50D/6.

Engineering Behaviour of Ashfield Shale

by

Mohammad Ghafoori
B.Sc., M.Sc.

A Thesis submitted for the Degree of Doctor of Philosophy

School of Civil and Mining Engineering
The University of Sydney
Australia

Feb, 1995

CONTENTS

SYNOPSIS

Intact specimens of Ashfield shale have been used in this study to investigate its engineering behaviour. Ashfield shale is a sedimentary rock of the Wianamatta sequence from the geological region known as the Sydney basin in New South Wales, Australia. This rock outcrops over parts of the Sydney metropolitan area. Many structures and deep excavations have been constructed in the Ashfield shale, and it is sometimes used as a construction material.

One of the primary aims of this investigation has been to identify index property tests useful for determining the engineering properties of shale. A further aim of the study has been to evaluate the effects of lamination orientation, with respect to the principal stress directions, on the shear strength, shear strength parameters and deformation of Ashfield shale.

Thin sections, X-ray diffraction and scanning electron microscopy analysis have been used to determine the clay mineralogy and fabric of the shale. Slake durability tests have been performed on samples of shale with varying degrees of weathering to investigate the deterioration of the rock from cycles of wetting and drying. Correlations between the slake durability index, the natural water content, Atterberg limits, uniaxial compressive strength, and the weathering grade of the shale have been investigated. The natural moisture content has been found to be a good predictor and a useful index for the durability, index properties, clay content, and the strength of the intact shale.

The point load test is widely used to determine the uniaxial compressive strength indirectly. Correlations have been made between the point load

strength index and the measured values of uniaxial compressive strength in direction perpendicular to laminations. The strength anisotropy, the ratio of point load strength in the strongest and weakest directions, was measured for the samples tested in these two directions.

This study also presents the results of a comprehensive series of triaxial and uniaxial compression tests on Ashfield shale. Triaxial compression tests have been performed over a range of confining pressures from 0 to 10 *MPa*. The orientation of the laminations, relative to the axial direction, in the triaxial apparatus has been varied between 0 and 90 degrees at intervals of 15 degrees. The lateral and longitudinal strains have been measured by gauges mounted on the core samples. These tests have been used to determine the effects of the anisotropy, caused by the laminations, on the strength and stiffness of the shale. The strength data were compared with basic failure theories and the applicability of these strength criteria for Ashfield shale was examined. Of the three criteria used for intact rock, Bieniawski's (1974) criterion appears to be the most appropriate one for Ashfield shale. The single plane of weakness theory (Jaeger, 1960) and the modified variable cohesive strength theory (McLamore and Gray, 1967) have shown good validity for Ashfield shale and fit the experimental data fairly well. The theoretical predictions also show good general agreement with the experimental values of the secant modulus of elasticity, measured at 50% of the peak strength across the full range of β (angle between lamination and axial stress direction) values.

For practical purposes a single criterion has been suggested. This criterion is capable of accurately predicting the strength of Ashfield shale over the full range of β values, and therefore capture accurately the anisotropic nature of the strength.

A series of direct shear tests has been carried out on the Ashfield shale to determine the influence of the boundary conditions on the strength parameters and the degree of anisotropy. Direct shear tests have been

performed at a variety of normal stresses within the range from 0.3 to 1.6 *MPa*, and peak and residual strength parameters have been determined. The peak strengths were usually mobilised at relatively small shear displacements and the shearing resistance was reduced abruptly with further shearing beyond the peak. It was found that the strength parameters were significantly affected by the direction of shearing. The triaxial and direct shear experimental results confirmed the existence of anisotropy in the shear strength parameters.

A numerical study of the deformation of an anisotropic rock, such as shale, in direct shear tests is presented. The study has investigated the effects of the orientation of the bedding planes to the shearing direction, and of the boundary conditions imposed in the test. A cross-anisotropic elastic model has been used to represent the pre-failure stress-strain behaviour of the rock and an extensive parametric study has been carried out of the behaviour of this material in direct shear. Implications for the interpretation of actual test data are discussed, and illustrated by comparison of the theoretical predictions with experimental results for Ashfield shale. The predicted direct shear stiffness shows good general agreement with the secant shear stiffness measured at 50% of the peak strength in the direct shear test. This implies that the direct shear test is capable of detecting accurately the nature of the anisotropy of shale. Furthermore, the secant values of the moduli determined from uniaxial and triaxial compression tests are consistent with the secant shear stiffnesses measured in direct shear tests.

PREFACE

The work described in this thesis was carried out during the period from 1991 to 1994. All the work was performed in the School of Civil and Mining Engineering at the University of Sydney. The candidate was supervised by Professor J.P. Carter and Dr. D.W. Airey in this school.

The By-Laws of the University of Sydney require a candidate for the degree of Doctor of Philosophy to indicate which sections of the thesis are original. In accordance with these By-Laws any material or ideas derived or obtained from other sources has been acknowledged in the text. Those sections of the thesis for which the candidate claims originality are as follows:

(1) In Chapter 3, all XRD, scanning electron and optical microscope results.

(2) In Chapter 4, the results of the slake durability and point load tests, uniaxial compression tests, the Atterberg limit tests, the results of the tests for porosity and dry density and clay fraction less than 2 microns. The analysis and discussion of the relationship between moisture content, *UCS* and dry density.

(3) In Chapter 5, all the results of triaxial and uniaxial compression tests on Ashfield shale samples with different lamination directions. The analysis and discussion of the results.

(4) In Chapter 5, the suggested empirical criterion for Ashfield shale and the analyses and comparisons between the predicted and

experimental results.

(5) In Chapter 6, all direct shear test results on shale samples with different lamination directions under constant normal stress conditions. The analysis and discussion of the test results.

(6) In Chapter 7, the numerical modelling of the Ashfield shale as an anisotropic material in direct shear tests and comparisons between the predicted and experimental results.

LIST OF PUBLICATIONS

A number of papers and reports was prepared and published by the Author and others during the period of candidature. They are submitted in support of this thesis and listed as follows:

Ghafoori, M., Mastropasqua, M., Carter, J.P. and Airey, D.W., (1993), "Engineering properties of Ashfield shale", Bulletin of the International Association of Engineering Geology, No. 48, pp. 43-58, and Research Report No. R663 (1992), School of Civil and Mining Engineering, University of Sydney.

Ghafoori, M., Carter, J.P & Airey, D.W., (1993), " Anisotropic behaviour of Ashfield shale in the direct shear test", in Geotechnical Engineering of Hard Soils-Soft Rocks, Anagnostopoulos et al. (eds), Balkema, Rotterdam, Vol. 1, pp. 509-515.

Ghafoori, M., Airey, D.W. and Carter, J.P., (1993), "Correlation of moisture content with the uniaxial compressive strength of Ashfield shale", Australian Geomechanics,No. 24, pp. 112- 114.

Ghafoori, M., Carter, J.P & Airey, D.W., (1994), "Analysis of anisotropic rock in direct shear", Computer Methods and Advances in Geomechanics, Siriwardane & Zaman (eds), Balkema, Rotterdam, pp. 2247-2252.

Ghafoori, M., Airey, D.W. and Carter, J.P., (1994), "The durability of Ashfield shale", Proceedings, 7th International Congress, International Association of Engineering Geology, Oliveira et al. (eds), Balkema, Rotterdam, pp. 3315-3321.

ACKNOWLEDGEMENTS

This investigation was carried out in the School of Civil and Mining Engineering of the University of Sydney under the supervision of Professor J.P. Carter and Dr. D.W. Airey. I wish to express my deep sense of gratitude to Professor Carter and Dr. Airey for their constant support, valuable supervision, encouragement and guidance with all aspects of this work. I am indebted for their co-operation and kind help they rendered from time to time.

I appreciate the help that I received from the other academic staff of the School of Civil and Mining Engineering, especially Professors John Booker, Harry Poulos, John Small, Drs Peter Brown, and Tim Hull. Acknowledgement is also due to the technical staff, particularly, R. Barker, I. Hoggard, A. Reyno, P. Witty, A.Farago, P. Li, A. Townsend and C. Hennessey for their co-operation and friendship. I am very thankful to the microscope unit staff (EMU), particularly Dr. I. Kaplin, Mr. A. Sikorski, T. Romeo and T. Joyce in preparing the polished sections, in the image analysis and in printing the photomicrographs. Dr. G. Deleon and Mr D. Nobbs from the Department of Chemical Engineering in XRD study and analysis and Mr. P. Maning in the Department of Geology in the study of porosity are gratefully acknowledged. I also wish to express my thanks to Ron Brew and Kim Pham for their assistance in preparing a number of figures.

The author is grateful to many people and organisations for making available some test data used in this study. Particular thanks are extended to Longmac Associates Pty. Ltd., Coffey Partners International Pty. Ltd., D.J. Douglas & Partners Pty. Ltd. and the Geomechanics group of the New South Wales Roads and Traffic Authority for making available many of their

geotechnical reports and associated data. The provision of the core samples of Ashfield shale by the Roads and Traffic Authority's Geomechanic groups is gratefully acknowledged.

I take this opportunity to thank my friends and fellow workers especially Dr. C.J. Leo, J.T. Tabucanon, G.R. Lashkaripour, M. Makarchian, F. Moghaddas Nejad, P. Kelleher, Axel Ng , N. Fernando, Le Ta for their friendship and sincerity. A note of gratitude is extended to Dr. C.J. Leo, who shared the same office with the author for about four years, for many constructive discussions about various aspects of this study and for his unconditional friendship and encouragement.

For their patience, encouragement and help throughout my study I should like to thank my family, especially my wife Zahra and my dauther Maryam and my son Ali. In appreciation of all the good things that God has made possible through them, this thesis is dedicated to them.

Finally, I wish to acknowledge the support of a scholarship provided by the Ministry of Culture and Higher Education, Islamic Republic of Iran.

NOTATION

Some of the more commonly used symbols in this thesis are listed below. In the test, all symbols and notation have been defined whenever they are first used.

β	angle between lamination and axial stress direction
β	value of the orientation angle, β, at which the strength is minimum (generally 30 degrees).
ε	infinitesimal strain
ε_x	strain components in x direction
ε_y	strain components in y direction
ε_z	strain components in z direction
ϕ	friction angle
ϕ_d	friction angle in the plane of weakness ($\beta = 30^\circ$)
ϕ_p	friction angle at peak shear strength
ϕ_r	friction angle at residual shear strength
γ_{xy}	strain components in xy direction
γ_{yz}	strain components in yz direction
γ_{zx}	strain components in zx direction
γ_d	dry unit weight of the rock (also known as the dry density)
γ_w	unit weight of water (1 t/m^3 or 64 lb/ft^3)
μ	coefficient of internal friction
ν	Poisson's ratio
ν_l	Poisson's ratio, describing the behaviour in the planes of the laminations in response to normal stress applied parallel to the laminations.

ν_2	Poisson's ratio, describing the behaviour in the direction perpendicular to the laminations in response to normal stress applied parallel to the laminations.
σ	normal stress
σ_1	major principal stress
σ_2	intermediate principal stress
σ_3	confining pressure (minor principal stress)
σ_c	uniaxial compressive strength
σ_{cj}	uniaxial compressive strength at a particular orientation angle
σ_x	stress components in x direction
σ_y	stress components in y direction
σ_z	stress components in z direction
τ	shear strength
τ_{xy}	stress components in xy direction
τ_{yz}	stress components in yz direction
τ_{zx}	stress components in zx direction
c_o	cohesion intercept
c_d	the cohesion intercept in the plane of weakness ($\beta = 30°$)
c_p	cohesion intercept at peak shear strength
c_r	cohesion at residual shear strength
e	total void ratio
h	distance between loading points
m_c	moisture content (%)
n	an anisotropy factor, also the total porosity (%)
A	the minimum cross section area of a plane through the loading cone contact points
D	distance between loading points in diametral test
E	Young's modulus
E_β	Young's modulus at direction of β

E_1	Young's modulus in the plane of isotropy, i.e. parallel to the laminations
E_2	Young's modulus perpendicular to the plane of isotropy, i.e. perpendicular to the laminations
E_i	initial tangent modulus
F	a size factor
G_2	the independent shear modulus, describing the shearing behaviour in planes perpendicular to the laminations
I_d	slake durability index
I_{d2}	slake-durability index (second cycle)
I_s	uncorrected point load strength index
K	modulus number
K_b	brittleness factor
K_s	shape factor
K_s	shear stiffness
K_{si}	initial tangent shear stiffness
K_{sp}	peak shear stiffness
K_{ss}	secant shear stiffness
L	length (distance between the loading cones in an axial test)
P	failure load
P_a	Atmospheric pressure (0.1 Mpa or 14 lb/in^2)

CHAPTER 1 INTRODUCTION

CHAPTER 1

INTRODUCTION

1.1 STATEMENT OF THE PROBLEM

Shale is the most abundant sedimentary rock in the earth's crust. Shale constitutes 47% of all sedimentary rocks and occurs over approximately 35% of the total land area (Pettijohn, 1957). In nature, shale may range from soft soil-like to hard rock-like materials with laminated or massive forms. The laminated shales tend to split parallel to the bedding planes, whereas the massive ones often tend to break into blocks. Lamination is mainly due to variations in grain size and changes in composition, and the laminations are generally parallel to the bedding planes.

Shale is one of the most complex and problematic and least understood geological materials. It is characterised by a wide variation in its engineering properties, particularly its resistance to short term weathering by wetting and drying. Grain size, mineralogy, cementation and fabric are the main factors that affect the engineering properties of shale. These factors are also important in the geological classification of shale. Shales contain a wide range of particle types which usually include the clay minerals and silt sized minerals, mainly quartz. Shale with a lesser clay mineral content is generally coarse-grained or

silty. The type of clay mineral and the ratio of clay mineral to quartz content have significant effects on the physical and mechanical properties of shale. Shales deteriorate mainly in response to changes in the temperature and humidity of the surrounding environment. This deterioration has long been recognised, especially in the coal mining industry, as a serious problem affecting the operation, stability, maintenance and safety in underground structures (Hartmann and Greenwald, 1941). Shale moisture variations, especially those involving wetting and drying cycles, are important in the weathering process.

Both engineers and geologists are interested in shale. Normally geologists are interested in the conditions in which the shale was formed, and their classification is based on mineral assemblages and physical properties. Engineers are more interested in the behaviour of shale as a construction material or as a foundation material for structures.

Shale masses frequently contain discontinuities such as joints and bedding planes which affect the mechanical behaviour of the rock substance and the rock mass. In particular, the bedding planes and laminations have significant effects on the shear strength of the shale mass. They may weaken the rock mass, but, importantly, they also make the rock substance behave anisotropically. The shear strength of the shale and its anisotropic behaviour are considered to be of major importance in a number of geotechnical problems, such as the design of underground structures in shale, in determining the behaviour of shale masses surrounding deep excavations, in understanding the behaviour of abutments for dams, and in assessing the stability of rock slopes in shale.

Knowledge of the mechanical properties of shale, e.g. how it deforms or fails under the action of applied forces, is essential for designing and/or evaluating the stability of a structure in rock. Unlike other engineering

materials such as metals and concrete, the composition and structure of shales are highly variable. Many different tests are run on core rock specimens to determine their mechanical properties and behaviour. Static mechanical property tests are designed to measure the deformation and strength of rock specimens and include the uniaxial compression, triaxial compression and direct shear tests.

The Sydney metropolitan area is founded on three major rock units, the Wianamatta group, the Hawkesbury sandstone and the Narrabeen group. These three rock units are overlain by Quaternary/Tertiary alluvium. The Wianamatta group rocks, especially the Ashfield shale, and their weathering products are of engineering importance as they form the foundations for most of the central business district and western Sydney. The shales also provide earth-fill and brick clay for construction projects throughout the Sydney region, and because of the widespread availability of Ashfield shale in the Sydney region, it has been used in road construction. Many zones of instability are reported in Wianamatta group in sydney metropolitan area (e.g. Branagan, 1985; Fell, 1985). Existing knowledge of shale behaviour in this region is largely empirical and conventional design of structure on rock is based primarily on empirical bearing capacities. There is limited data on deformation behaviour of shale. The uncertainties in this approach may necessitate the use of relatively high factors of safety. Because of the deeper excavations in the central business district and Chatswood area and increasing development in Western Sydney, greater knowledge is now required. This thesis is an attempt to provide some information about the engineering and deformation behaviour of shale.

1.2 PURPOSE AND SCOPE OF INVESTIGATION

One of the primary aims of this investigation has been to identify tests useful

for determining the index properties of shales. A major part of this investigation deals with the uniaxial compressive strength, the point load strength index, the slake durability, the degree of weathering, the moisture content, the dry unit weight and the bulk unit weight, and the relationships between them. Also included is an examination of the important influence of moisture content and the degree of weathering on the mechanical properties, particularly the strength. It will be demonstrated that the natural moisture content is a good predictor of the durability, strength and index properties.

The mechanical behaviour of shales is dependent on their mineralogy, and especially the type and quantity of any clay mineral present. To understand the mineral composition, especially the clay mineralogy of the Ashfield shale, X-ray diffraction analyses, scanning electron microscopy, and optical microscopy have been conducted.

To simulate the loading which may occur in the field in a rock material around an excavation or under a foundation, a series of triaxial tests have been performed for a range of confining pressures and lamination orientations. The aim of this study was to evaluate the effect of confining pressure and the lamination directions with respect to the principal stress direction, on the shear strength, shear strength parameters and deformation of Ashfield shale.

The mechanical behaviour of rock with weakness planes may have direct importance in many mining and engineering projects. For example, the stability of rock slopes and tunnel walls is often controlled by the shear strength of weakness planes. To measure the peak and residual shear strength and shear strength parameters, a programme of direct shear tests is essential. The conventional direct shear device has been used to obtain the shear strength parameters of the laminated Ashfield shale. In these tests the normal stress has been held constant, boundary condition that is relevant for a number of practical problem, e.g. slope stability problems. The effect of lamination

direction on the strength parameters has been evaluated.

From the laboratory investigation, a model based on the theory of elasticity was used to predict the shear stiffness of Ashfield shale in the direct shear test. The various model parameters were obtained from the uniaxial compression tests. Comparisons were made between the predicted and experimental shear stiffnesses.

1.3 OUTLINE OF THE THESIS

Experimental and numerical methods are presented in this thesis for evaluating the engineering properties and predicting the engineering behaviour of Ashfield shale. These methods are presented in five main chapters.

Chapter 2 presents a brief review of previous studies on the geology mineralogy, classification and engineering behaviour of shales. In particular, the review includes a study of index tests, triaxial and direct shear tests on samples of shale. The various strength criteria for isotropic and anisotropic rocks and their assumptions are also reviewed.

The geology, mineralogy and physical properties of Ashfield shale are described in Chapter 3.

Chapter 4 describes the index tests carried out in this investigation. A major part of this chapter deals with the uniaxial compression strength, the point load strength index, and the slake durability test. The correlation between different physical properties and index tests results is investigated. The natural moisture content has been found to be a good predictor of the durability, strength, and the clay content of the shale.

Chapter 5 describes the uniaxial and triaxial testing progrmme and testing procedure. The results of uniaxial and triaxial compression tests on Ashfield shale for samples with different lamination orientations are presented. The tests have been used to determine the effects of the laminations and confining pressure on the deformation and strength parameters of Ashfield shale. The strength and deformation data are generally described well by existing theories for anisotropic materials.

Chapter 6 describes the results of a comprehensive series of direct shear tests on Ashfield shale. The laboratory testing programme and the procedure for monotonic direct shear tests under constant normal stress conditions are described. The effect of normal stress and lamination direction relative to the direction of applied shear force on the peak and residual shear strengths, the shear strength parameters, and stiffness are presented.

Chapter 7 describes the results of an investigation into the pre-failure behaviour of a cross-anisotropic material in the direct shear test. A numerical study is conducted to investigate the effects of parameters such as the degree of anisotropy, the shape of the test specimen, and the boundary conditions of the shear test on the shear response. The implications of the numerical study for the interpretation of actual test data are discussed, and are illustrated by comparisons of the theoretical predictions with the experimental results for Ashfield shale.

Chapter 8 presents the main conclusions and some recommendations for further research.

CHAPTER 2 LITERATURE REVIEW

CHAPTER 2

LITERATURE REVIEW

2.1 INTRODUCTION

The engineering behaviour of soils and rocks is complex and variable. Certain properties are more important than others for a given engineering application. For sedimentary rocks, such as shale, the engineering properties are mainly controlled by the degree of weathering, the mineral components, the type of cementation, the texture and structure. These factors influence the water content, specific gravity, bulk density and the total void ratio (e), total porosity (n), and degree of saturation (s).

The objective of this chapter is to present an overview of previous studies into the engineering behaviour of argillaceous rocks with particular emphasis on shales. The mineralogical and physical properties, and classification of argillaceous sedimentary rocks are reviewed to determine suitable definitions for these rocks. Various laboratory tests for determining the strength and stiffness of rock are reviewed to determine suitable tests for the investigation of Ashfield shale. Data from previous studies of Ashfield shale are reviewed.

2.2 DEFINITION AND CLASSIFICATION OF SHALE

2.2.1 General background

Shale is the most abundant sedimentary rock in the earth's crust. The geological literature shows that the terminology used to describe the entire group of argillaceous sediments is not standardised and there are numerous inconsistencies in the classification and nomenclature of shales (Pettijohn, 1948).

There are different opinions about the classification and identification of this kind of rock. The term shale has been used by some authors for all argillaceous sediments, including claystone, siltstone and mudstone (Ingram, 1953; Krumbein et al., 1963). Others have specified the large group as the mudstone group and classified shale as a member of this group (Twenhofel, 1937; Muller, 1967). Terzaghi (1946) stated two essential properties for materials to be called shale:
(1) the material should give a clear ring when it is struck by a hammer, and
(2) the volume should not be changed while the material is immersed in water

Argillaceous rocks such as shale, mudstone, claystone, siltstone, and clay shale are characterised by wide variations both in their engineering properties and composition. The common characteristics of this group of rocks are that all members are fine-grained and composed predominantly of clay and silt sized materials.

2.2.2 Classification for geological purposes

2.2.2.1 Based on origin

Pettijohn (1975) classified clays and shales as residual or transported materials. This classification is shown in Figure 2.1. The residual clays are a soil or a product of the soil forming processes that formed in situ. The character of in situ

materials is dependent upon climate, drainage, and parent rock materials. The transported clays and shales obtain their components from three sources:

(a) products of abrasion,

(b) end products of weathering,

(c) chemical and biochemical additions.

Twenhofel (1937) classified the fine grained materials based on two variables, state of induration and the relative amounts of silt and clay components. This classification was used later by Pettijohn (1975) and is shown in Figure 2.2. Twenhofel extended the term mudstone to include the whole family of argillaceous rocks. Most writers, including Picard (1953) and Pettijohn (1975), used the term mudstone for those rocks that have the grain size and composition of a shale but without laminations or fissility.

Mead (1936) suggested a classification for shales that divides them into two broad groups (Figure 2.3):

(a) Compacted or soil like shales, without intergranular cement, which have been consolidated by the weight of overlying sediment,

(b) Rock like shales as a cemented or bonded material in which the cementing material may be calcareous, siliceous, ferruginous, gypsiferous, etc., or if lacking a cementing agent, the shale may be bonded by recrystalisation of its clay minerals.

To distinguish between compacted and cemented shale, he suggested the slaking test by immersing dry samples in water. Those shales which do not fall apart after drying and wetting are termed cemented shales. Underwood (1967) also used the term "soil-like" shale for compacted shale, and "rock-like" shale or bonded shale for cemented shale.

A simple weathering test consisting of 5 cycles of drying and wetting for distinguishing compacted shale from cemented shale was described by Philbrick (1950). He suggested that the shales that reduced to grain sized particles be

termed compacted shales and those that were unaffected or which reduced to "flakes" be termed cemented shales.

Based on stress history, Bjerrum (1967b) classified shales as overconsolidated plastic clays with strongly developed diagenetic bonds and clay-shales as overconsolidated plastic clays with well developed diagenetic bonds. Similarly, Terzaghi and Peck (1967) classified shales based on the fragment size to which the intact shale material is reduced upon submersion. According to this classification, shales can be categorised as "well bonded" or "poorly bonded" with "rock-like" shales and "clay-shales" at each extreme of induration, respectively.

A distinction between soil-type and rock-type argillaceous materials is possible based on the strength loss, the rate of softening and amount of strength loss in triaxial tests during softening (Morgenstern and Eigenbrod, 1974). The results of the strength softening tests suggested that for "rock-type" materials, e.g. shales, the undrained shear strength (C_u) is greater than 1800 *kPa* and the strength loss during softening is less than 40% of its original strength. Figure 2.4 shows the classification of argillaceous materials based on the results of strength softening tests.

Morgenstern and Eigenbrod (1974) also tried to distinguish between soils and rocks based on slaking tests. They found that both the quantitative slaking test and the rate of slaking test are useful index tests for distinction of soil and rock. Figure 2.5 shows the classification of argillaceous materials based on slaking characteristics. In this classification, the maximum amount of slaking expressed in terms of liquid limit (W_L) and the rate of slaking test (ΔI_{Li}) expressed in terms of the change of liquidity index (ΔI_L).

For the very low plasticity and non-plastic materials slaking is not the most destructive mechanism. The quantitative slaking test is a simple but very time consuming test and therefore not well suited for classification. Hamrol (1961)

and Franklin (1970) suggested tests similar to the rate of slaking test. Hamrol suggested the water content of oven-dried specimens after they had been immersed in water for approximately 1 - 2 hours and named this as the alteration index. He found that this parameter correlated well with the shearing resistance and modulus of elasticity of the rock investigated. Hamrol's rate of slaking test and Franklin's test both provide a durability index. Both measure the rate of slaking of oven dried specimens after immersion in water. Hamrol's rate of slaking test determines the amount of disintegration by measuring the water content after water immersion for 2 hours, while Franklin's slake durability tests determines the amount of disintegration after water immersion and mechanical disturbance for 10 minutes. Both tests give similar results. The disadvantage of Hamrol's test compared with Franklin's test is the longer test time, but no special equipment is needed and also the mechanical process does not affect the test result.

It is highly desirable to have a single, standard slaking test, which should be accepted universally, to differentiate the rock-type and soil-type argillaceous materials. Based on the literature on the slaking characteristics of argillaceous rocks, Franklin and Chandra's (1972) slake durability index test was recommended by many people. More detail about the slake durability literature is described in the another section of this chapter.

According to the classification schemes of Mead (1936), Philbrick (1950), Underwood (1967), Terzaghi and Peck (1967), and Morgenstern and Eigenbrod (1974), the Ashfield shale can be classified as a well bonded and cemented shale.

2.2.2.2 Based on texture and structure

Many researchers also classified argillaceous materials based on texture and structure. The size, shape, and arrangement of particles within a rock is known as the texture or fabric of a rock. Particle size distributions of clays and shales

have been extensively investigated by many researchers. Pettijohn (1975) stated that most shales contain a higher proportion of silt. Krynine (1948) estimated the average shale to be about 50% silt. Shales are often classified as clayey, silty, or sandy shales based on the grain size distribution. A common texture in laminated shales is a preferred orientation of the platy clay minerals parallel to the bedding plane. In some clays and shales, clay minerals show a random orientation (Keller, 1946). In some cases this may be as the result of authigenic crystal growth in place.

Shales are also characterised by the property of fissility. Fissility is one of the most critical mechanical aspects in shale as it can lead to strong anisotropy. Fissility is the tendency of a rock to split, or separate, along relatively smooth surfaces parallel to the bedding planes (Pettijohn, 1975; Spears, 1976). Some shales are markedly fissile, others weakly so. The consensus of a group of investigators is that fissility is usually associated with a preferred parallel arrangement of clay particles which is mainly promoted by the properties of the depositional environment (Ingram, 1953; White, 1961; Mead, 1966) and enhanced by sediment overburden (Lambe, 1958; Odom, 1963, 1967; O'Brien, 1963, 1970). The presence of organic materials can also produce well developed fissility (O'Brien, 1970; Gibson, 1965; Ingram, 1953; Odom, 1967). Spears (1976) found no direct relationship between fissility and clay orientation for some carboniferous shales. He found fissility to be entirely controlled by laminations that is varves, consisting of dark discontinuous lenses containing slightly more organic materials and clay minerals.

Alling (1945) and Ingram (1953) tried to establish a scale of fissility and to relate fissility to the composition. Both investigators noted that an increasing siliceous or calcareous content decreases fissility of a shale.

Laminations, which are also a common sedimentary structure in shale, are a primary feature useful in reconstructing the original sedimentary conditions of

argillaceous rocks. A lamination is the thinnest recognisable unit layer and is usually less than 10 *mm* (commonly 0.05 to 1 *mm*) in thickness (Bates and Jackson, 1987). Laminations appear to be of three kinds: alternations of coarse and fine particles, such as silt and clay; alternations of light and dark layers distinguished only by organic content, which is responsible for their colour; and alternations of calcium carbonate and silt (Pettijohn, 1975). These alternations may be the result of differential settling rates of the various components or of differing rates of supply of these materials to the basin of deposition.

In summary, sedimentologists have generally restricted the term shale to a material with particular structure, e.g. fissility and lamination, but most engineers and some geologists have used the term shale based on degrees of induration and deterioration. In spite of the many attempts to standardise the terms mudstone and shale for the massive type and fissile type of argillaceous materials, respectively (Ingram, 1953; Gamble, 1971), in practice these two terms are used in a general sense depending on geographical location (e.g. in the USA the term shale is the common name for both fissile and massive rocks, but in Britain the term mudstone is the common name for these materials). This shows that still there is no unique universal definition to be used for practical purposes. This lack of agreement is due largely to the difficulty of quantifying the degree of induration and rate of deterioration of argillaceous rocks.

2.2.2.3 Mineral composition

The mineral composition of an argillaceous material is one of its most important characteristics. Shale contains a wide range of minerals which are usually a mixture of clay-size particles, mainly clay minerals, and silt size particles, mainly quartz. The mineralogy of shale has a significant influence on the engineering behaviour especially when clay minerals are dominant. The main clay minerals found in shales are illite, kaolinite, montmorillonite, and chlorite. The type of clay mineral is a function of the source rocks, climate and diagenetic history.

Smectite and kaolinite are more common in non-marine shales, whereas illite and chlorite are more common in marine shales (Brown et al., 1977). Different clay minerals have different effects on the engineering behaviour of shale. Shales containing the smectite group, of which the most common member is montmorillonite, are usually more troublesome than others.

The clay mineral content in shale may vary from 40% percent or less to 100%. In the shales with higher clay content, the clay mineral particles are small, normally less than 0.002 *mm*. Shales with less clay minerals are generally coarse grained or silty. The ratio of clay mineral to quartz content is also a useful mineralogical parameter in shale. Increasing quartz content has been shown to result in reducing liquid and plastic limits (Spears and Taylor, 1972; Attewell and Farmer, 1976), increasing uniaxial compressive strength and uniaxial tensile strength of shale (Gunsallus and Kulhawy, 1984; Dusseault et al., 1986).

2.2.3 Classification for engineering purposes

From an engineering standpoint rock can be divided in two groups, that is, intact rock and in-situ rock. The rock material which can be sampled and tested in the laboratory is known as intact rock. In large scale engineering structures in rock, in situ tests are usually used to determine design parameters on the deformability of the rock mass. Because of the cost, where in situ testing is not possible, design parameters may be based on properties of the intact rock material determined in the laboratory. These properties are usually the uniaxial compressive strength, the modulus of elasticity and Poisson's ratio. The quantitative or at least semi-quantitative description of rock cores recovered during site investigation is a necessary step in the assessment of the rock mass. This assessment and the allocation of descriptive classes is now advocated for general use (Anon., 1981), and is a logical extension of the early proposals of Deere (1963) that were later elaborated by Deere and Miller (1966) for rock material, and by Deere, Merritt and Coon (1969) for in situ rock.

There are several important engineering properties to consider in the classification of rocks, e.g. compressive, tensile and shear strength, modulus of elasticity. The most extensive work on the classification of intact rock for engineering purpose based on laboratory values have been done by Coates (1964), Coates and Parsons (1966) and Miller (1965).

Coates and Parsons classified intact rocks according to uniaxial compressive strength (σ_c) and deformation parameters that were determined in the laboratory. They classified the rock into weak ($\sigma_c < 35\ MPa$), strong ($35 < \sigma_c < 123\ MPa$) and very strong $\sigma_c > 123\ MPa$ categories. Based on their classification, most shales would be classified as weak rocks.

Deere and Miller (1966) proposed an engineering classification based on two important engineering properties of the rock, the uniaxial compressive strength and the modulus of elasticity. This classification seems to be sensitive to mineralogy, fabric and degree of anisotropy of the rock material.

Deere, Merritt, and Coon (1969) reviewed classification systems for in-situ rocks and suggest two methods of indexing rock quality: rock quality designation (RQD) and velocity index. The RQD is the ratio of length of core recovered, counting all sound core over 4 inches long to the total drilled length of the core for each run. The velocity index is the square of the ratio of in-situ to laboratory sonic velocity.

A classification of shales based on compressive strength or undrained shear strength has been used by some investigators (Underwood, 1967; Morgenstern and Eigenbrod, 1974; Oliver 1979a). Underwood (1967) proposed a classification for shale based on some engineering considerations and significant properties of shales based on laboratory testing and field observations to differentiate the problematic from non-problematic shales. Among the significant engineering properties of shales, he suggested compressive strength, peak and residual shear

strengths, modulus of elasticity, moisture content, density, void ratio, permeability, swelling potential and activity ratio for classification of shales. To evaluate the in situ engineering behaviour of shale, he considered state of stress, slope stability, rebound of excavated surfaces, deterioration of shale surfaces, and pore pressure. According to Underwood (1967), the compressive strength of shale ranges from less than 180 *kPa* for weaker compaction shales to more than 108 *MPa* for well cemented shales.

Franklin (1970) extensively reviewed the problem of classification of rock in general, and his primary concern was with a classification system that requires a minimum of laboratory preparation and testing and applicability to in-situ properties. Gamble (1971) included other properties such as swelling potential, plasticity characteristics and residual shear strength which are peculiar to and important in the engineering behaviour of shales and other mudrocks.

2.3 PHYSICAL PROPERTIES

2.3.1 Density and porosity of shale

The density of a rock is one of its most fundamental properties. The density is influenced by the mineral composition, porosity, joints and other open spaces present. For the same rock type, the density will generally be increased as the depth increases (Athy, 1930; Hedberg, 1936; Jones, 1944). This increase is because of the decrease of open cracks under pressure of the overlying rocks. The density will be also affected by the organic content. Reported values of density of shales fall within the range 2.0 to 2.73 t/m^3 (Duly, Manger and Clark, 1966).

Porosity is also an important physical property of rock in the field of geology, geophysics, petroleum engineering and rock mechanics. Porosity is a rock

property that affects the density, strength and elasticity and it is an important factor in assessing strength of rocks. Many factors influence the porosity of a shale, and porosity also varies during the geological history of shale. The porosity will be increased as a result of erosion, stress relief, and weathering. The initial porosities of deposited mud may be as much as 70 to 80% (Trask, 1931), but the porosity of shale is much less. Porosity decreases with compaction rather than by filling of pores. Muller (1967) demonstrated that grain size, clay mineral compaction, and temperature play an important role in the reduction of porosity below a depth of about 500 *m*. Although the average clay has a porosity of 30 to 35%, the porosity of shale under an overburden of 1800 *m* is only 9 to 10 percent (Hedberg, 1936). This decrease in porosity is a result of the substantial compaction at depth.

Many researches have reported the effect of porosity on the mechanical properties of rocks. All strength properties of rocks decrease with increase in porosity (Price, 1960; Kowalski, 1966; Smordinov et al., 1970; Rzhenky and Noviki, 1971; Vernik et al., 1993).

2.3.2 Moisture content

It has been well established that the moisture content in shales can have significant effects on their physical and mechanical properties. The natural moisture content of shales varies from less than 5% upwards to as high as 35% for some of the clay shales (Underwood, 1967). Various researchers compared the uniaxial compressive strength of many rock types under different conditions, e.g. oven dry, air dry and wet conditions. Analysis of their data shows that for all rock types, the strength is significantly lower in wet conditions. This reduction in strength is higher in the case of sedimentary rocks.

For shales, Salustowics (1965) found that the presence of moisture may

decrease the strength by as much as 60%. Colback and Wiid (1965) performed uniaxial compression tests on quartzitic shale samples under various relative humidities and observed a decrease in compressive strength with an increase in moisture content. Colback and Wiid found that the compressive strength of quartzitic shale under saturated conditions was about 50% of that under dry conditions (Figure 2.6). As this figure shows the change in moisture content from saturated to dry for this rock is very small, i.e. in the order of 1%. Colback and Wiid (1965) also performed triaxial compression tests on cylindrical specimens of a quartzitic shale and found that the Mohr strength envelope of water saturated samples had the same shape as the Mohr envelope of dry samples, but the saturated samples had lower strengths.

The effects of moisture on the strength of argillite were studied by Burshtein (1969). He found that the strength may decrease to a third of its initial value with an increase of 1.5% in the moisture content. For the Beaufort shales in South Africa, Oliver (1979b) observed that both the uniaxial compressive strength and tensile strength of specimens at in situ moisture conditions were generally 1.5 to 3 times that of specimens immersed in water for 24 hours. Similar effects of moisture on strength reduction have been given by other authors (e.g. Jumikis, 1966; Ballivy et al., 1976; Venkatappa Rao et al., 1983, 1986).

2.3.3 Weathering

Weathering, defined as the process of alteration of rocks occurring under the direct influence of the atmosphere and the hydrosphere (Sounders and Fookes, 1970), is an important process for shales. Since weathering is the main factor that weakens rocks, the quantitative classification of weathering grades and the mechanical behaviour of the weathered rocks are two important aspects of any engineering study of shales. Many investigators have tried to classify rock weathering according to the purpose of the engineering projects which involved the rocks, (e.g. Moye, 1955; Ruxton and Berry, 1957; Hamrol, 1961; Iliev, 1966).

These have generally been qualitative rather than quantitative classifications, and the previous work has mostly been related to granitic rocks. Dearman (1976) proposed a modified version of the weathering grade classification system to be used in field assessments of both rock material and the rock mass for engineering purposes. A similar approach was followed by Pells et al. (1978) to categorise the Ashfield shales into five classes on the basis of the uniaxial compressive strength (*UCS*) and the degree of fracturing. Hadfield (1981) later defined three weathering zones for these shales, which incorporated the classification of Pells et al. Table 2.1 shows the resulting classification system for Ashfield shale.

Shales are characterised by a wide variation in their engineering properties, particularly their resistance to short term weathering by wetting and drying. The durability of shales and other mudrocks to weathering upon exposure to surface and underground conditions following excavation is of particular interest. One of the most common forms of breakdown in argillaceous rocks such as shale is slaking which is the disintegration of these materials when exposed to air or moisture, or to drying and wetting.

Environmental changes in humidity and temperature cause cycles of wetting and drying of shale. Compared with temperature, humidity variations play the most important role in shale deterioration (Hartman and Greenwald, 1941; Fish et al. 1944 ; Parker, 1966).

2.3.4 Slake durability

The slake durability test is used to measure the resistance of a rock sample to weakening and disintegration from a standard two cycles of wetting and drying. The main aim of this test is to evaluate the weathering resistance of shales. It is important in many projects, i.e. the stability of slopes in road, canal, spillway, and other cuts, and in underground excavations. (Hartman and Greenwald, 1941; Ingram, 1953; Underwood, 1967; Morgenstern and Eigenbrod, 1974). Problems

in using shale as a construction material or as a foundation material have occurred in numerous applications, such as embankment failures, slope instability, and unstable subgrade. The assessment of the durability of such rock types is very important for engineering geological classification purposes.

Many researchers have studied moisture adsorption as an indicator of rock durability (e.g. Grice, 1968; Chenevert, 1970; Aughenbaugh, 1974; Van Eeckhout and Perig, 1975; Harper et al., 1979; Richardson, 1984). In most studies samples were placed in environments of different relative humidities ranging from 12% to 100%. Grice in the study of the deterioration of shale in tunnels concluded that with control of humidity and temperature over long time periods a quantitative measure of progressive fissuring and disintegration will be provided without disturbing the rock mass.

Anisotropic expansion of shale by moisture adsorption is a factor responsible for differential swelling which may cause local failure and material disintegration. The strain anisotropy (different strains perpendicular and parallel to bedding planes) will result from both shale moisture increase upon either unconfined exposure to higher humidity environments (Hartman and Greenwald, 1941; Van Eeckhout, 1976; Oliver, 1979b; Harper et al., 1979) or water immersion (e.g. Murayama and Yagi, 1966; Onodera and Duangdeum, 1981) and shale moisture decrease upon unconfined exposure to lower humidity environments (Chenevert, 1970a; Harper et al., 1979).

Taylor and Spears (1970) found that in laminated shale the disintegration was controlled by lamination thickness. In general, shales with high illite and mica content disintegrated more rapidly in water than shales with kaolinite as the dominant clay mineral. Russell (1982) found that the form and amount of calcite has a major control on slake durability of shales. High durability is caused by the presence of hard bands which are richer in calcite than typical shales. However, in samples with homogeneous calcite dissemination, durability is more controlled

by calcite content than the abundance of clay minerals. Later Russell and Herman (1985) found that calcite content controls the frequency and types of the discontinuities as well as the intact strength and slake durability of the Queenston shale.

There have been many test procedures for estimating the slake durability of shales. All methods essentially consist of cycles of drying and wetting by water or some other fluid. Franklin (1970), Chandra (1970), Taylor and Spears (1970) discussed the results of various methods of testing for durability. A slake durability test apparatus was developed and tested at Imperial College by Franklin (1970) and Chandra (1970). It has since been included in a suggested test method by the commission on standardisation of laboratory and field tests of the International Society for Rock Mechanics (1970). In the slake durability test developed by Franklin and Chandra (1972), ten representative lumps of shale each weighing 50 to 60 grams are oven dried and placed in a drum. After 10 minutes rotating in a partly immersed drum constructed of 2 *mm* mesh, the retained material in the drum is oven dried at 105°C for at least 6 hours and weighed. The cycle is repeated and the slake durability index is the dry weight percentage of material retained after the second cycle.

Franklin and Chandra (1972) and Gamble (1971) have performed a wide range of the slake durability tests and devised a simple, but very useful classification for evaluating the weathering resistance of shales. Gamble classified rock by using the slake durability index (I_d) after two cycles of slaking. Deo (1972, 1973) used some index tests, such as slake-durability, Atterberg limits, particle size distribution, X-ray diffraction, California bearing ratio and bulk density, for identification of shale suitable for use in embankments. The slaking and compression softening tests were used by Morgenstern and Eigenbrod (1974) for identifying shale types. They performed the slaking test on various clay shale samples and other stiff clays. They found a linear relationship between the maximum water content, obtained during the slaking test, and the liquid limit of

the unweathered shale. Deo and Wood (1972) carried out further tests on shales and other slaking materials. They modified the test by increasing the number of revolutions to 500.

Venter (1980) performed a series of slake durability tests using different sizes of meshes and at different temperatures for a number of shales samples. He concluded that the slake durability index was not affected by the different mesh sizes or different temperatures.

According to a number of researchers (Grice, 1968; Franklin and Chandra, 1972; Aughenbaugh, 1974; Aughenbaugh and Bruzewski, 1976; Oliver, 1979a, 1979b; Chugh and Missavage, 1981), the submergence slake durability test is not an accurate way to evaluate the time dependent deterioration response of shale exposed to atmospheric conditions. Grice (1968) found a great difference in the disruptive effect on shale specimens subjected to cycles of realistic humidity, temperature changes, and cycles with alternating water saturation and oven drying. He studied the effect of temperature and humidity fluctuations on the disintegration of a non expandable Ordovician shale from Canada.

Gordon (1976) conducted some slake durability index tests on dark grey moderately weathered and fresh Ashfield shale. The results of three tests are summarised by Won (1985). Based on these limited data the fresh grey shale has shown slake durability index values of 80% after 30 minutes test duration. A more comprehensive series of shale durability tests will be presented later in this dissertation.

The slake durability test is a good test for distinguishing and characterising different types of shales. This test is also a good indicator for evaluating of the weathering resistance of shales. The assessment of the durability of shale is very important for using shale as a construction material or as a foundation material.

2.4 STRENGTH TESTS

Strength is a quantitative engineering property of rock specimens. Knowledge of the strength of rocks is essential in the design and prediction of performance of a structure on or in the rock. The applied stress may be compressive, shear, or tensile in application, requiring the mobilisation of compressive, shear, and tensile strength. In addition, knowledge of the strength is essential for classification purposes, to assist with judgment about the suitability of these rocks for various construction purposes.

In shales, because of the difficulty in sampling, storing, and inherent anisotropy, e.g. lamination or fissility, strength tests are more complicated than other rocks. There are many factors that control the strength of shales, e.g. mineralogy, moisture condition, and lamination or bedding. In this section a review of the basic strength tests is given, with the aim of identifying index tests and properties useful for defining engineering properties of shale.

2.4.1 Point load test

The point load strength test provides a rapid and accurate strength index value that is useful for strength classification of rock material. The test can be conducted quite rapidly and inexpensively on-site, and thus it provides a useful supplement to more expensive laboratory strength tests. Indeed, values of the index may be used to predict other strength parameters in cases where appropriate correlations have been obtained. This test is also capable of measuring the strength anisotropy index, which is the point load strength ratio in two different directions which in general are taken parallel and normal to the laminations. The point load test is normally performed with portable equipment on typically either core samples or irregular specimens. Several researchers (Franklin, 1981; Oakland and Lovell, 1982; Richardson, 1985) recommended the point load index for use in classification of shale.

The International Society for Rock Mechanics (ISRM, 1985) procedure has been adopted as a standard method for testing cores (axially and diametrically), blocks, and irregular lumps. The sample is placed between two conical platens, and the distance (D) between the platens is recorded. A measured load (P) is applied until a fracture surface passes through the specimen. The point load strength index (I_s) is then given by the following equation (Broch and Franklin, 1972).

$$I_s = \frac{P}{D^2} \tag{2.1}$$

where

I_s = the point load strength index

P = the applied load

D = the distance between the loading points.

Bergh-Christensen and Selmer-Olsen (1970) and Selmer-Olson and Blindheim (1970) used the diametral point load test as an index test in their work on drillability of rocks in Norway. Bieniawski (1975), Carter and Sneddon (1977) and Hassani et al (1980) concluded that more accurate and repeatable index values are derived from diametral testing.

From a very comprehensive series of tests reported in the literature (e.g. Reichmuth, 1963, 1968; D'Andrea et al., 1965; McWilliams, 1966; Broch and Franklin, 1972) it was shown (Reichmuth, 1968, Broch and Franklin, 1972) that the shape and dimensions of the test specimen have a significant effect on the point load index value. From the experimental data a size correction chart was proposed by Broch and Franklin for a diameter of 50 *mm* in diametral point load index. This chart was suggested as the standard reference. This chart is reproduced in Figure 2.7.

Many correlations have been presented in the literature from which uniaxial compressive strength can be predicted. Broch and Franklin (1972) gave a conversion factor of 24 between the uniaxial compressive strength and the point load index. Bieniawski (1975) was perhaps the first to indicate that the correlation factor is size dependent. He obtained the correlation factor values of 24, 21, and 18 for *NX*, *BX* and *EX* size cores, respectively, using the diametral point load test. Pells (1975) used the point load test to predict the uniaxial compressive strength of rock materials from a number of sites (13 different rock types). He concluded that, "for certain rock materials the *UCS* value that is predicted using the diametral point load test and a conversion factor of 24 (or the conversion factors given by Bieniawski) is sufficiently accurate for many engineering design purposes, particularly classification (error less than 20%)". He also stated "there are certain rock materials, not identifiable visually, for which the point load test predicts uniaxial strengths that are significantly in error (error greater than 20%)". Because of these conclusion Pells (1975) recommended that whenever point load test results are used to predict uniaxial or triaxial material strengths, at least some conventional uniaxial compression tests should be performed. Hassani et al. (1980) carried out the point load test using an expanded data base with tests on three rock types at seven core diameters and modified the size correction chart that is used to reference point load values from core with different diametral sizes to the standard size of 50 *mm*. Figure 2.8 shows the new size-correction chart. Hassani et al. (1980) found a conversion factor of 29 between uniaxial compressive strength and diametral point load index for all rock types.

Broch and Franklin (1972), Pells (1975), Read et al. (1980), Greminger (1982), Forster (1983), and Tsidzi (1991) performed point-load tests on anisotropic rocks in order to evaluate the effect of anisotropy on point load test results.

Pells (1975) found that it was impracticable to use diametral $I_s(50)$ results to

estimate uniaxial compressive strength values for highly anisotropic rocks. Read et al. (1978) carried out tests on rocks in the Melbourne area the results of which support Pells' recommendations. They suggested a length to diameter ratio of 0.65 for anisotropic rocks in the axial point load test. In anisotropic rocks such as shale it is useful to test pieces both diametrically and axially to obtain a measure of the variations in strength due to anisotropy.

Hadfield (1981) and the State Rail Authority for the Eastern Suburbs Railway (1976) reported limited point load test data for the Ashfield shale. Based on these data Won (1985) suggested correlation factors of 14 to 21 between *UCS* and the axial point load strength and 22 to 35 between *UCS* and the diametral point load strength. These correlations have been based on limited data. More data would be required to find reliable correlation factors between *UCS* and axial and diametral point load strengths. These are investigated in the present research programme.

2.4.2 Uniaxial compression test

The uniaxial compressive strength is one of the most important and commonly used properties of rocks. The main purpose of the uniaxial compression tests is to investigate the strength characteristics as well as to determine the elastic parameters of rocks. The uniaxial compressive strength has been widely used as a basis for classification of rock for engineering purposes.

The effect of specimen size, shape and aspect ratio (*L/D*, where *L* and *D* are the length and diameter of a cylindrical specimen, respectively) on uniaxial compressive strength have been studied by several investigators (Gonnerman, 1925; Obert et al., 1946; Thaulow, 1962; Hobbs, 1964; Mogi, 1966; Green and Perkins, 1968). They found that generally the uniaxial compressive strength decreases as *L/D* increases, following some form of hyperbolic or exponential relation. Based on the above studies, ISRM (1972) recommended an *L/D* ratio

of 2.5 to 3 as the standard for specimens in the uniaxial compression test.

Hawkes and Mellor (1970) and Hawkes et al. (1973) have done major work on uniaxial testing in rock mechanics. The test conditions and the size of the specimen are particularly important in this kind of test. The cylindrical samples with a diameter *NX* (54 *mm*) core size and a length to diameter ratio of 2 to 2.5 was specified by ASTM D2938 for uniaxial compressive tests. Where it is necessary to test smaller cores, Hawkes and Mellor suggested that the specimen diameter must be at least 20 times the maximum mineral grain diameter. Figure 2.9 shows the effects of the ratio of *L/D* on uniaxial compressive strength based on data that were collected by Hawkes and Mellor. As this figure shows for rough and rigid platens, the apparent uniaxial strength decreases as the *L/D* ratio increases. In general terms for better results, test specimens should be straight and their diameter should be constant and the ends should be flat, parallel and normal to the long axis.

To avoid edge effects on the strength and deformation results, a cylindrical shape was chosen for the experiments reported in the current study. In spite of the ISRM recommendation for the *L/D* ratio of 2.5 to 3 as the standard, because of the coring problems in shale, an *L/D* ratio of 2 was used for uniaxial compression test in this study.

Previous UCS data for slightly weathered to fresh Ashfield shale in the Sydney metropolitan area were reported by Burgess (1977), Chesnut (1983) and Won (1985). According to Won (1985), Ashfield shale has a uniaxial compressive strength ranging from 5 to 75 *MPa* with a mean strength of 25 *MPa*. This result is based on a sample size of 200 tests and agrees with previously published data by Burgess (1977) and Chesnut (1983).

2.4.3 Triaxial test

In nature, soils and rocks exist in a general stress state. To understand the strength behaviour of in-situ rock masses, triaxial testing of intact rocks is of prime importance. With all soils and rocks the confining pressure plays an important role, affecting both the strength and moduli. This can be investigated in triaxial tests.

2.4.4 Shear strength of anisotropic rocks

A material is called anisotropic if properties of this material are not the same in all directions. In general, the anisotropic properties of rocks may be due to primary structures, for example bedding, or due to secondary structures such as jointing and cleavage. An ideal cylindrical anisotropic rock specimen is shown in Figure 2.10 specifying a plane of weakness making an angle β to the axial direction. Anisotropic rocks (i.e. shale, slate, and schist) show a variation in their compressive strength when the direction of the laminations is varied with respect to the direction of the axial stress.

Theoretical and laboratory studies to assess the strength and deformation properties of anisotropic rocks in relation to the weakness plane direction have been performed by many investigators (e.g. Jaeger, 1960; Donath and Cohen, 1960; Donath, 1961, 1964, 1972a,b; Hoek, 1964; McLamore and Gray, 1967; Fayed, 1968; Pomeroy et al., 1971; Attewell and Sandford, 1974; Brown et al., 1977; Lekhnitskii, 1981; Arora, 1987; Ramamurthy et al., 1988; and Singh, 1988).

The effects of lamination orientation in shales have been studied by many researchers. The maximum strength generally occurs when the laminations are at 0 or 90° to the axial direction and the lowest strength at about 30° (e.g. Donath, 1961, 1964; Chenevert and Gatlin, 1965; Youash, 1966; McLamore and

Gray, 1967).

2.4.5 Empirical failure criteria for rocks

One of the most difficult problems encountered in analysing the stability of structures built on or in rock, is the determination of the most realistic failure criterion for discontinuous rock masses. In a homogeneous isotropic rock the strength parameters belong only to the intact rock medium itself. In contrast, in an anisotropic rock mass containing weakness planes, the strength parameters of the weakness planes are likely to be dominant variables.

In the past many strength criteria have been proposed on different bases. Of the various theories of failure that have been proposed, only those that have been found on the basis of experiment to be reasonably valid for rock are considered here. There is no unique criterion that is valid for all rocks. Following is a review of various strength criteria proposed by different investigators.

The simplest and best known criterion is the internal friction criterion associated with the names of Coulomb (1776) and Navier (1883). In this criterion maximum shear stress is predicted by:

$$|\tau| = c_o + \mu\sigma \qquad (2.2)$$

where:

τ and σ are the shear and the normal stress on the failure plane, c_o is often referred as the cohesive shear strength and μ is the coefficient of internal friction.

Mohr (1900) generalised the Coulomb criterion and proposed that the normal stress, σ, and the shear stress, τ, across the failure plane are related by the functional relation

$$\tau = f(\sigma) \tag{2.3}$$

This equation will usually be represented by a usually concave downwards curve in the σ - τ plane, which may be determined experimentally as the envelope to the Mohr circles corresponding to failure under a variety of stress conditions. It is assumed that the intermediate principal stress, σ_2 has no influence on the failure. In the linear case, the Mohr criterion is equivalent to the Coulomb criterion, with slope equal to the coefficient of internal friction.

Bieniawski (1974) found that a normalised form of an equation originally proposed by Murrel (1965) gave good predictions of rock strength. This is written

$$\frac{\sigma_1}{\sigma_c} = 1 + B\left(\frac{\sigma_3}{\sigma_c}\right)^{\alpha} \tag{2.4}$$

where

σ_1 = major principal stress

σ_3 = minor principal stress

σ_c = uniaxial compressive strength

α and B are material constants.

This equation has been widely used in practice in recent years. From a study of a range of South African rocks, Bieniawski suggested that α is a constant equal to 0.75 for all rock types and B is equal to 3 for siltstone and mudstone. According to Bieniawski, if a value of σ_c for the intact rock is known, the triaxial shear strength can be predicted to within 10%.

An empirical failure criterion, capable of modelling the highly non-linear relationship between major and minor principal stresses for isotropic and anisotropic rocks was proposed by Hoek and Brown (1980). This criterion in

terms of principal stresses and uniaxial compressive strength is stated as:

$$\sigma_1 = \sigma_3 + \sqrt{(m\sigma_c\sigma_3 + s\sigma_c^2)} \qquad \textbf{(2.5)}$$

where

m and s are dimensionless parameters which characterise the degree of interlocking between particles, in a jointed rock mass. m is a function of rock type and quality which controls the curvature of the σ_1 versus σ_3 curve and s is a material constant that for intact rocks is equal to 1 and for a completely broken mass is equal to 0.

They suggested the value of $m = 10$ for argillaceous rocks such as mudstone, siltstone, shale and slate. It has been demonstrated that the Hoek-Brown criterion provides good predictions of strength for Green River shale (McLamore and Gray, 1967). The Hoek-Brown criterion does not explicitly allow for anisotropic behaviour even though it does include the effect of jointing.

An empirical strength criterion based on Mohr-coulomb's criterion has been proposed by Rao (1984), Ramamurthy et al. (1985), Rao et al. (1985) and Ramamurthy (1986). This criterion is applicable for both intact and jointed rocks. This strength criterion has been expressed as

$$\frac{(\sigma_1 - \sigma_3)}{\sigma_3} = B\left(\frac{\sigma_c}{\sigma_3}\right)^{\alpha} \qquad \textbf{(2.6)}$$

where α and B are material constants. A constant value of $\alpha = 0.8$ was suggested for all rock types and a value between 1.8 and 3 was suggested for B, the precise value depending on the rock type. For argillaceous rocks (shale, mudstone, claystone, siltstone) a value, $B = 2$, was suggested.

Johnston (1985) proposed a criterion which he claimed is applicable to a wide range of intact material ranging from soft clays through to very hard rocks for

both compressive and tensile stress regions. This criterion is as follows:

$$\sigma_{1n} = \left[\frac{M}{B}\sigma_{3n}+1\right]^{B} \tag{2.7}$$

where B and M are constants. M is a function of σ_c and material type whereas B is a function of σ_c only.

This is the only criterion which assumes that the basic parameters are not only dependent on material type but also on the uniaxial compressive strength of the rock. He suggested the following expression for B and M:

$$B = 1-0.0172\ (\log\sigma_c)^2 \tag{2.8}$$

$$M = 2.065+K\ (\log\sigma_c)^2 \tag{2.9}$$

where K is equal to 0.231 for argillaceous rocks, and σ_c is expressed in MPa.

2.4.6 Strength criteria for anisotropic rocks

Strength criteria for anisotropic rocks is are more complicated than those used for isotropic rocks. This is largely because of possible variations between the directions of the weakness plane and the maximum principal stress. A few investigators have proposed empirical failure criteria for anisotropic rocks based on the classical Coulomb-Navier and Griffith's failure criteria but involving certain limiting assumptions. In this section, a brief review of these criteria with their assumptions and limitations is presented.

2.4.6.1 Single plane of weakness theory

This theory, proposed by Jaeger (1960), assumes that the body fails in shear and has a different cohesion and coefficient of internal friction at different

orientations. This theory is a generalised form of the well-known Mohr-Coulomb linear envelope failure theory which describes an isotropic body containing a single plane or a system of parallel planes of weakness. For failure within the matrix material the theory suggests that

$$(\sigma_1-\sigma_3) = \frac{2\,(c\,\cos\phi+\sigma_3\sin\phi)}{(1-\sin\phi)} \qquad \textbf{(2.10)}$$

where

c = cohesive strength of the matrix material

ϕ = friction angle of the matrix material

When failure occurs along the weak planes the strength is given by

$$(\sigma_1-\sigma_3) = \frac{2\,(c_d+\sigma_3\tan\phi_d)}{(1-\tan\phi_d\,\tan\beta)\sin2\beta} \qquad \textbf{(2.11)}$$

where β is the angle between σ_1 and the plane of weakness, and c_d and ϕ_d are the cohesive strength and friction angle in the plane of weakness. The material constants in this theory are evaluated by performing triaxial tests at β = 0, 90, and 30 degrees at various confining pressures. The values of c, ϕ, c_d, and ϕ_d are then estimated from the Mohr-Coulomb envelopes.

2.4.6.2 Variable cohesive strength theory

This theory was also proposed by Jaeger (1960) to describe a body that fails in shear having a constant value of internal friction, $tan\phi$, but variable cohesive strength, c. The equation describing failure for this case is

$$(\sigma_1-\sigma_3) = \frac{2\,(c+\sigma_3\tan\phi)}{\sqrt{\tan^2\phi+1}\;-\tan\phi} \qquad \textbf{(2.12)}$$

where:

$$c = A - B\,[\cos 2\,(\xi - \beta)] \qquad (2.13)$$

In this equation ξ is the value of β corresponding to a minimum value of c, generally 30 degrees, at which the strength is also minimum, and A and B are constants that can be evaluated by conducting triaxial tests at 0, 30 and 90 degrees at different confining pressures. By plotting Mohr-Coulomb envelopes, the respective values of $tan\phi$ and c for the above orientations are evaluated. The limitations of this theory are that a wide range of triaxial tests are needed to plot the Mohr-Coulomb envelopes for $\beta = 0, 30,$ and 90 degrees, and also it does not predict well the end parts of the anisotropy curve (deviatoric stress versus β) in shale.

Jaeger's variable cohesive strength theory was modified by McLamore and Gray (1967). They suggested that the variation of c in Equation (2.13) can be more closely described by the following relationship:

$$c = A_{1,2} - B_{1,2}\,[\cos 2\,(\xi - \beta)]^n \qquad (2.14)$$

where A_1 and B_1 are constants that described the variance over the range $0 < \beta < 30°$ and A_2 and B_2 over the range $30 < \beta < 90$ degrees. n is an "anisotropy type" factor and Mclamore and Gray suggested that it has a value of 1 to 3 for cleavage and schistosity type anisotropy and a value of 5 to 6 for bedding plane type anisotropy. Figure 2.11 illustrates the form of Equation (2.14) for different values of n. In this figure, the value of c at $\beta = 0$ and 90 degrees was assumed to be 41.4 *MPa* and for $\beta = 30$ degrees it was assumed to be 20.7 *MPa*.

The main limitations of this theory are that a number of triaxial tests are needed at $\beta = 0, 30$ and 90 degrees, and that the value of n has to be precisely estimated based solely on the presumed type of anisotropy. Furthermore, the strength prediction must be done in two separate parts, from $\beta = 0$ to 30 degrees and from $\beta = 30$ to 90 degrees.

2.4.6.3 Non-linear Mohr-Coulomb criterion for anisotropic rock

This empirical strength criterion proposed by Rao (1984) has also been extended for layered or foliated rocks which show anisotropic response (Ramamurthy et al., 1988; Ramamurthy and Arora, 1994). It can be written as:

$$\frac{(\sigma_1-\sigma_3)}{\sigma_3} = B_j \left(\frac{\sigma_{cj}}{\sigma_3}\right)^{\alpha_j} \qquad \textbf{(2.15)}$$

where

σ_{cj} = uniaxial compressive strength at a particular orientation angle (β)

α_j and B_j = constants, the values of which depend on the rock type and orientation of the planes of weakness.

Ramamurthy et al. (1988) observed that the values of α_j and B_j vary systematically with σ_{cj} as a function of β in anisotropic rocks. The following two empirical equations have been suggested:

$$\frac{\alpha_j}{\alpha_{90}} = \left(\frac{\sigma_{cj}}{\sigma_{c90}}\right)^{1-\alpha_{90}} \qquad \textbf{(2.16)}$$

and

$$\frac{B_j}{B_{90}} = \left(\frac{\alpha_{90}}{\alpha_j}\right)^{0.5} \qquad \textbf{(2.17)}$$

where

σ_{c90} = uniaxial compressive strength at $\beta = 90°$,

α_{90} and B_{90} = constants for a particular rock at $\beta = 90°$, obtained by conducting triaxial tests at this orientation.

Limited data for triaxial compression tests on Ashfield shale samples were reported by Won (1985). The triaxial tests were performed on sample of Ashfield shale from the Redfern area of Sydney by the New South Wales Department of

Construction. The following shear strength parameters were given for intact shale, tested perpendicular to the lamination direction, $c = 3\ MPa$ and $\phi = 52°$. The post peak failure envelope parameters were, $c = 400\ kPa$ and $\phi = 52°$. A friction angle of 37 degrees has been determined from the post peak failure envelope for shale samples with lamination angles at 45 degrees to the major principal stress direction.

2.5 DEFORMATION PARAMETERS

The elastic parameters, are usually required as input for finite element analyses, characterisation of intact rock, or rock mass deformability evaluations. The modulus of elasticity (E) and Poisson's ratio (ν) are usually determined from strain measurements made axially and diametrally in a uniaxial compression test. Several test methods have been suggested for determining uniaxial compressive strength, modulus of elasticity, and Poisson's ratio (e.g. International Society for Rock Mechanics, ISRM, 1978).

Effects of various mechanical factors on elastic parameters have been studied by a few researchers. In homogeneous rocks, the stress strain curves in the prefailure range are observed to be least affected by a variation in the L/D ratio. A systematic study on marble with L/D ratios between 3 to 0.33 was conducted by Hudson, Brown and Fairhurst (1972). They observed that the modulus values are independent of the L/D ratio and size of the specimens. This observation was confirmed by Lama and Gonano (1976), by conducting experiments on plaster and marble with L/D ratio of 0.25 to 2.75. Perkins et al. (197o) noticed very slight variation on the modulus values for specimens of L/D ratio of 1.5 and 2.

The effects of lamination orientation on the stiffness and shear strength parameters of shale have been also studied. Chenevert and Gatlin (1965) found that there is no variation in Young's modulus within the bedding plane (plane of

anisotropy), but there is considerable variation in the modulus between this plane and the plane perpendicular to this plane. They also stated that Young's modulus is not significantly affected by confining pressure. This statement is in disagreement with the results of other studies. For Longwood shale tested in triaxial compression in which ϕ was found, by Donath (1961), to be in the range of 20° when testing parallel to bedding and in the range of 30° when testing perpendicular to bedding.

2.6 DIRECT SHEAR TEST

The shear strength and shearing characteristics of jointed rocks are considered to be of major importance in a number of key geotechnical problems, such as the design of underground structures, in deep excavations and in assessing the stability of rock slopes. The purpose of the direct shear test is to measure the direct shear strength, shear stiffness and shear strength parameters of a joint or weakness plane after applying a constant normal stress to the plane. Graphs of shear stress versus shear displacement and normal displacement versus shear displacement are plotted to identify the peak and residual shear strength and dilation of the sample.

Barton (1973) states that the ratio of peak strength to residual strength for rock joints seldom exceeds 4, and it is always greater than unity. The ratio decreases with increasing normal stress. The strength envelope for a joint is a graph of shear strengths versus normal stresses. Shear strengths, particularly peak shear strengths increase with increasing normal stress, so joints at greater depth seem to be stronger.

Direct shear tests depend more on equipment capabilities than on an attempt to simulate field condition (Mouchoarab and Benmokrane, 1994). Many direct shear devices have been designed during the last three decades (Obert et al.,

1976; Natau et al., 1979; Crawford and Curran, 1981; Lam and Johnston, 1982; Gould, 1982; Ooi and Carter, 1987a; Hutson and Dowding, 1987a; Benjelloun et al., 1989; Skinas et al. 1990; Kana et al., 1991; Mouchaorab and Benmokrane, 1994).

2.6.1 Shear strength of anisotropic rocks in direct shear

In order to investigate the mechanical behaviour of anisotropic rocks, direct shear tests has been conducted by many researchers (e.g. Krasmanovic and Langof, 1964; Krasmanovic, 1967; Lajtai, 1969a,b; Hayashi, 1966; Kawamoto, 1970; Uff and Nash, 1967; Kobayashi and Sugimoto, 1981; Walker, 1981). Krasmanovic and Langof conducted direct shear tests on stratified and jointed limestone. They did tests on three different types of samples. In the first type, shearing occurred through the intact or solid rock. In these rocks the maximum shear strength occurred at small deformation (approximately 0.1 to 0.5 *mm*). The ratio of maximum shear strength to residual shear strength was always greater than 2. In the second type of test, shearing occurred along the stratification surface (or bedding joint) and the maximum shear resistance occurred at greater deformation (approximately 2 to 5 *mm*) and the ratio of maximum shear strength to residual shear strength was between 1 and 2. The third series of test was done on samples with rough fissures containing detrital materials. In this case the ratio of maximum shear strength and residual shear strength was approximately equal to 1 and great deformations were necessary for mobilisation of the shear resistance.

Hayashi (1966) carried out 450 direct shear tests on layered, crossed, intermittent and parallel jointed models of plaster. The results of this investigation are as follows:

(a) the shear load at failure of a specimen with transversal joints decreased with an increase in the number of joints,

(b) the shear load at failure of a continuously jointed (layered) material under one side constraint showed that specimens with a positive joint system were

weaker than those with a negative joint system. The load at failure increased with increase in the constraining force N and if no dilatancy was allowed, the value of constraining force required was extremely high. In the case of a negative joint system the constraining force N required is far higher than for a positive joint system. The positive and negative joint system are illustrated in Figure 2.12

Kawamoto (1970) conducted a series of direct shear tests on jointed and layered plaster-sand models. The intermittent parallel joint systems were prepared by inserting a number of small steel sheets of 0.1 *mm* in thickness. The jointed models were classified in the positive system ($\theta = 0$ to $90°$) and the negative system ($\theta = 0$ to $-90°$). The maximum shear strength occurred at angle $\theta = -22.5°$. The failure by pure shearing rupture occurred only when $\theta = 0°$. In the case of the positive joint system, combined ruptures mainly occurred. Figure 2.13 shows the failure patterns of selected jointed media in the direct shear tests.

The pattern of the results obtained by Kawamoto (1970) is similar to that obtained by Hayashi (1960) with the difference that the maximum shear strength obtained by Kawamoto occurred at an angle $\theta = -22.5$, while the maximum shear strength obtained by Hayashi was at an angle of about $\theta = 45°$. It seems that the confining of lateral dilatancy influences the results.

Similar tests were performed by Kobayashi and Sugimoto (1981) on specimens containing artificial discontinuous planes. The peak shear strengths were small in the region of $\theta = 45°$. The results of these tests are in disagreement with those of Hayashi (1966).

The shear strength of a shale along the bedding planes in various directions from dip to strike was measured by Uff and Nash (1967), using a shear box. Parallel to these planes the strength parameters c and ϕ were found to vary with the orientation relative to the dip. According to them, the maximum peak values

of friction angle and cohesion in the bedding plane occur in the directions of strike and dip respectively, with the minimum values at right angles. The values of residual friction and cohesion appear to be constant.

It must be noted that the most of the previous work has been done on artificially jointed samples. For design purposes, further research on the behaviour of natural specimens with weakness planes is obviously required. This is investigated in the present research programme. The shear stiffness and the effects of the weakness plane direction on stiffness will be investigated.

2.7 CONCLUSION

In this chapter the literature on geological classification of argillaceous sedimentary rocks was reviewed to find the background for the definitions and classification of shales. Grain size, lamination, mineral composition and slaking behaviour are among the important properties to consider in the classification of argillaceous rocks, at least when related to engineering purposes. It was found that the shale deterioration and loss of its natural induration as a result of weathering upon exposure to wetting and drying cycles is by itself a major engineering problem. According to the geological classifications, the Ashfield shale can be classified as a well bonded and cemented shale.

The various strength criteria for isotropic and anisotropic rocks have been reviewed and their assumptions and limitations were discussed. An extensive review of the behaviour of anisotropic rocks in uniaxial and triaxial stress states and in direct shear has been presented. In all these cases, the direction of the laminations with respect to the axial stress is an important parameter influencing the test results. Many strength criteria have been proposed for shales but because of the variability of these rocks, further tests are required to determine appropriate parameters for Ashfield shale.

From the literature it was found that a few studies have been carried out on the behaviour of anisotropic rocks in direct shear tests and most of the work was performed on specimens containing artificial discontinuity planes.

In spite of many attempts made in the past to describe the engineering behaviour of intrinsically anisotropic rocks, it was noted that very little consideration has been given to the effect of weakness planes on the stiffness of anisotropic rocks.

Thus, this review has set the directions for both the experimental investigation and the numerical modelling carried out as part of the present work.

Table 2.1 Weathering Zones for Ashfield Shale (after Hadfield, 1981)

Zone	Degree of weathering	RQD %	Classification for shale (after Pells, 1978)			
			Class	General description and field guide	*UCS* (*MPa*)	Fracturing
A	Extremely weathered	0	V	Mainly shaley clay-hard clay with thin zones of weak shales	Not normally measurable	Highly fractured or fragmented
B	Highly-moderately weathered	20 to 60	IV	Weak shale - core sections can be heavily scored or cut with steel knife alternatively, interbedded medium strong and very weak shale	Not normally measurable	Highly fractured or fragmented
			III	Medium strong shale - core sections can be deeply scored with a steel knife	2 - 7	Fractured to highly fractured
C	Slightly weathered to fresh	60 to 90	II	Medium to strong shale - core sections can be scored with steel knife	7 - 16	Fractured
			I	Strong shale - core sections can only be slightly scratched with steel knife	16	Slightly fractured

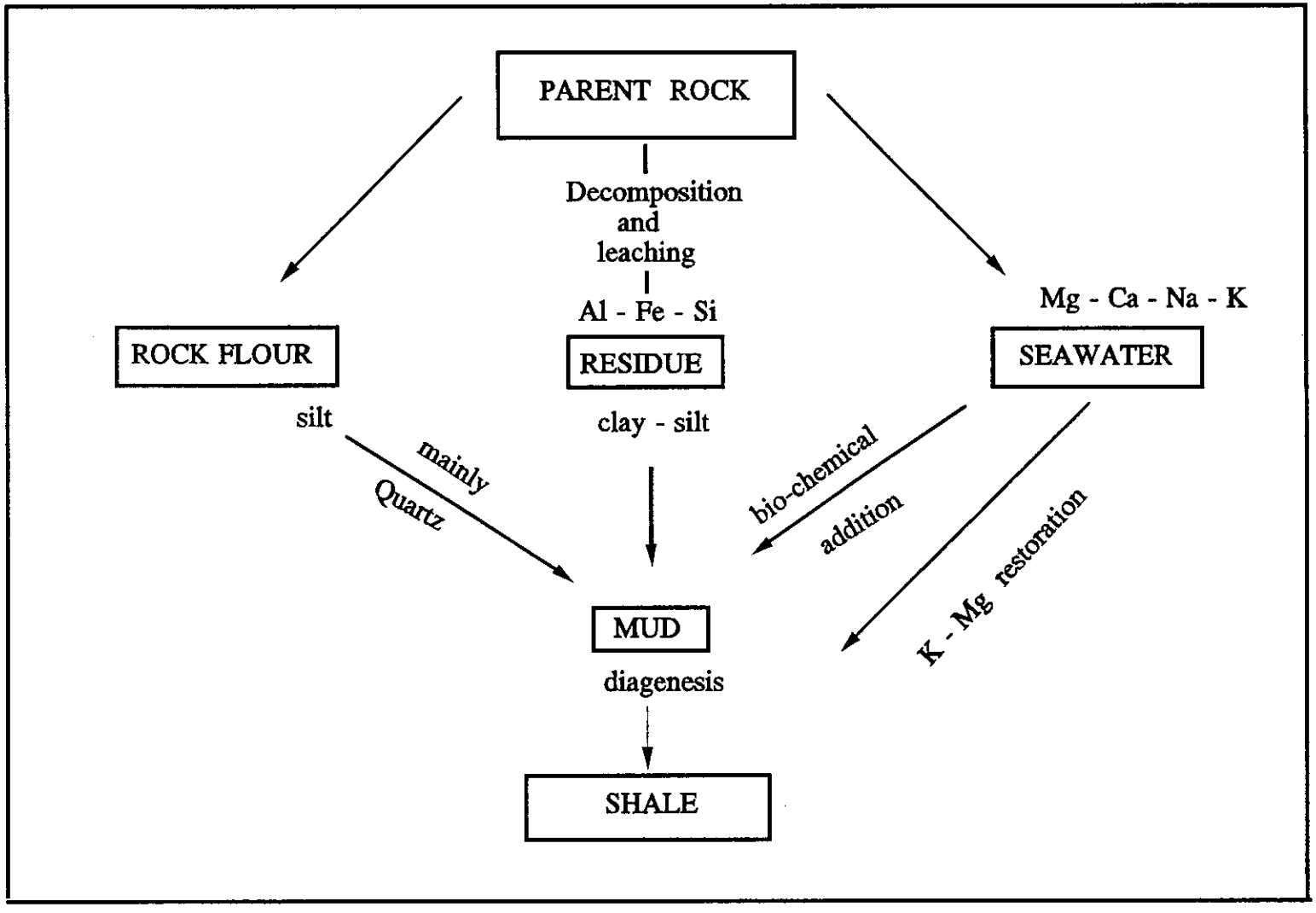

Figure 2.1 Origin of shale (after Pettijohn, 1975)

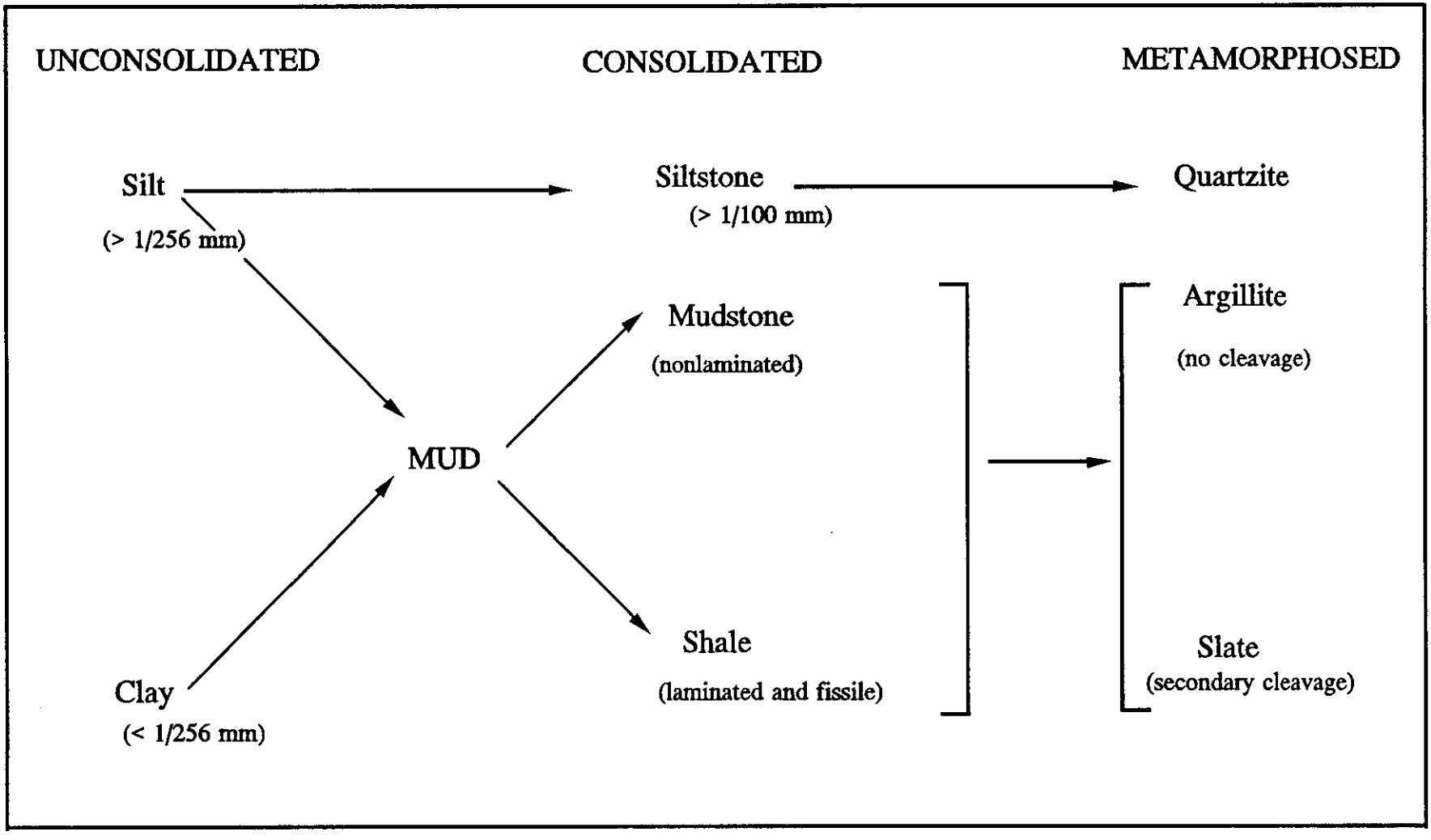

Figure 2.2 Terminology of the argillaceous sediments (after Pettijohn, 1975)

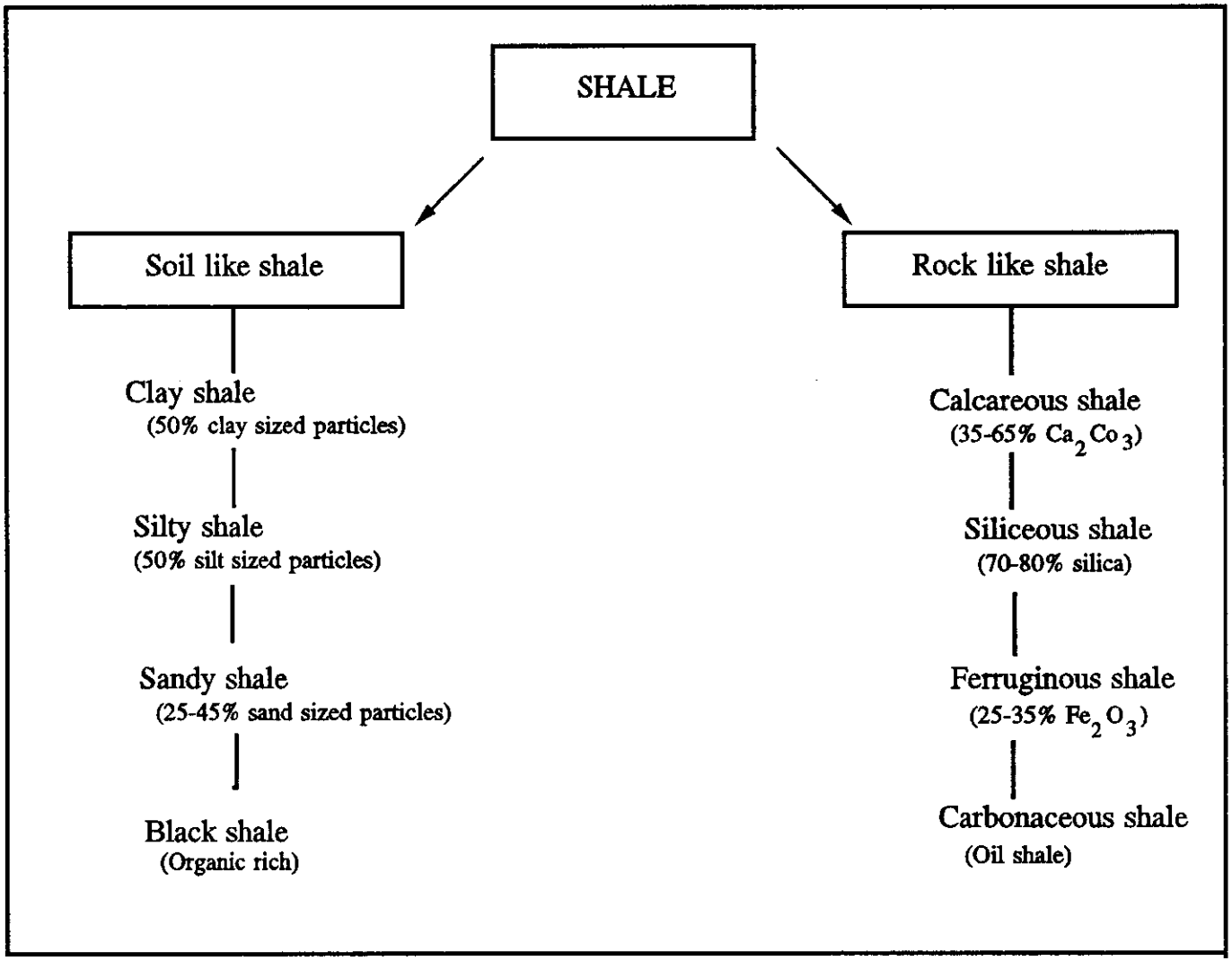

Figure 2.3 Geological classification of shale (after Mead, 1936)

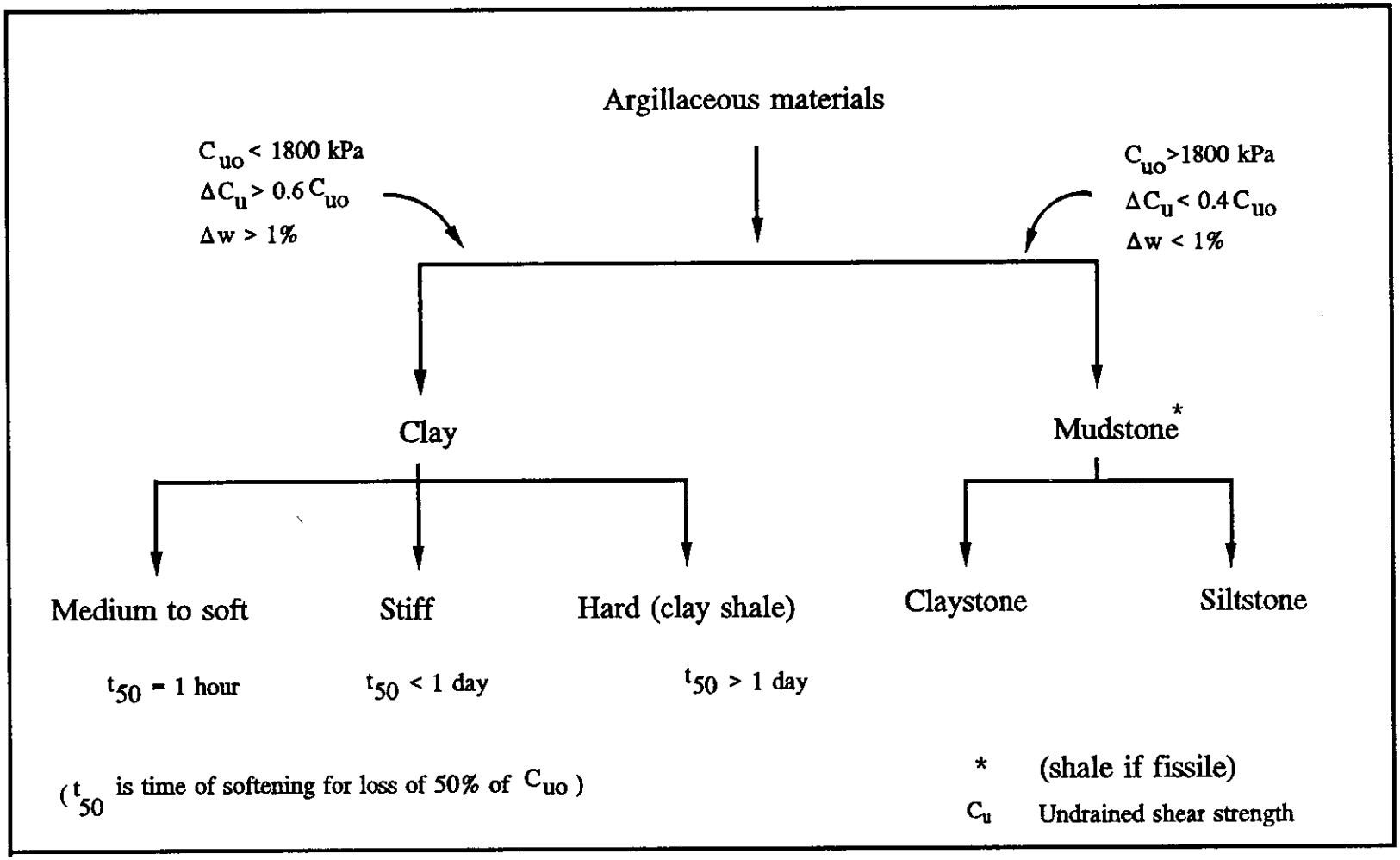

Figure 2.4 Engineering classification of argillaceous materials (after Morgnstern and Eigenbrod, 1974)

W_L Liquid limit

ΔI_L Liquidity index

Rate of Slaking $\Delta I_{Li} = \frac{I_{Li} - I_{L0}}{\text{2h water immersion}}$		Amount of Slaking $W_S - W_L$				
		Very low VL $W_L < 20$	low L $20 < W_L < 50$	medium M $50 < W_L < 90$	high H $90 < W_L < 140$	very high VH $W_L > 140$
	slow S $\Delta I_L < 0.75$	VS S	L S	M S	H S	VH S
	fast F $0.75 < \Delta I_L < 1.25$	VS F	L F	M F	H F	VH F
	very fast VF $\Delta I_L > 1.25$	VS VF	L VF	M VF	H VF	VH VF

Figure 2.5 Classification in terms of slaking characteristics (after Morgenstern and Eigenbrod, 1974)

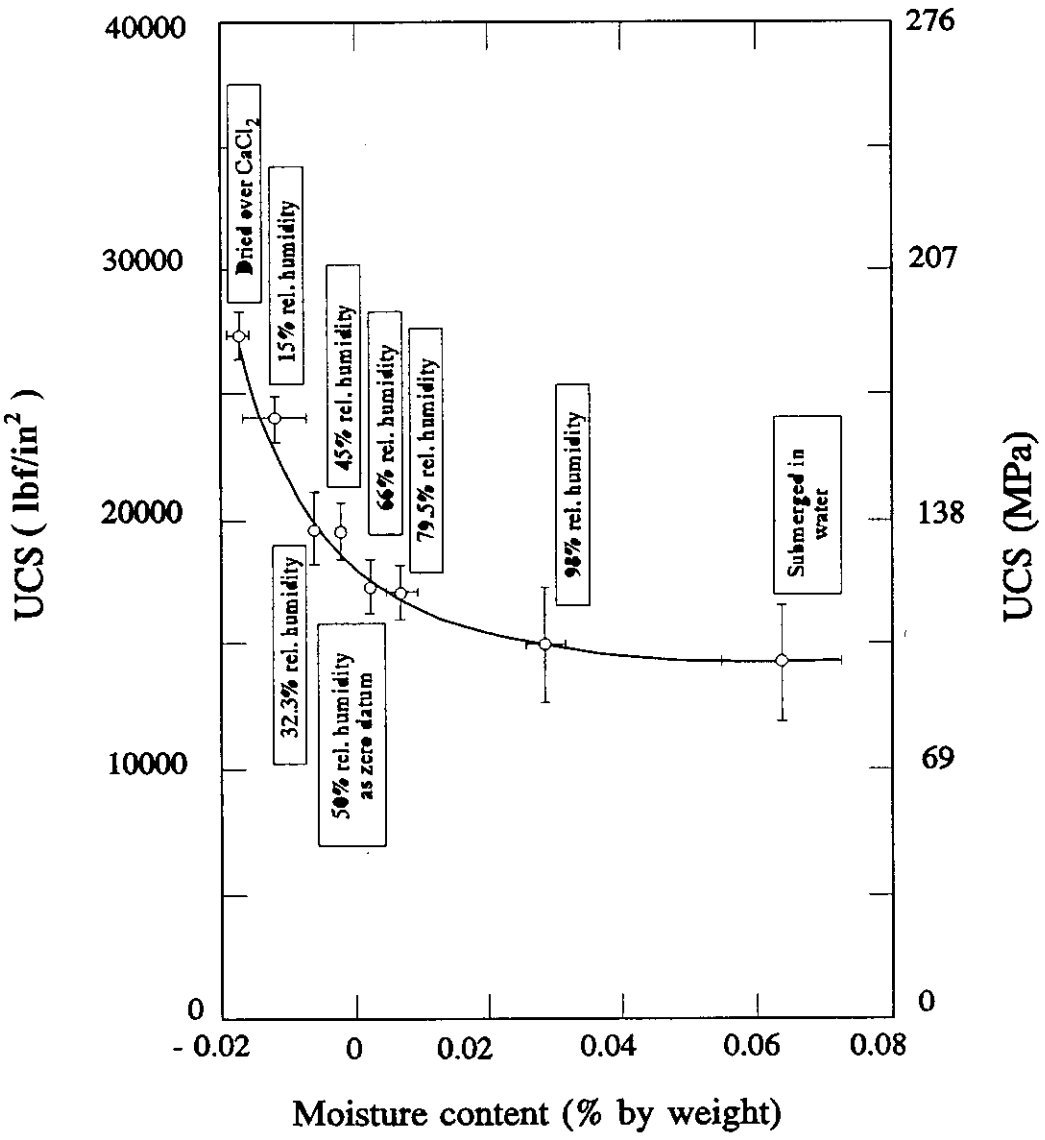

Figure 2.6 Relationship between compressive strength and moisture content for quartzitic shale specimens (after Colback and Wiid, 1965)

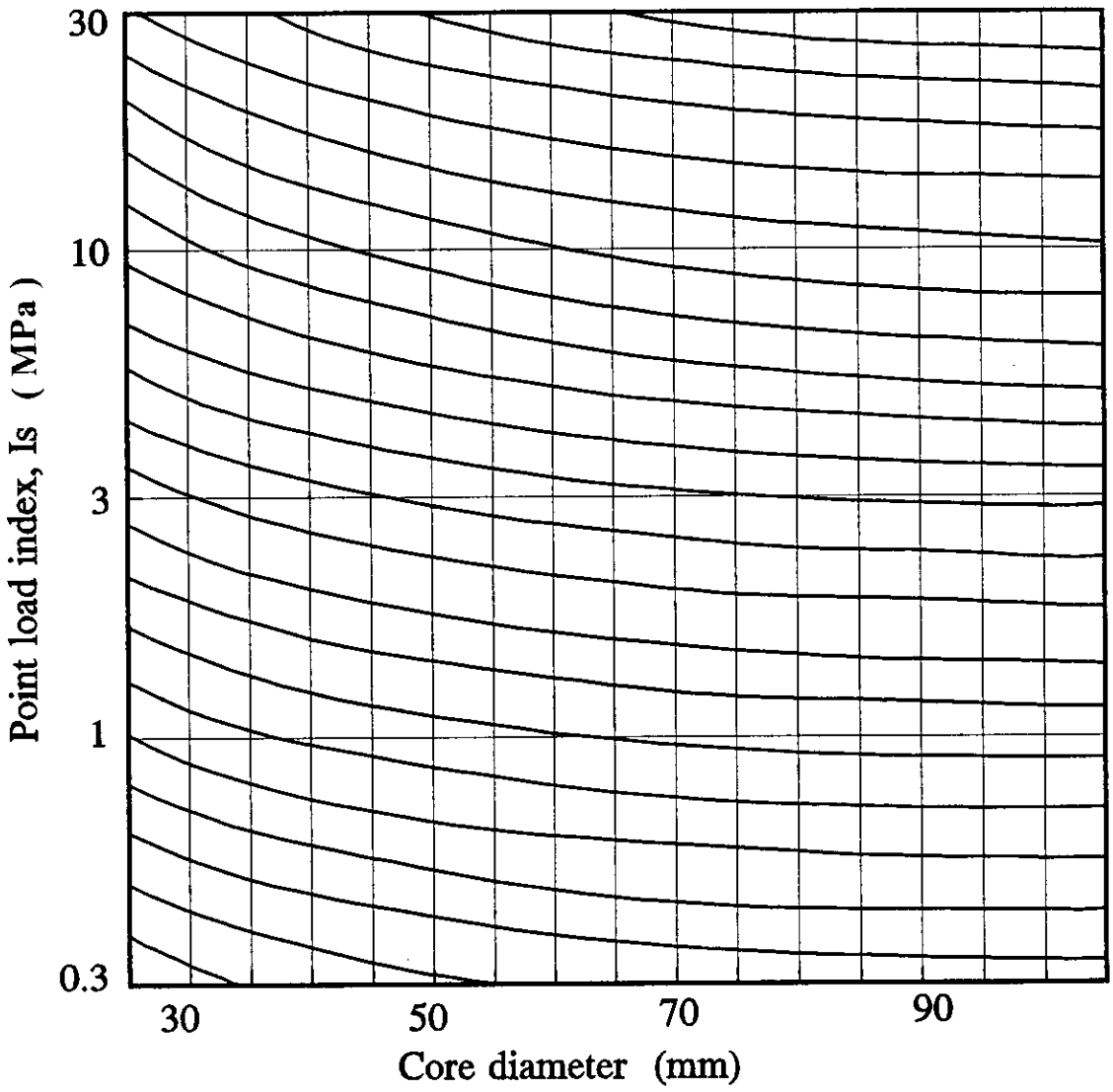

Figure 2.7 Size correction chart (after Broch and Franklin, 1972)

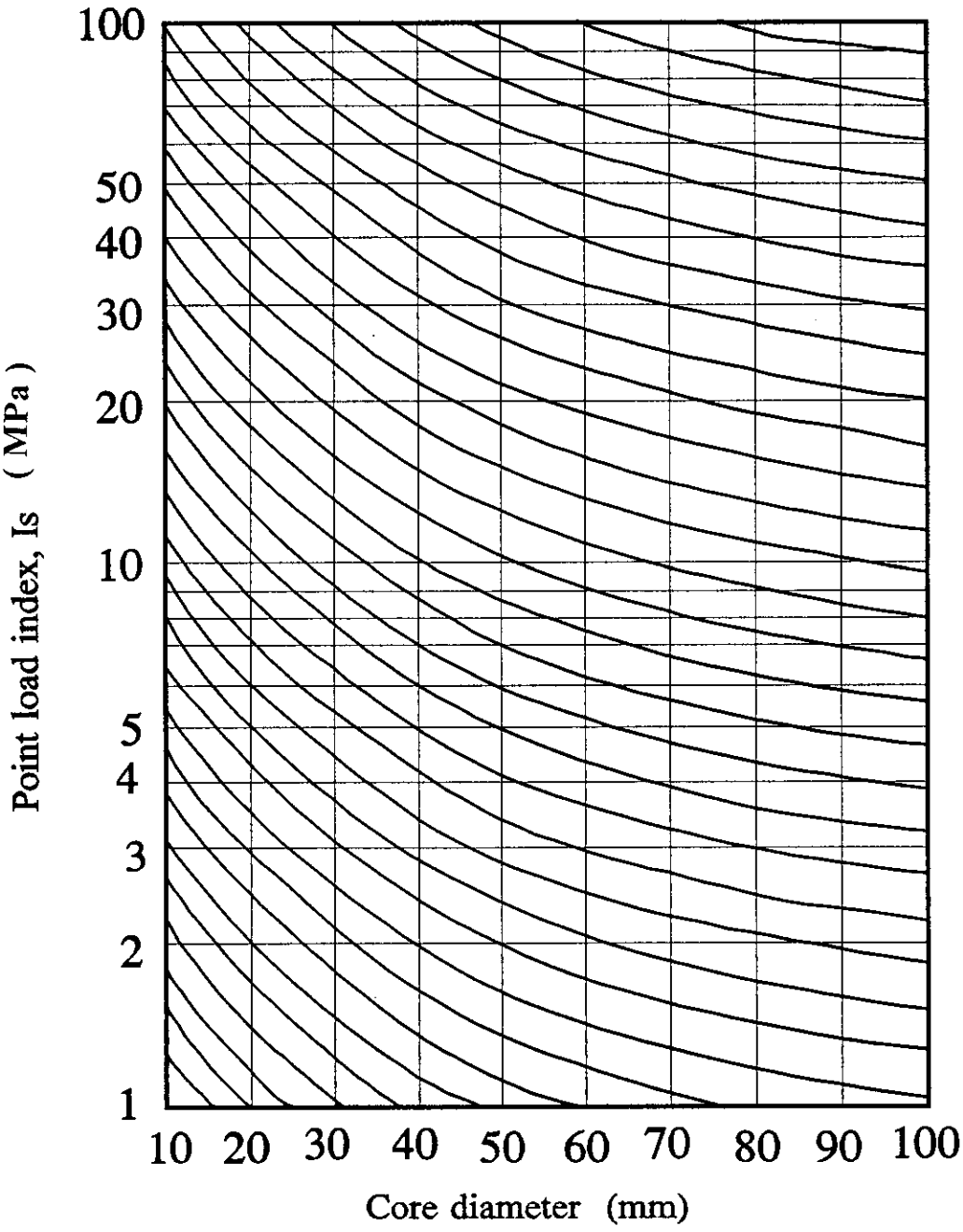

Figure 2.8 Modified size correction chart (after Hassani et al., 1980)

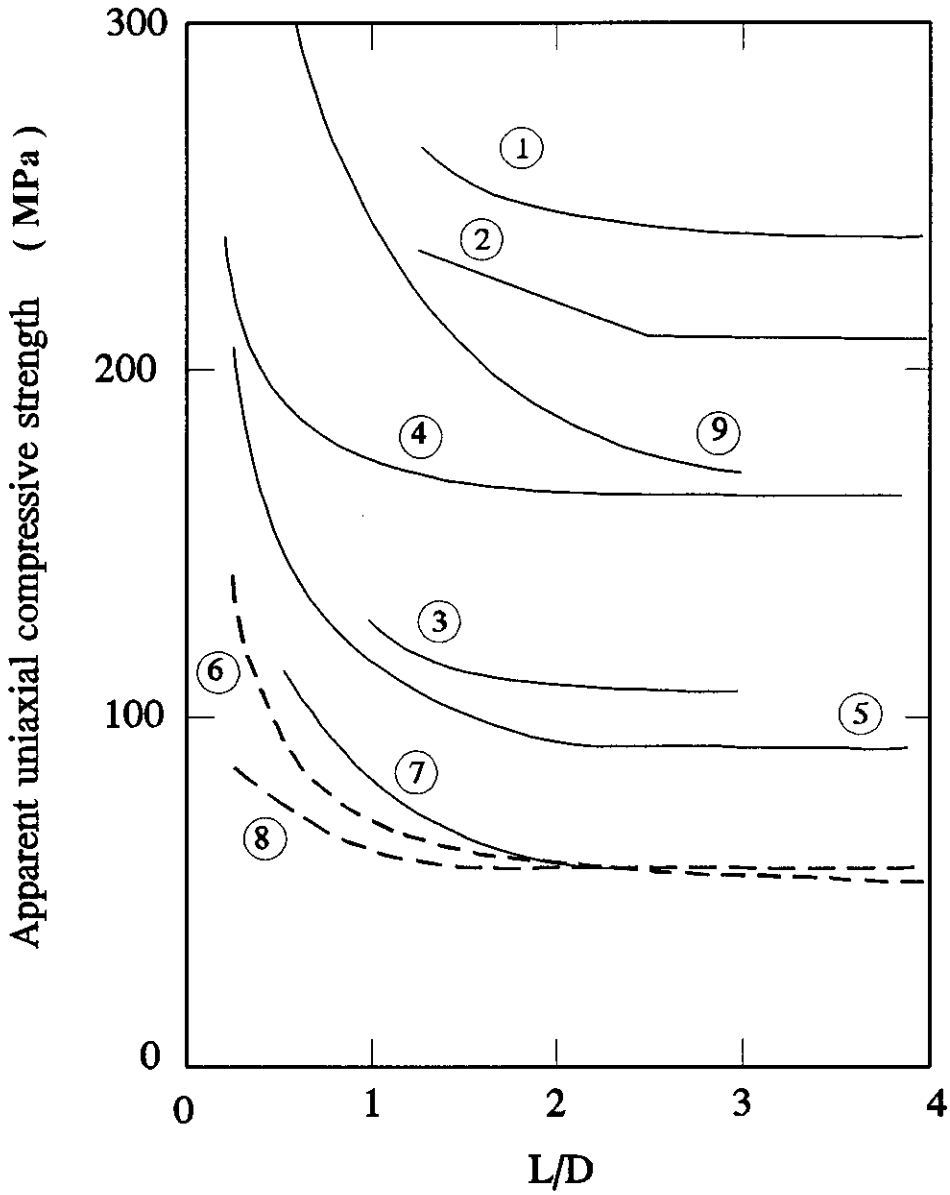

Figure 2.9 Influence of length/diameter ratio (L/D) on uniaxial compressive strength of granite (1) dolomite (2), trachyte (3), sandstone and siltstone (4.8), and saturated grinite (9), from various sources (after Hawkes and Mellor, 1970)

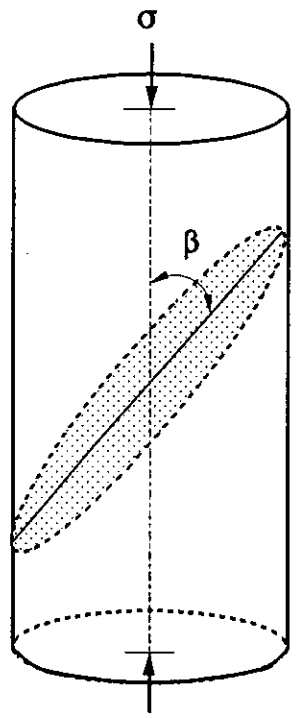

Figure 2.10 View of a typical anisotropic sample

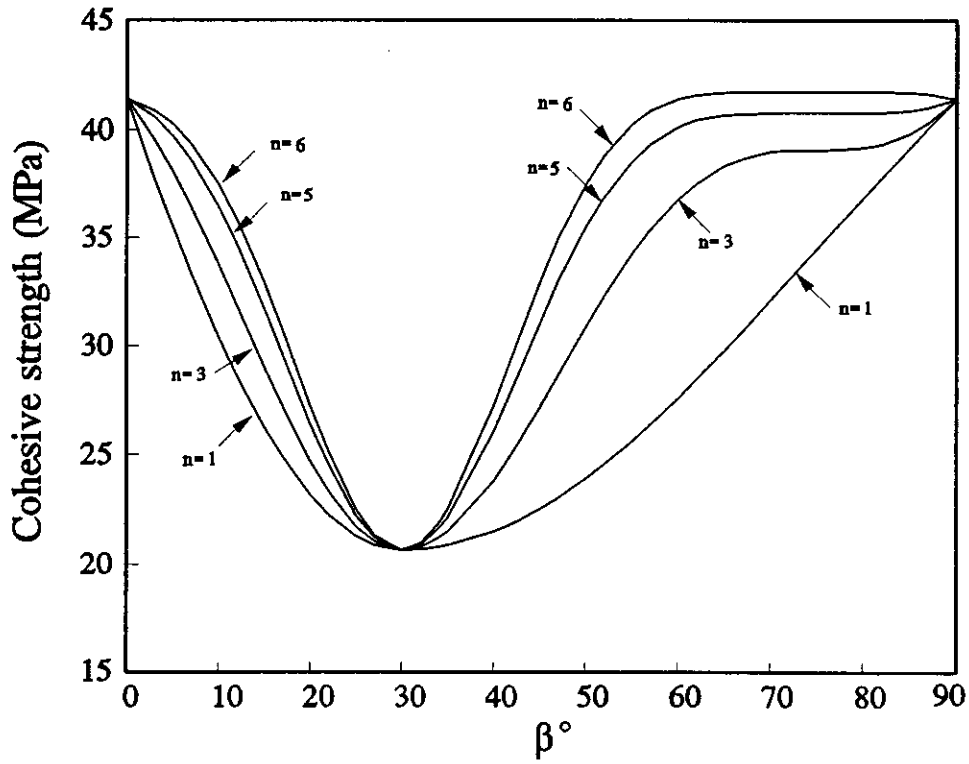

Figure 2.11 Cohesive strength versus β for various values of n (after McLamore and Gray, 1967)

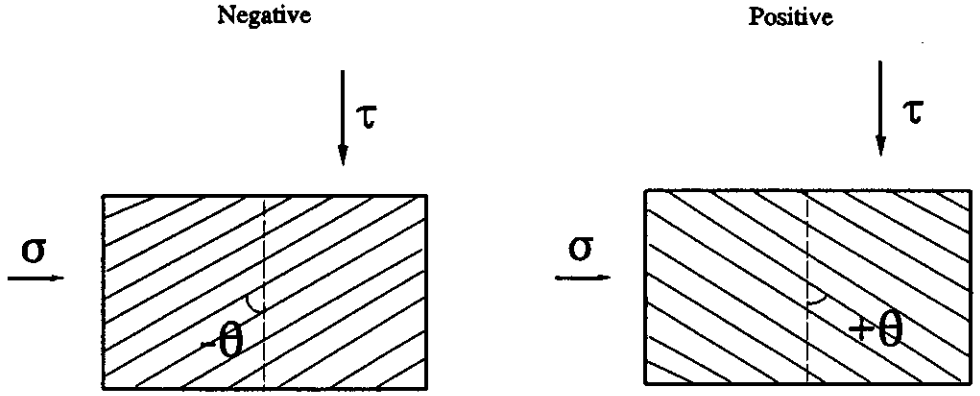

Figure 2.12 Orientation of laminations respect to the shear direction

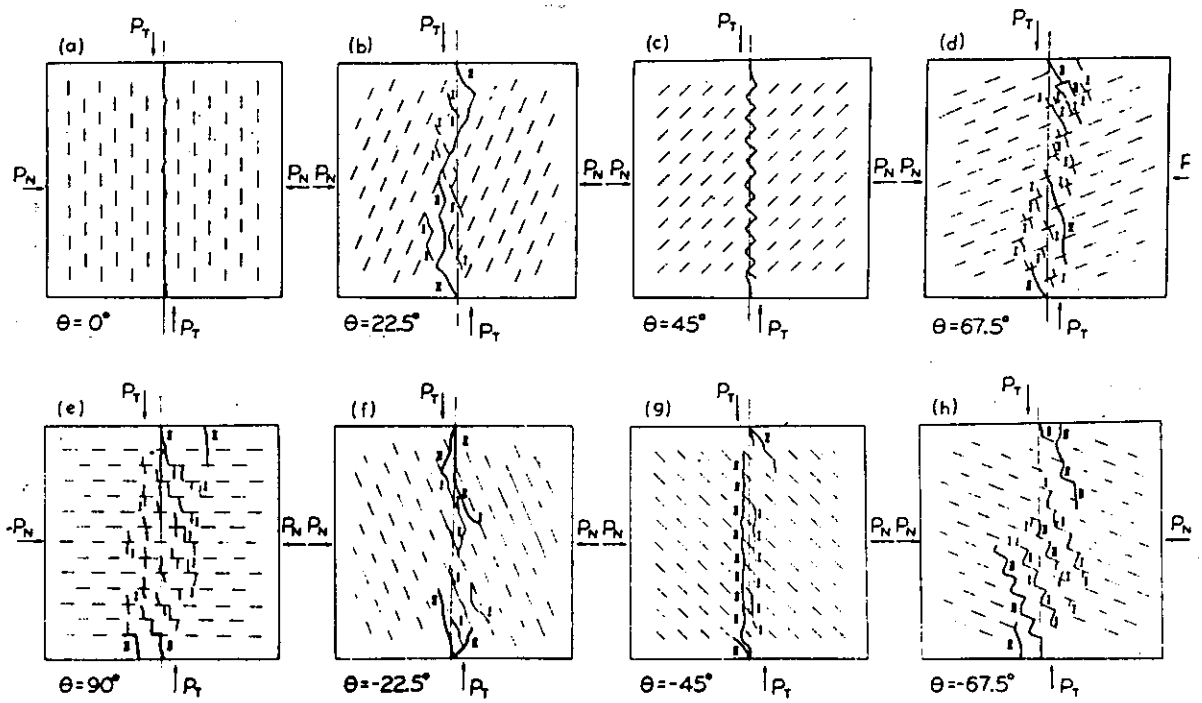

Figure 2.13 Failure patterns of jointed media by direct shear test (after Kawamoto, 1970)

CHAPTER 3 GEOLOGY AND PHYSICAL PROPERTIES OF ASHFIELD SHALE

CHAPTER 3

GEOLOGY AND PHYSICAL PROPERTIES OF ASHFIELD SHALE

3.1. INTRODUCTION

The near surface rocks of engineering significance in the Sydney region consist mainly of sandstones and shales. The objectives of this chapter are to present a broad introduction to the geology of the Sydney region, a more detailed geology of the Ashfield shale, and to present a detailed study of Ashfield shale from three sites. The microfabric and mineralogy of Ashfield shale have been studied using a variety of techniques including X-ray diffraction, optical microscopy and scanning electron microscopy. The scanning electron microscope (SEM) with energy dispersive X-ray spectroscopy analysis (EDS) has been used to study the micromorphology and mineralogy of this rock. In this chapter some of the basic engineering properties of Ashfield shale have also been considered, viz. the moisture content, the density, and the porosity and the correlations between them demonstrated.

Liquid limit and plastic limit tests have been performed on ball-milled samples of Ashfield shale from three sites under study, with geological

descriptions ranging from fresh to highly weathered shale. The clay size fraction, as determined from sedimentation analysis, was determined on samples of highly weathered to fresh Ashfield shale from one of the sites.

3.2. GEOLOGY

The geology of the Ashfield shale within the Wianamatta group has been described by Herbert (1979). The main features described by Herbert are reproduced below. Rocks of sedimentary origin are the dominant rocks in the Sydney region. They have been deposited within a broad zone of subsidence known as the Sydney basin. In the Sydney basin the Hawkesbury sandstone is overlain by a series of fine grained rocks known as the Wianamatta group. The Wianamatta group occupies the central portion of the Sydney Basin (Figure 3.1) extending to the west of Sydney, about 50 *km* from Port Jackson to Penrith, and to the south, about 80 *km* from Windsor to the Picton area. This sedimentary sequence has a maximum recorded thickness of 304 *m* (Herbert, 1980) and is divided into the Ashfield shale, the Minchinbury sandstone, and the Bringelly shale (Figure 3.2). The Ashfield shale was deposited in a shallow marine or brackish environment (Herbert, 1979). The Ashfield shale, the basal formation of the Wianamatta group and the upper part of the Hawkesbury sandstone are the only rock units outcropping in the city area. The Ashfield shale has a minimum complete thickness of 44.6 *m* in the Picton area and a maximum thickness of 62 *m* near Erskine park (Herbert, 1980). Lovering (1954a) and Herbert (1970, 1976) proposed the subdivision of the Ashfield shale into four members, which from the base upwards are: the Rouse Hill siltstone, the Kellyville laminite, the Regentville siltstone, and the topmost Mulgoa laminite (Figure 3.2). The Ashfield shale is comprised of a lower sequence of dark-grey to black, sideritic claystone and siltstone horizons which grade upwards into a fine sandstone and siltstone laminite, and then into the overlying Minchinbury sandstone. In some places, because of the absence of the underlying Mittagong

formation, the Ashfield shale rests directly on the Hawkesbury sandstone. Because of the weathering, the Ashfield shale is rarely well exposed except in quarry faces.

The basal unit of the Ashfield shale, the Rouse Hill siltstone, is composed of dark-grey to black, sideritic, silty claystone which is slightly carbonaceous in some areas. The Kellyville laminite is defined by a marked increase in the number of lithic-quartz sandstone laminations. The Regentville siltstone consists of black to dark-grey siltstone. In some areas, e.g. south-east of Moss Vale, it gradually becomes more sandy towards the top where it is overlain by the Minchinbury sandstone. The Mulgoa laminite is composed of dark-grey siltstone and fine, light-grey sandstone laminae. Based on microspore and pollen determinations, a Mid Triassic age has been demonstrated for the Wianamatta group by Helby (1973).

According to this geological classification, the term Ashfield shale has been used to cover siltstone, claystone and laminite. From the engineering point of view, it is important to find if the engineering behaviour of each member is the same or different. A classification for Ashfield shale based on engineering considerations must take this into account.

Samples for this study came from three widely spaced locations in the Sydney metropolitan area. The Sydney 1:100,000 geological sheet and Figure 3.1 indicate that the three sites studied, i.e. Ryde, Surry Hills and Moorebank, are underlain by Ashfield shale, the lowest member of the Wianamatta group. The presence of the Ashfield shale was confirmed by the rock exposures and by examination of cores from the three sites.

Figure 3.3 shows the weathered outcrop of the Ashfield shale at the Ryde-interchange site. The layers of Ashfield shale in this site are generally horizontal. The majority of the samples were obtained from borehole coring at the Ryde-

interchange site in northern Sydney. The field work at the Ryde-interchange site comprised the drilling of 5 angled boreholes with 51 *mm* core diameters and 4 angled boreholes with 61 *mm* core diameters with orientations from 30 to 90 degrees from the horizontal. The boreholes were drilled by large truck mounted rigs provided by the Roads and Traffic Authority of New South Wales (RTA), as illustrated in Figure 3.4.

The boreholes at the Ryde-interchange encountered relatively uniform conditions over the site within the clay/shale sequence, with clays to depths of 0.5 - 2 *m* underlain by extremely weathered to highly weathered light grey to yellow brown shales which graded into moderately weathered grey and brown shales to slightly weathered and strong grey shales below vertical depths of 5 and 9 *m* from the surface. The residual clay, below 0.5 *m*, derived from the weathering of shale. The rocks of the site consist of Ashfield shale, which are generally yellow brown and dark grey shale with pale grey silty laminations and lenses. The weathered outcrop of the Ashfield shale at the Ryde-interchange shows that the silty parts are more resistant to erosion than the other parts. In most of the boreholes the shale was interbeded with many very thin light grey silty bands, so that there was an alternating sequence of clayey and silty bands. Coloured photographs of core samples recovered from boreholes where the drilling was carried out in the direction perpendicular to the bedding plane are shown in Figure 3.5. They indicate that residual clay overlies shaley clay and clayey shale which in turn overlies the intact shale. The degree of weathering was estimated by visual assessment following the ISRM guidelines.

Blocks of shale were also obtained from excavations in Surry Hills near the central railway station in Sydney and in Moorebank, in western Sydney. In the Surry Hills site an excavation was cut to a maximum depth of about 3 *m*. In this area the fresh shale has been found as close as 0.2 *m* below the soil and weathered rock interface. The rocks of the site consist of Ashfield shale, which are generally dark grey, horizontally bedded with coarse light grey and fine

grained laminations and lenses. In the Moorebank site, the Ashfield shale consists of generally black to dark grey shales with laminated silty bands. The bedding in Ashfield shale is uniformly thin with individual layers ranging up to 50 *mm* in thickness.

Core samples were obtained from these blocks of shale using a drilling machine in the laboratory. All samples were kept at their natural moisture content before testing by coating the samples with a moisture sealant called "Valvoline Tectyle" and then protected by a thin plastic film, "Gladwrap", as soon as possible after coring.

Subsurface data from several boreholes, drilled at different sites in the Sydney metropolitan area (e.g. Chatswood, Parramatta, Surry Hills, Redfern, Ashfield, etc.) by various geotechnical consultants and agencies (Ghafoori et al., 1993) show results similar to those from the sites under study here. Data from these investigations have been used in this thesis to extend the database.

Based on visual assessment the Ashfield shale from the Ryde-interchange area consists of finer grained materials than the shales from Surry Hills and Moorebank. In the Moorebank and Surry Hills sites the Ashfield shale consists of generally dark grey to grey silty and sandy shales with laminated silty bands.

3.3 MINERALOGY

Both geologists and engineers are interested in knowledge of the distribution of minerals within rocks and sediments. The microfabric and mineral analysis of soils and sediments have been studied for several decades using a variety of techniques including optical microscopy, X-ray diffraction, transmission electron microscopy, and scanning electron microscopy. The spatial arrangement of constituent particles and voids are frequently defined as microfabric. This may

contain important data regarding diagenesis and the behaviour of soil or rock under stress. The scanning electron microscope (SEM) with energy dispersive X-ray spectroscopy analysis (EDS) is a useful tool that can offer an insight into the nature of a rock, and permit a study of micromorphology and mineralogy. Since the first micrograph of a geological specimen was taken by Smith (1956), numerous micrographs have provided qualitative insight into geological processes. Using the SEM, it is also possible to acquire X-ray maps showing the distribution of elements across the field of view. The scanning electron microscope has been less successful in the study of argillaceous rocks than for other rock types because of their closed-packed, usually platy grains, and very small pore spaces. Recent improvement in back-scattered detectors in the last ten years has meant that useful information about the micromineralogy and petrography can now be obtained (e.g. Krinsley et al., 1983, Huggett, 1984; Pye and Krinsley, 1984, 1986; Krinsley and Manley, 1989). Important information can be also obtained from powder analyses in which the initial sample has been severely disrupted. For instance, X-ray diffraction (XRD) is widely used to determine mineralogy.

This section presents the results of X-ray diffraction, optical microscopy and scanning electron microscopy on samples of Ashfield shale from the three selected sites.

3.3.1 Sample preparation and examination methods

3.3.1.1 XRD samples

X-ray diffraction (XRD) is the main tool for the identification and quantitative analysis of clay minerals. Two methods of sample preparation for X-ray diffractometry were used in this study:

1) unoriented mounts of powder of dry clay in aluminium holders, and
2) oriented clay formed by settling the clay slurry on a glass slide or ceramic tile.

To make powder samples for X-ray diffraction, representative samples of shale were crushed by a ball-mill. For the oriented test, some of the powder was diluted in distilled water after treatment with ethylene glycol and boiling for 1 hour at 90 to 100°C. The solution was then transferred to a 100 cc measuring cylinder, stirred, and then allowed to settle for about 3.5 hours. The top 10 to 20 cc of the solution in the measuring cylinder was taken by a pipette and centrifuged for 15 minutes at 3000 rpm. After decanting the water, the remaining slurry was used to make the oriented mount on a tile or glass slide. This process was followed to ensure that the remaining particles would be less than 2 microns.

3.3.1.2 SEM samples

Samples for the electron microscope studies were cut from the shale specimens with dimensions approximately 15 mm in diameter and 10 mm thick. They were embedded in epoxy resin and vacuum impregnated. They were then heated at approximately 60°C overnight to cure the impregnated resin. The resulting blocks were ground and polished perpendicular to the bedding planes with abrasive paper to give a suitable surface for observation in the desired direction. During the polishing process, progressively finer grades of abrasive paper were used. The samples were coated with a thin film of carbon in a vacuum evaporator to eliminate charging. A thin film of gold provides better electrical and thermal conductive properties, but carbon coatings are preferable when specimens are to be subjected to X-ray microanalysis (e.g. Goldstein et al. 1981). The finished polished sections were then mounted and examined in a Phillips 505 scanning electron microscope. Scanning electron microscopy with X-ray analysis was undertaken to evaluate the micro-mineralogy of the Ashfield shale. In particular, the size, shape, and distribution of the individual components were studied. Such information can provide additional evidence on the origin and nature of the materials.

Thin sections of Ashfield shale samples are also prepared to investigate the

size, shape, and distribution of the components within this shale.

3.3.2 Clay mineral analysis

Clay minerals have a significant influence on the engineering behaviour of shales. They are essentially a weathering product resulting from the chemical decomposition of igneous and some metamorphic rocks. The most important factors that characterise clay mineralogy are particle size and shape. They are a group of hydrous alumino-silicates, the majority of which consist of composite layers of sheet silicate structures. These layers may be linked by cations or water molecules in the interlayer sites (Brindley & Brown 1980).

From an engineering viewpoint the minerals can be divide into two groups, those with swelling and non-swelling clay minerals. The clay minerals with interlayer water molecules as a part of their structure, such as the smectites, are classified as swelling clay minerals because they are susceptible to changes in the number of water molecules. The clay minerals without interlayer water molecules, such as kaolinite and illite, have relatively stronger bonds between the layers and are classified as non-swelling clay minerals.

3.3.3 Results

3.3.3.1 XRD results

Eighteen samples of Ashfield shale from the three sites were analysed as part of this study to determine the clay minerals present in the Ashfield shale. The procedures for X-ray diffraction analysis and interpretation followed Carroll (1970), Grim (1953, 1962) and Brown (1961). Both the bulk material and material finer than 2 microns have been analysed. The samples were further analysed after heating to 550°C. To confirm the reliability of the experimental procedure, duplicate and in some cases triplicate samples were prepared.

The mineral contents of the Ashfield shale were identified by the XRD patterns using a Phillips X-ray diffractometer model 11300 and also a Siemens D5000 powder diffractometer. The X-ray diffractometer is run by Siemens software, Diffract V3.0, installed on a PC 486-DX33. Users have access to the powder diffraction data base with more than 60,000 standard data files. The SIROQUANT V7 program from the CSIRO, running under Windows, was used for quantitative analyses.

Oriented clays were X-rayed from 3° to about 50° along the 2Θ axis, using CuKα radiation and a scanning speed of 1° 2Θ/minute. The X-ray diffraction traces were obtained for each specimen. Selected samples were subjected to additional treatment after heating at 550°C in order to selectively destroy certain clay mineral species. The peaks themselves were labelled with their *d* reflection (spacing) values and with an abbreviation for minerals. By using the SIROQUANT software a quantification of the X-ray data was carried out in this study. Figure 3.6a (a´, b´, c´) shows typical X-ray diffraction traces for the Ashfield shale from the three sites.

The clay mineralogy of the less than 2 microns fraction of the Ashfield shale from Ryde-interchange, Surry Hills and Moorebank (Figures 3.6a) is dominated by kaolinite as evidenced by the strong 7.2 Å peak, and mica by the 10.2 Å peak. The strong 4.26 Å peak of quartz indicates that it forms an important constituent of the less than 2 micron fraction of the shale samples.

To distinguish between the 7.1 Å kaolinite (001) and 7 Å chlorite (002) diffraction intensities, all the oriented samples were X-rayed after heating to 550°C. The subsequent X-ray diffraction patterns did not show any peaks in the 7 Å area indicating that the 001 kaolinite had collapsed, and confirming the absence of chlorite in the samples of Ashfield shale.

In the clay mineralogy of the less than 2 microns fraction of the Ashfield shale

kaolinite was abundant in all the samples, all the other components were paired with the intensity of this mineral. In this analysis the 7.1 Å peak of kaolinite (001) was used for comparing the 10 Å mica (001) and 4.26 Å diffraction of quartz (001). For the Ashfield shale from the Ryde-interchange site, the intensity ratio of mica to kaolinite is about 50% and the intensity ratio of quartz to kaolinite is about 9%. For samples of shale from Surry Hills, the ratios for mica and quartz are 43 and 26%, respectively, and from the Moorebank area the ratios are 57% for mica and 18% for quartz. This gives an indication of the relative proportions of these minerals in the samples.

Powder patterns run on the Ashfield shale from the three sites showed that quartz was very abundant in this shale. The powder pattern gave X-ray peaks for quartz and clay minerals only. Figure 3.6b shows typical X-ray traces for the Ashfield shale from the three sites.

The X-ray trace of the less than 2 micron fraction shows that kaolinite and micaceous clay minerals are the dominant clay minerals in the Ashfield shale, and that on average kaolinite is more abundant. Similar results were obtained from the bulk samples (Figure 3.6b). The micaceous clay mineral in the Ashfield shale is illite. The other main mineral in the Ashfield shale is quartz.

The quantitative X-ray diffraction analysis of the minerals in the samples from the three sites was made using the SIROQUANT software and the powder patterns. Mean mineral contents using this method are given in Table 3.1. This indicates that the clay minerals comprise about 50 percent of the shale samples and that kaolinite and the mica group are the predominant clay minerals. Quartz constitutes about 50 percent of the Ashfield shale from the three sites. Previous studies of the Wianamatta group shales have also indicated (Table 3.2 a,b) that clay minerals comprise from 45 to 60 percent of the material and that kaolin and illite are the predominant clay minerals (Loughnan, 1960, Dolanski, 1971, Slansky, 1973 and Herbert, 1979). Previous studies have also indicated that quartz

comprises from 25 to 45 percent of the Ashfield shale (e.g. Herbert, 1979; Table 3.2b).

The current results indicate that kaolinite is more abundant than illite. Based on the XRD quantitative analysis the current results agree well with previously published data.

The thin sections of Ashfield shale were examined in optical microscopy with ordinary and polarizan lights. It was shown that the laminations in Ashfield shale range from about 0.05 to 1.0 mm in thickness and appear to be of alternations of coarse and fine particles, such as angular quartz and clay minerals (Figure 3.7).

3.3.3.2 SEM results

The prepared samples of Ashfield shale were examined in both the secondary electron (SE) and backscattered electron (BE) modes with the SEM operating at 20 kV and with the electron beam normal to the specimen surface. The magnification chosen was varied between 100 and 3000 times, as this proved most useful in observing the range of particle sizes present. The nature of the samples examined in the secondary image and the back-scattered mode is illustrated by the micrographs in Figure 3.8. In normal photographic recording of back-scattered images, it is common to slightly saturate the white areas and the dark areas, as this provides a better visual presentation. Once the contrast range has been set, the specimen is scanned slowly to acquire the digital image. For quantitative chemical analysis of samples of Ashfield shale an X-ray analyser, attached to a scanning electron microscope, was used. Once the back-scattered image had been stored, the SEM was operated in the X-ray mode and a trace obtained to determine the elements present in the sample. This enabled windows to be drawn about each elemental peak for use in subsequent X-ray mapping. The clay minerals and other mineral components were differentiated on the basis of their chemical composition as indicated by qualitative X-ray microanalysis.

Figure 3.8 (a and b) shows the backscattered electron (BE) and secondary electron (SE) mode photographs at magnification (100x) for a sample of Ashfield shale from the Ryde-interchange site, respectively. Scanning electron microscopy (SEM) with energy dispersive X-ray spectroscopy analysis (EDS) responses from certain elements (Fe, Ca, Mg), suggest that the white spots in BE or dark spots in SE mode photographs are siderite. EDS responses from certain elements (K, Al, Si) suggest that some of these flat surfaces around the white spots (Figure 3.8a) are oriented flakes of illite. In all figures, numerous flat surfaces are exposed.

A linear fabric characteristic was observed most clearly on surfaces cut perpendicular to the laminations. This fabric is produced by numerous roughly parallel linear features. Figure 3.9,at a higher magnification (3000x), shows many such individual lineations. The observations at higher magnification suggest that these linear trends are because of the orientation of the clay particles. In this figure the white large mineral (A) in the middle contains Phosphorus (P). The trace elements, Cerium, Lanthanum, Thorium (Ce, La, and Th) were found in the phosphate (X-ray spectroscopy A, Figure 3.9). The phosphate in the Ashfield shale is mainly concentrated in nodules. The Phosphate nodule is surrounded by kaolinite and illite. A previous study also confirmed the presence of Phosphate, mainly as nodular concretions in the Ashfield shale (Herbert, 1979). EDS responses (X-ray spectroscopy B) from certain elements (K, Al, Si) suggest that some of these flat surfaces around the white mineral (Figure 3.9) are oriented flakes of illite.

Aluminium is a good indicator of clay minerals, and large amounts were present in the samples of Ashfield shale under study. The back scattered electron image and X-ray analysis responses of the Ashfield shale from Surry Hills are shown in Figures 3.10 (a) and (b). EDS responses from certain elements, Potassium, Aluminium, Silicon (K, Al, Si) in Figure 3.10 (a), suggest that some of these flat surfaces are illite. The photo shows that the bulk of the matrix of

the sample is composed of platy clay minerals which show a definite preferred orientation. The white spots in BE (Figure 3.10a, F) with certain elements, Iron, Calcium, Magnesium (Fe, Ca, Mg), (X-ray spectroscopy F) suggest that some of these are siderite. Numerous SEM observations have been made of the silt-sized detrital grains in the shale samples. Quartz is most commonly observed. Figure 3.10 (b) shows the back scattered electron image, with magnification of 1300x, image for Ashfield shale from Moorebank. The large grey high relief grain (C) is quartz (X-ray spectroscopy C). As this figure shows, quartz is surrounded by clay minerals (D). Some siderite is also evident in this figure. The bulk of the matrix of the rock is composed of kaolinite and illite.

Previous studies have indicated that two minor but significant minerals within the Ashfield shale are Siderite and Feldspars. Electron microscopy and optical microscopy have revealed that the Siderite is finely dispersed in the Ashfield shale. Based on optical microscopy compared to other components Siderite comprises about 8 to 10 per cent. Previous studies have indicated Siderite contents of about 10 to 12 percent (Ferguson and Hosking, 1955). No significant Feldspar was detected in the samples used in this study, although at other locations they have been detected (for instance Herbert, 1979 reported Feldspar amounts of about 0.2 per cent).

X-ray diffraction, scanning electron microscopy and optical microscopy studies of the Ashfield shale from the three sites show no significant difference in mineralogy between the sites. The current results agree well with previously published data. It appears that there are no significant differences in mineralogy throughout the Ashfield shale.

3.4 PHYSICAL PROPERTIES

In this section some of the basic properties of Ashfield shale are considered, viz.

the moisture content, the density, and the porosity. Some of the data used in this section to illustrate these properties have been obtained from geotechnical consultants and agencies in the Sydney region (see Ghafoori et al., 1993). They include Ashfield shale samples from many locations in the Sydney Basin, with geological descriptions ranging from intact to highly weathered.

Physical property tests on shales, as with other materials in the earth's crust, have been performed for many years. Because of the grain size and the complexity of their clay mineral fraction, shales are among the most difficult rocks to analyse completely. The physical properties of shale are closely interrelated and it is difficult to discuss one property without mentioning the others (Underwood, 1967). Properties such as natural water content, specific gravity of particles and bulk density are fundamental to the understanding of the relationships between the different phases in a rock or soil. Suggested methods for measuring the properties of intact rock are detailed in ISRM (1979b) and have been followed in this study.

3.4.1 Moisture content

It has been well established that the moisture content in argillaceous rock masses such as mudstones and shales can have significant effects on their physical properties. Changing the moisture content of a rock can significantly alter its mechanical properties.

For the samples of Ashfield shale considered in this study and a large number of samples from different locations with different degrees of weathering (Ghafoori et al., 1992, 1993) the natural moisture contents range between 1.12 and 8.76%. The moisture content referred to here is based on the weight of the water in a shale specimen divided by the weight of the oven dried specimen, and is expressed as a percentage. The mean moisture content of all samples was calculated to be 3.0%, with a standard deviation of 1.2%.

To compare the Ashfield shale from the three specific sites considered in this work, the natural moisture contents of more than twelve samples of fresh shale from these sites were determined and the results are presented in Table 3.3. They indicate that the natural moisture content of fresh Ashfield shale ranges between 2% for the Surry Hills and Moorebank sites to about 4.5% for the Ryde-interchange site.

3.4.2 Porosity

The porosity of a rock is the volume of the pores or air spaces expressed as a percentage of the total volume of the sample. Porosity is an important physical property of rock in the field of geology, geophysics, rock mechanics and petroleum engineering. The density, strength, sorption and in general rock elasticity will be affected by porosity. This is particularly important in weak rocks where the porosity is relatively high. The porosity of a rock depends upon the shape of the grains, size of the grains, distribution of the grains, orientation of the grains and also on the mineralogy, texture and cementing material.

There are several different methods for the determination of porosity, but because of the disintegration of the samples in water most of these methods are not applicable for the Ashfield shale. A gas porosimeter apparatus, which works basically on air displacement, was used to determine the porosity of the Ashfield shale samples in this study. The gas saturation method provides the effective porosity, which gives the volume of interconnected pores, and not necessarily the true porosity.

All the rock samples prepared in this study were cylindrical cores with 25 *mm* diameter and 25 to 30 *mm* length. The ends of each sample were cut to be plane and parallel. All the samples were oven dried prior to test and thereafter cooled in a desiccator before estimation of their porosity. The porosity measurement by the gas porosimeter was rapid and each measurement took between 5 and 10

minutes. The pore volume was calculated from the difference in bulk and grain volumes. The bulk volume of each sample was determined in a volumetric apparatus that used the displacement of mercury.

The porosities of fourteen samples of fresh Ashfield shale from the three sites were determined and the results are presented in Table 3.5. Table 3.5 shows the porosity of fresh Ashfield shale ranges between 5% for the Surry Hills and Moorebank sites to about 13% for the Ryde-interchange site. Using the data in Table 3.5, a plot of porosity versus dry density was prepared and this is also shown in Figure 3.11. It indicates a linear relationship between the porosity and dry density. The following equation provides a good fit to the data:

$$\gamma_d = (2.711 - 0.025n)\gamma_w \qquad (3.1)$$

in which

n = Porosity (%)

γ_d = dry density of the rock, and

γ_w = unit weight of water (1 t/m^3 or 64 lb/ft^3)

Regression analysis shows that equation (3.1) fits the data with a correlation coefficient of $r^2 = 0.89$. A total of 14 data points were used in this study and the standard deviation was $0.026\gamma_w$.

From porosity measurements (Table 3.5) the mean value of the specific gravity, $G_s = 2.74$ was obtained. The theoretical relation between dry density and porosity is given by

$$\gamma_d = G_s(1-n)\gamma_w \qquad (3.2)$$

Using Equation (3.2), a plot of porosity versus theoretical dry density was prepared and this is also shown in Figure 3.11. Figure 3.11 shows there is a close agreement between the empirical and theoretical equations.

3.4.3 Density

The density or unit weight of a rock is defined as its weight per volume. Mineralogy, porosity, joints, and other open spaces in rock all influence its density. The mechanical properties of the intact rock can be expected to depend on the density.

The dry densities of all shale samples considered in this study and a large number of samples from different locations with different degrees of weathering (Ghafoori et al., 1992, 1993) range from 2.15 to 2.7 t/m^3, and the mean dry density was calculated to be 2.47 t/m^3, with a standard deviation of 0.11 t/m^3. A plot of dry density versus moisture content is shown in Figure 3.11, which indicates that the dry density decreases with an increase in the moisture content. Figure 3.11 indicates a linear relationship between dry density and moisture content. The following equation provides a good fit to the data:

$$\gamma_d = (2.711 - 0.064 m_c)\gamma_w \qquad (3.3)$$

in which

m_c = moisture content (%)

γ_d = dry density of the rock, and

γ_w = unit weight of water (1 t/m^3 or 64 lb/ft^3)

Regression analysis shows that equation (3.3) fits the data with a correlation coefficient of $r^2 = 0.91$. A total of 50 data points were used in this study and the standard deviation was $0.031\gamma_w$. Because of the closeness of this correlation and because the natural moisture content of a shale sample is a relatively simple parameter to determine in practice, equation (3.3) provides an indirect but very convenient means of estimating γ_d for Ashfield shale.

A mean value of $G_s = 2.74$ has been obtained from porosity measurements of samples of Ashfield shale (Table 3.4). If it is assumed that the shale is saturated then the relation between dry density and moisture content may be

obtained from the following theoretical equation,

$$\gamma_d = \frac{G_s \gamma_w}{1+e} \tag{3.4}$$

$$e = m_c G_s \tag{3.5}$$

Using Equations (3.4) and (3.5), a plot of moisture content versus dry density was prepared and this is also shown in Figure 3.11. Again there is close agreement between the empirical and theoretical equations.

The natural water content has been calculated assuming fully saturated samples ($s=1$), using Equations (3.4) and (3.5) and measured values of dry density and a mean value of $G_s = 2.74$ (Table 3.4). The water contents estimated in this way are also shown in Table 3.4. Comparing these estimated water contents with direct measurements of water content (Table 3.3), it was found that all samples of the Ashfield shale were close to being fully saturated in-situ, so the natural water content gives a direct measure of the porosity of the shale. Conversely, because the samples of the Ashfield shale were almost fully saturated in-situ, it follows that the changes in moisture content mostly reflect changes in porosity of the shale rather than the degree of saturation.

From a sample size of 51, the bulk density of Ashfield shale was found to have a range from 2.34 t/m^3 to 2.73 t/m^3. The mean bulk density was calculated to be 2.54 t/m^3 with a standard deviation of 0.073 t/m^3. In an earlier study of 'hard' Ashfield shale the in situ density was found to range from 2.43 t/m^3 to 2.64 t/m^3 (Chesnut, 1983).

The distribution of densities with depth below the surface for five boreholes at the Ryde-interchange site is shown in Table 3.5 and a plot of bulk density against depth is shown in Figure 3.12. The range of depths covered is from 3.5

to 11.5 *m*. Table 3.5 and Figure 3.12 show the concentration of points in the range from 2.34 to 2.66 t/m^3. In general, the trend is one of density increasing with depth, but because of the limited depths for the existing data no great significance can be attached to this result.

3.5 WEATHERING

Whenever argillaceous rocks are either exposed or lie close to the surface, weathering processes begin to take effect. Both physical and chemical processes are important in controlling the weathering of argillaceous rocks. The physical processes are generally a prerequisite for subsequent chemical weathering. Discolouration of the rock material gives evidence of weathering, and as the degree of weathering increases the discolouration tends to increase. The weathering process is often associated with an increase in clay content and this will change the engineering properties of the shale. In particular, it will increase the porosity and decrease the density and strength.

Definitions of the various grades of weathering that are based on visual assessment of the rock samples (usually made in the field) are given in Table 3.6. The definitions given in this table are very similar to those that have generally been used by the supervising geologists and geotechnical engineers in the field classification of many of the samples considered in this study. Similar definitions for the degrees of weathering may be found in the appropriate ISRM guidelines (e.g. see Brown, 1981) and in the Australian standard for site investigation (SAA, 1981).

3.6 ATTERBERG LIMITS

The index tests proposed by Atterberg (1911), which were introduced into soil

mechanics by Terzaghi (1962), measure the water contents at which the soil mass passes from one state to the next. The indices which are most useful for engineering purposes are the liquid and plastic limits and their numerical difference, named the plasticity index. These limits are expressed as percent water content, measured by weight. Atterberg limits and activity can provide a rough guide to the clay mineralogy (see Skempton, 1953).

To determine the liquid and plastic limits of Ashfield shale, the material passing from the drum in the slaking test (Chapter 4) was used. For the more durable samples the retained portion of material in the slaking tests was crushed by ball-milling. The Australian standard procedure (AS 1289 C1, 1977) for the determination of the liquid and plastic limits was used.

A total of 20 liquid limit and plastic limit tests were performed on materials used in the slaking tests. For every test, after determining the liquid limit (LL) and the plastic limit (PL), the plasticity index (I_p) was calculated from the following equation:

$$I_p = LL - PL \qquad (3.6)$$

A summary of the Atterberg limits for Ashfield shale is given in Tables 3.7 and 3.8. As can be seen in Table 3.7, the Ashfield shale has very low plasticity, ranging from a plasticity index of 2.9 to 6.2. A plot of the previous (Herbert, 1979) and present test results on the Casagrande "A"line chart is shown in Figure 3.13. Figure 3.13 shows that the majority of the samples of Ashfield shale tested plot near the A-line of the plasticity chart in the low plasticity range. On the basis of the Atterberg limits, the Ashfield shale components may be classified as silt and clay with low plasticity (CL-ML). The previous study of the Ashfield shale by Herbert (1979) also showed very low plasticity, with a plasticity index ranging from 1.2 to 6.9.

Figure 3.14 shows the relationship between the liquid and plastic limits for the

present and previous data. There is a clear trend of increasing plastic limit, and plasticity index, with increasing liquid limit. Figure 3.15 shows a plot of liquid limit against natural water content. It can be seen that there is a rough trend for the liquid limit to increase with increasing natural water content.

3.7 CLAY CONTENT

The clay size fraction, as determined from sedimentation analysis and Stokes's law, describes the particles with an equivalent spherical diameter of less than 2 micron. Four samples of highly weathered to fresh Ashfield shale from the Ryde site were used for the clay size fraction in this study. The samples were ground and passed through a 425 μm mesh sieve. In the sedimentation analysis, only those particles which were finer than 75 micron size were included. The Australian standard procedure (AS 1289.C6.3, 1977) was used to determine the clay fraction less than 2 microns. The results of these tests indicated clay fractions of about 30% whereas the mineralogical studies indicated clay fractions of about 50% in all samples. This discrepancy presumably reflects the presence of significant quantities of large kaolin particles. This could be caused by cementation (fusing of the clay particles at high temperature and pressure). The process of weathering causes a breakdown of the cementation. Thus clay mineral content remains constant, but clay particle size fraction increases. This could also explain increasing of the liquid limit, I_p, and durability of Ashfield shale. Because of the limited number of samples tested, the results can not be considered conclusive, but trends are as expected.

Figures 3.16 and 3.17 present the variations of the liquid limit and plasticity index versus clay fraction less than 2 microns, respectively, for highly weathered to fresh Ashfield shale. Figures 3.16 and 3.17 show that increasing clay fraction (less than 2 micron) is associated with an increase in liquid limit, which as noted above is associated with an increase in plasticity index. The relationship between

weathering grade and clay fraction is shown in Figure 3.18. This figure shows that as the shale weathers the clay fraction (less than 2 microns) tends to increase. The results for four samples of Ashfield shale are typical of many shales in that weathering increases the clay fraction and increases the water content.

Activity is the ratio of the plasticity index to the percentage of clay less than 2 microns (Skempton and Northey, 1953). The activity of the four samples tested varied between 0.2 to 0.27. Based on Skempton's classification, all four samples would be described as inactive. This low activity was expected because of the predominance of kaolinite and the absence of smectite in the Ashfield shale, and the swelling potential can be expected to be very low.

3.8 CONCLUSIONS

X-ray diffraction analyses of the Ashfield shale show no chlorite, no mixed-layer clays, and no smectite. The X-ray trace of the less than 2 micron fraction shows that kaolinite and micaceous clay minerals (illite) are the dominant clay minerals in Ashfield shale, and that on average kaolinite is more abundant. Quartz is the major non-clay constituent of the Ashfield shale.

A number of large mineral grains were shown within the platy fine-grained matrix. Quantitative chemical analysis of samples of Ashfield shale showed that silicon, aluminium and potassium (Si, Al, K) were the main constituents and iron (Fe) was present to some extent in all samples. The presence of iron within the Ashfield shale samples reflects the presence of siderite in this rock. Siderite was found to be finely dispersed in the Ashfield shale and no feldspars were detected in this study.

The effect of weathering is to increase the clay and moisture contents. However, different fresh unweathered shales had different moisture contents.

The variability of the natural moisture content can be correlated with mineralogical factors. Increasing moisture content was associated with increasing clay content (particles less than 2 microns) and in turn this was associated with an increase in plasticity index and plastic and liquid limits. The natural moisture content has been found to be a good predictor of the index properties and clay content of the shale.

Throughout the Sydney region the depth to fresh shale has been found to vary quite considerably. For example, in the Ryde area where the shale outcrops, fresh shale has also been found at depths between 5 and 9 m below the surface. In other places, where residual soils overly the shale, fresh shale has been found as close as 0.2 m below the soil-rock interface.

Comparing the estimated water contents ($s=1$) with measured values of water contents, it was found that all samples of the Ashfield shale to be essentially fully saturated in-situ so the natural water content gives a direct measure of the porosity of the shale. Measurements of the porosity and water content of some shale samples indicate that the changes in moisture content mostly reflect changes in porosity of the shale.

Based on visual assessment, the Ashfield shale from the Ryde-interchange area consists of finer grained materials than Ashfield shale from Surry Hills and Moorebank. In the Moorebank and Surry Hills sites the Ashfield shale consists of generally dark grey to grey silty and sandy shales with laminated silty bands. The porosity of fresh Ashfield shale ranges between 5% for the Surry Hills and Moorebank sites to about 13% for the Ryde-interchange site. The natural moisture content of fresh Ashfield shale also ranges between 2% for the Surry Hills and Moorebank sites to about 4.5% for the Ryde-interchange site.

Table 3.1. Average clay minerals and quartz composition in the Ashfield shale determined in this study

Ashfield shale site	Kaolinite %	Illite %	Quartz %
Ryde-interchange	27	23	50
Surry Hills	27	18	55
Moorebank	26	22	52

Table 3.2a. Average clay mineral composition in the Wianamatta group shales

Rock type %	Kaolinite %	Illite %	Illite-Smectite %	Source
Ashfield shale	60	40	-	Herbert (1979)
Ashfield shale	55	45	-	Loughnan (1960)
Bringelly shale	45	35	20	Loughnan (1960)

Table 3.2b Mineralogy of claystone-siltstone in the Wianamatta group (after Herbert, 1979)

Rock type	Total clay minerals %	Quartz %	Other minerals %
Upper Bringelly shale	45-65	25-52	usually < 10
Ashfield shale and lower 30 *m* of Bringelly shale	40-60	20-45	usually < 16

Table 3.3 Moisture content for the Ashfield shale from three sites

Sample number	Moisture content (%)		
	Ryde-interchange	Surry Hills	Moorebank
1	4.6	1.7	2.1
2	4.3	1.6	2.3
3	4.5	1.8	1.9
4	4.4	2	2.1

Table 3.4. Porosity and dry density of Ashfield shale from three sites

Sample name	Grain vol. (cm^3)	Bulk vol. (cm^3)	S. grain density (g/cc)	Dry density (g/cc)	Porosity (%)	Moisture con. $S=1$
R1	11.30	12.83	2.73	2.40	11.92	4.99
R2	10.89	12.11	2.71	2.44	10.10	4.16
R3	20.23	23.08	2.75	2.41	12.35	5.07
R4	13.17	14.94	2.76	2.44	11.84	4.81
R5	11.07	12.45	2.78	2.47	11.09	4.55
R6	20.23	22.31	2.70	2.45	9.34	3.76
R7	19.76	22.11	2.74	2.45	10.65	4.34
S1	16.24	17.00	2.76	2.63	4.48	1.73
S2	12.38	13.12	2.67	2.52	5.65	2.28
S3	20.66	21.83	2.72	2.57	5.38	2.12
F1	16.43	17.40	2.76	2.60	5.57	2.18
F2	12.73	13.56	2.74	2.57	6.12	2.44
F3	19.01	20.14	2.72	2.57	5.60	2.16

R = Ryde S = Surry Hills F = Moorebank

Table 3.5 Bulk densities at different depths for five boreholes in Ryde-interchange site.

Bore. No. 1		Bore. No.2		Bore. No.3		Bore. No.4		Bore. No.5	
Depth (m)	Density (t/m³)	Depth (m)	Density (t/m³)	Depth (m)	Density (t/m³)	Depth (m)	Density (t/m³)	Depth (m)	Density (t/m³)
6.72	2.36	5.78	2.47	6.29	2.48	3.64	2.43	5.58	2.34
7.68	2.46	6.34	2.57	6.79	2.55	4.54	2.49	7.48	2.49
8.75	2.44	7.50	2.45	7.10	2.51	5.58	2.48	9.90	2.48
9.59	2.48	8.09	2.53	8.75	2.56	6.57	2.53	11.52	2.57
10.44	2.56	8.80	2.51	10.08	2.61	7.58	2.49		
		9.44	2.54	11.11	2.66	9.55	2.57		
		10.70	2.60			10.46	2.59		

Table 3.6 Definitions of the Degrees of Weathering

Grade	Symbol	Description	Definition
1	F	Fresh	Rock substance is unaffected by weathering.
2	SW	Slightly weathered	Rock substance is affected by weathering to the extent that staining or partial discolouration of the rock substance by limonite has taken place. The colour and texture of the fresh rock is recognisable. The strength properties are essentially those of the fresh rock substance.
3	MW	Moderately weathered	The rock substance is affected by weathering to the extent that limonite staining extends throughout the whole of the rock substance and the original colour of the rock is no longer recognisable.
4	HW	Highly weathered	The rock substance is affected by weathering to the extent that limonite staining or bleaching affects the whole of the rock substance and signs of chemical and physical decomposition of individual minerals are usually evident. The porosity and strength may be increased or decreased when compared to the fresh rock substance, usually as a result of the leaching or deposition of iron. The colour and strength of the original fresh rock substance is no longer recognisable.
5	EW	Extremely weathered	The rock substance is affected by weathering to the extent that the rock exhibits soil properties, i.e. it can be remoulded and can be classified according to the Unified Classification System, but the texture of the original rock is still evident.

Table 3.7 A summary of the Atterberg limit test results (present study)

No. of sample	Liquid Limit (%) *LL*	Plastic Limit (%) *PL*	Plasticity Index (%) I_p
SLP1	20.2	15.4	4.8
SLP2	21.3	16.8	4.5
SLP3	19.1	15.0	4.1
SLP4	18.9	16.0	2.9
SLP5	18.9	15.2	3.7
SLP6	21.5	16.6	4.9
SLP7	22.4	17.8	4.6
SLP8	18.3	14.7	3.5
SLP9	22.3	16.5	5.8
SLP10	20.4	15.8	4.6
SLP11	19.5	15.4	4.1
SLP12	23.3	17.1	6.2
SLP13	23.0	17.1	5.9
SLP14	19.1	15.0	4.1
SLP15	18.0	14.2	3.8
SLP16	17.6	14.0	3.6
SLP17	20.8	15.6	5.2
SLP18	19.5	14.3	5.2
SLP19	20.9	15.5	5.4
SLP20	24.1	17.9	6.2

Table 3.8 A summary of the Atterberg limit test results (after Herbert, 1979)

No. of sample	Plastic Limit (%) *PL*	Liquid Limit (%) *LL*	Plasticity Index (%) I_p
Ba20	11.7	17.4	5.6
Ba21	13.2	19.1	5.9
Ba22	14.7	21.1	6.4
Ba23	13.0	17.9	4.9
Ba24	14.9	20.0	5.1
Ba25	12.8	15.7	2.8
Ba26	12.8	16.2	3.4
Ba27	13.4	20.3	6.9
Ba28	15.1	21.9	6.8
Ba29	12.3	18.1	5.8
Ba30	13.3	18.7	5.4
Ba31	13.2	18.2	5
Ba32	13.6	15.4	1.8
Ba33	14.7	21.2	6.5
Ba34	14.0	19.9	5.9
B21	16.0	17.2	1.2
B22	15.4	20.0	4.6
B23	15.3	20.7	5.4
B24	13.6	16.2	2.6
M1	16.0	18.0	2.0
M2	14.0	18.0	4.0
M3	14.0	16.0	2.0
M4	14.0	17.0	3.0

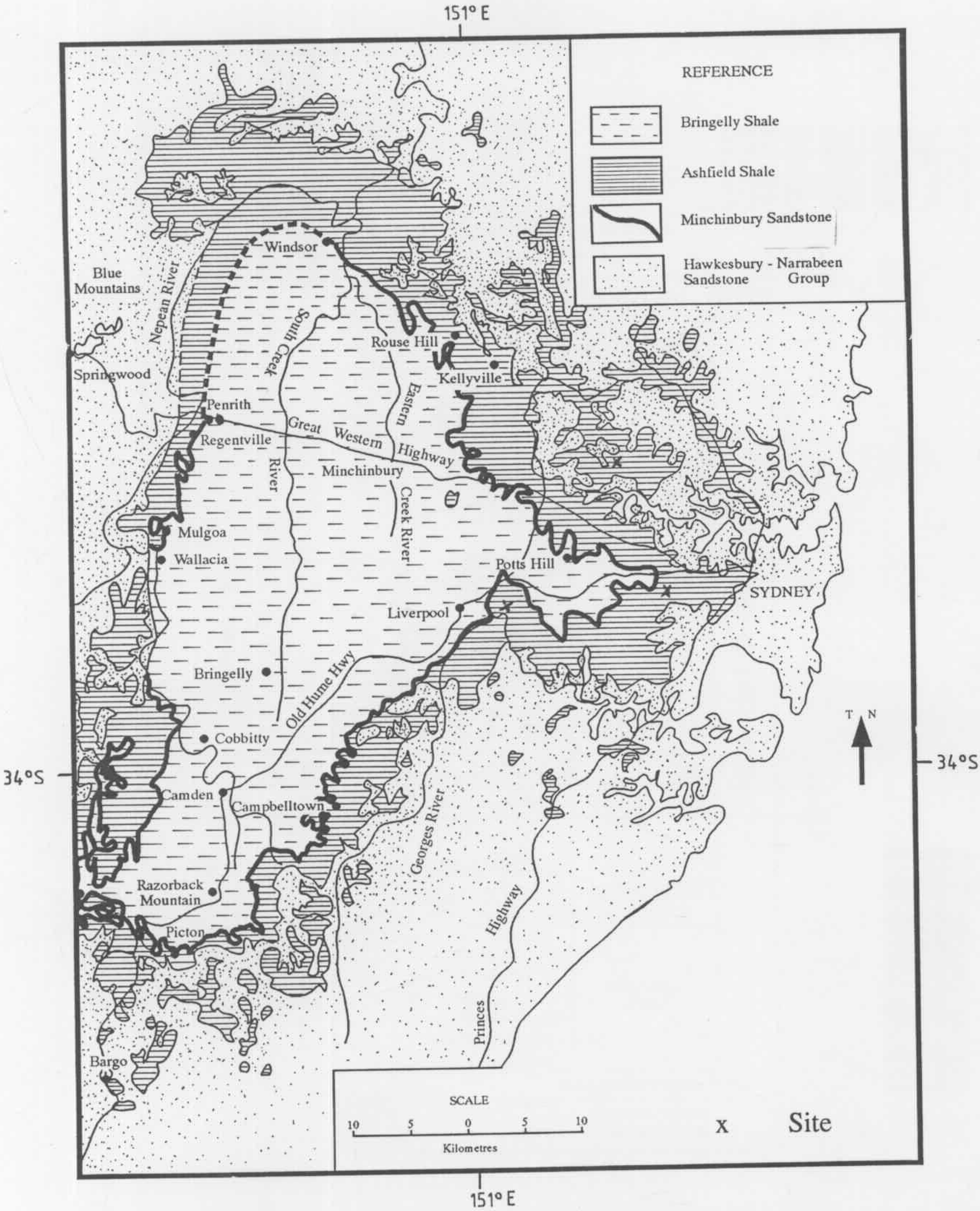

Figure 3.1 Distribution of Wianamatta Group rocks (after Herbert, 1979, 1980)

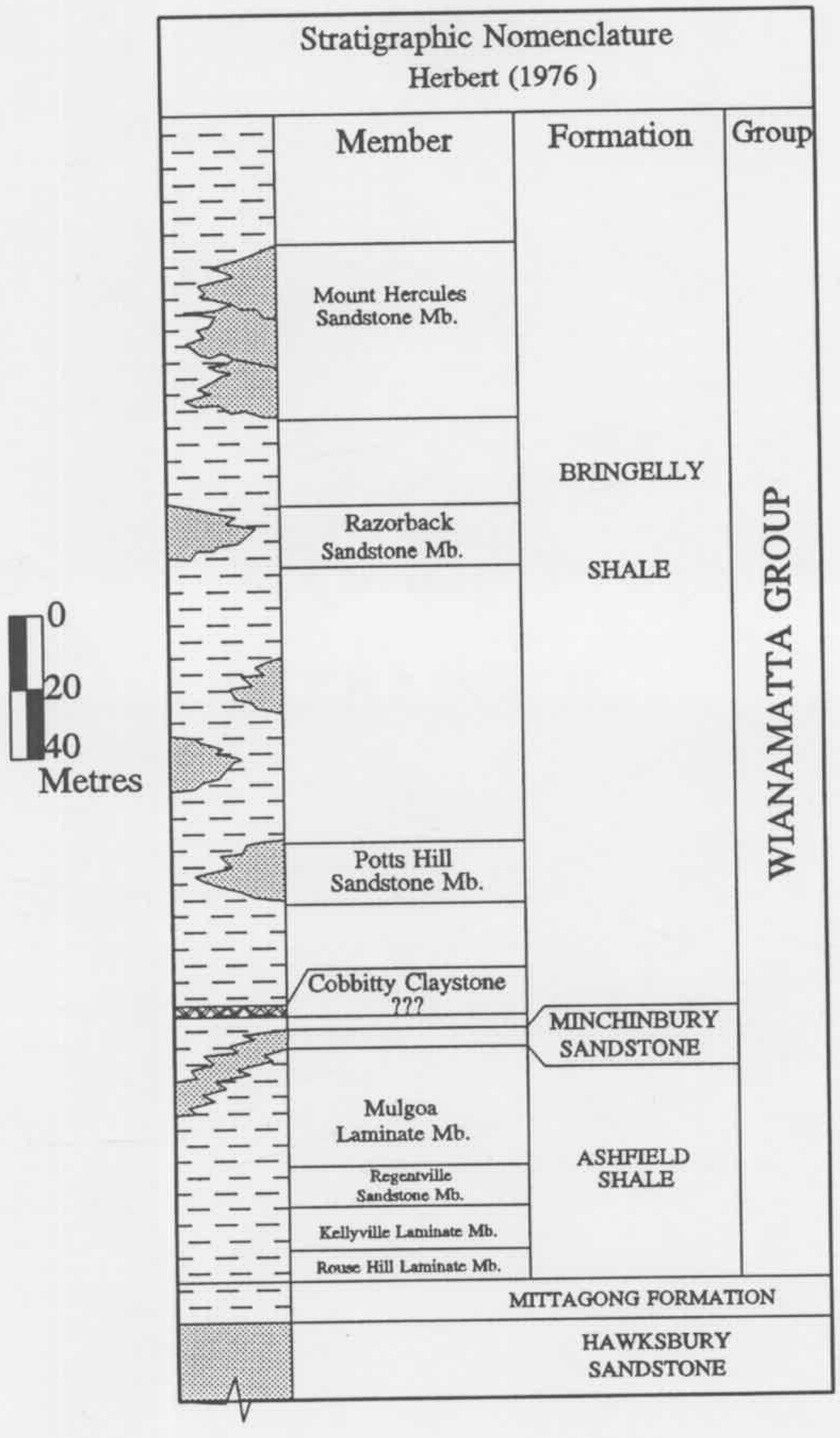

Figure 3.2 Wianamatta Group stratigraphy
(after Herbert, 1979, 1980)

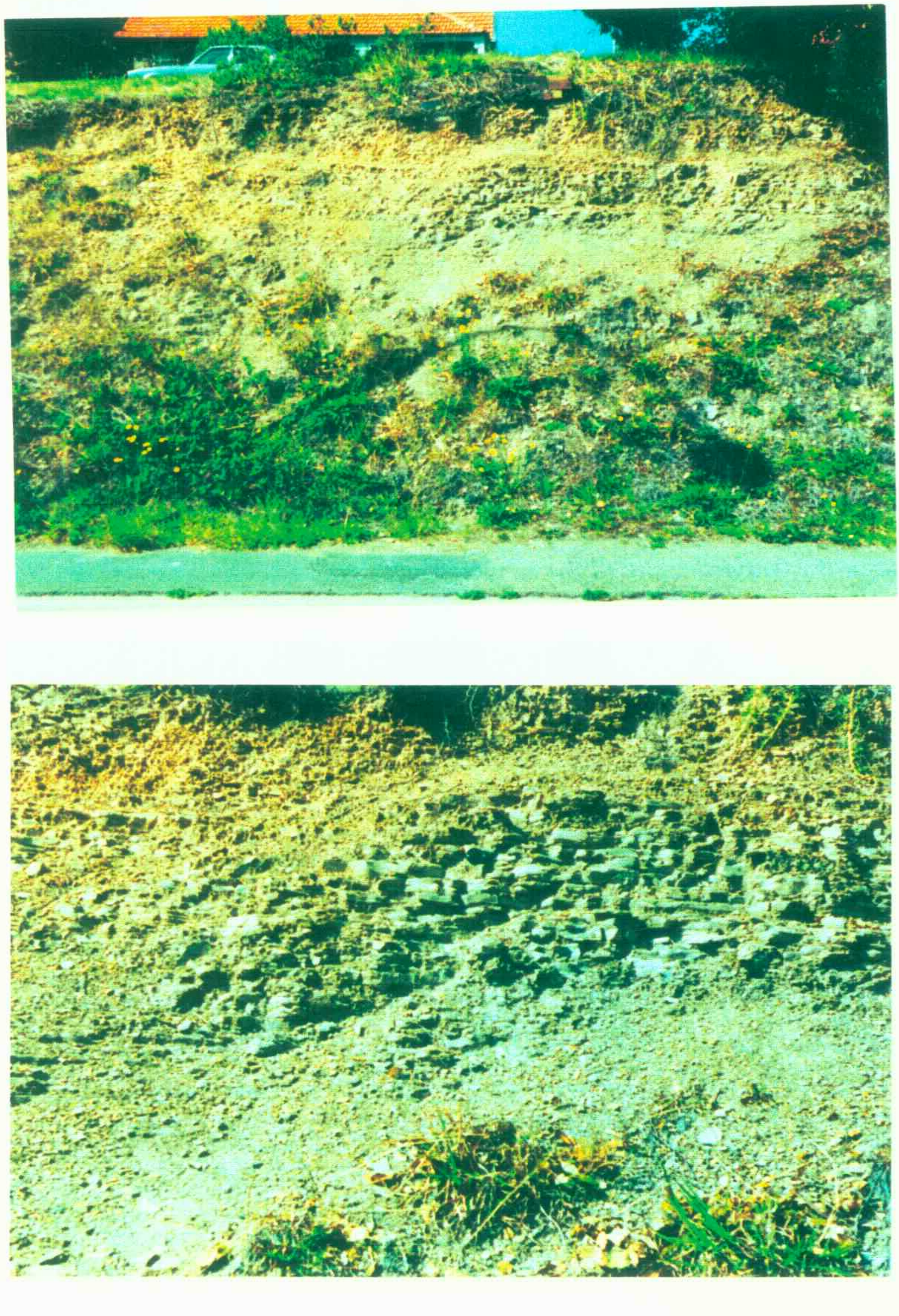

Figure 3.3 Weathered outcrop of the Ashfield shale at the Ryde site

Figure 3.4 Large truck mounted drilling rig

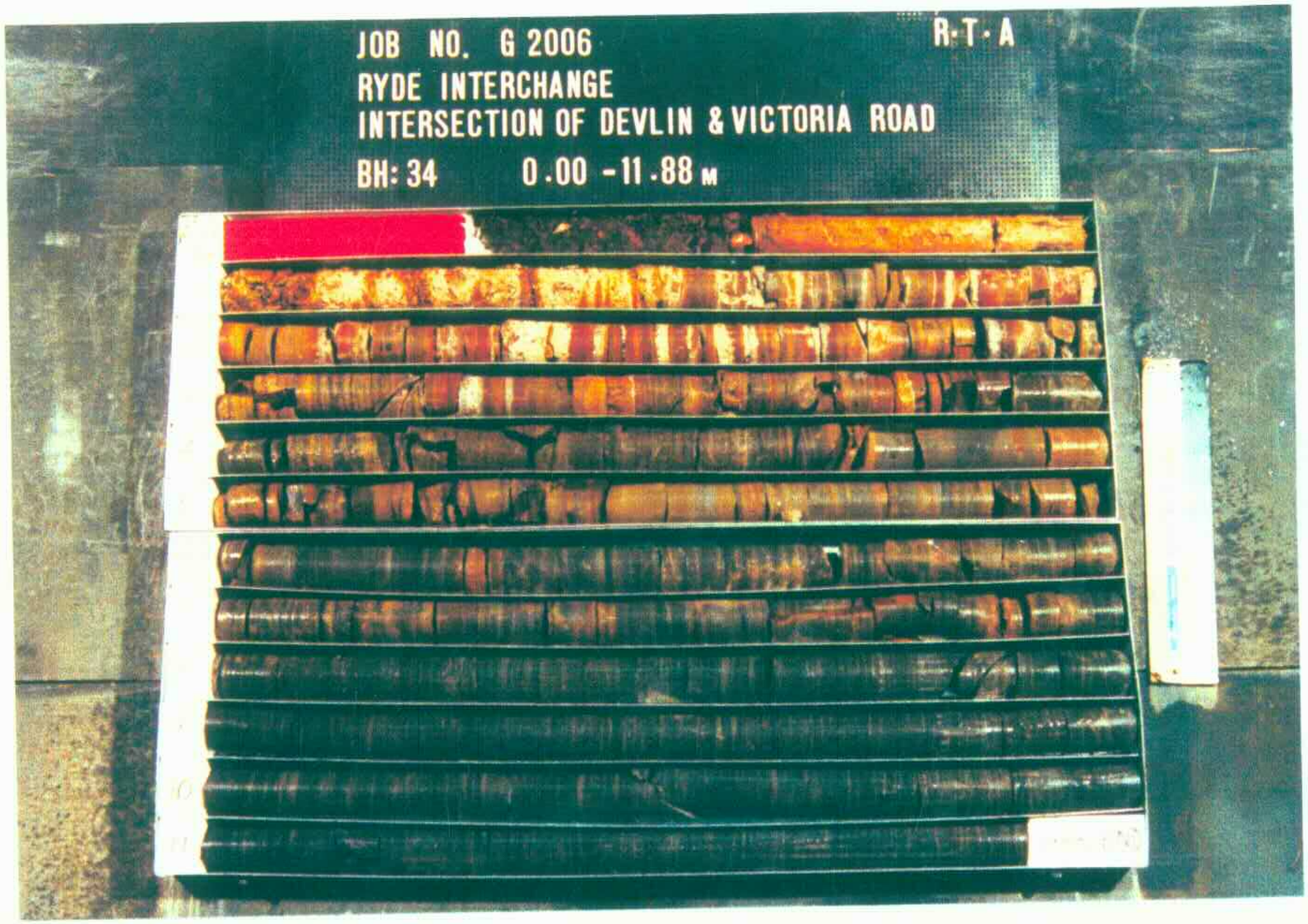

Figure 3.5 Recovered core samples from borehole at Ryde site

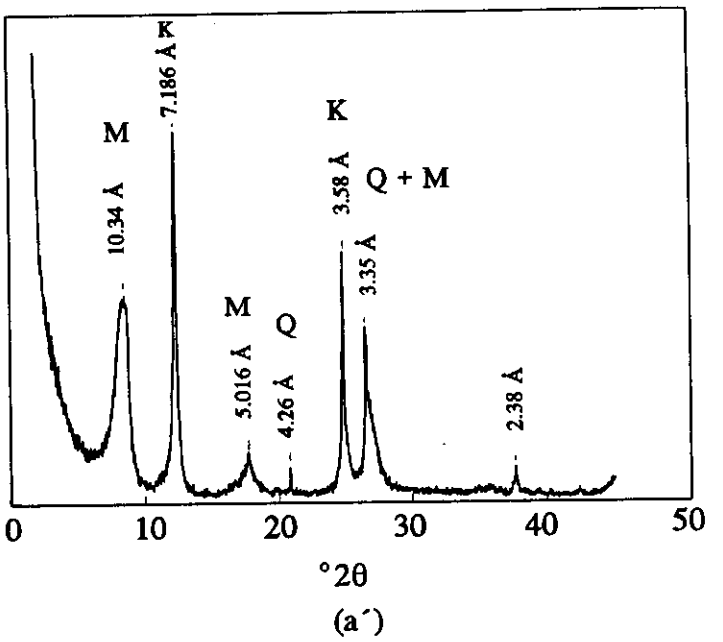

(a´)

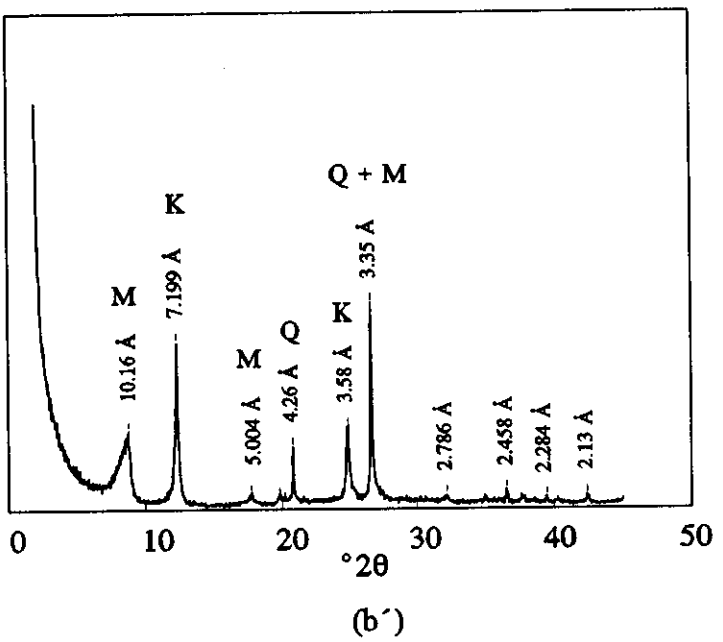

(b´)

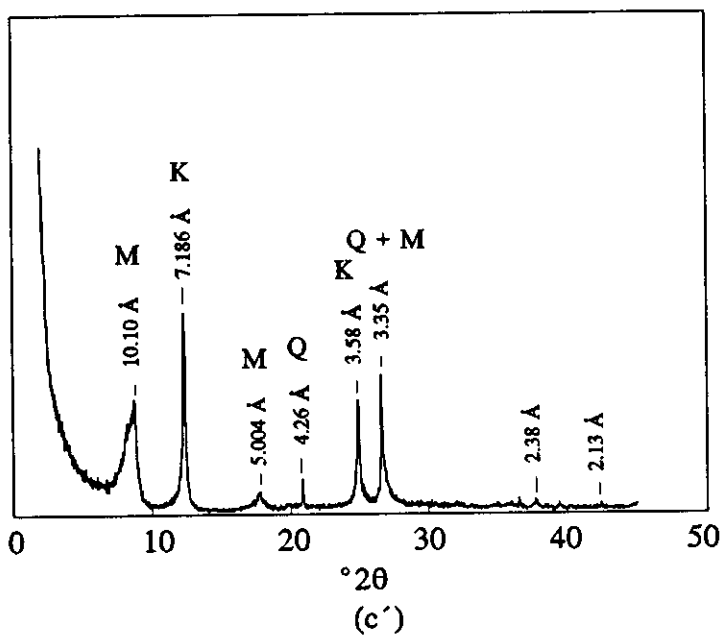

(c´)

Figure 3.6a Typical X-ray diffraction trace, 2 μ fraction of Ashfield shale (a´): Ryde, (b´): Surry Hills, (c´): Moorebank

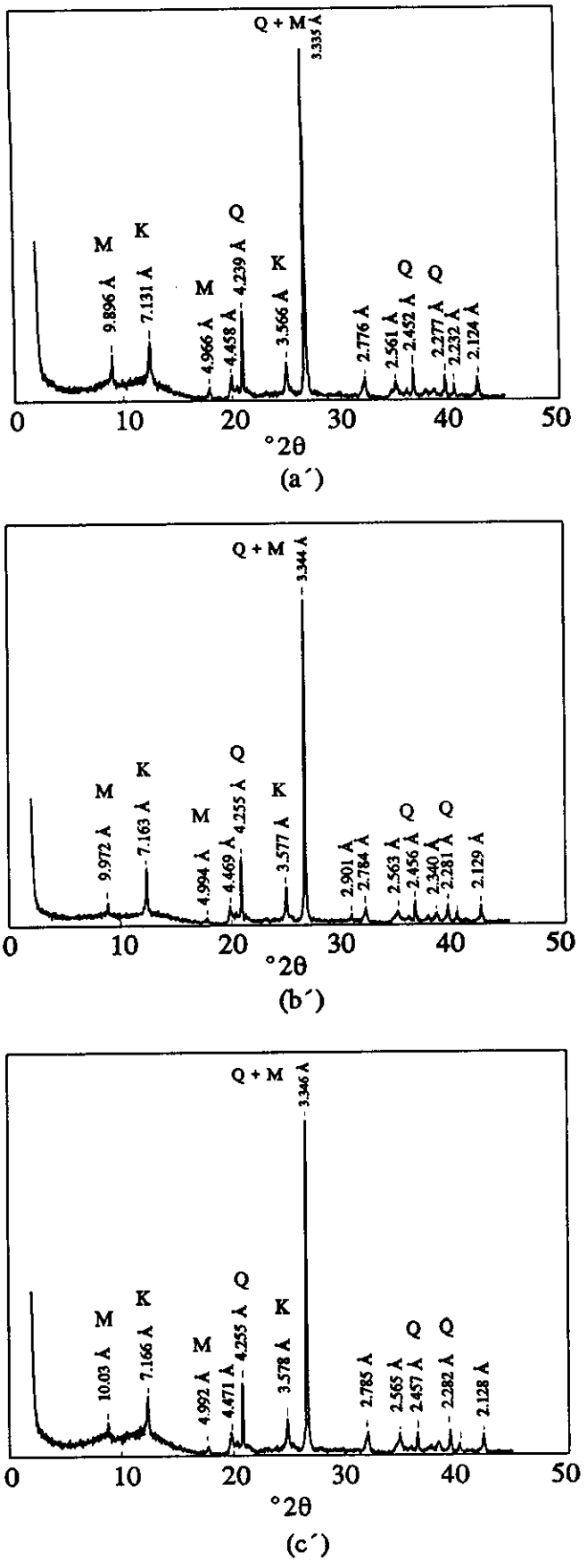

Figure 3.6b Typical X-ray diffraction trace for Ashfield shale (powder)
(a´): Ryde, (b´): Surry Hills, (c´): Moorebank

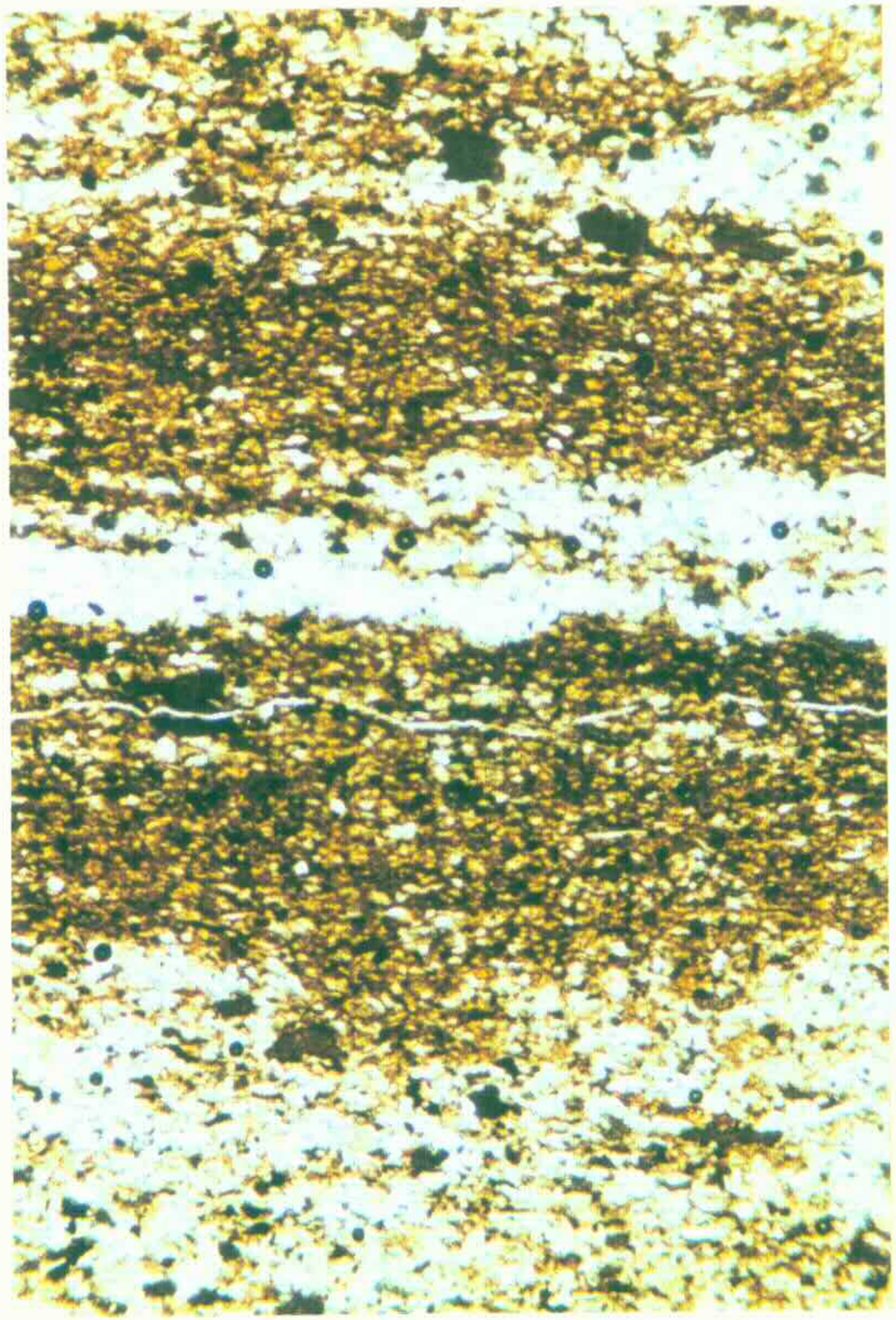

(a)

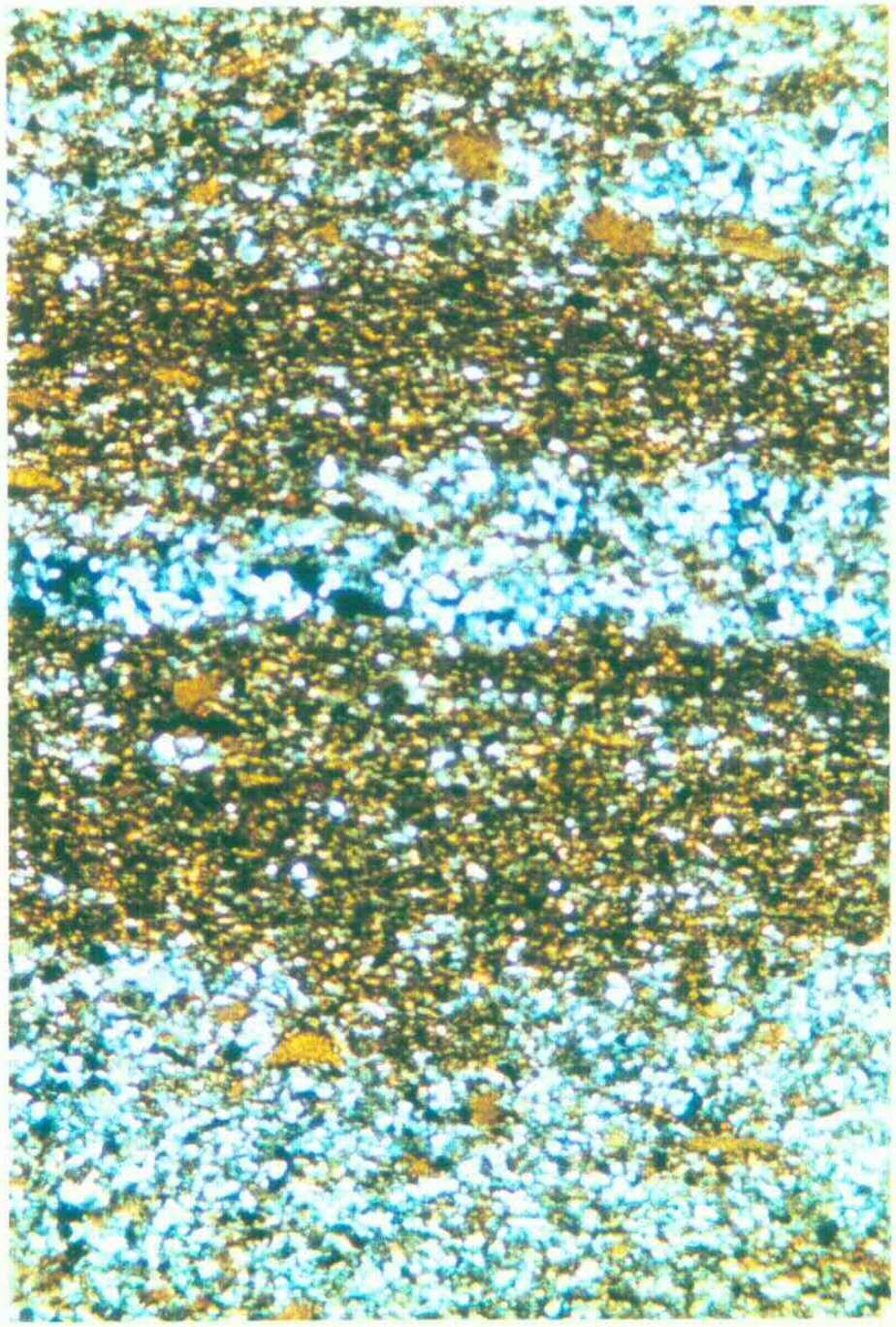

(b)

Figure 3.7 Photographs of the thin section of Ashfield shale, (a) ordinary light, (b) polarizan light, x25

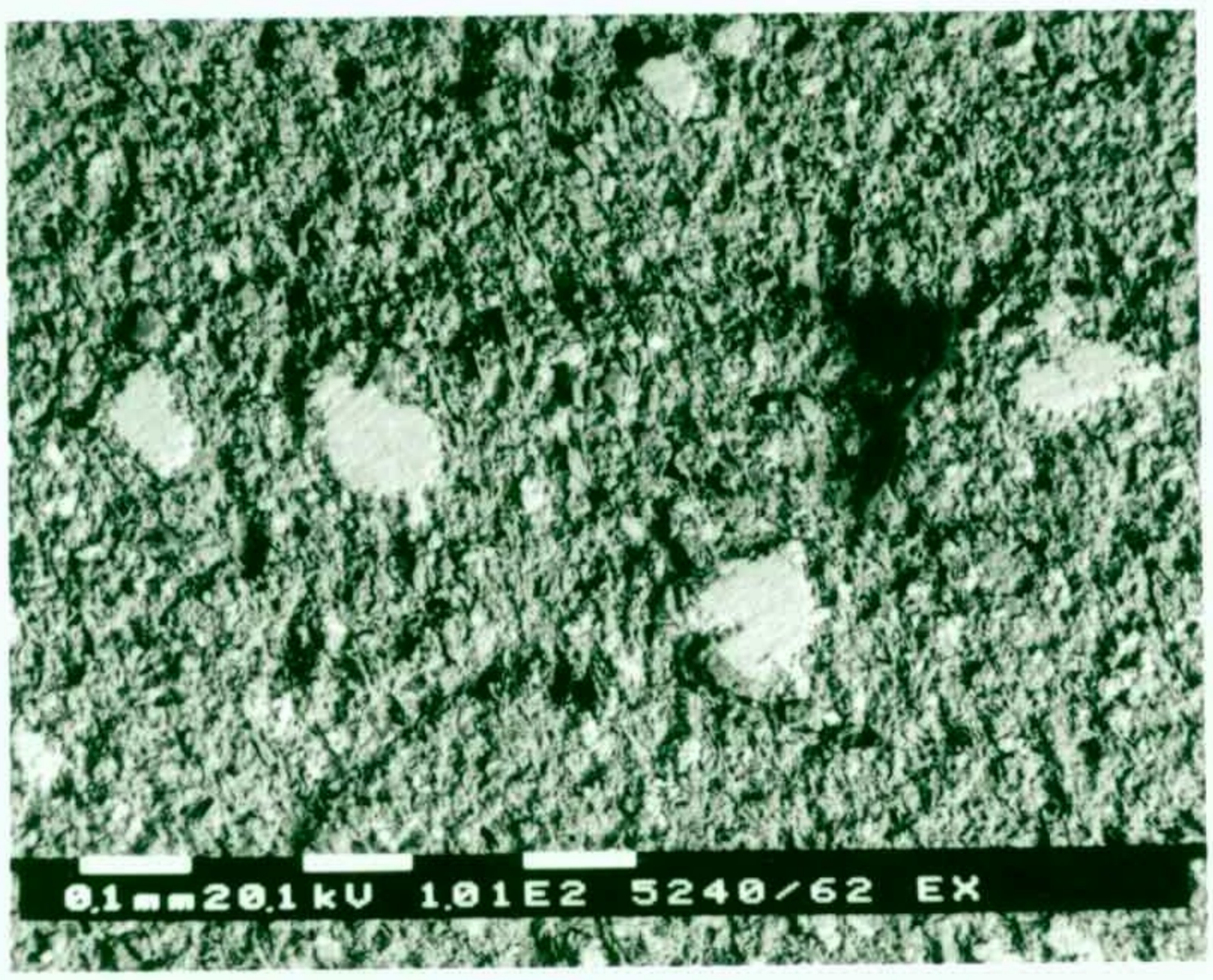

(a)

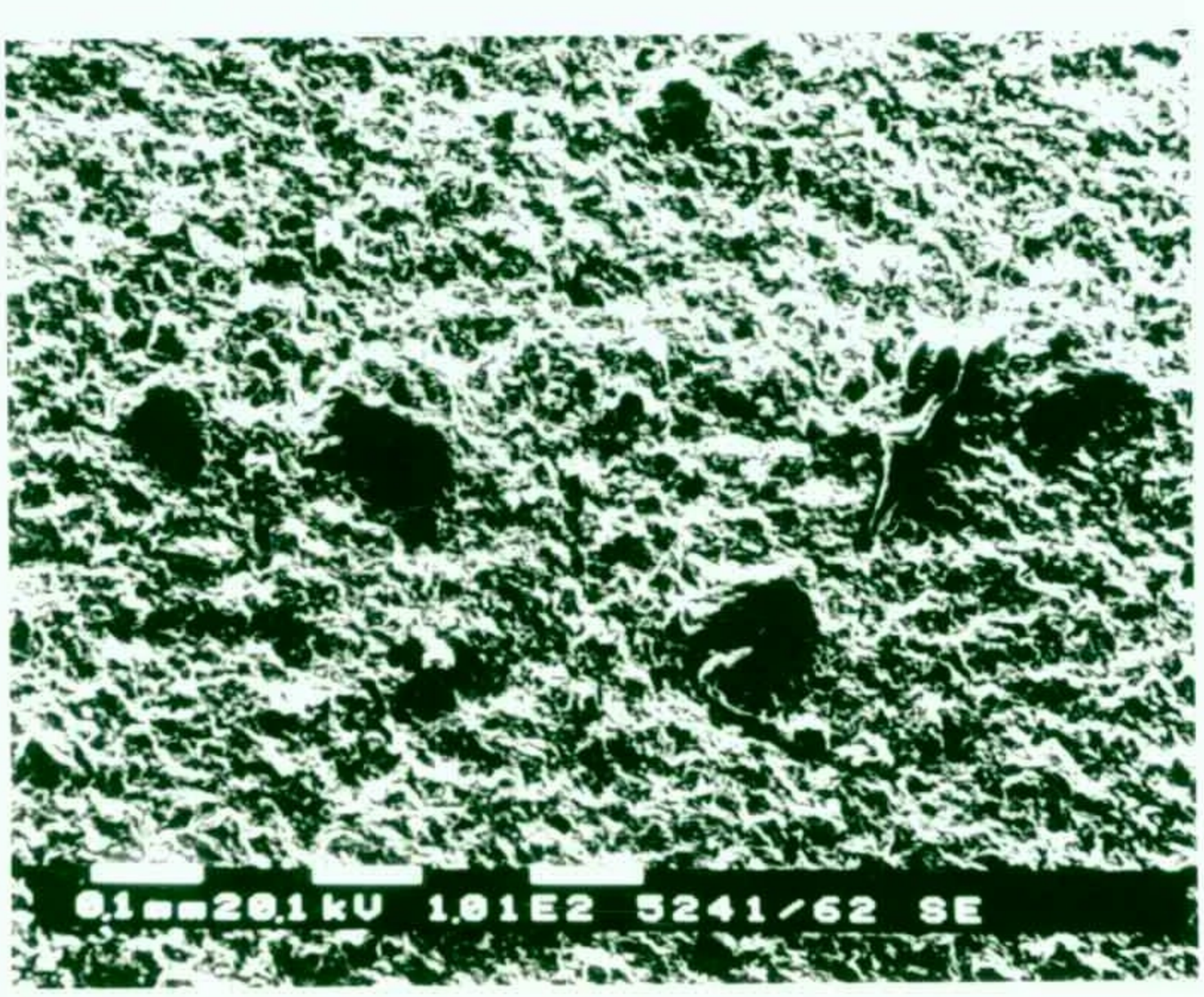

(b)

Figure 3.8 Scanning electron micrographs, (a): Back-scattered electron image and (b): Secondary electron image, of Ashfield shale. Magnification = 100x

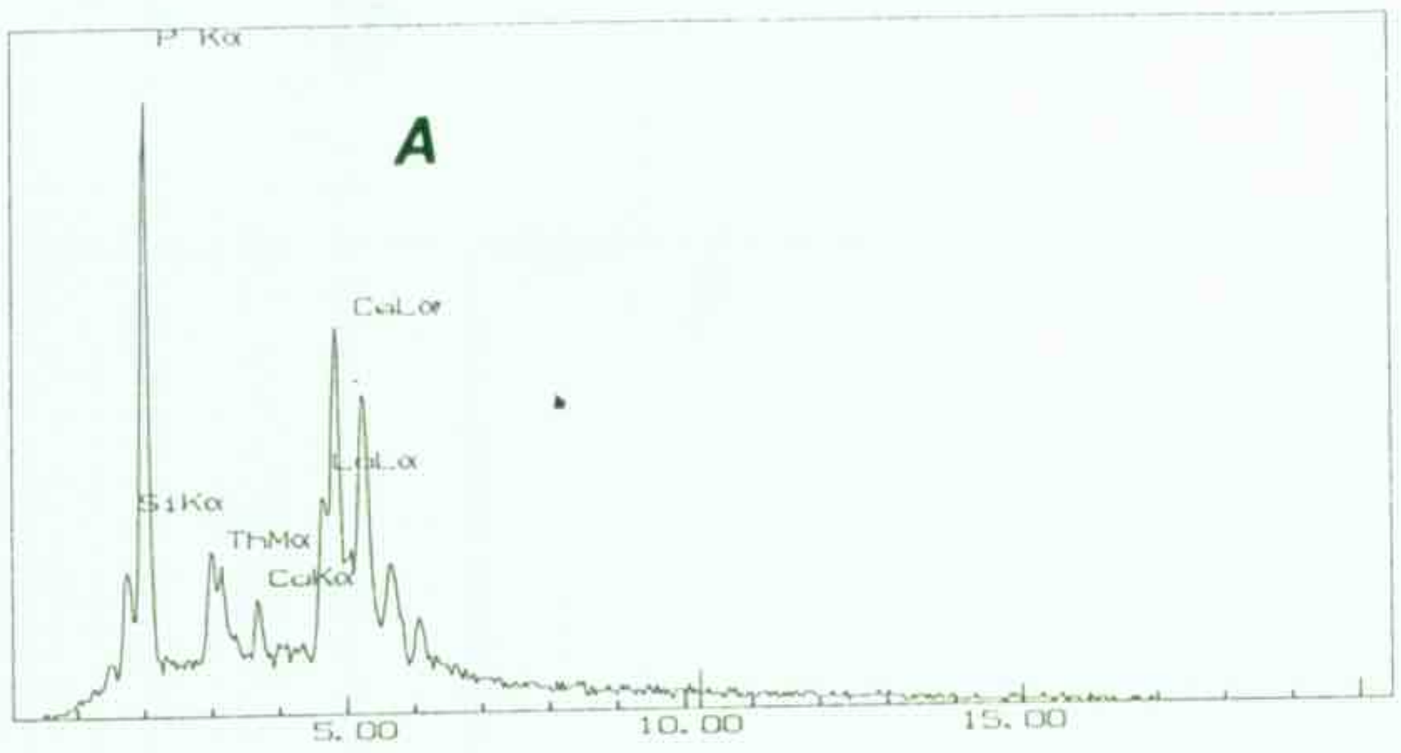

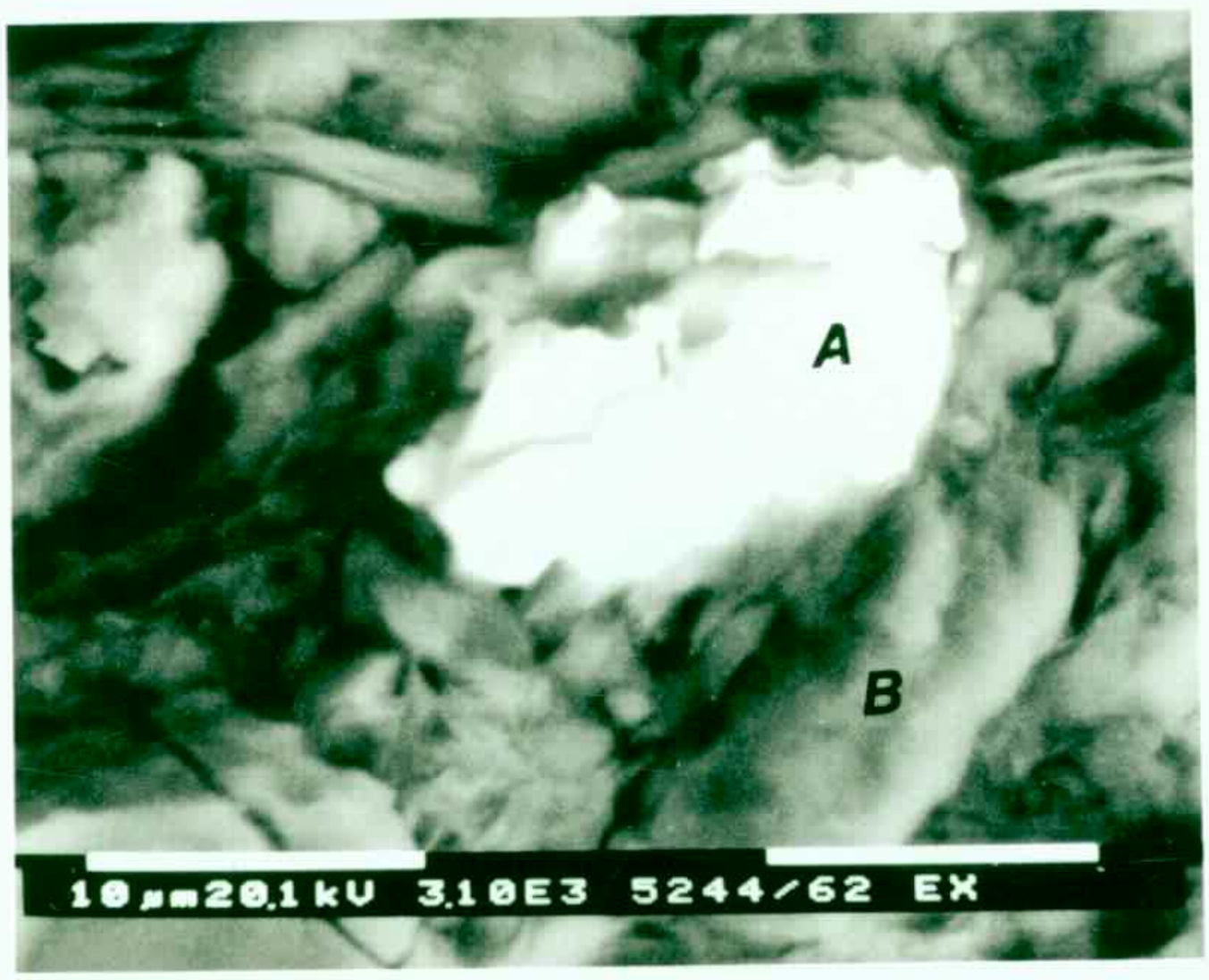

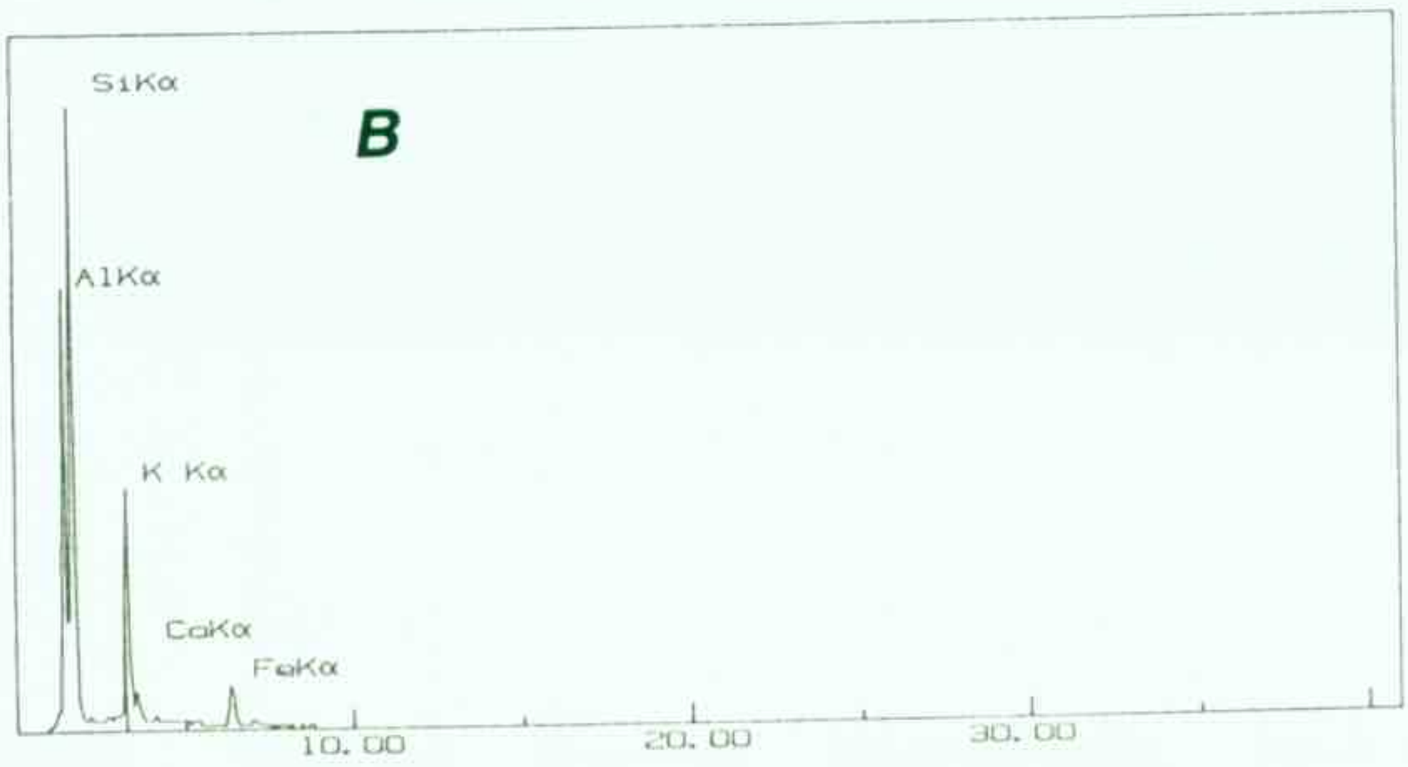

Figure 3.9 Scanning electron micrographs, back-scattered electron image, of Ashfield shale. Magnification = 3000x

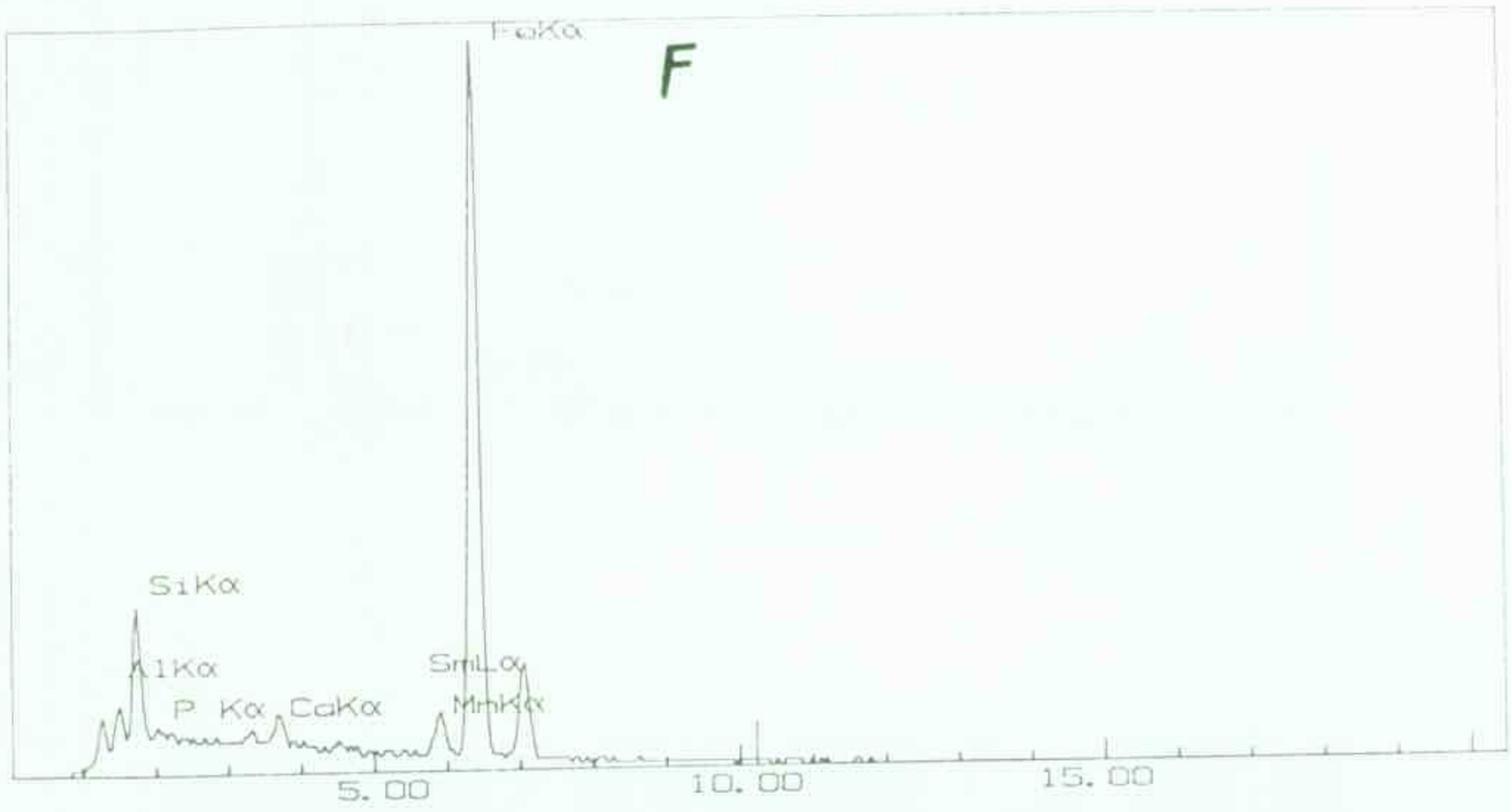

Figure 3.10 (a) Scanning electron micrographs, back-scattered electron image, of Ashfield shale.
Magnification = 40x

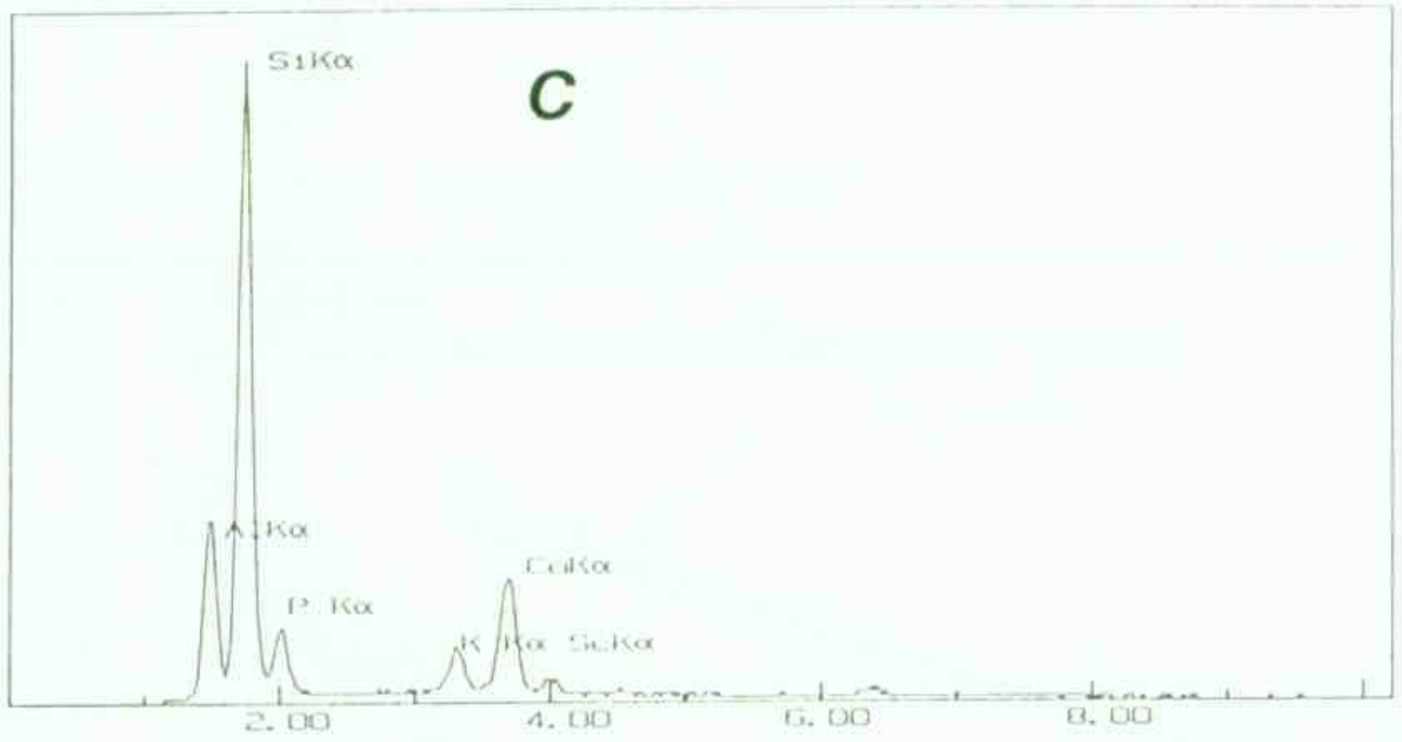

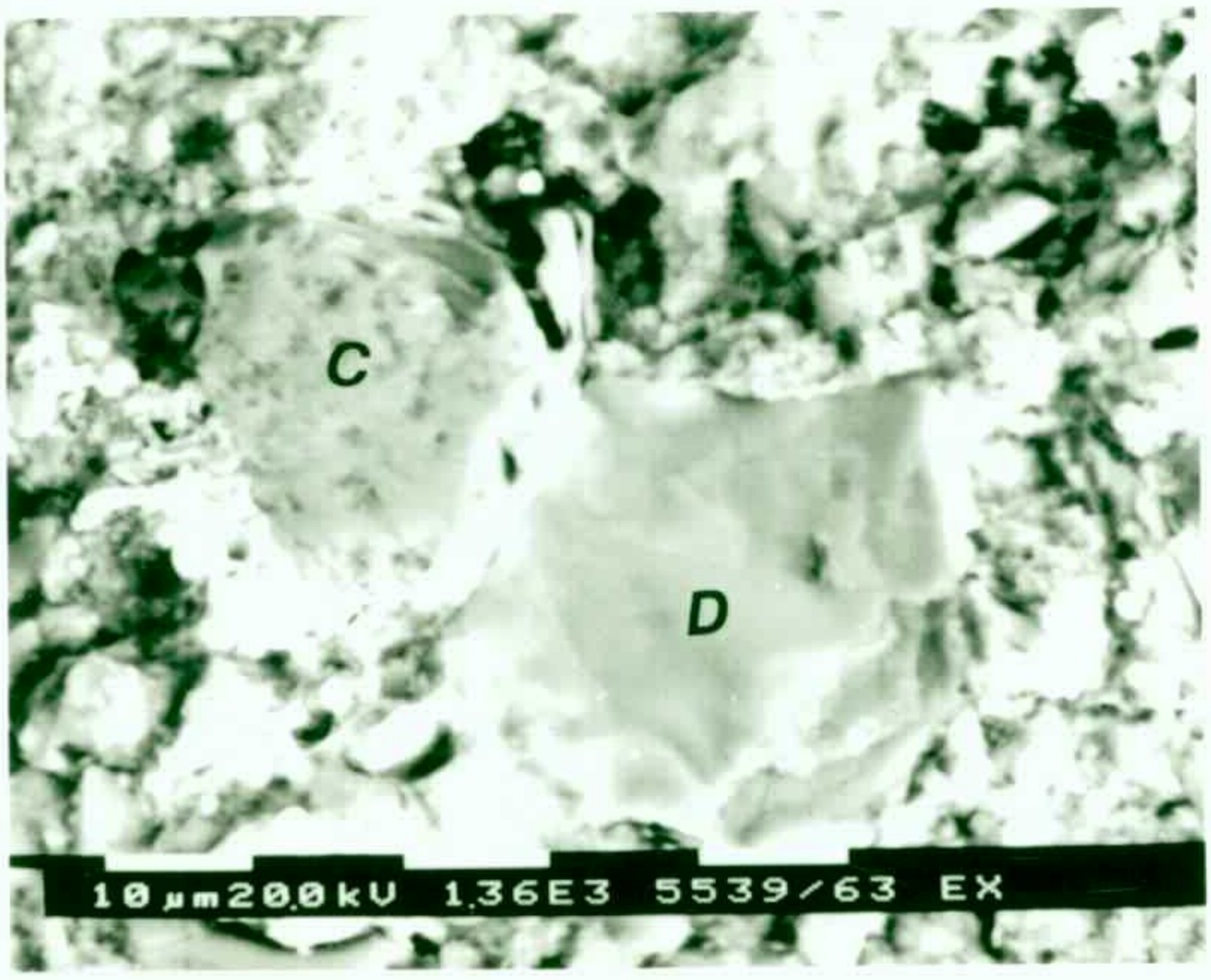

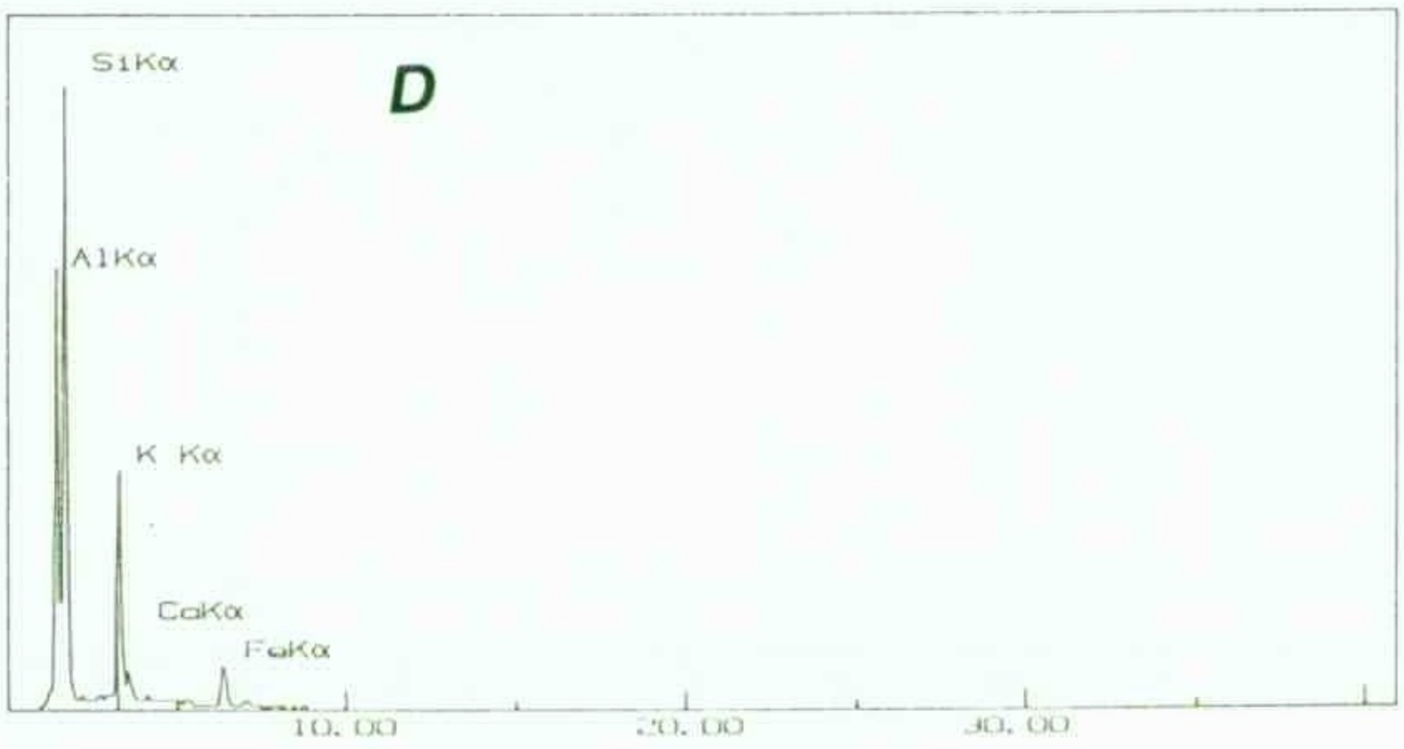

Figure 3.10 (b) Scanning electron micrographs, back-scattered electron image, of Ashfield shale.
Magnification = 1300x

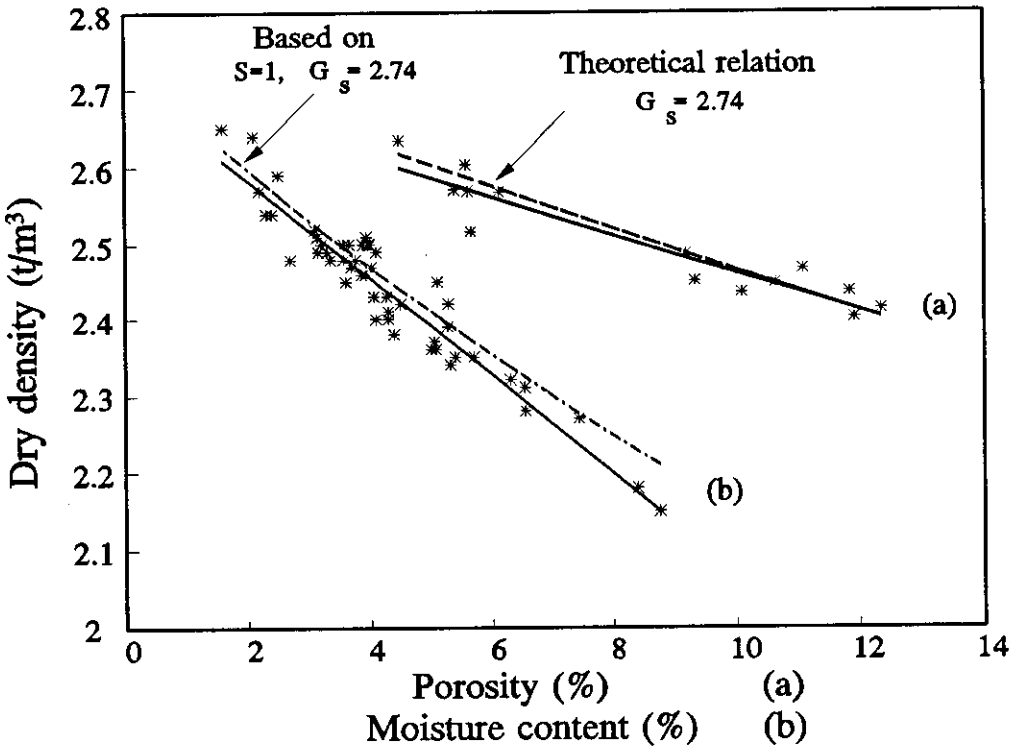

Figure 3.11 Dry density versus porosity and moisture content for Ashfield shale

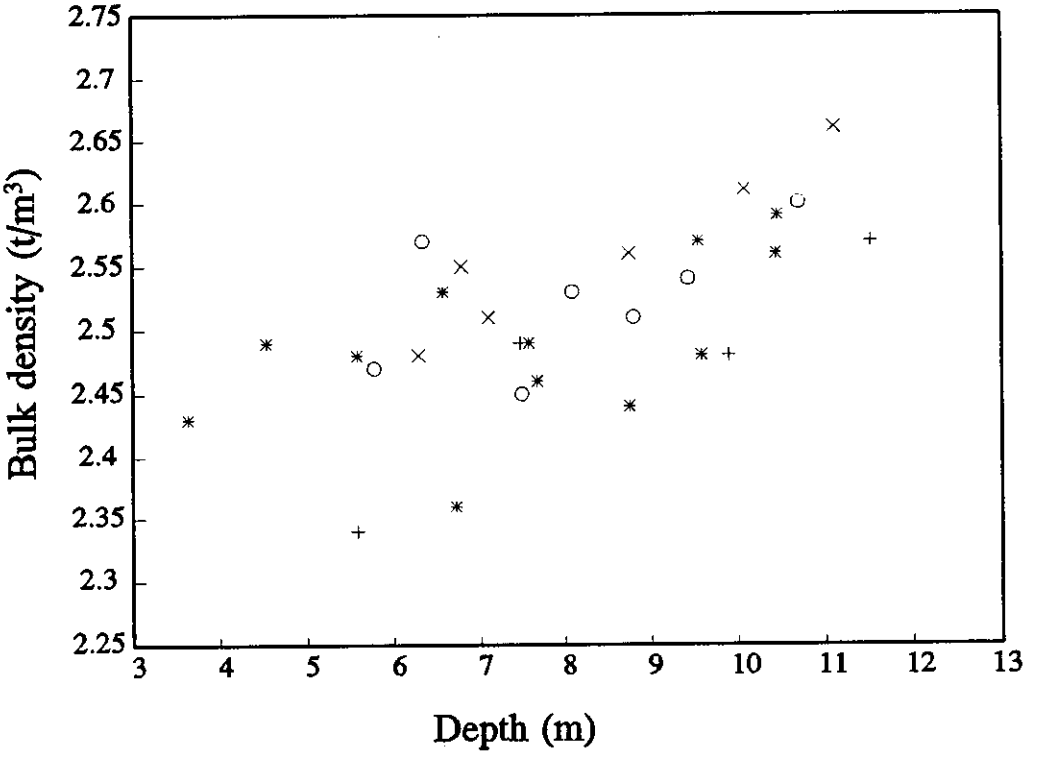

Figure 3.12 Variation of bulk density with depth

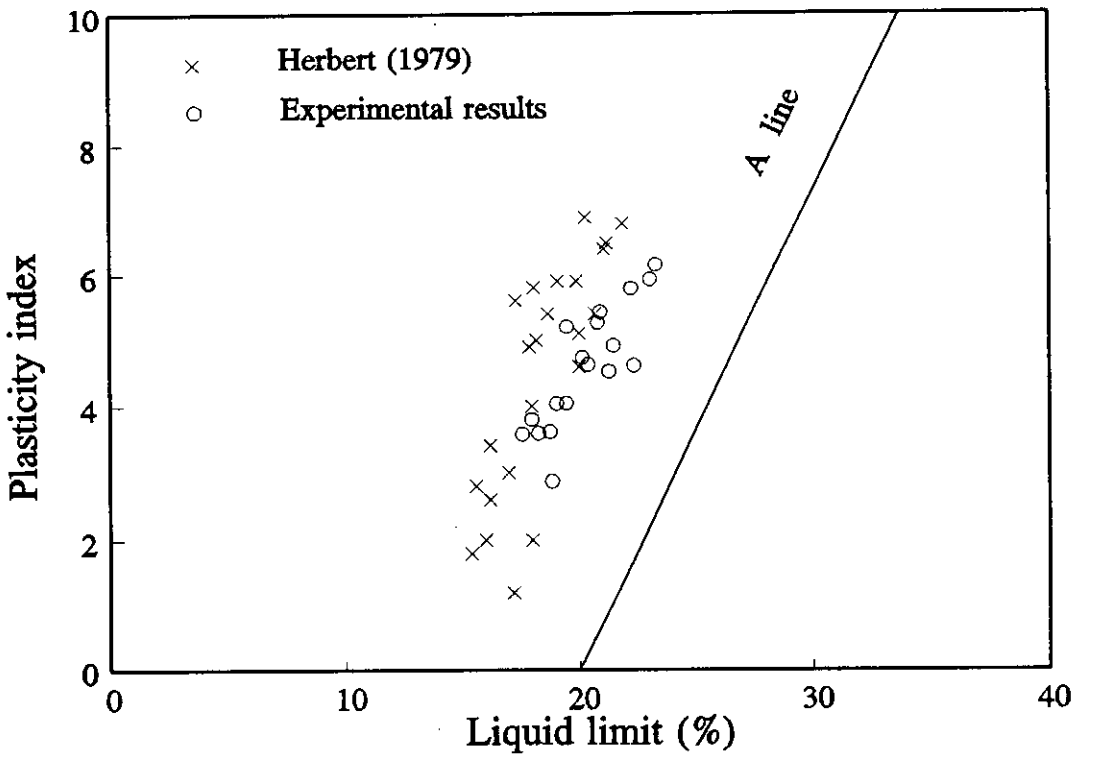

Figure 3.13 Plasticity index versus liquid limit for Ashfield shale

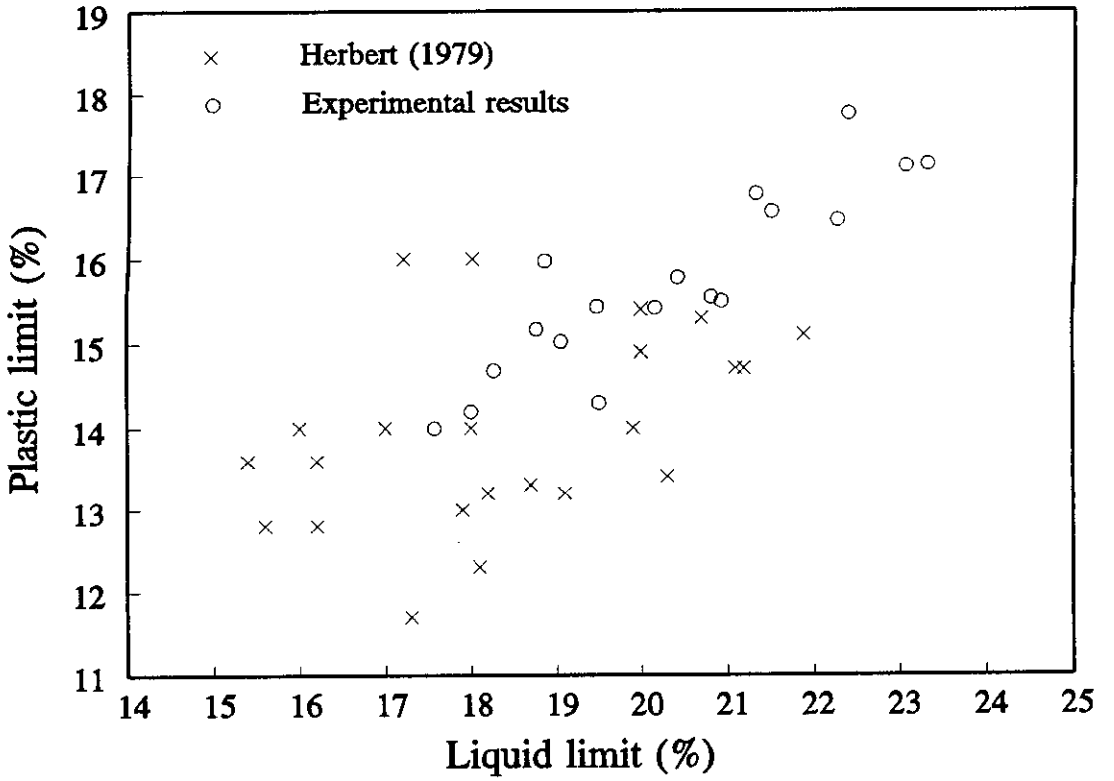

Figure 3.14 Relationship between liquid limit and plastic limit

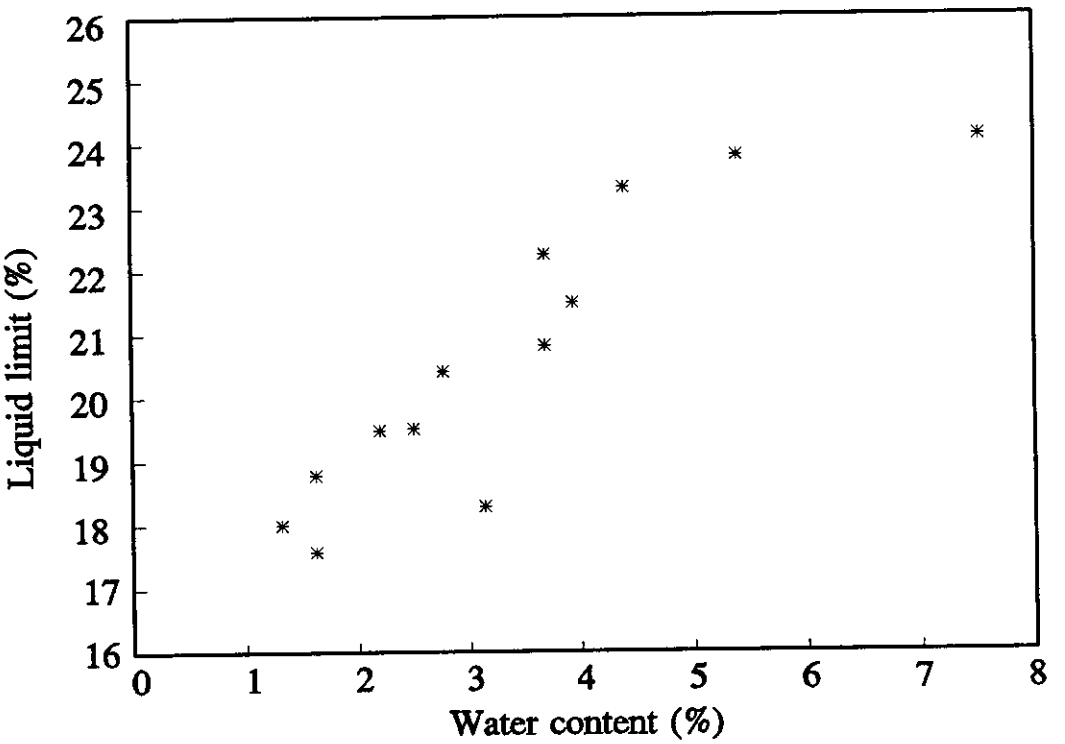

Figure 3.15 Liquid limit versus natural water content

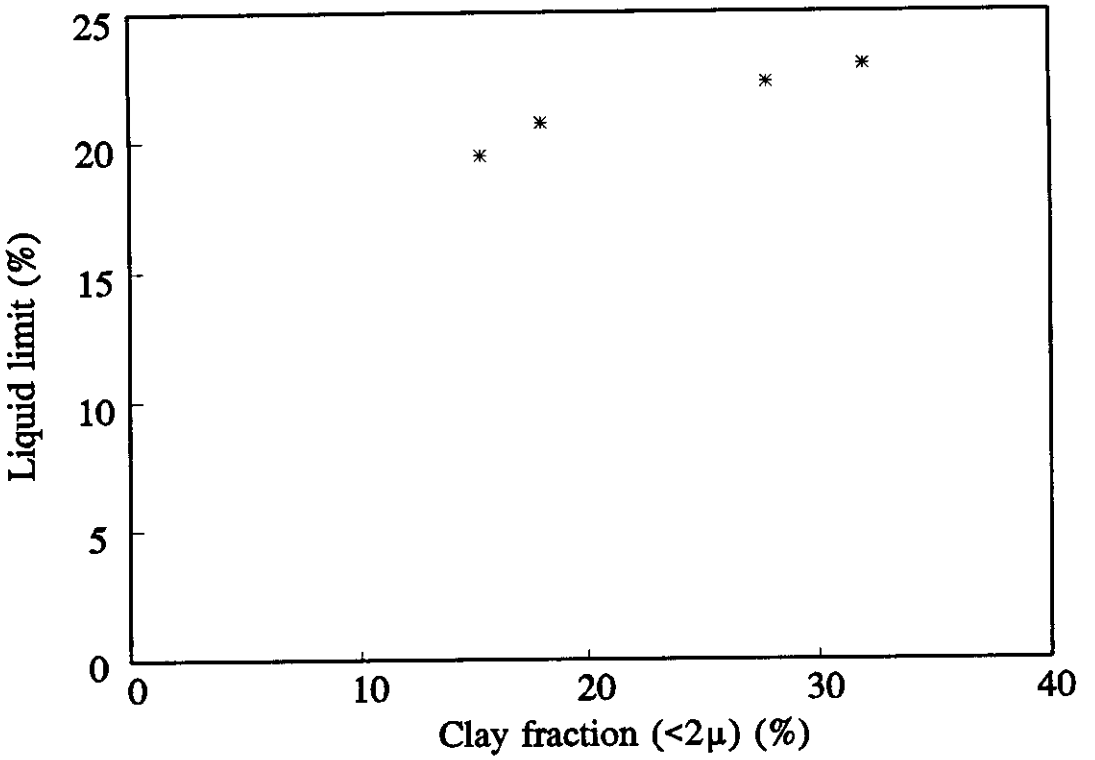

Figure 3.16 Liquid limit versus clay fraction

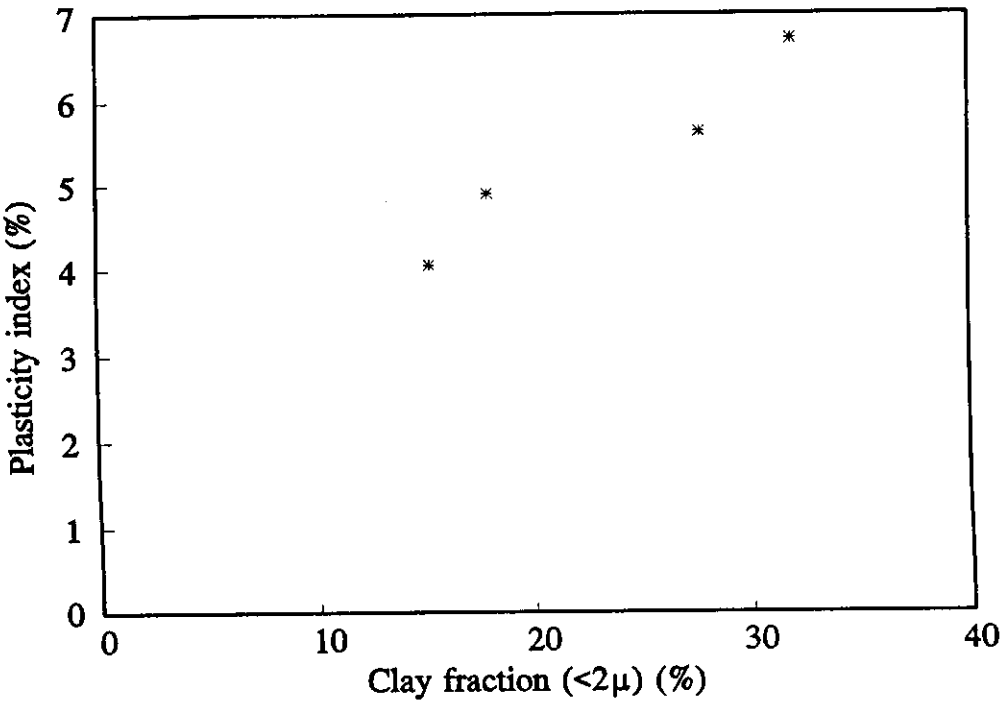

Figure 3.17 Plasticity index versus clay fraction

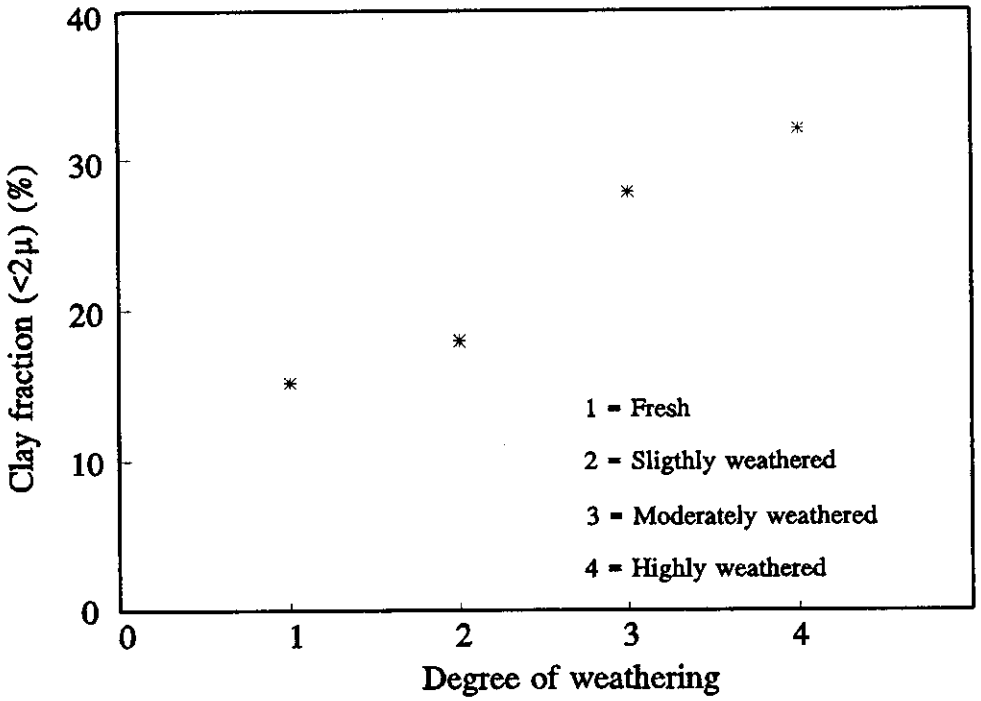

Figure 3.18 Relationship between weathering grade and clay fraction

CHAPTER 4 INDEX TESTS

CHAPTER 4

INDEX TESTS

4.1 INTRODUCTION

Simple index tests has been performed to investigate the mechanical and physical properties of Ashfield shale. Intact shale specimens have been used for all the uniaxial compression tests, point load tests and slake durability tests performed.

The uniaxial compressive strength (*UCS*) is possibly the most broadly used parameter in rock engineering. To investigate the strength of Ashfield shale in general, a large number of uniaxial compression tests were carried out on prepared cylindrical samples cored perpendicular to the laminations. The aim of this series of tests was to establish a correlation between the results of uniaxial compression tests and various other physical and mechanical properties. A series of uniaxial compression tests was also performed on samples of Ashfield shale with different lamination directions to determine the anisotropic strength variation and deformational behaviour of Ashfield shale. The results of this series of tests are presented in Chapter 5.

To investigate the strength of Ashfield shale in general, a large number of diametral and axial point load tests have been carried out on prepared core samples. The aim of these tests was to investigate the effect of sample geometry, degree of weathering and loading configuration on the point load strength index, and to establish a correlation between the results of uniaxial compression tests and diametral and axial point load tests. The ratio of the point load strength indices measured parallel and normal to the laminations has also been determined. This has given a measure of the strength anisotropy.

This chapter also summarises the findings of a study of the slaking behaviour of Ashfield shale. The results of slake durability tests are presented in this chapter and the relation of the durability to other properties is investigated. The degree of breakdown of the Ashfield shale upon drying and wetting was measured using slake-durability apparatus. Normally argillaceous rocks such as shale have low durability to weathering and breakdown upon exposure to drying and wetting.

Slaking is a short-term physical disintegration process that may occur in some geological materials that are exposed at the surface. Material characteristics and local environmental conditions are the two important factors that control this disintegration. In slake durability tests the deterioration of a rock from cycles of wetting and drying is investigated. All rocks will be affected to some extent by cycles of wetting and drying, but the effects on shales can be very pronounced. It has been suggested that the slake durability test can also be used to predict the engineering performance of shales (Gamble, 1971).

A description of the index tests and test results for Ashfield shale are individually presented in this chapter. Data on moisture contents, degree of saturation, porosity and density were presented in Chapter 3.

4.2 INDEX TEST PROGRAMMES

A total of 150 uniaxial compression tests, 250 axial and 100 diametral point load tests and 60 slake durability tests have been performed on the Ashfield shale. Table 4.1 summarises the laboratory test programme. Addition *UCS* and point load test results have been obtained from previously unpublished data kindly provided by geotechnical consultants and agencies that are active in the Sydney region (Ghafoori et al., 1993). These include Ashfield shale samples from many locations in the Sydney basin, with geological descriptions ranging from intact to highly weathered shale. For brevity, only selected test results are presented in the figures of this chapter. However, all test data are included in the analysis of the results.

4.3 TEST EQUIPMENT

4.3.1 Uniaxial compression tests

The uniaxial compression tests were performed on cylindrical core specimens, using a 250 *kN* capacity servo controlled testing machine (INSTRON, MODEL TT-KM). The INSTRON consists of an integrated loading frame and control system in which the cross-head applies the load necessary at a rate that can be controlled manually. This machine can be adjusted to supply a constant stress or strain rate. In the tests reported here the axial load was applied with a constant rate of axial deformation (a constant cross-head rate). In this series of tests a rate of cross-head movement of 0.2 mm/minute was selected on the basis of a nominal time to failure of 10 to 15 minutes from the beginning of loading. To reduce the specimen end effects all uniaxial compression tests were performed with steel end platens with smooth surfaces, the same diameter as the test specimen, with a spherical seat in the upper platen, following the recommended ISRM test procedure. The system had an

automated data logging program to record the progress of the test. The data read during the test were stored on a computer hard disk for later processing.

A linear variable differential transformer (LVDT) was used for measuring the axial deformations caused by the axial loading. In accordance with the ISRM suggestion the LVDT was graduated to read in 0.002 *mm* units and was accurate within 0.002 *mm* in any 0.02 *mm* range and within 0.005 *mm* in any 0.25 *mm* range. A high magnification micrometer was used to calibrate the LVDT.

The magnitudes of the applied uniaxial compressive load and axial displacement were monitored throughout each test. The uniaxial compressive load was measured by a load cell mounted on the cross-head of the testing machine. The precision and linearity of the cell were confirmed by a calibration test prior to use. The load cell has a maximum capacity of 250 *kN*. The voltage outputs of the load cell and LVDT were suitably amplified and then fed into an analog-digital converter and stored in the memory of a computer system for later processing.

4.3.2 Point load tests

The point load test was performed on core samples of about 52 *mm* diameter. Details of the loading arrangements are illustrated in Figure 4.1. A portable apparatus consisting of a loading frame, pump, ram and cones, as shown in Figure 4.2, was used. This simple point load apparatus is light and has a capacity of 12 tons. The hydraulic pressure gauge connected to the ram was used to measure the failure load required to break the specimen. The diameter and length of all samples were measured to $\pm$ 0.1 *mm* by using a vernier calliper in accordance with ISRM procedures.

4.3.3 Slake durability tests

The slake durability tests have been performed on samples of Ashfield shale using a device similar to that developed by Franklin and Chandra (1972), following the suggested ISRM (1979a) method. The apparatus consisted of an electric motor, a test drum and a slaking trough. The test drum with 2 *mm* standard mesh was a cylinder, 100 *mm* in length and 140 *mm* in diameter, with at one end a solid fixed base and at the other end a solid removable lid. The drum can withstand a temperature of 105°C and it is strong enough to retain its shape during the test. The drum was rotated about a horizontal axis by the electric motor at a speed of 20 revolutions per minute in a trough with the slaking fluid (usually water) to a level of 20 *mm* below the drum axis. This apparatus was constructed according to the dimensions given by Franklin and Chandra (1972) and it is shown in Figure 4.3.

4.4 SPECIMEN PREPARATION

4.4.1 Uniaxial compression tests

To obtain samples for uniaxial compressive strength tests boreholes were drilled by large truck mounted rigs provided by the Roads and Traffic Authority of New South Wales (RTA) at the Ryde interchange site. Details have been given in chapter 3. Cores were also obtained from block samples recovered from an excavation in Surry Hills near the Central railway station in Sydney. Core samples were obtained from the blocks of shale using a drilling machine in the laboratory. The blocks were firmly clamped onto the drilling table so that good quality core specimens could be obtained. Water was used for cooling and flushing during the drilling. All samples were coated with Valvoline Tectyl immediately after coring to prevent moisture content changes. All the core samples were cut to length with a small diamond saw and their

ends were ground by sandpaper to make them smooth and perpendicular to the longitudinal axis according to the ISRM (1981) recommendation.

The diameter of all samples was approximately 52 *mm*. The diameter and height of the specimens were measured with a vernier calliper according to the ISRM suggested methods. The diameter of each specimen was measured to the nearest 0.1 *mm* by averaging two diameters measured at 90 degrees to each other at about the mid height and the upper and lower ends of the specimen. The average diameter was used for the cross-sectional area calculation. The height of each specimen was measured to the nearest 0.1 *mm* by averaging two diametrically opposed height measurements.

4.4.2 Point load tests

The core samples for the point load tests were taken only from the Ryde-interchange. Some of these cores were drilled in the Ryde-interchange area in about 1991 and were brought from the New South Wales Roads and Traffic Authority (RTA) stores for testing in 1993.

In all the diametral tests, core samples with a length to diameter ratio greater than 1.0 were selected for testing and all samples were split along the laminations. In the axial test, core samples with a length to diameter ratio between 0.5 and 1 were chosen for testing perpendicular to the laminations. Suitably sized samples for axial point load tests were obtained either from samples first split by diametral testing or by diamond saw cutting.

4.4.3 Slake durability tests

Samples for this study came from three sites in the Sydney metropolitan area. The majority of the samples were obtained from borehole coring at the Ryde-interchange site in northern Sydney. At the Ryde site the shale varied from

fresh unweathered to highly weathered. Other fresh samples were obtained from blocks of shale obtained from excavations at Moorebank, in western Sydney, and from Surry Hills, near the business centre of the city.

Slake durability tests have been performed on samples varying from fresh intact to highly weathered shale. Tap water and in some tests distilled water at room temperature (about 22°C) were used as the slaking fluid. There was not any significant difference between the results of slake durability, using tap water or distilled water.

4.5 TEST PROCEDURES

4.5.1 Uniaxial compression tests

All specimens tested in uniaxial compression were right circular cylinders with a height to diameter ratio of approximately 2. Each specimen was carefully placed concentrically with the load cell and the base platen. Axial load on the specimen was applied by providing a constant deformation rate such that failure occurred within 5 to 10 minutes of loading. The ISRM (1981) suggested method for determination of the uniaxial compressive strength of rock materials was followed.

4.5.2 Point load tests

The sample preparation and the testing procedures used for point load testing generally followed the suggested methods of the International Society for Rock Mechanics (1985). Each sample of Ashfield shale was placed into the testing apparatus such that the laminations were either parallel or normal to the loading axis.

4.5.2.1 Calculation procedure

The International Society for Rock Mechanics suggested method for calculation of the point load strength index, $I_{s(50)}$, was adopted. The equation used to calculate the point load index is as follows

$$I_s = \frac{P}{D_e^2} \tag{4.1}$$

where D_e, the equivalent core diameter, was given by:

$$D_e^2 = D^2 \quad \textit{for diametral tests;} \tag{4.2}$$

and

$$D_e^2 = \frac{4A}{\pi} \quad \textit{for axial tests;} \tag{4.3}$$

The symbols used in these equations have the following meanings:

P = Failure load

I_s = Uncorrected point load strength index

D = Diameter (distance between loading points in diametral test)

A = L x D, the minimum cross sectional area of a plane through the loading cone contact points.

L = Length (distance between the loading cones in an axial test)

Point load tests in the two directions parallel and perpendicular to the laminations were performed. The strength anisotropy index, the ratio of point load strengths in these two directions, I_a, was measured.

4.5.2.2 Size correction

The test sample shape and size have significant effects on the derived index

value, so in order to obtain a unique point load strength value for the rock sample a size correction must be applied. The results should be corrected to a standard thickness of 50 *mm*. Greminger (1982) found that the size and shape effects in point load testing are independent of the degree of anisotropy and loading direction. The point load strengths are a function of D (in diametral tests) and D_e (in axial tests). In the current work the following equation, as suggested by the International Society for Rock Mechanics (1985), was used for the size correction:

$$I_{s(50)} = F \times I_s \tag{4.4}$$

where:

F = a size correction factor

I_s = uncorrected point load strength

and the size correction factor can be obtained from the following expression:

$$F = \left(\frac{D_e}{50}\right)^{0.45} \tag{4.5}$$

where *De* is measured in *mm*.

For tests on samples near the standard 50 *mm* size, the following approximate expression has also been suggested in the ISRM procedures:

$$F = \left(\frac{D_e}{50}\right)^{0.50} \tag{4.6}$$

In the case of Ashfield shale, the diameter of all samples tested was about 52 *mm*, so equation (4.6) has been used to calculate the size correction.

4.5.3 Slake durability tests

The slake durability sample consisted of ten representative shale lumps, nearly equ-dimensional in size, each with a mass between 40 to 60 grams, to give a

total sample mass of 450 to 550 grams. The following steps describe the test procedure.

(a) The specimens were placed in the drum and oven dried for at least 6 hours to a constant weight at a temperature of 105° C. The weight (A) of the drum plus specimens was recorded and then both were cooled at room temperature for about 30 minutes. The drum containing the specimens was mounted in the trough and coupled to the motor.

(b) The trough was filled with slaking fluid (tap water, or in some tests with distilled water, at 22°C) to a level 20 *mm* below the drum axis, and the drum was rotated at 20 revolutions per minute for ten minutes.

(c) At the end of the test, the drum was removed from the trough and the lid removed from the drum and the drum and the retained portions of the specimen were oven dried (for at least 12 hours) to a constant weight at 105°C. The combined weight was recorded (B).

(d) The retained material was then subjected to a second cycle of slaking and steps (b) - (c) were repeated and the weight (C) of the drum plus the retained portions of the specimen was recorded. For more cycles, the above procedure was repeated.

(e) The drum was brushed clean and its weight (D) was recorded.

(f) The slake-durability index was calculated as the percentage ratio of the amount of shale remaining after each cycle to the initial dry sample weight as follows:

$$I_{d2} = \frac{C-D}{A-D} \times 100\% \qquad (4.7)$$

where:

I_{d2} = Slake-durability index (second cycle)

The second cycle slake-durability index was proposed by Gamble (1971) for use in rock classification. The samples of Ashfield shale were further characterised by their first, third and fourth cycles for evaluating the effects of the number of cycles and slaking duration on the slake-durability indices.

4.6 UNIAXIAL COMPRESSION TEST RESULTS

The experimental programme was designed (Table 4.1) to characterise the uniaxial compressive strength of the Ashfield shale, to assess the relationship between uniaxial compressive strength and various other physical and mechanical properties, and to assess the anisotropic behaviour of the Ashfield shale. The anisotropic behaviour of the Ashfield shale will be discussed in detail in Chapter 5.

4.6.1 Results of tests with axial loading perpendicular to the laminations

From a total of 150 samples from this study and other sources (Ghafoori et al., 1993), the measured *UCS* values ranged from 1.8 to 60.2 *MPa*. Thirty four of the samples were classified as fresh Ashfield shale and they had *UCS* values ranging from 12.7 to 60.2 *MPa*. The mean strength for this latter group of samples was calculated to be 28.2 *MPa*, with a standard deviation of 14.1 *MPa*. This distribution of strengths for the fresh samples agrees well with previously published data by Burgess (1977), Chesnut (1983) and Won (1985). Figure 4.4 presents the *UCS* data for Ashfield shale in the form of a histogram chart.

4.6.2 Distribution of *UCS* test results

The distribution of *UCS* test results is presented in Figure 4.5, using the classification into strength groups suggested by the International Society of Rock Mechanics (1972). According to this classification the fresh Ashfield shale samples may be described as predominantly a moderately strong to strong rock.

4.6.3 Correlation of *UCS* with other physical properties

4.6.3.1 Moisture content

It has been well established that the moisture content in argillaceous rocks such as mudstone and shale can significantly affect their physical and mechanical properties. The results reported in this section have been obtained from Ashfield shale samples from many locations in the Sydney Basin, with geological descriptions ranging from intact to highly weathered. For these samples the moisture contents were in the range from 1.12% to 8.76%. The mean moisture content of all samples was calculated to be 3.85%, with a standard deviation of 1.8%. A plot of *UCS* versus moisture content is shown in Figure 4.6. This graph indicates that *UCS* decreases with an increase in the moisture content, which is consistent with previous findings for other shales (Salustowicz, 1965; Colback and Wiid, 1965; Jumikis, 1966; Burshtein, 1969; Van Eeckout, 1976).

As shown in Figure 4.6, the relationship between *UCS* and moisture content appears to be exponential. A small increase in moisture content causes a large reduction in *UCS*. The variations shown on this figure are described well by the following equation:

$$UCS = 600 p_a e^{-0.415 m_c} \qquad \textbf{(4.8)}$$

in which

m_c = moisture content (%), and

p_a = atmospheric pressure (0.1 *MPa* or 14 lb/in^2).

Regression analysis shows that equation (4.8) fits the data with a correlation coefficient of $r^2 = 0.93$. A total of 53 data points, with known moisture content and *UCS*, were used in this study and the standard deviation was $25 p_a$.

Because of the closeness of this correlation and because the natural moisture content of a shale sample is a relatively simple parameter to determine in practice, equation (4.8) provides an indirect but very convenient means of estimating *UCS* for Ashfield shale. These results demonstrate that a simple classification based on the natural moisture content, an easily measured quantity, could be adopted for the Ashfield shale. The fresh shale samples from Surry Hills and Moorebank had lower moisture contents and higher strengths than the samples from the Ryde site.

4.6.3.2 Unit weight

It is also of interest to investigate the relationship between the density (unit weight) and other mechanical properties of the intact rock. The mechanical properties of the intact rock can be expected to depend on the unit weight, as the strength has been shown previously to be simply related to the moisture content. Figure 4.7, based on the data accumulated in this study, shows a clear curvilinear relationship between the *UCS* and dry unit weight for Ashfield shale, in which the *UCS* generally increases with the dry unit weight. The variation shown on the figure is best described by the following equation:

$$UCS = 2.05\times10^{-4}\left[e^{5.38(\gamma_d/\gamma_w)}\right] p_a \qquad \textbf{(4.9)}$$

where

γ_d = the dry unit weight of the rock (also known as the dry density),

γ_w = the unit weight of water

p_a = is atmospheric pressure (0.1 *MPa* or 14 lb/in^2).

Regression analysis shows that equation (4.9) fits the data with a correlation coefficient of $r^2 = 0.77$. A total of 60 data points were used in this study and the standard deviation was 45.5 p_a.

The dry unit weight of the shale samples considered here ranged from 2.15 to 2.7 t/m^3, and the mean dry unit weight was calculated to be 2.47 t/m^3, with a

standard deviation of 0.11 t/m^3.

4.7 POINT LOAD TEST RESULTS

4.7.1 Axial point load tests

A total of 237 axial point load tests were performed on core specimens from the Ryde site which had different degrees of weathering. Because of the laminations, it was found that the samples with a length to diameter ratio of 1.1 as suggested by Broch and Franklin (1972) either rotated between the loading cones of the test equipment or broke at the edges of the sample. Consistent results were obtained when the length to diameter ratio was between 0.6 to 0.7. The axial point load results varied between 2.92 *MPa* for fresh to 0.05 *MPa* for highly weathered Ashfield shale. For 191 fresh to slightly weathered samples, the axial point load indices were in the range from 2.92 to 0.25 *MPa*. The mean axial point load strength of all these samples was calculated to be 1.02 *MPa*, with a standard deviation of 0.6 *MPa*.

4.7.2 Diametral point load tests

A total of 152 diametral point load tests were performed parallel to the lamination planes. In this case, the core samples were split in their weakest direction. Core specimens with length to diameter ratios greater than 1 were used for these tests. The distance L between the contact loading point and the nearest free end (Figure 4.2) was chosen to be at least 0.7 times the core diameter for the majority of the samples.

The diametral point load results varied between 1.07 *MPa* for fresh to 0.03 *MPa* for highly weathered Ashfield shale. For 66 fresh to slightly weathered samples of Ashfield shale the diametral point load strengths were in the range

from 1.07 to 0.18 *MPa*. The mean diametral point load strength of all these samples was calculated to be 0.61 *MPa*, with a standard deviation of 0.22 *MPa*.

4.7.3 Distribution of point load test results

The distributions of axial and diametral point load strength test results are presented in Figures 4.8 and 4.9, respectively. The classification into strength groups based on values of the point load strengths is that suggested by the International Society of Rock Mechanics (1972). According to this classification the fresh to slightly weathered Ashfield shale samples may be described as predominantly a moderately strong to strong rock.

4.7.4 Effect of *L/D* ratio on axial point load strength

A series of tests was performed to study the effect of *L/D* ratio on the axial point load strength index of the Ashfield shale core samples, each with a diameter of about 52 *mm*. A summary of the results obtained for this series of tests is presented in Table 4.2. The results are shown graphically in Figure 4.10. This graph indicates that the axial point load strength generally decreases with an increase of the thickness to diameter (*L/D*) ratio. Similar effects of *L/D* ratio on axial point load have also been described by Broch and Franklin (1972) and Forster (1983). It has previously been reported (e.g. Greminger, 1982; Tsidzi, 1989) that I_s values are unreliable when the specimen thickness is less than 35 *mm*. This corresponds to $L/D=0.67$ for the 52 *mm* specimens used in this study. As a results no tests were performed on samples less than 35 *mm* thick.

4.7.5 Comparison of point load index and *UCS*

To compare the results of the point load tests with those of uniaxial compression tests on Ashfield shale, twenty core samples with length to diameter of 2 were also prepared for uniaxial compression testing. The off-cuts of these cores were used

for axial and diametral point load tests. The uniaxial compressive strengths perpendicular to the bedding plane ($\beta=90°$) and the results of the diametral and axial point load tests for these twenty samples and data from other sources (Ghafoori et al., 1993) are given in Table 4.4. Correlations have been made between the point load strengths and the measured values of uniaxial compressive strength from these tests and other sources. Figures 4.11 and 4.12 show the uniaxial compressive strength plotted against the axial and diametral point load strength indices, respectively, for all the results obtained from this and other sources (Ghafoori et al., 1993). These figures show straight line relationships with average correlation factors of 24.1 and 38.2 between the axial and diametral point load strengths and the uniaxial compressive strength, respectively. Regression analysis shows that the correlation coefficients are 0.85 and 0.87, respectively.

4.7.6 Measurement of strength anisotropy

The Ashfield shale samples that were used for point load tests had been cored perpendicular to the bedding planes. Each sample was placed into the point load apparatus such that the lamination was either parallel or perpendicular to the loading axis. To find the strength anisotropy in point load tests, forty eight core samples with diameters of about 52 *mm* were tested with point loading in the direction of the laminations, and a further forty eight with point loading in the direction perpendicular to the laminations.

For anisotropic rocks, both the axial and diametral point load tests were suggested by Broch and Franklin (1972) to estimate the strength anisotropy, using the anisotropy index (I_a) where,

$$I_a = \frac{I_s\ (axial)}{I_s\ (diametral)} \qquad \textbf{(4.10)}$$

Table 4.3 shows the results of point load tests conducted parallel and perpendicular to the laminations. As this table shows, there is clear evidence of the influence of lamination, the primary anisotropic fabric, on the point load strength of Ashfield shale. The point load strength index $I_{s(50)}$ values obtained when the samples were tested diametrally, parallel to the laminations were always less than the values obtained for samples tested axially perpendicular to the laminations. The strength anisotropy, I_a, the ratio of point load strength in the strongest and weakest directions was measured for the samples tested in these two directions. From a total of 48 samples, the strength anisotropy index considered here ranges from 3.18 to 1.16 and the mean strength anisotropy index was calculated to be 2 with a standard deviation of 0.5. However, from the correlations with *UCS* a ratio of $I_a = 1.6$ can be determined. The difference between the anisotropy ratios from the individual point load test results and from the correlations with *UCS* results indicates the difficulty of determining the anisotropy from point load tests. This is probably caused by natural variability in the samples which can be expected to be more significant in the smaller point load tests samples.

With this kind of rock, failure normally tended to occur along the bedding planes rather than through the rock substance. Pells (1975) found that it was not practicable to use diametral $I_{s(50)}$ results to obtained *UCS* values for highly anisotropic sandstone. For the shale the scatter in the relation between I_{sd} and I_{sa} and *UCS* is similar, suggesting that either index could be used. However, single tests cannot be relied on to determine *UCS* and this is likely to limit the usefulness of these index tests.

4.8 SLAKE DURABILITY TEST RESULTS

Tests were performed on four sub-samples of four fresh Ashfield shale specimens from the Ryde site to investigate the effect of slaking time on the durability

results. The test results are summarised in Table 4.5. The relationship between slaking time and the slake durability index is shown in Figure 4.13. The rate of slake loss was found to be nearly linear for these fresh samples, but different samples showed variable resistance to slaking. The longer periods of slaking time in each cycle improved the discrimination between the shale samples.

To investigate the effects of numbers of cycles on the durability of Ashfield shale, tests were performed on eight samples with varying degrees of weathering from the Ryde site. In these tests a constant slaking time of 10 minutes was used in each cycle. The results are summarised in Table 4.6. The effect of increasing numbers of cycles of wetting and drying is shown in Figure 4.14. This shows that the percentage of the samples retained decreases steadily with number of cycles, and decreases with increasing degree of weathering.

Different procedures have been recommended for classifying the durability of shales from these tests. For the Ashfield shale two ten minute cycles, as suggested by Gamble (1971), give reasonable distinction between the samples, but the single cycle results, as suggested by Franklin and Chandra (1972), are less satisfactory. However, if the time for the wetting phase of the cycle is increased good distinction can be obtained from a single cycle (Figure 4.13).

A series of tests was performed on fresh Ashfield shale from three sites in the Sydney metropolitan area. Table 4.7 shows the effects of slaking on samples of fresh shale from these three different sites. The test results are also shown graphically in Figure 4.15. It can be seen that the durability of "fresh" shale is not constant but varies slightly from location to location.

Following the classification scheme established by Gamble (1971) and Franklin and Chandra (1972), these results indicate that the durability of Ashfield shale varies from high for fresh intact material to low for highly weathered material. The high durability of fresh Ashfield shale is consistent with the

mineralogical assessment (chapter 3) and in particular with the absence of smectitic clays. The mineralogical investigations revealed that the Ashfield shale from the Ryde site consisted of finer grains and contained a slightly lower quartz and higher clay content than from the other sites. This may explain the difference in the durabilities of the fresh shales.

4.8.1 Correlation of slake durability with other engineering indices

4.8.1.1 Atterberg limits and slaking durability

A quantitative slaking test in combination with the Atterberg limits has been suggested (Gamble, 1971) as a useful way of classifying argillaceous rocks for engineering purposes. Figures 4.16 (a and b) and 4.17 (a and b) show plots of liquid limit and plasticity index versus one and two cycles slake durability indices of Ashfield shale. The figures show a clear correlation between the slake durability index and the liquid limit for the Ashfield shale, with increasing liquid limit and plasticity index associated with a reduction in slake durability.

4.8.1.2 Durability - plasticity classification

Following the scheme proposed by Gamble (1971) the Ashfield shale would be classified as follows. The fresh Ashfield shale from the Ryde-interchange site would be classified as a medium high durability - low plasticity shale; the slightly to moderately weathered Ashfield shale from this site would be classified as a medium durability -low plasticity shale; the Ashfield shale from the other two sites (Surry Hills and Moorebank) would be classified as a very high durability - low plasticity shale.

4.8.1.3. Natural water content

It has been well established that the moisture content in the Ashfield shale can

have significant effects on its engineering behaviour. A good correlation has been shown to exist between uniaxial compressive strength and natural water content for a large number of samples from different locations with different degrees of weathering (Figure 4.6). This correlation indicates that the uniaxial compressive strength decreases with an increase in the moisture content, as might be expected.

The fresh shale samples from Surry Hills and Moorebank had lower moisture contents and higher strengths than the samples from the Ryde site, and as noted above the former samples were more durable. Figure 4.18 shows the relation between natural water content and the 2 cycle slake durability index. This figure shows a clear trend of increasing water content being associated with reducing durability of the Ashfield shale. The durability decreases as the natural water content increases. These results again demonstrate that a simple classification based on the natural moisture content, an easily measured quantity, could be adopted for Ashfield shale.

Figure 4.19 presents the variation of the 2 cycle slake durability index versus clay fraction less than 2 microns for highly weathered to fresh Ashfield shale. Figure 4.19 shows that the increasing clay fraction, which is normally related to increasing porosity, is associated with decreasing durability, as expected.

4.8.2 Discussion

The mineralogy of Ashfield shale has been described in detail in chapter 3. The predominant clay minerals recorded in this study and by earlier researchers are mainly kaolin and illite. In the Ashfield shale breakdown due to clay minerals should be low compared to other shales. Calcite is relatively rare and the most common carbonate is siderite which occurs most commonly as finely disseminated particles and not as a matrix cement.

Bedding planes or stratifications are the most common structure in sedimentary rocks. Normally this structure may give rise to a plane of weakness. Bedding planes or laminations also occur in argillaceous rocks. The interaction between shale and water can be regarded as the main reason for shale deterioration. A study of Ashfield shale has revealed that the laminations occur because of alternating coarse and fine grained materials. Because of a lack of the expansive clay minerals, the swelling in the Ashfield shale is thought to be due to the uptake of water between grains along the interfaces of the laminations and to thus be controlled by the fabric. This suggestion is consistent with the observation that the samples one easily broken along the laminations. Negative pore pressure following the desiccation of the shale may also contribute to the fractures parallel to the laminations. It has been noted (e.g. Kennard et al., 1967; Taylor and Spears, 1970) that these fractures are the main cause of the breakdown of shale samples parallel to laminations.

4.9 EFFECT OF WEATHERING ON INDEX TESTS

Some data for Ashfield shale with different degrees of weathering have been obtained from different sources (Ghafoori et al., 1993). The determination of the degree of weathering for each sample was made by the various engineering geologists and geotechnical engineers during site investigations. The weathering grades reported here have been taken directly from the borehole logs, and these have generally been determined according to the definitions in Table 3.6. The influence of weathering processes on the engineering properties of Ashfield shale have also been determined and are described in this chapter.

4.9.1 Relationship between UCS and weathering grade

The relationship between *UCS* and weathering grade is shown in Figure 4.20. As expected, Figure 4.20 shows that the average value of the *UCS* decreases with the degree of weathering, but there is an indication that the range of strengths for each weathering class also reduces with the degree of weathering. The reasons for this variation in the strength ranges may be because of a wide range of moisture contents or porosities due to small changes in the mineralogy. This indicates how difficult it is for the field geologist to discriminate between the various grades of weathering, particularly grades 1 and 2.

Pells et al. (1978) categorised the Ashfield shales into five classes on the basis of the uniaxial compressive strength (*UCS*) and the degree of fracturing. Hadfield (1981) later defined three weathering zones for these shales, which incorporated the classification of Pells et al. The resulting classification system was shown in Table 2.1 Chapter 2.

From this study it has been found that the rock classifications recommended by Pells et al. (1978) for Ashfield shale are still useful classification for design purposes. In the present study it is suggested that the natural moisture content of the shale is a useful index for determining other engineering properties, especially the strength of the intact rock. The important correlation over the range of moisture contents has been summarised in equation (4.8), and the strength of the intact rock could be determined from this equation. It may prove that this equation is useful in practice during the preliminary stages of design of structures upon, or in, the Ashfield shale. Another important parameter in Ashfield shale to be considered is the anisotropy due to the laminations. More details about this behaviour are discussed in the following chapters.

4.9.2 Relationship between point load strength index and weathering grade

The relationships between axial and diametral point load strengths and weathering grade are shown in Figures 4.21 and 4.22, respectively. A clear relationship between axial and diametral point load strength and weathering grade is depicted. As expected, the average value of the axial and diametral point load strengths decrease with the degree of weathering (Figures 4.21 and 4.22), but there is an indication that the range of strengths for each weathering class also reduces with the degree of weathering. The general decrease of both measures of the point load strength index with weathering grade reflects the trend observed for the uniaxial compressive strength data (Figure 4.20).

4.9.3 Relationship between slake durability and weathering grade

Some tests were run on Ashfield shale from Ride site with different degrees of weathering to check the effect of weathering on the durability results. The relationship between weathering grade and slake durability index is shown in Figure 4.23 which shows that the percentage of the samples retained decreases steadily with increasing degree of weathering.

Trends in the data (though widely scattered) suggest correlations may exist between the degree of weathering and the engineering properties of this material. However, natural moisture content or porosity appears to provide better predictions of the behaviour than the more subjective geological definitions of weathering. Definitions of the various grades of weathering are based on visual assessment of the rock samples in the field. The scattered data may indicate how difficult it is for the field geologist to discriminate between the various grades of weathering, particularly fresh to slightly weathered samples.

4.10 CONCLUSION

4.10.1 Uniaxial compressive strength

From this and previous studies it is concluded that generally the fresh Ashfield shale can be categorised as moderately strong to strong rock, according to the engineering classification of intact rocks proposed by the ISRM (1972). The data described in this chapter have enabled an investigation of the correlations between various engineering properties of Ashfield shale. It is suggested that the natural moisture content of the shale is a useful index for determining other engineering properties, especially the strength of the intact rock. A range of natural moisture contents from 1.12 to 8.76% has been investigated for fresh to highly weathered samples of shale. The important correlation over this range has been summarised in equation (4.8), and it may prove to be useful in practice during the preliminary stages of design of structures upon or in the Ashfield shale. It is not known whether this correlation also applies outside the range of moisture contents investigated. Indeed, caution should be exercised in the use of equation (4.8) beyond this range. The variation of strength with moisture content is more related to changes in the porosity of the samples than to changes in the degree of saturation. The samples were saturated at their in-situ moisture content.

A correlation has been made between the dry unit weight and the measured values of *UCS*. There is a curvilinear relationship between the *UCS* and dry unit weight for Ashfield shale, in which the *UCS* generally increases with the dry unit weight, see equation (4.9). Although this correlation is less accurate than the correlation with moisture content, it does not require the assumption that the samples are saturated.

4.10.2 Point load indices

The point load strength test is a simple, relatively quick and inexpensive method for determination of rock strength and the strength classification of rock materials. According to the ISRM classification scheme most of the samples considered in this study were of moderately strong to strong rock. The general decrease of both measures of the point load strength index with weathering grade was observed, and this is consistent with the trend observed for the uniaxial compressive strength. There is a consistent variation in the axial point load with respect to the thickness to diameter (*L/D*) ratio. The axial point load strength generally decreases with an increase in *L/D* of sample.

The point load test is widely used to determine the uniaxial compressive strength indirectly. Correlations have been made between the point load strengths and the measured values of uniaxial compressive strength in direction perpendicular to laminations. Average correlation factors of 24.1 and 38.2 with correlation coefficients of 0.85 and 0.87 are indicated between the axial and diametral point load strengths and the uniaxial compressive strength, respectively. However, owing to the scatter in the data the point load tests do not appear to be reliable for estimating *UCS* values.

Primary anisotropic fabric such as lamination has a significant effect on the engineering behaviour of Ashfield shale. The strength anisotropy index has been defined as the ratio of values of $I_{s(50)}$ measured perpendicular and parallel to the laminations. For Ashfield shale the strength anisotropy index varies between 3.18 and 1.16 with a mean of 2 and a standard deviation of 0.5, But from the correlations with *UCS* a lower value of 1.6 was determined

4.10.3 Durability

There is a clear correlation between the slake durability index and the liquid limit for the Ashfield shale, with increasing liquid limit, and plasticity index, associated with a reduction in slake durability. Correlations between the durability, strength and natural moisture content of the Ashfield shale have been demonstrated, with durability and strength increasing with decreasing moisture content.

The effect of weathering is to increase the clay and moisture contents and thereby reduce the strength and durability. However, different fresh unweathered shales had different moisture contents and different strengths and durabilities.

The variability of the natural moisture content can be correlated with mineralogical factors. Increasing moisture content was associated with increasing clay content (particles less than 2 microns) and in turn this was associated with an increase in plasticity index and plastic and liquid limits. The higher strengths and durabilities of some fresh shales were associated with higher quartz contents. The natural moisture content has been found to be a good predictor of the durability, strength, index properties and clay content of the shale.

Table 4.1 Summary of the test programme

Type of test	No. of test	Aim of test
Uniaxial compressive test	150	To find the mean strength and relationship with moisture content, dry unit weight and weathering grade ($\beta = 90°$)
Axial point load test	34	To find correlation factor with *UCS*
	155	To investigate the effect of weathering on axial point load strength
	48	To investigate the strength anisotropy
Diametral point load test	41	To find correlation factor with *UCS*
	63	To investigate the effect of weathering on diametral point load strength
	48	To investigate the strength anisotropy
Slake durability test	60	To investigate the deterioration of the Ashfield shale from cycles of wetting and drying

Table 4.2 Effect of length to diameter ratio (L/D) on axial point load strength

Specimen No.	$I_{sa(50)}$	L/D	Specimen No.	$I_{sa(50)}$	L/D
RSH1	1.03	1.22	RSH14	1.60	0.84
RSH2	1.14	1.20	RSH15	1.90	0.84
RHS3	1.15	1.13	RSH16	1.95	0.83
RHS4	1.33	1.09	RSH17	1.97	0.82
RHS5	1.24	0.99	RSH18	1.84	0.78
RSH6	1.22	0.97	RSH19	1.91	0.75
RSH7	1.36	0.95	RSH20	1.78	0.74
RSH8	1.65	0.91	RSH21	1.95	0.73
RSH9	1.36	0.90	RSH22	1.99	0.71
RSH10	1.54	0.90	RSH23	2.24	0.7
RSH11	1.69	0.88	RSH24	2.26	0.69
RSH12	1.57	0.87	RSH25	2.10	0.67
RSH13	1.80	0.85	-	-	-

Table 4.3 The strength anisotropy index, I_a, for Ashfield shale

Specimen No.	$I_{sd(50)}$	$I_{sa(50)}$	I_a
RS1	0.85	2.36	2.8
RS2	0.82	1.87	2.28
RS3	0.68	2.07	3.04
RS4	0.82	1.58	1.93
RS5	0.69	1.62	2.37
RS6	1.03	2.95	2.88
RS7	1.02	2.45	2.4
RS8	1.02	2.28	2.23
RS9	0.82	1.91	2.33
RS10	0.82	2.13	2.60
RS11	1.79	2.64	2.60
RS12	0.82	1.93	2.35
RS13	1.02	1.92	1.88
RTS1	1.50	1.89	1.93
RTS2	1.03	2.4	2.34

Table 4.3 The strength anisotropy index, I_a, for Ashfield shale (continued)

Specimen No.	$I_{sd(50)}$	$I_{sa(50)}$	I_a
RTS3	1.02	2.77	2.70
RTS4	1.36	2.13	1.57
RTS5	0.83	2.15	2.60
RTS6	1.71	2.86	1.67
RTS7	1.23	2.24	1.82
RTS8	0.82	2.57	3.13
RTS7	1.03	2.35	2.29
RTS8	0.69	2.18	3.18
RTS9	1.15	2.52	2.18
RTS10	1.15	2.16	1.87
RTS11	1.02	1.76	1.72
RTS12	1.02	1.65	1.62
RTS13	0.95	1.64	1.72
RTS15	1.16	2.52	2.17
RTS16	1.22	2.15	1.76
RTS17	1.30	2.21	1.70
LS1	0.50	0.70	1.40
LS2	0.50	0.60	1.20
LS3	0.43	0.58	1.35
LS4	0.043	0.83	1.93
LS5	0.40	0.80	2.00
LS6	0.40	0.60	1.50
LS7	0.40	0.53	1.33
LS8	0.57	0.66	1.16
LS9	0.65	0.80	1.23
LS10	0.30	0.60	2.00
LS11	0.90	1.30	1.44
L312	0.61	1.06	1.74
LS13	0.64	1.23	1.92
LS14	0.39	0.70	1.79
LS15	0.05	0.11	2.20
LS16	018	0.35	1.94
LS17	0.90	1.60	1.77

Table 4.4 *UCS* and axial and diametral point load test results

Specimen No.	*UCS* (MPa)	$I_{sd(50)}$ (MPa)	$I_{sa(50)}$ (MPa)	*Specimen No.*	*UCS* (MPa)	$I_{sd(50)}$ (MPa)	$I_{sa(50)}$ (MPa)
RTA1	59.80	2.19	1.70	RTA19	34.34	0.95	1.64
RTA2	62.89	2.4	1.71	RRS1	19.00	-	0.60
RTA3	45.36	2.36	1.03	RR32	21.00	0.31	0.68
RTA4	63.25	2.71	1.72	RRS3	15.00	0.58	0.78
RTA5	50.00	2.10	1.02	RRS4	21.00	0.38	0.60
RTA6	30.84	1.51	0.83	RRS5	23.00	0.42	0.50
RTA7	62.65	2.30	1.71	RRS6	20.00	0.53	0.77
RTA8	59.87	2.13	1.49	RRS7	1.80	0.28	0.35
RTA9	51.56	1.89	1.03	RRS8	3.00	0.16	0.35
RTA10	49.88	2.17	1.23	RRS9	19.60	0.65	0.89
RTA11	39.50	1.65	1.16	RRS10	21.70	0.53	1.17
RTA12	63.60	2.10	1.38	RRS11	27.00	0.62	1.88
RTA13	66.60	2.78	1.74	RRS12	30.90	1.00	1.63
RTA14	58.43	2.61	1.36	RRS13	35.60	1.00	1.78
RTA15	66.96	2.26	1.74	RRS14	34.00	-	1.50
RTA16	53.61	2.17	1.50	RRS15	31.00	0.57	1.40
RTA17	51.56	2.15	1.02	RRS16	35.30	1.00	-
RTA18	56.76	2.27	1.22	RRS17	41.80	1.21	-

Table 4.5 Effect of slaking time on slake durability for the Ashfield shale

Slake durability cycle time (minute)	Slake durability index (% retained)			
	Sample Numbers			
	S1	S2	S3	S4
10	97.73	95.31	99.1	97.9
20	95.28	89.76	98.55	96.6
30	93.49	86.21	97.46	95.43
40	89.72	78.37	96.53	93.72

Table 4.6 Effect of degrees of weathering on slake durability of Ashfield shale

Sample Numbers	Degree of weathering	Slake durability index (% retained)			
		No. of slaking cycles			
		1	2	3	4
SN1	Fresh	96.52	93.86	90.93	88.33
SN2	Fresh	98.10	94.22	90.96	88.48
SN3	Slightly weathered	92.80	83.70	73.50	64.27
SN4	Slightly weathered	95.30	87.60	75.90	64.60
SN5	Moderately weathered	80.00	54.90	40.50	26.12
SN6	Moderately weathered	88.03	62.64	41.60	28.30
SN7	Highly weathered	66.55	36.43	18.80	17.70
SN8	Highly weathered	66.50	40.91	27.48	19.48

Table 4.7 Durability of Ashfield shale from three different sites

No. of cycles	Ryde Samples		Moorebank Samples		Surry Hills Samples	
	1	2	1	2	1	2
1	98.1	96.52	99.05	99.12	99.27	99.23
2	94.22	93.86	98.34	98.41	98.68	98.62
3	90.96	90.93	97.82	97.84	98.21	98.21
4	88.48	88.33	97.15	97.17	97.66	97.64

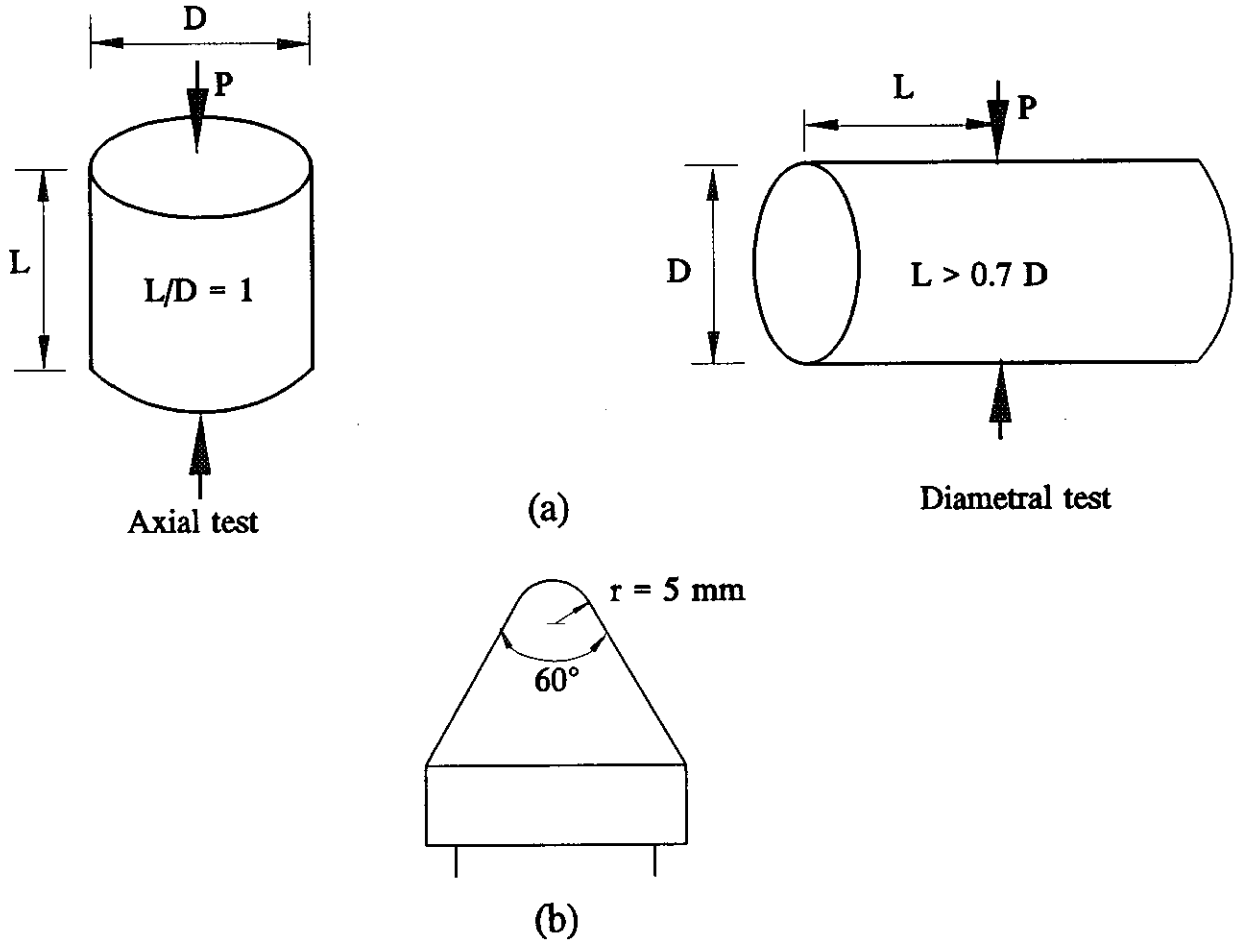

Figure 4.1 (a) Details of the point loading

(b) Dimensions of the standard loading cone

Figure 4.2 A simple portable point load test apparatus

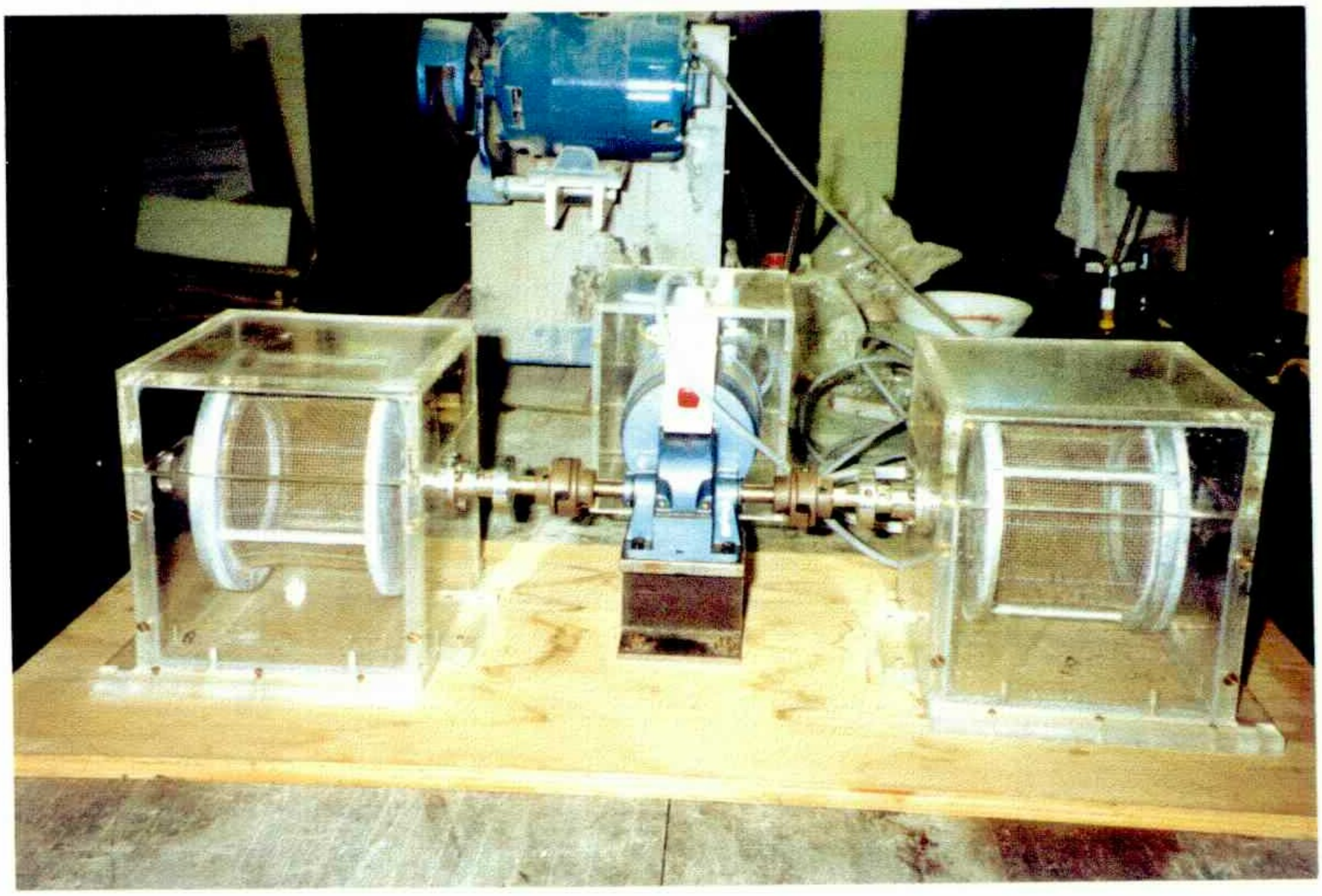

Figure 4.3 Slake durability testing equipment

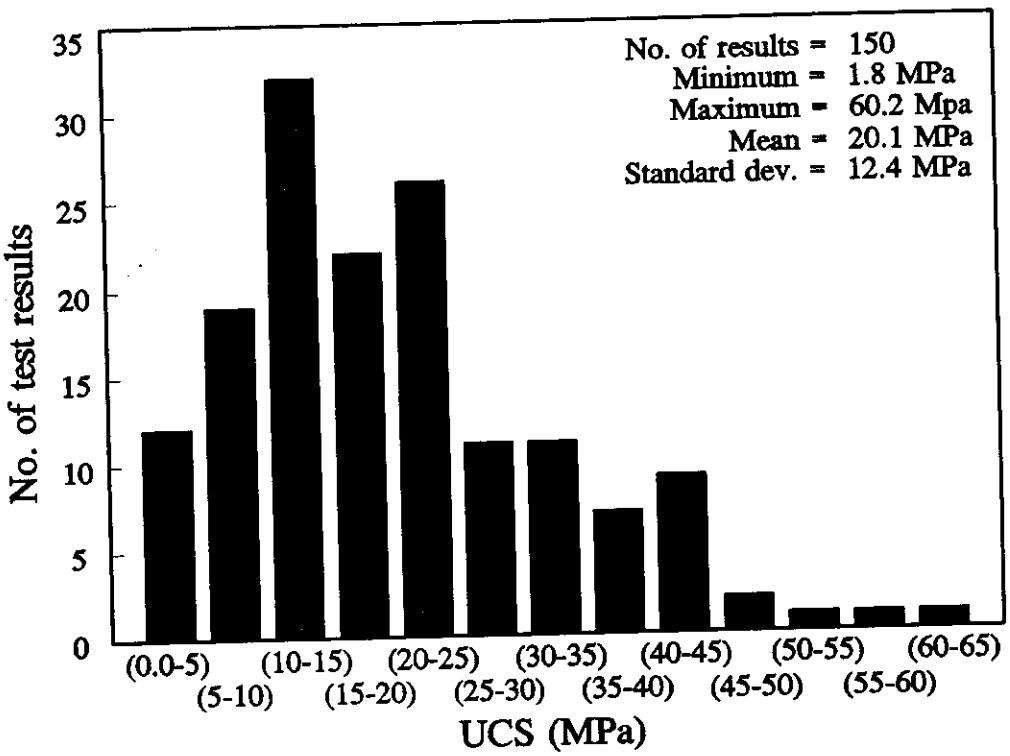

Figure 4.4 Histogram of UCS data for Ashfield shale

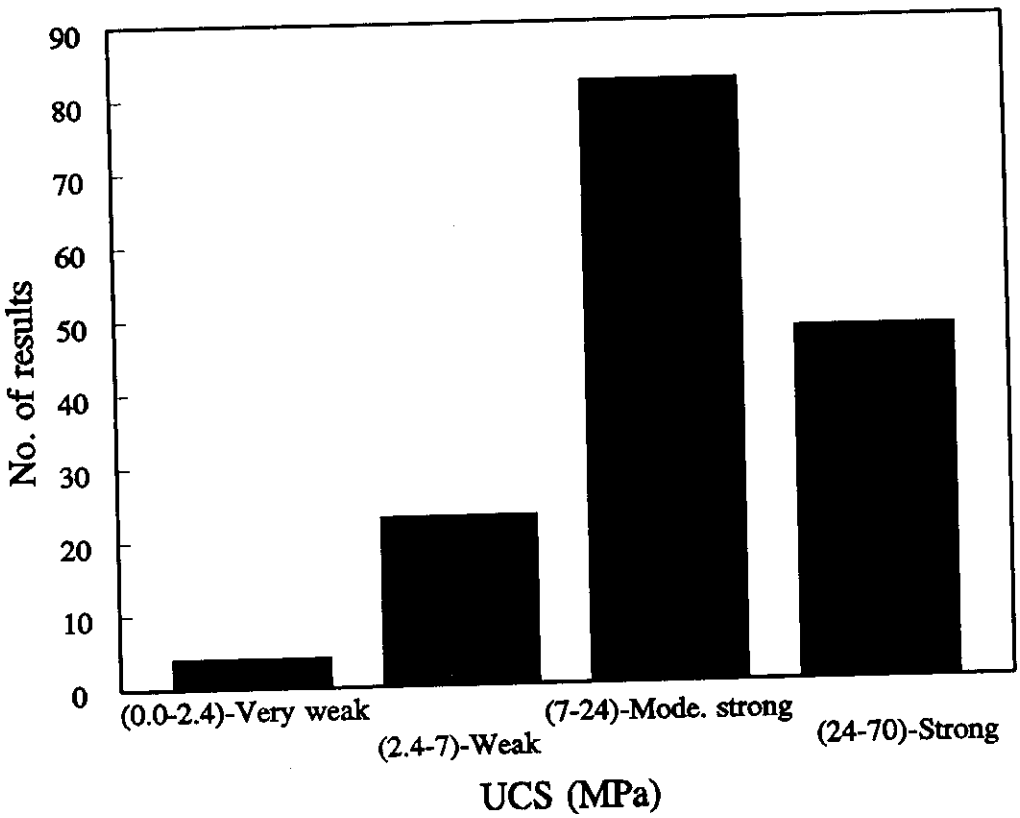

Figure 4.5 Distribution of UCS values for Ashfield shale

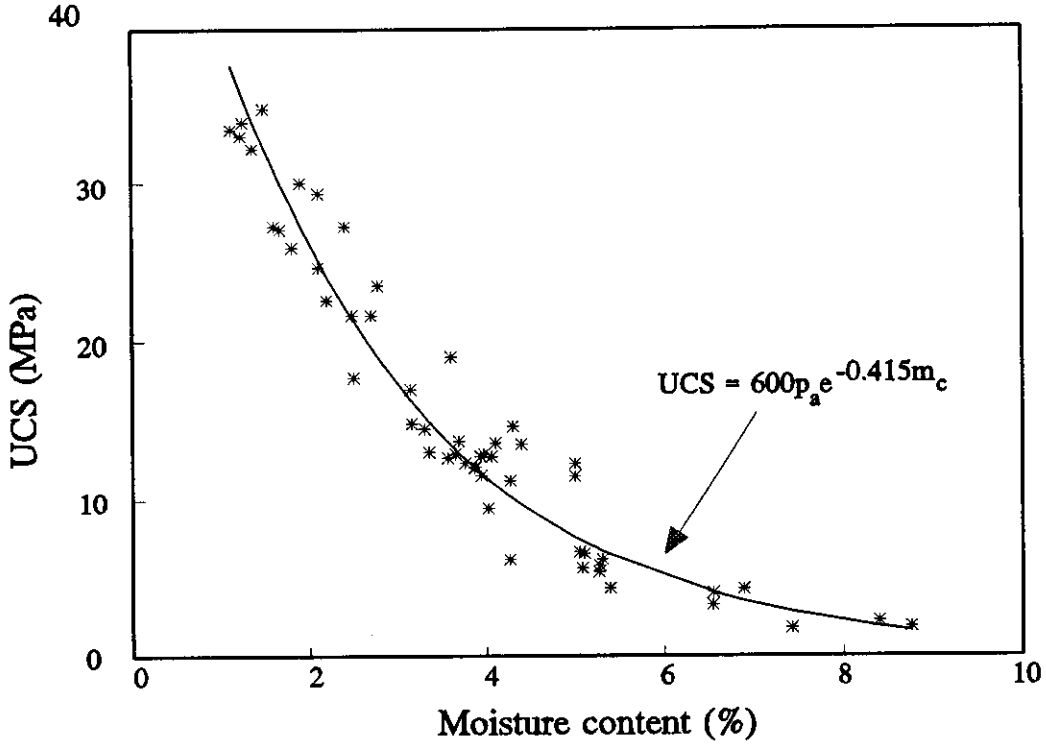

Figure 4.6 UCS versus moisture content for Ashfield shale

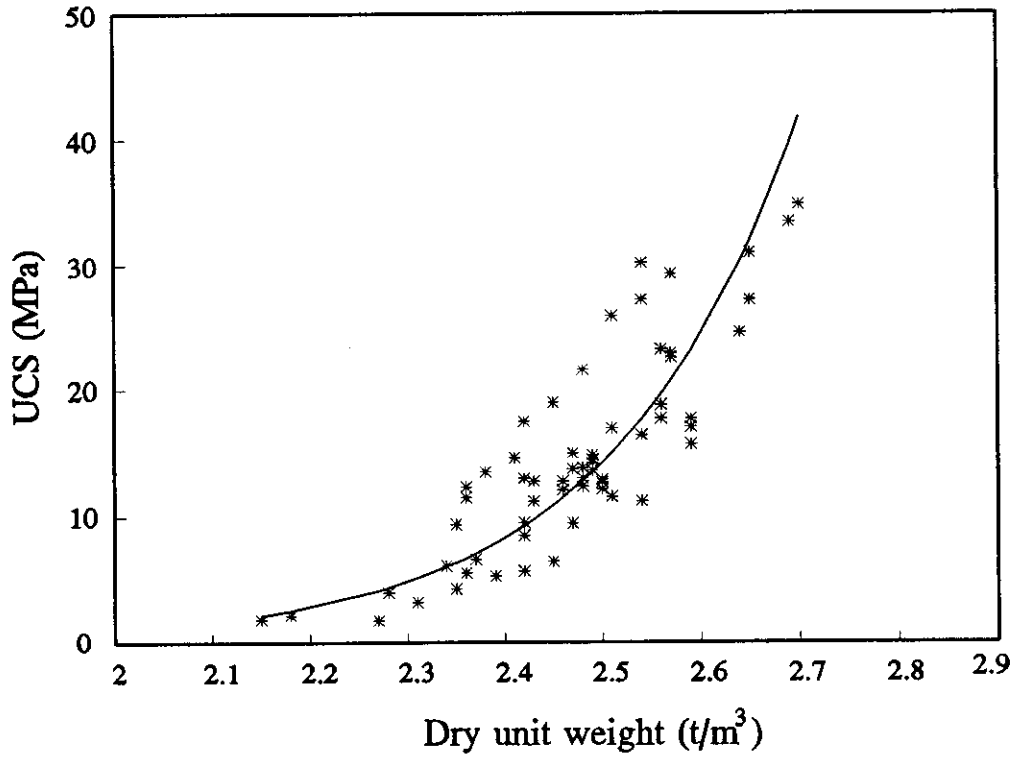

Figure 4.7 UCS versus dry unit weight for Ashfield shale

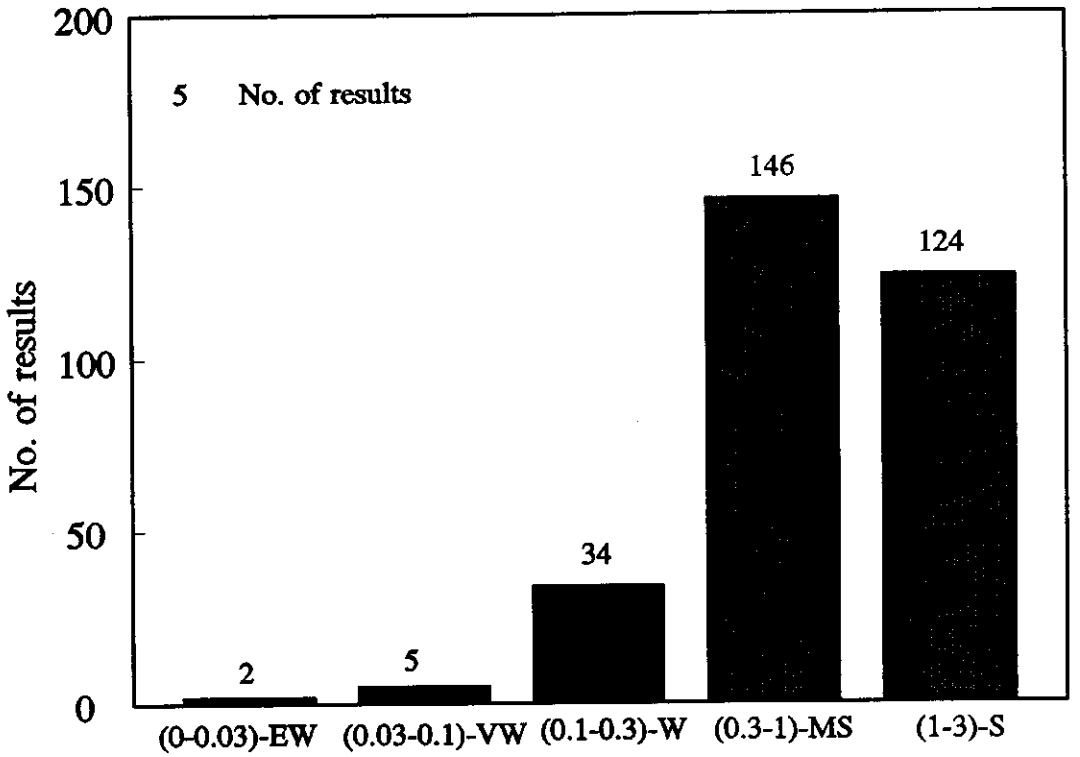

Axial point load strength index (MPa)

Figure 4.8 Distribution of axial point load strength index

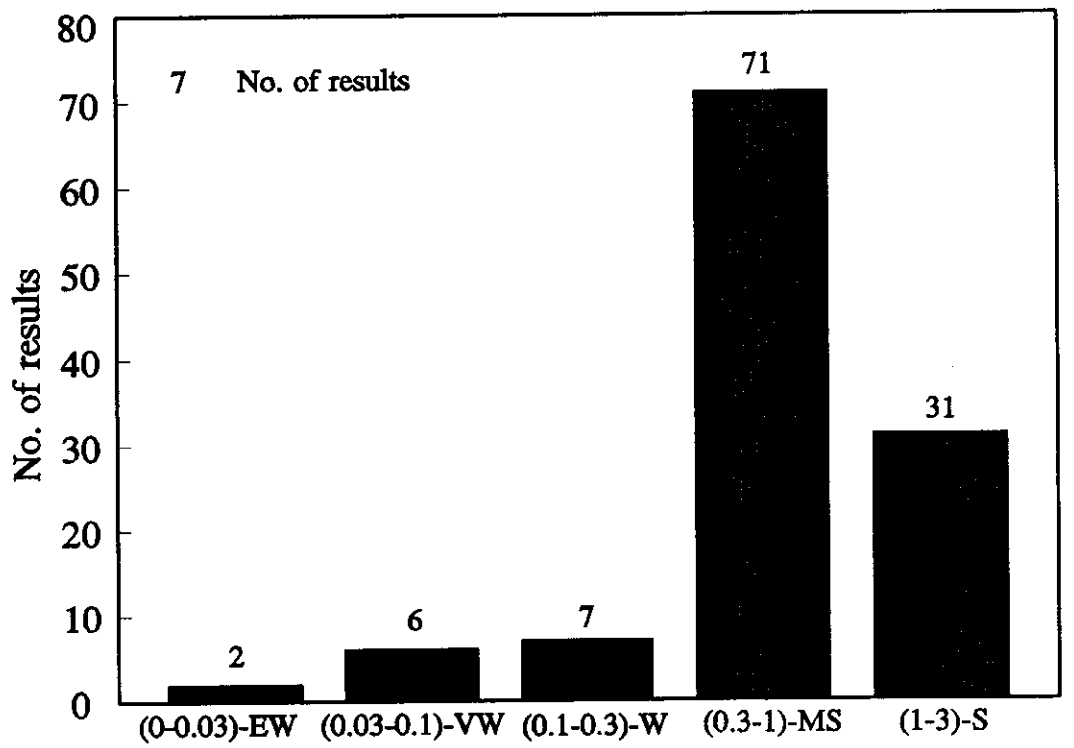

Diametral point load strength index (MPa)

Figure 4.9 Distribution of diametral point load strength index

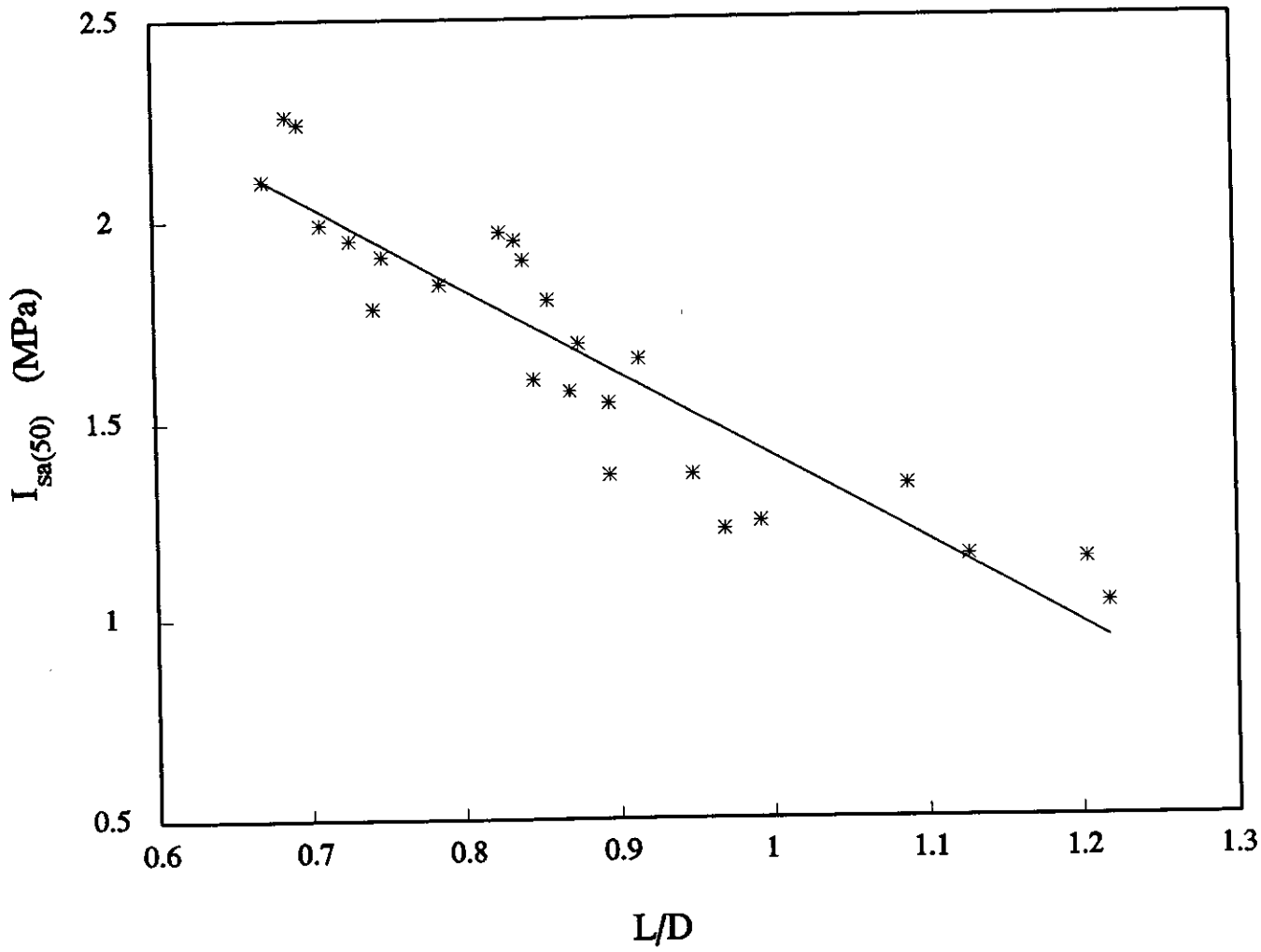

Figure 4.10 Effect of L/D ratio on axial point load strength index

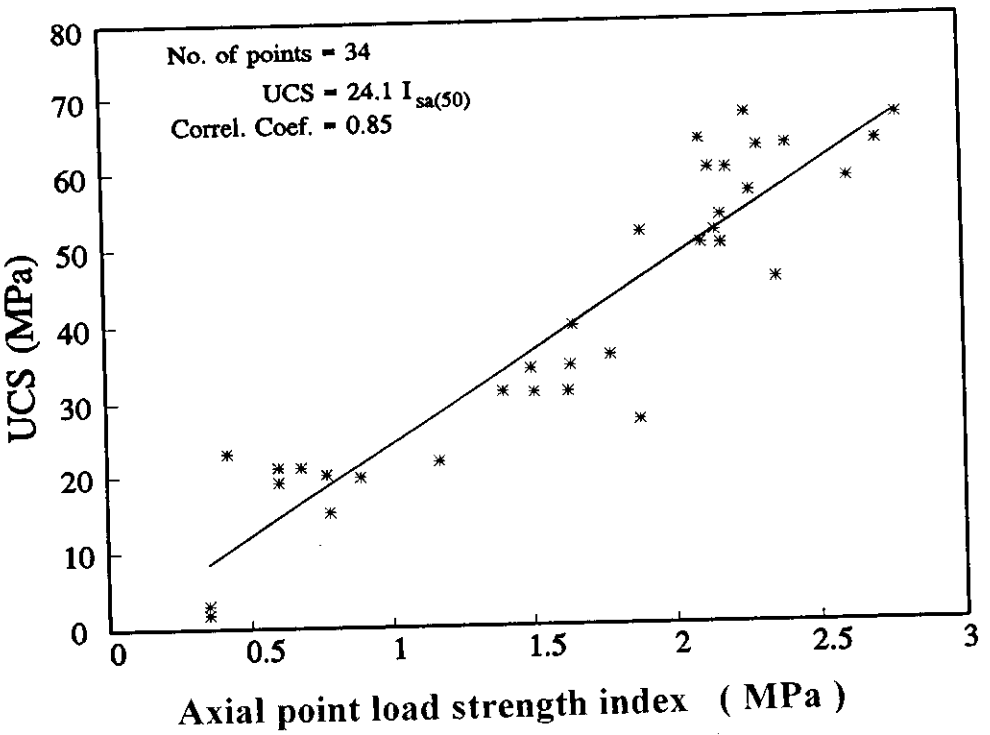

Figure 4.11 UCS versus axial point load strength index

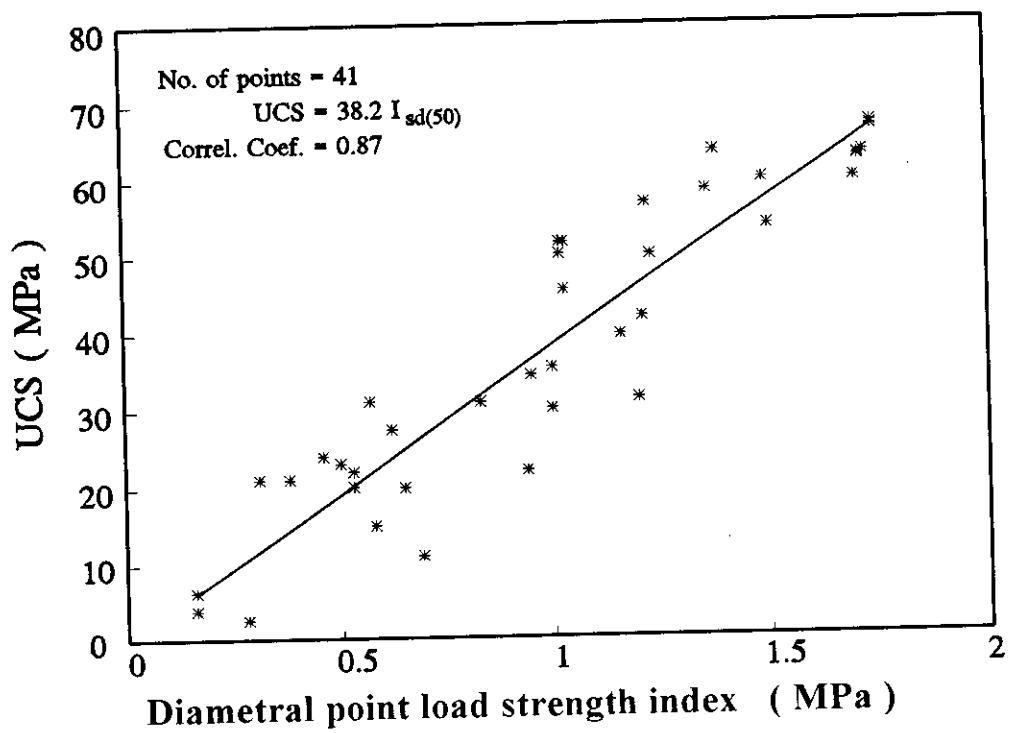

Figure 4.12 UCS versus diametral point load strength index

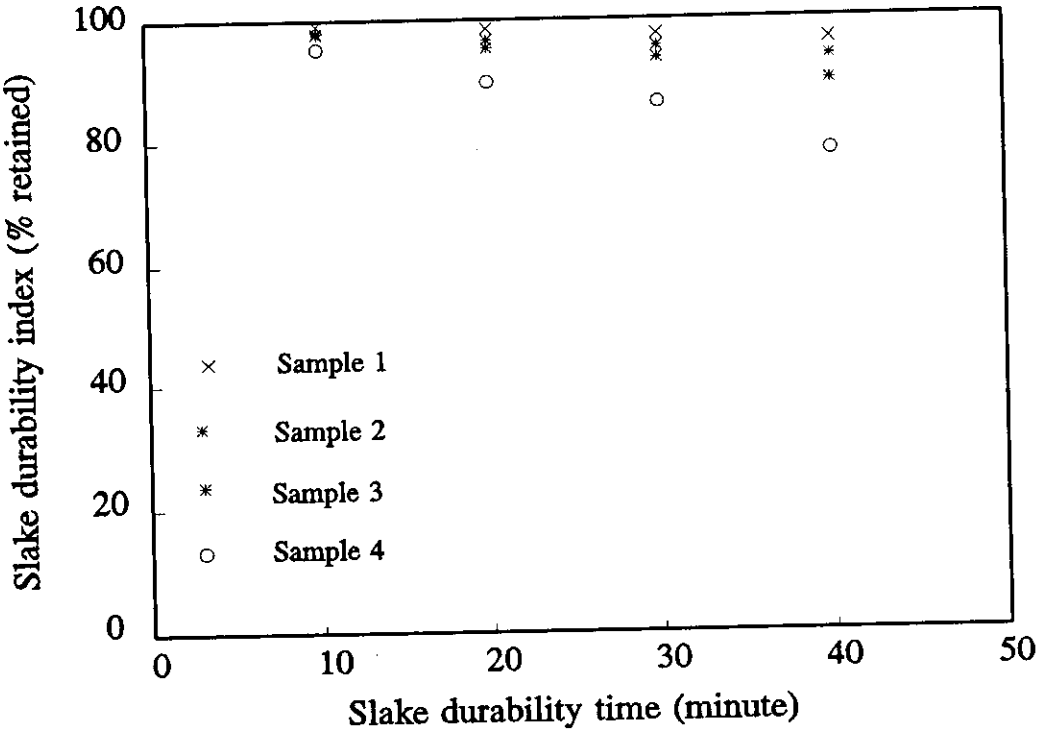

Figure 4.13 Relationship between slaking time and durability

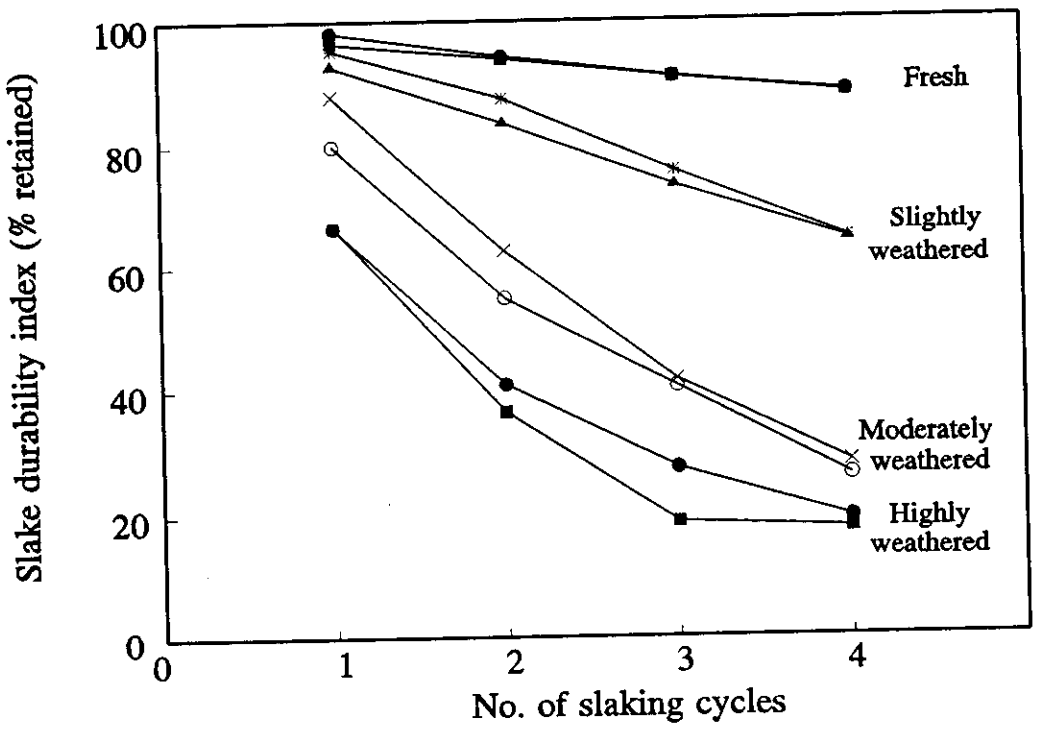

Figure 4.14 Effect of number of cycles

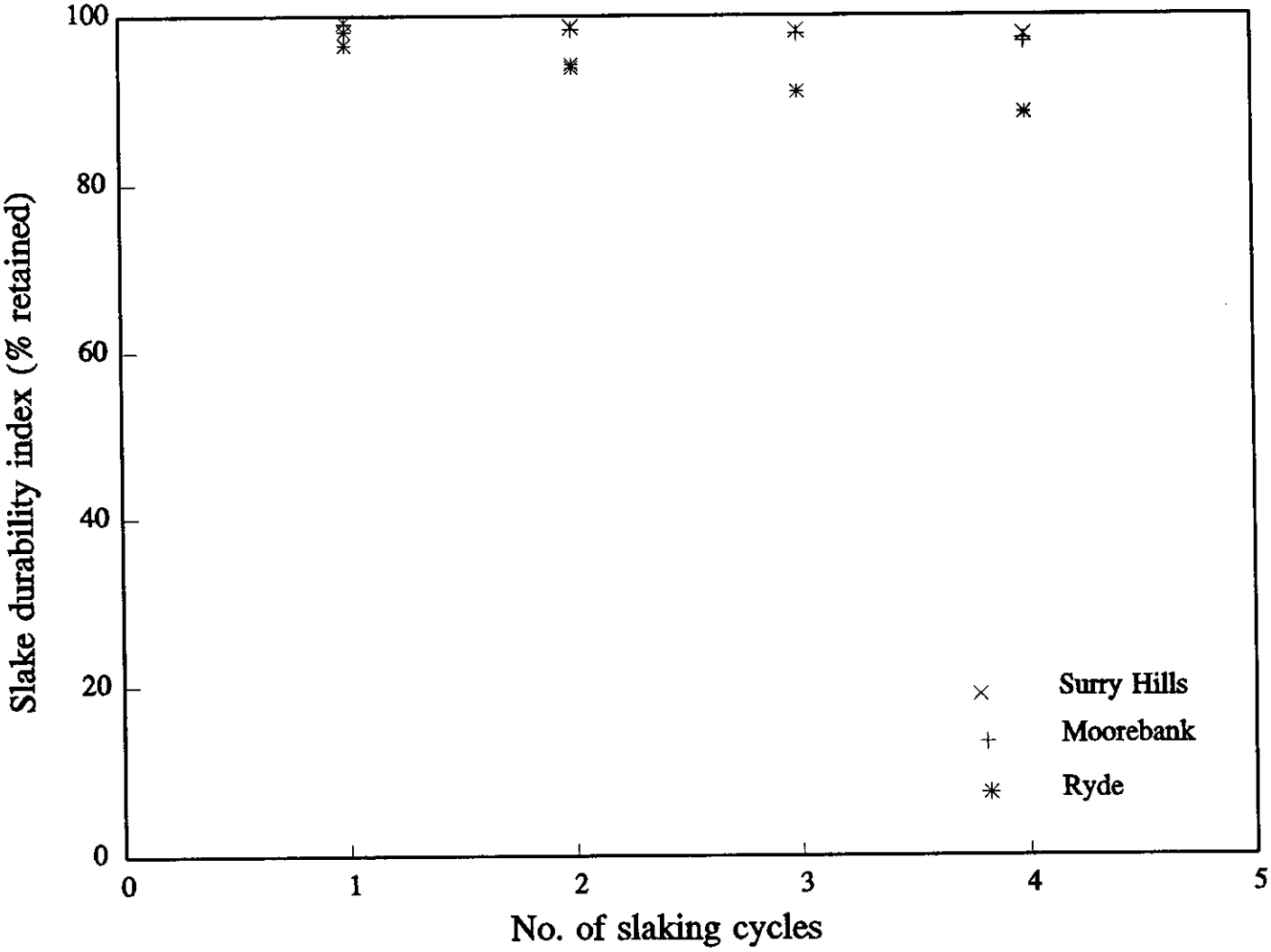

Figure 4.15 Effect of slaking cycles on samples of fresh shale from different sites

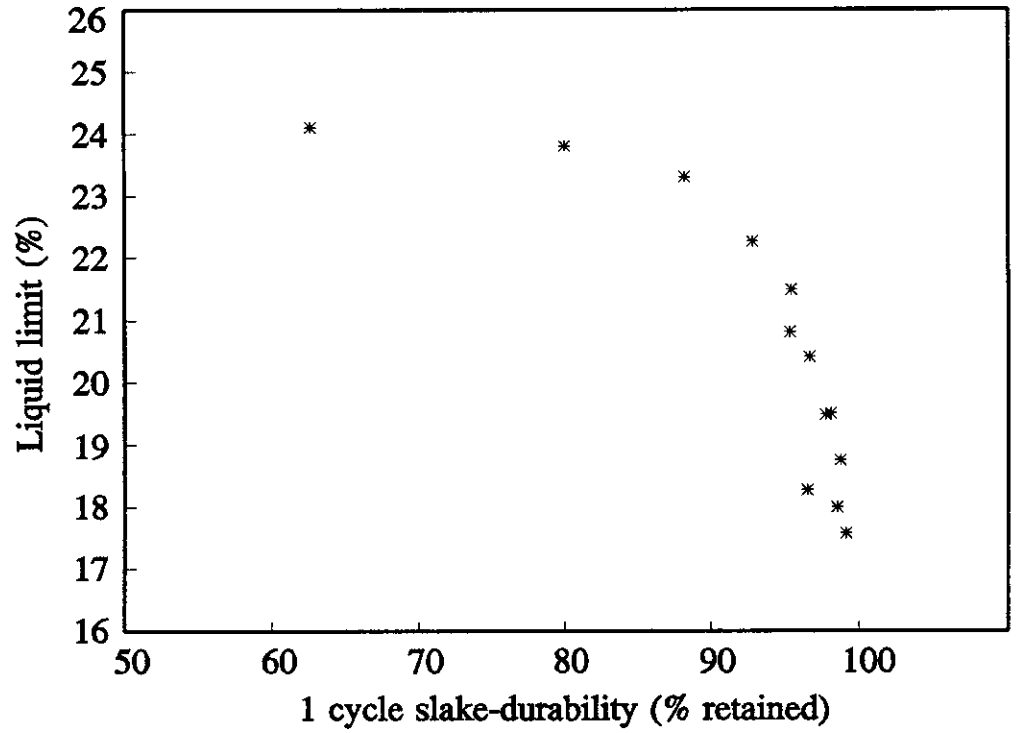

(a)

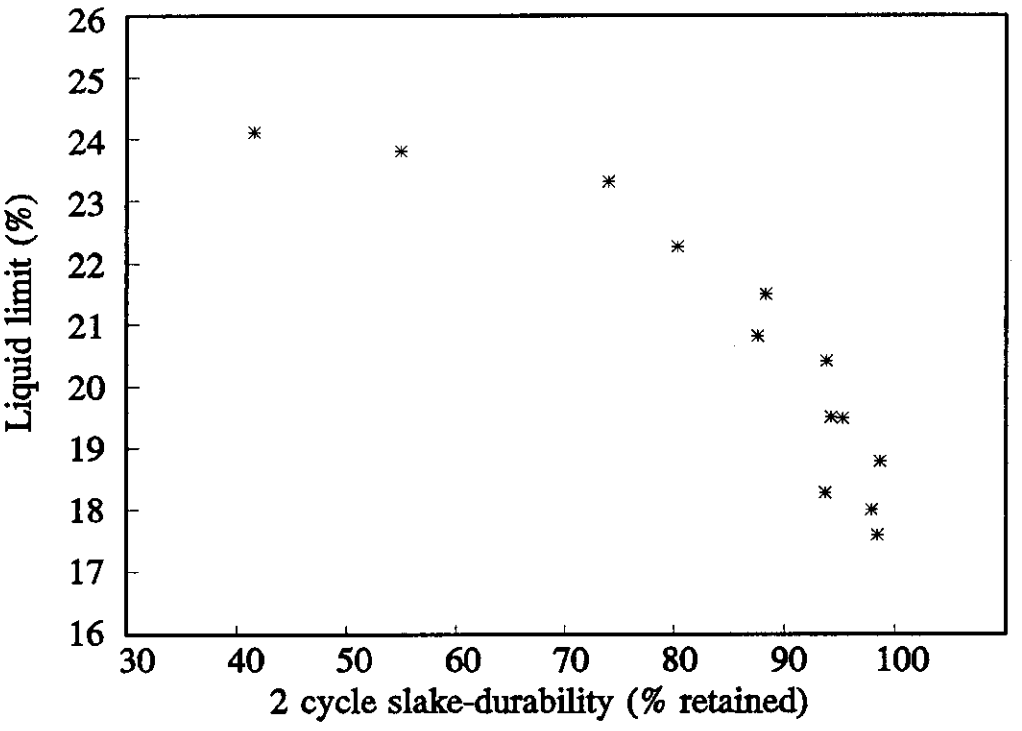

(b)

Figure 4.16 Liquid limit versus (a) one cycle and (b) two cycle slake durability index

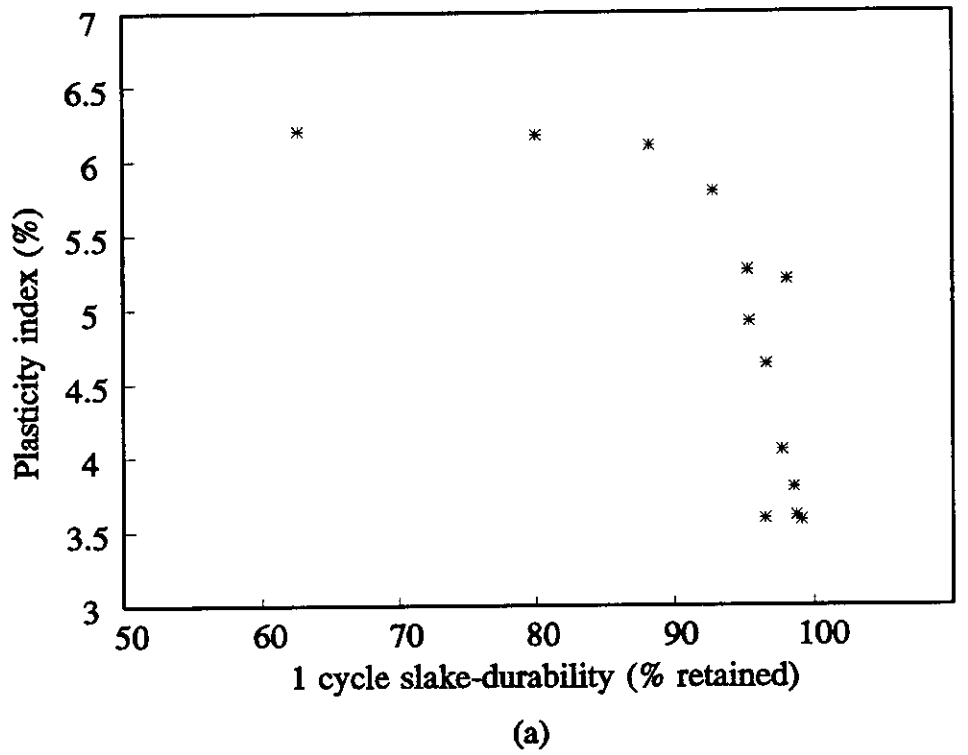

(a)

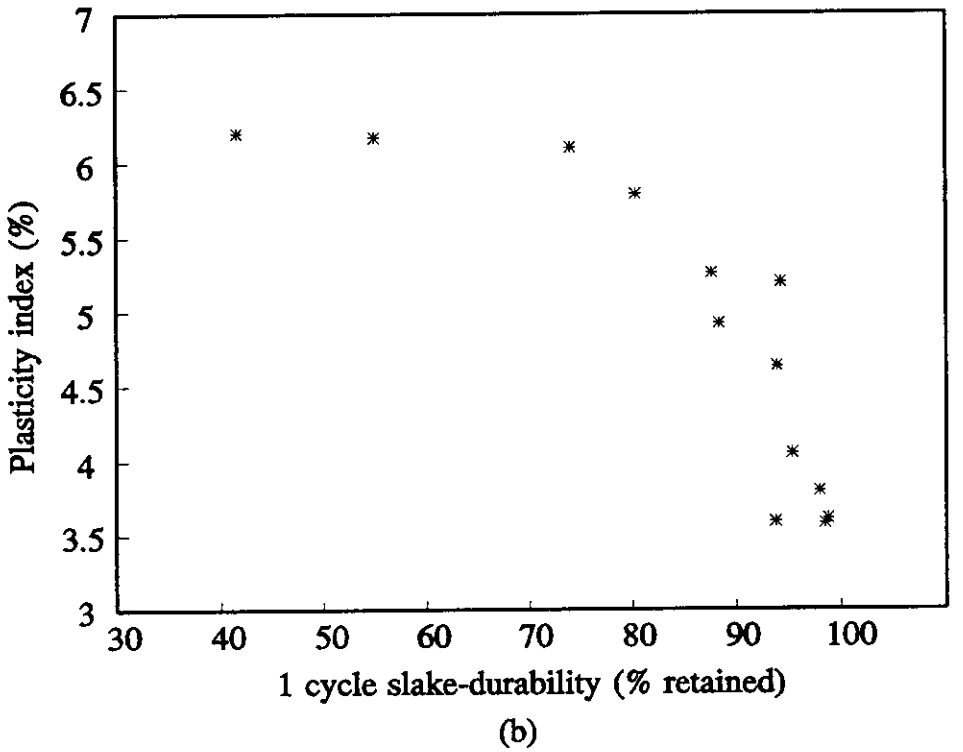

(b)

Figure 4.17 Plasticity index versus (a) one cycle and (b) two cycle slake durability index

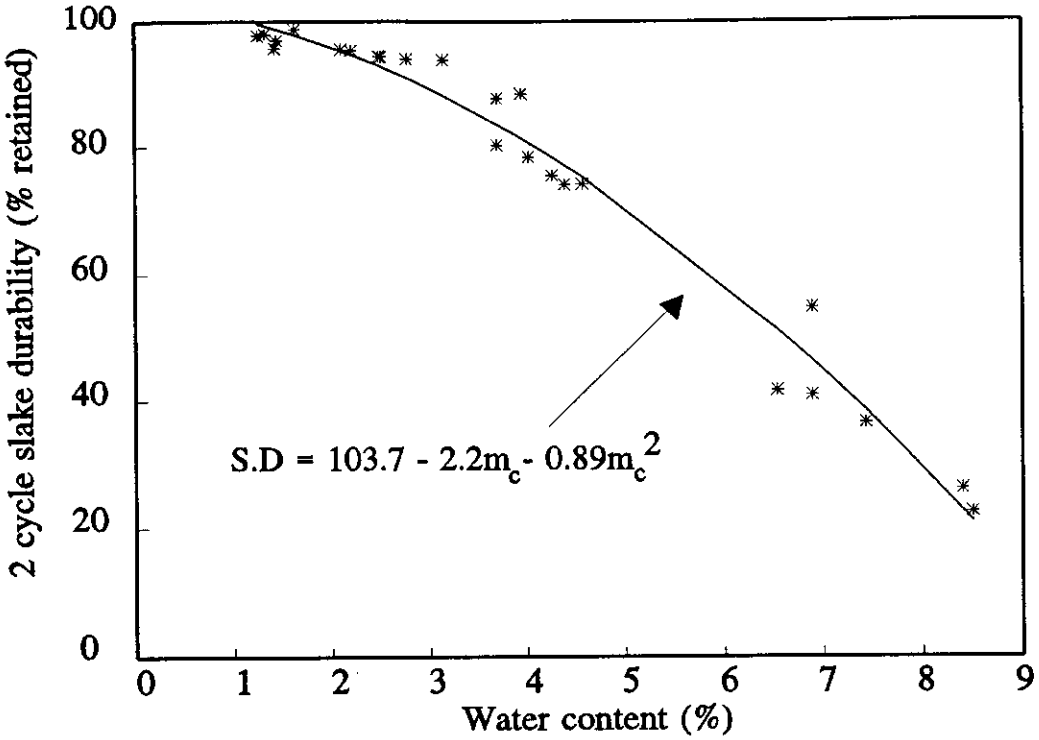

Figure 4.18 Relationship between two cycle slake durability and moisture content

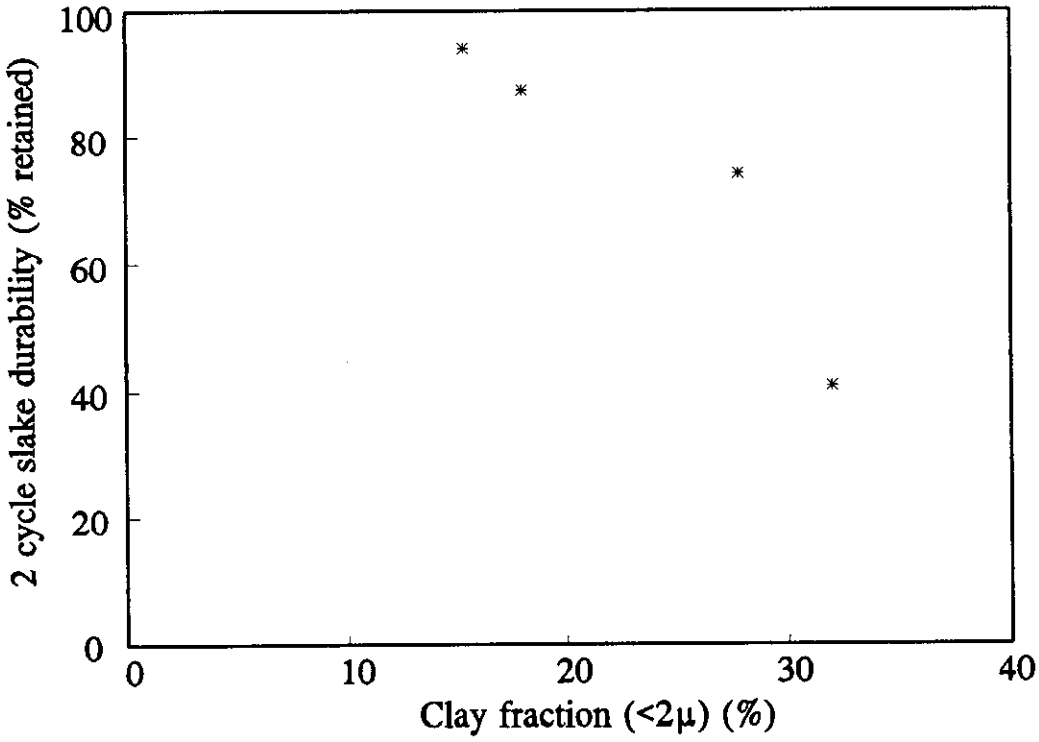

Figure 4.19 Slake durability versus clay fraction

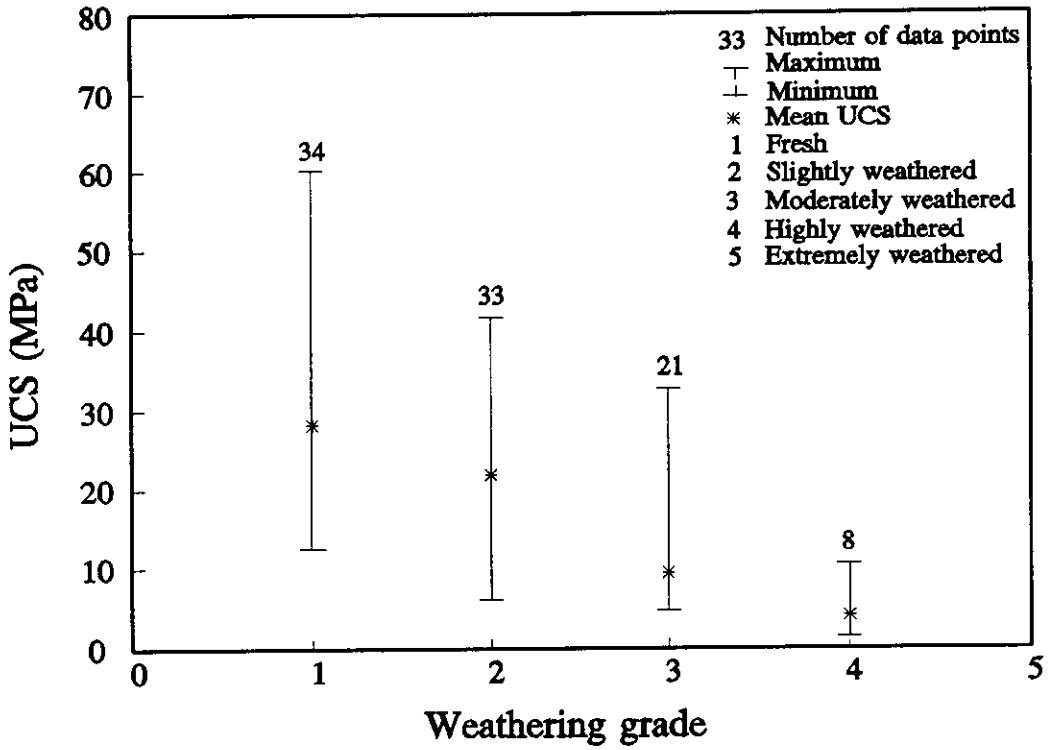

Figure 4.20 Relationship between UCS and weathering grade

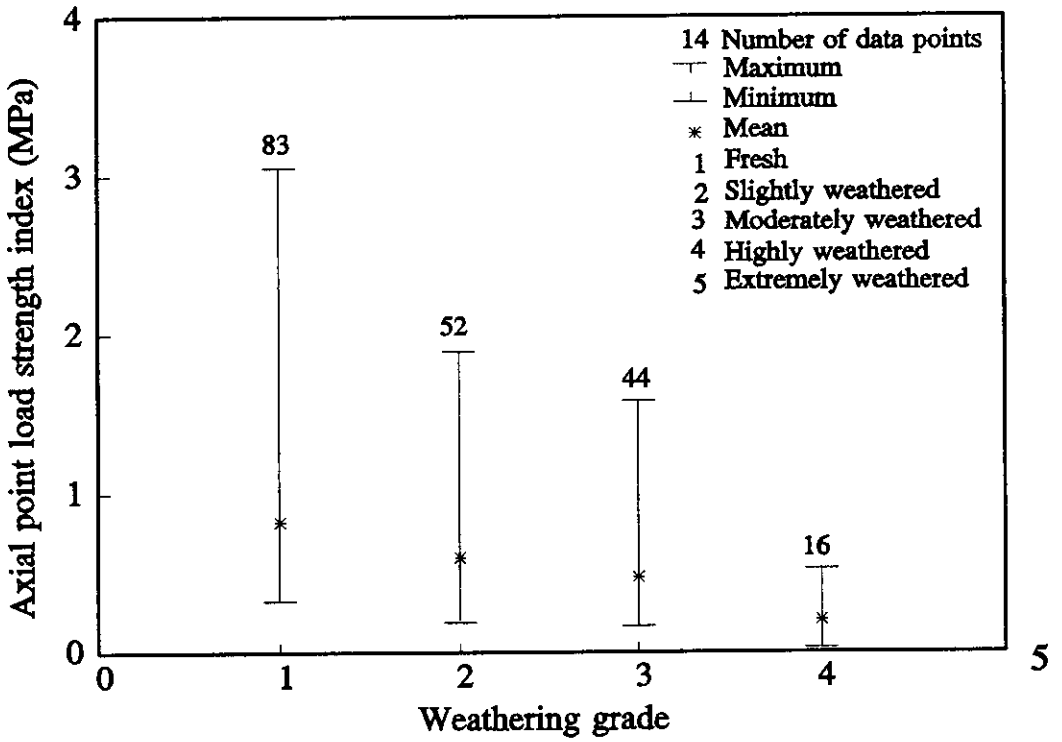

Figure 4.21 Relationship between axial point load strength and weathering grades

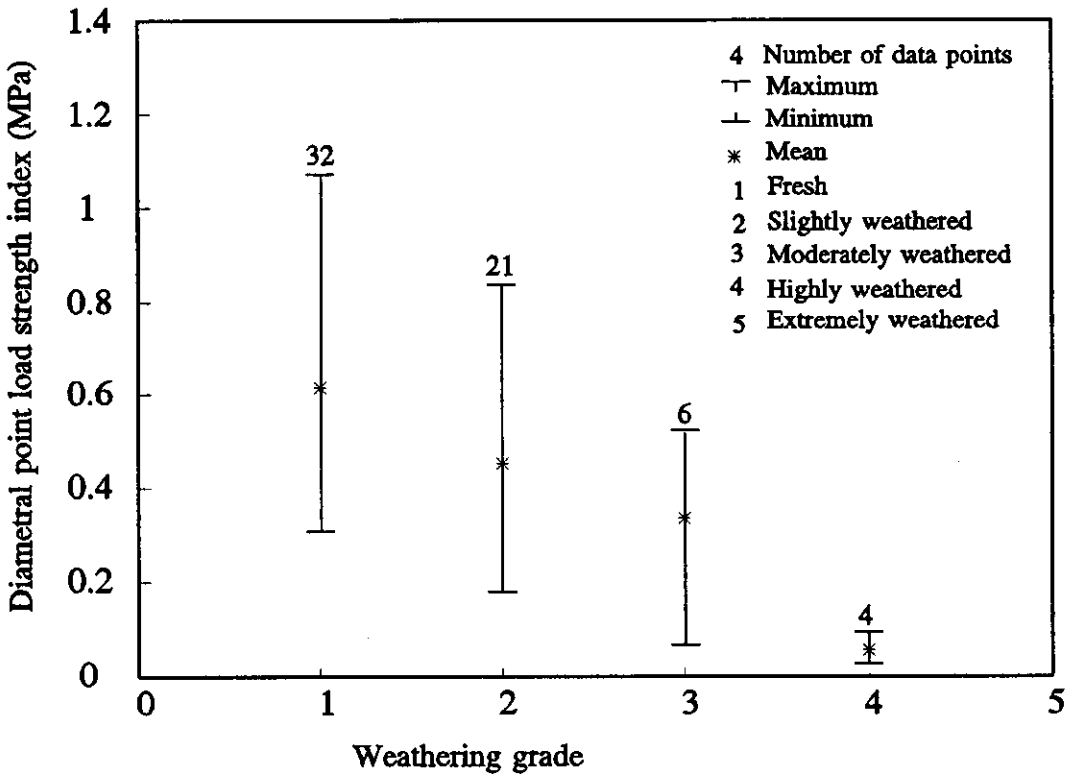

Figure 4.22 Relationship between diametral point load strengt and weathering grades

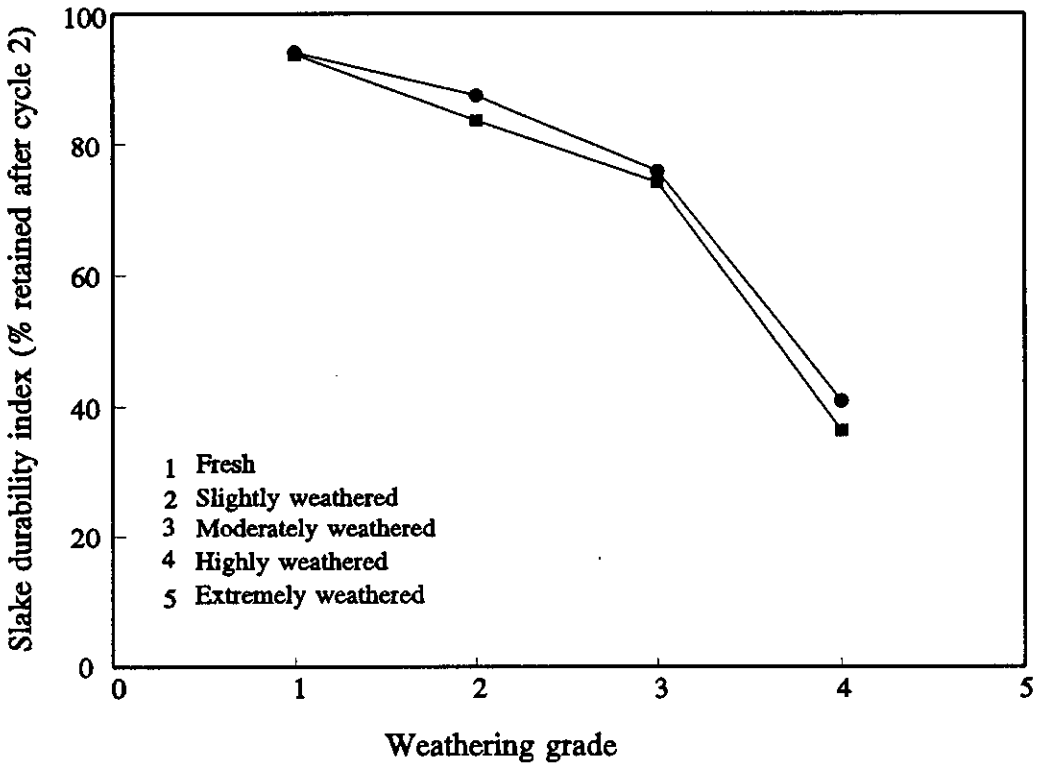

Figure 4.23 Relationship between slake durability and weathering grades

CHAPTER 5 UNIAXIAL AND TRIAXIAL COMPRESSION TESTS

CHAPTER 5

UNIAXIAL AND TRIAXIAL COMPRESSION TESTS

5.1 INTRODUCTION

Lamination, a primary sedimentary anisotropic fabric element has a significant effect on uniaxial and triaxial compressive strengths and the deformation behaviour of Ashfield shale. The schematic representation of an anisotropic sample and the typical cylindrical test samples are shown in Figures 5.1 and 5.2, respectively. As these figures show, the specimens have laminations oriented at an angle β with the direction of the axial principal stress. It has been noted in the literature that anisotropic rocks usually show maximum uniaxial and triaxial compressive strengths at the orientations $\beta = 0$ or 90 degrees and minimum compressive strength at orientations $\beta = 30$ to 40 degrees. Hence, the estimation of compressive strength anisotropy of rocks must be obtained from samples that at least include values of $\beta = 30$ and 90 degrees.

The testing programme described in this chapter was carried out to study the anisotropic behaviour of Ashfield shale in uniaxial and triaxial compression. Two series of uniaxial and triaxial compression tests were carried out on the Ashfield

shale specimens. The first series of tests was performed on cylindrical specimens of the shale, without strain gauges. All tests in this series were performed to failure and stresses and strains were determined from a load cell and external LVDT, respectively. The second series of tests was performed on cylindrical specimens of the Ashfield shale with strain gauges mounted on them. All tests in this series were carried out until the deviator stress reached a level equivalent to about 50% of the maximum shear strength. In both series, uniaxial and triaxial compression tests were performed on specimens with the laminations at orientation angles (β) of 0, 15, 30, 45, 60, 75 and 90 degrees to the direction of the applied axial load (Figure 5.2).

The first series of triaxial compression tests was performed at confining pressures of 0.1, 1 and 10 *MPa*. The second series of triaxial compression tests was performed at confining pressures of 0, 0.1, 0.5, 1, 2, 5 and 10 *MPa*. This work is an attempt to study the effects of confining pressure and lamination direction on the maximum shear strength and deformation behaviour of the Ashfield shale. Comparisons have also made between the results of this experimental study and some empirical strength criteria.

The theory for a cross anisotropic elastic material has been used to analyse the deformation behaviour of this shale. Five independent elastic parameters describe this cross anisotropic system. These five independent elastic parameters have been obtained from the uniaxial and triaxial compression tests on samples with different orientations of the laminations to the axial load direction.

5.2 TESTING PROGRAMME

Table 5.1 gives details of the uniaxial and triaxial compression tests programme. A total of 43 uniaxial and 127 triaxial compression tests was carried out on samples of the Ashfield shale from the Ryde-interchange and Surry Hills sites.

The main aims of the first series of 75 uniaxial and triaxial tests were to obtain a clear understanding of the variation of shear strength as a function of confining pressure and lamination orientation, and to evaluate the shear strength parameters. The second series of uniaxial and triaxial tests (95 tests) was intended to investigate the deformation parameters of the Ashfield shale and the effects of lamination direction and confining pressure on the deformation parameters. For brevity, only selected test results are presented in the figures of this chapter. However, all test data are included in the analysis of the results.

5.3 TEST EQUIPMENT

5.3.1 Uniaxial compression test

The uniaxial compression test equipment was mentioned in detail in Chapter 4. In some uniaxial compression tests TML-PL20 strain gauges were used to measure both axial and circumferential strains during axial loading. Axial and diametral pairs of electrical resistance strain gauges were mounted diametrically opposed at mid-height of the specimen for determination of the modulus of elasticity and Poisson's ratio. These strain gauges had a resistance of 120 ohms, a gauge factor of 2 $\pm$ 0.5% and a gauge length of 20 *mm*.

Two Peekel strain indicators, type T 200, with two independent input circuits for the connection of strain gauges, were used to monitor signals from the strain gauges. Each indicator could measure readings from two strain gauges. In this study the quarter bridge, 120 ohm, two connection lead circuit was used. This type of strain indicator is designed for a fixed gauge factor of 2. To take readings from the Peekel strain indicator the loading machine was stopped with the axial load maintained, values of the four gauge strains were read manually, and the machine restarted. Readings were taken every 200 *kPa* change in axial stress. The strain indicator gives the result in microstrain and these were converted to

percentage values.

5.3.2 Triaxial compression test

To evaluate the shear strength and deformation characteristics of the Ashfield shale under triaxial conditions, high pressure triaxial equipment was used. Figure 5.3 shows a complete set-up of the triaxial equipment. The apparatus is described in detail below.

A high pressure Rockcell Model 10 triaxial cell with a cell pressure capacity of 70 *MPa* was used to apply controlled confining pressure to the sample. In the triaxial tests confining pressures from 0.1 to 10 *MPa* were used. For low confining pressure, i.e. 0.1 and 1 *MPa*, the cell pressure was provided by nitrogen gas through a gas water interface. For all tests at confining pressures greater than 1 *MPa*, the cell pressure was supplied by a GDS digital controller with a capacity of 20 *MPa*. A detailed description of the digital controller has been given by Menzies (1988).

For all triaxial tests a 500 *kN* capacity servo-controlled hydraulic actuator (MTS) was used in a rigid loading frame to apply the axial load. The axial load was transmitted through the upper loading platen to the specimen. The upper platen was spherically seated to the ram in an attempt to eliminate end-moments being applied to the specimen, particularly in cases where the flat ends of the cylindrical specimen were not exactly parallel. Care was taken to ensure that the centre of curvature of the seat surfaces coincided with the centre of the specimen ends. For the triaxial compression tests on the samples with strain gauges, a new ram, the same as the triaxial cell ram but without a spherical seat, was manufactured. Eight holes were inserted from the bottom to the top for passing the eight wires from the strain gauges through the ram. This modification was done to try to avoid any leakage of water into the shale specimen under confining pressure. In this case, a spherical seat was used for the lower platen.

For all the specimens, an impermeable and flexible 1.5 *mm* thick rubber membrane was used to isolate the sample from the water (confining fluid) within the test cell. Four O-rings were used to prevent the water from entering the specimen. Two brass clamps were applied to the top and bottom caps to strengthen the O-rings and prevent leakages. The two stiff end caps were made of hardened steel. The end caps had flat polished surfaces with a variation from flatness of less than 0.01 *mm*.

5.3.2.1 Stress and strain measuring devices

Axial load was measured by a model 661.23D-01 load cell installed beneath the MTS actuator. It had a capacity of 500 *kN*. Axial displacement was measured by an SN 488 linear variable differential transformer (LVDT) installed within the MTS actuator. It had a range of $\pm$ 12.5 *mm* and a resolution of approximately 0.006 *mm*.

For some of the specimens two TML-PL20 axial and two TML-PL20 circumferential electrical resistance strain gauges were mounted diametrically opposed at mid-height of the specimen for determination of the modulus of elasticity and Poisson's ratio. Each of the strain gauges was connected in an arm of a Wheatstone bridge circuit. For each gauge the Wheatstone bridge circuit was completed by three dummy gauges glued to pieces of shale core outside the triaxial cell. The outputs from the bridge circuits were amplified and measured by the A-D converter card in the computer. The amplification for each circuit was measured before each test. With this information and knowing the gauge factor was 2 $\pm$ 0.5% the strain could be determined. The position of the strain gauges on the samples with respect to the lamination direction is shown in Figures 5.4 a and b.

The magnitudes of the applied axial compressive load, axial displacement and axial and diametral strains were monitored throughout each test by an analog to

digital converter and stored in the memory of a computer system for later processing.

5.4 SPECIMEN PREPARATION

To obtain samples for uniaxial and triaxial compression tests, five boreholes with different angles, β, between the bedding planes and the axis of the borehole were drilled by large truck mounted rigs at the Ryde-interchange site. Details of the sample recovery have been described in Chapter 3. Samples with values of β in the range from 30 to 90 degrees were obtained from the Ryde site. Core samples were also obtained from blocks of shale recovered from an excavation in Surry Hills near the Central railway station in Sydney. Samples with orientations of β 0 to 90 degrees were obtained in this way. All retrieved cores were cut to the required length with a small diamond saw and their ends were ground by sandpaper to make them smooth and perpendicular to the longitudinal axis according to the ISRM (1981) recommendations.

As mentioned in Chapter 3, the shale from the Surry Hills site is generally stronger than shale from the Ryde-interchange site and there was no test data for β = 0 and 15 degrees at the Ryde site. This was taken into account by preparing core samples in three directions (β=0, 15 and 90°) from the block of shale from Surry Hills, and conducting uniaxial and triaxial tests in these directions. By comparing the results of tests on samples with a lamination angle of β=90° from the two sites, correlation factors between the two shales were obtained. Values of the shear strength and modulus of elasticity at β=0 and 15° for the Ryde shale were estimated by applying the appropriate correlation factors to the test data for the Surry Hills shales (β=0 and 15°). The data presented for the Ryde site in the remainder of this chapter for β=0 and 15° are from Surry Hills with the scale factor applied.

5.5 TEST PROCEDURES

5.5.1 Uniaxial compression test

All specimens tested in uniaxial compression were right circular cylinders with a height to diameter ratio of approximately 2. Each specimen was carefully placed concentrically with the load cell and the base platen. Axial load on the specimen was applied continuously by providing a constant deformation rate such that failure occurred within 5 to 10 minutes of loading. The ISRM (1981) suggested method for determination of the uniaxial compressive strength of rock materials was followed.

In the tests on specimens with strain gauges, a special loading sequence was applied. The samples were loaded to a stress level equal to approximately one-half of their strength and were then unloaded. Some of these samples were subsequently used in the triaxial tests. Curves of axial stress against axial and diametral strain were obtained. The modulus of elasticity and Poisson's ratios were calculated.

5.5.2 Triaxial compression test

The recording devices were prepared and calibrated before each test. One of the prepared samples was selected. Its diameter was determined to the nearest 0.01 *mm* by averaging measurements at the top, midpoint and bottom of the sample. Its length was measured to the nearest 0.01 *mm*. The triaxial cell was assembled with the specimen aligned between the platens. The spherical seat was lightly lubricated with mineral oil. The sample was protected from water by a rubber membrane. After a specimen was set up, the triaxial cell was filled with distilled de-aired water. The air bleeder hole was kept open to allow the air to escape through this hole during filling the cell and was closed after filling. A typical view of sample set up before and after test is shown in Figures 5.5 (a) and (b),

respectively.

To apply the pre-determined confining pressure, the axial load and the confining pressure were increased simultaneously in such a way that the axial load and confining pressure were approximately equal until the pre-determined confining pressure was reached. The magnitude of the confining pressure was controlled by a GDS pressure-volume controller. Subsequently, the axial load was increased continuously at a constant rate such that failure occurred within 10 to 15 minutes of loading.

For tests on strain gauged specimens a special loading sequence was applied. The samples were loaded to a stress level equal to approximately one-half of their strength and then unloaded. The confining stress was then increased and the samples re-loaded to the same stress level before unloading again. This process was repeated until the confining stress was 10 *MPa* where the samples were loaded to failure. Curves of axial stress against axial and diametral strain were obtained. From these curves the modulus of elasticity and Poisson's ratio were calculated.

5.6 SHEAR STRENGTH CHARACTERISTICS

In this section, the behaviour of Ashfield shale as an anisotropic material will be discussed. A series of uniaxial and triaxial compression tests has been performed on the Ashfield shale to study the influence of the laminations directions, with respect to the loading axis, on the strength values and on the mode of specimen failure. The effect of confining pressure on compressive strength at different lamination orientations has been studied. By drawing Mohr circles and Mohr-Coulomb envelopes to these circles, the shear strength parameters, c and ϕ, have been determined. The nature of the observed variations is discussed.

5.6.1 Uniaxial test results

Uniaxial compressive strength tests were performed on the Ashfield shale specimens with the laminations having different orientations (β) to the applied load. The orientation of the plane of anisotropy (β) was varied between 0 and 90 degrees. All samples tested in this study failed in a brittle manner with either vertical or subvertical splitting, or for the samples with β = 30 and 45 degrees, failure along the laminations. The strength results are summarised in Table 5.2.

In order to study the strength anisotropy of the Ashfield shale, the results were also plotted in the form of maximum axial stress against the orientation angle (β) in Figure 5.6. As this figure shows the maximum strength occurred at β = 90 degrees and the minimum strength at β = 30 degrees.

For Ashfield shale, dominated by a single set of laminations, the shape of the curve relating the *UCS* to the lamination angle, β, can be predicted by an equation similar in form to one proposed by McLamore and Gray (1967) for variable cohesion. The equation is in the form:

$$\sigma_c = A - B\left[\cos 2\left(\beta_m - \beta\right)\right]^n \qquad (5.1)$$

where

σ_c= uniaxial compressive strength at orientation angle, β.

β_m= value of the orientation angle, β, at which the strength is minimum (usually found to be approximately 30 degrees)

n = an anisotropy factor, which, according to McLamore and Gray, usually has a value of 1 or 3 for planar anisotropy.

A and B are constants.

The values A and B were determined over two ranges of β using the uniaxial compressive strength at β = 0 and 30 degrees, and 30 and 90 degrees. A value of n = 3 provides the best fit to the experimental results from this study. The

equations that best fit the observed data are:

$$\sigma_c = 25.5 - 17.1\ [cos2\ (30° - \beta)]^3 \qquad (5.2)$$

for $0 \leq \beta \leq 30°$

$$\sigma_c = 24.2 - 15.7\ [\cos2\ (30° - \beta)]^3 \qquad (5.3)$$

for $30° \leq \beta \leq 90°$

where σ_c is the predicted uniaxial compressive strength in *MPa*.

The predicted values of uniaxial compressive strength and the experimental results for Ashfield shale are compared in Figure 5.7. As Figure 5.7 shows, reasonably good agreement exists across the full range of β values for the shales from both sites.

The anisotropic strength ratio may be defined as the ratio of the maximum compressive strength to the minimum compressive strength over the full range of β values. The maximum uniaxial compressive strength for samples from Ryde-interchange was observed to be at the orientation of $\beta = 90$ degrees with a magnitude of 26.22 *MPa*, and the minimum compressive strength was observed to be at $\beta = 30$ degrees with the magnitude of 8.45 *MPa*. The anisotropy ratio ($\sigma_{c90}/\sigma_{c30}$) of the Ashfield shale from Ryde-interchange site therefore appears to be approximately 3.1. This is significantly greater than the anisotropy ratio of approximately 2 determined from the point load index tests.

5.6.2 Triaxial test results

Figures 5.8 and 5.9 show representative plots of the deviator stress (σ_1-σ_3) against axial strain (ϵ_1) at a confining pressure of 10 *MPa* for core specimens containing laminations oriented at $\beta = 90$ degrees to the axial load direction for shale from

the Surry Hills and Ryde sites, respectively. In both cases an almost linear elastic response up to the maximum deviator stress was observed, followed by a rapid reduction in the deviator stress with further strain beyond the peak. The peak deviator stresses occurred at relatively small strains that were in the range from approximately 1 to 2%.

For loading in the direction parallel to the laminations (Figure 5.10), the axial strains at the peak deviator stress were lower than the strains observed when the axial loading was applied in the direction normal to the laminations (Figure 5.8). As Figures 5.8 and 5.10 show, the sample loaded parallel to the laminations shows greater stiffness than the sample loaded perpendicular to the laminations.

Figure 5.11, which is a plot of typical stress-strain curves for specimens of Ashfield shale with $\beta = 75°$ compressed at various confining pressures, indicates a trend that is typical of all orientations. This figure shows that the confining pressure has an effect upon the stress-strain properties and the strength of the Ashfield shale. It is clear that increasing the confining pressure generally increases the peak shear strength. In this case ($\beta = 75°$) the shale had a uniaxial compressive strength of about 24.9 *MPa* and exhibited brittle failure for all values of confining pressure. At a confining pressure of 10 *MPa* the compressive strength (σ_1-σ_3) increased to about 50.9 *MPa*.

In order to study the strength anisotropy of the Ashfield shale, the triaxial tests results were also plotted in the form of the peak deviator stress (σ_1-σ_3) against the orientation angle (β) as a function of the confining pressure (σ_3) in Figure 5.12. As this figure shows the maximum deviator stress occurred at β = 90 degrees and the minimum deviator stress at β = 30 degrees for all confining pressures.

It is also noted that an increase in the confining pressure slightly reduces the effect of anisotropy. The relationship between compressive strength anisotropy

and confining pressure is shown in Figure 5.13. This graph indicates that the ratio between the values of the maximum and minimum strength, corresponding to the directions $\beta = 90$ and $\beta = 30$ degrees respectively, reduces from 3.1 at zero confining pressure to 1.85 at a confining pressure of 10 *MPa*.

The variation of maximum axial stress (σ_1) with the confining pressure (σ_3) and the lamination directions, β, is shown in Figure 5.14. This figure shows that an increase in the confining pressure increases the maximum strength of the Ashfield shale specimens for all values of β. The rate of increase is approximately the same for all orientations.

Inspection of the modes of failure in the specimens of the Ashfield shale revealed that for the range $15° < \beta \leq 45°$ failure usually occurred as a shear slip on the laminations. In the specimens with lamination angles of $\beta \leq 15$ degrees, failure occurred by extension fracture, i.e. parting of some of the laminations. For $\beta \geq 60$ degrees the failure plane intersected the laminations and formed at an angle between 20 to 30 degrees with the direction of the maximum principal stress. Figures 5.15 (a) and (b) shows schematic and typical representation of these failure modes. The confining stress had no influence on the mode of failure, for the range of stresses used.

5.6.3 Shear strength parameters

To understand further the shear strength parameters of the Ashfield shale as functions of the confining pressure and the lamination orientation, Mohr circles were constructed for each specimen of Ashfield shale from the Ryde-interchange and for specimens oriented at three directions (i.e. 0, 15, 90 degrees) from Surry Hills. The states of stress at failure for samples with lamination directions defined by $\beta = 30, 45, 75$ and 90 degrees from the Ryde site are presented in Figures 5.16 and 5.17. The Mohr-Coulomb envelopes were drawn as the best fit tangents to the Mohr stress circles. All the envelopes obtained are approximately

parabolic towards the origin. For the purpose of comparison a linear relation has been assumed over the range of normal stress from 5 to 30 *MPa* to obtain the cohesion intercept c on the vertical axis and the angle of friction ϕ. The shear strength parameters (c_i, ϕ_i) for the tangent to the envelopes approaching zero stress have also been obtained. The values of c and ϕ and c_i and ϕ_i deduced in this way are functions of the angle β and the results for all lamination directions are listed in Table 5.3.

The variation of cohesive intercept with the lamination angle for both parts of the strength envelopes is also shown graphically in Figure 5.18. The general trends for both curves are the same and the shapes of the curves are generally similar to those of the curves obtained for the peak strengths, as might be expected. Figure 5.18 shows that the orientation of the laminations to the axial direction has a significant effect on the cohesive intercept of the Ashfield shale. The maximum cohesions for both cases occur at β = 90 degrees and the minimums at β = 30 degrees. A comparison of the results in Figure 5.18 indicates that the cohesions derived from the Mohr-Coulomb envelopes between 5 and 30 *MPa* are approximately twice the cohesions derived from the initial tangents to the Mohr-Coulomb envelopes.

The variations of the friction angles, ϕ, ϕ_i, with the lamination angle are shown in Figure 5.19. This figure shows that the friction angle from the linear part of the envelope varies only slightly, between 30 and 34 degrees, except close to β = 30 degrees, where it dropped to 24 degrees. The friction angles derived from the tangent to the initial part of the envelope varied between 56 to 63 degrees, except for β = 30 degrees, where it dropped to 47 degrees. A comparison of the results in Figure 5.19 shows that the friction angles derived from the initial tangent to the envelopes are approximately twice the friction angles derived at stresses between 5 and 30 *MPa*.

5.6.4 Strength criteria for intact rock

Three empirical strength criteria suggested by Bieniawaski (1974), Hoek and Brown (1980), and Ramamurthy (1986) have been compared with the experimental results. These criteria make no explicit allowance for strength anisotropy, i.e. the influence of β, but this can be included implicity by a change in the value of the normalising parameter, σ_c, for each individual value of β. This has been done for all the results presented. The values of maximum axial stress, σ_1, have been obtained for four different confining pressures, $\sigma_3 = 0, 0.1, 1$ and $10\ MPa$. The values of the various strength "constants" suggested by each of the authors for "shales" have been used in the comparisons presented here.

The empirical strength criterion proposed by Bieniawski is:

$$\frac{\sigma_1}{\sigma_c} = 1 + B\left(\frac{\sigma_3}{\sigma_c}\right)^{\alpha} \qquad \textbf{(5.4)}$$

where σ_c is the uniaxial compressive strength of intact rock at a particular orientation angle (β), and B and α are constants. Bieniawski suggested that $\alpha = 0.75$ and $B = 3$ for shale.

The empirical criterion proposed by Hoek and Brown (1980) is:

$$\frac{\sigma_1}{\sigma_c} = \frac{\sigma_3}{\sigma_c} + \sqrt{\left(m\frac{\sigma_3}{\sigma_c} + s\right)} \qquad \textbf{(5.5)}$$

where m and s are material constants, σ_c is the uniaxial compressive strength of intact rock at a particular orientation angle (β). For intact shales Hoek and Brown suggested that $s = 1$ and $m = 10$.

The empirical criterion proposed by Ramamurthy (1986) is:

$$\frac{(\sigma_1-\sigma_3)}{\sigma_3} = B\left(\frac{\sigma_c}{\sigma_3}\right)^{\alpha} \qquad (5.6)$$

where σ_c is the uniaxial compressive strength at a particular angle β and B and α are constants. Values of $\alpha = 0.8$ and $B = 2.2$ have been suggested by Ramamurthy as appropriate for shales. Ramamurthy claimed that this criterion is applicable for all values of σ_3 larger than 5% of the uniaxial compressive strength, which would limit its applicability to confining stresses greater than about 1 *MPa* for this shale.

The above mentioned values of the empirical constants were used to predict peak values of σ_1 at various confining pressures (σ_3). The prediction and typical test results for the Ashfield shale specimens with $\beta = 90$ and 30 degrees are given in Figure 5.20. This figure shows a comparison of the experimental and predicted values, and clearly indicates that, in general, the Bieniawski (1974) and Hoek and Brown (1980) criteria predict the strength of Ashfield shale reasonably well. The criterion proposed by Ramamurthy (1986) is observed to slightly under predict the peak stress values. A comparison of the strengths predicted using the Bieniawski (1974) strength criterion, and the experimental results for Ashfield shale is shown in Figure 5.21 for different lamination directions. This figure shows that in general there is good agreement between the experimental results and predicted values across the full range of β, provided an appropriate value of σ_c is used for each value of β.

5.6.5 Strength criteria for anisotropic material

Ashfield shale is dominated by a single set of laminations. The shape of the anisotropy curve throughout the range of the lamination angle (β) may be predicted by an anisotropic failure criterion. Different strength criteria have been proposed for the prediction of the strength of anisotropic rocks, and these

have already been discussed in Chapter 2. Three strength criteria suggested by Jaeger (1960), McLamore and Gray (1967), and Ramamurthy et al. (1988) have been compared with the experimental results.

The single plane of weakness theory, proposed by Jaeger (1960), was compared with the experimental results. In this theory Jaeger postulated that if failure occurs through the intact rock only, the shear strength is determined by

$$\sigma_1 - \sigma_3 = (N_\phi - 1)\sigma_3 + 2c\sqrt{N_\phi} \qquad \textbf{(5.7a)}$$

$$\textit{where} \qquad N_\phi = \frac{1+\sin\phi}{1-\sin\phi}$$

and c, ϕ are the cohesion intercept and friction angle, respectively, for the intact rock. On the other hand, if shear failure occurs only along the planes of weakness then the strength is determined by

$$(\sigma_1 - \sigma_3) = \frac{2c_d + 2\sigma_3 \tan\phi_d}{(1 - \tan\phi_d \tan\beta)\sin 2\beta} \qquad \textbf{(5.7b)}$$

where c_d, ϕ_d are the cohesion intercept and friction angle for the discontinuity (β = 30°). The single plane of weakness theory was evaluated by substituting the values of c and ϕ, that were obtained from the experimental results at β = 0 and 90 degrees, into equation 5.7a, and the values of c_d and ϕ_d obtained for β = 30° into equation 5.7b. Figure 5.22 shows the comparison of the experimental results with Jaeger's single plane of weakness criterion. Examination of Figure 5.22 shows that Jaeger's single plane of weakness theory fits the experimental results of Ashfield shale fairly well over the whole range of β. The fact that c and ϕ are stress level dependent is a major drawback to the use of this criterion. The values of c, ϕ, c_d, and ϕ_d must be known in order for this theory to predict the strength. The Mohr-Coulomb envelopes are therefore required for the 0, 30 and 90 degrees

orientations, and these are obtained by conducting several triaxial tests at these orientations. The need for this extensive data set represents a basic limitation of this theory.

The variable cohesive strength theory, suggested by Jaeger (1960) and modified by McLamore and Gray has also been compared with the experimental results. This theory assumes a variable cohesive strength (c) in the direction β to the maximum stress direction and a constant value of friction angle (ϕ). This theory is described by

$$(\sigma_1 - \sigma_3) = \frac{2(c + \sigma_3 \tan\phi)}{\sqrt{\tan^2\phi + 1} - \tan\phi} \qquad \textbf{(5.8)}$$

where

$$c = A - B[\cos 2(\beta_m - \beta)]^n \qquad \textbf{(5.9)}$$

and

$\tan\phi$ = constant

where

β_m = value of the orientation angle, β, at which the strength is minimum (generally 30 degrees).

A and B = constants.

n = anisotropy factor that is assigned a value of 1 or 3, as suggested by McLamore and Gray for planar anisotropy.

For Ashfield shale, dominated by a single set of laminations, the shape of the curve relating the cohesion intercept to the lamination angle, β, can be predicted by Equation (5.9) and known values of cohesion at $\beta = 0, 30$ and 90 degrees. The values of the constants A and B in this equation were determined in two sets, as suggested by McLamore and Gray, using data for β = 0 and 30 degrees, and β

= 30 and 90 degrees. The value of $n = 3$, as suggested by McLamore and Gray, was used for the planar anisotropy factor in this prediction. The empirical equations for predicting the values of c (in *MPa*) for the Ashfield shale have been determined as:

$$c = 7.68 - 3.9\ [cos2\ (30° - \beta)]^3 \qquad \textbf{(5.10)}$$

for $0 \leq \beta \leq 30°$, and

$$c = 7.36 - 3.58\ [cos2\ (30° - \beta)]^3 \qquad \textbf{(5.11)}$$

for $30° \leq \beta \leq 90°$

The values of c_i for Ashfield shale were also predicted using equations having the same form as equations 5.10 and 5.11, i.e.

$$c_i = 3.78 - 2.28\ [cos2\ (30° - \beta)]^3 \qquad \textbf{(5.12)}$$

for $0 \leq \beta \leq 30°$, and

$$c_i = 3.27 - 1.77\ [cos2\ (30° - \beta)]^3 \qquad \textbf{(5.13)}$$

for $30° \leq \beta \leq 90°$

The coefficients in these last two equation were also determined by fitting the McLamore and Gray theory at $\beta = 0$, 30 and 90 degrees.

The experimentally determined cohesion intercepts (c) were compared to the modified variable cohesive strength theory. The cohesions (c) predicted using equations 5.10 and 5.11 and the experimental results for Ashfield shale are shown in Figure 5.23. Good agreement exists between the experimental data and the predictions across the full range of β values, not just at the points where the theory was fitted to the test data ($\beta = 0°, 30°, 90°$). The same procedure was used to compare the initial cohesion intercepts (c_i) to the modified variable cohesive strength theory. As shown in Figure 5.23, good agreement also exists between the experimental data (c_i) and the predictions across the full range of β

values.

Jaeger's variable cohesive strength theory was evaluated by substituting the values of c from equations 5.10 and 5.11 and a constant value of $\phi = 32°$ into equation 5.8. The predicted values of deviator stress and the experimental results for Ashfield shale are shown together in Figure 5.24. As this figure shows, reasonably good agreement exists between experimental and predicted results across the full range of β values with different confining pressures, except at $\beta =$ 30 degrees for higher confining pressure.

Compared to the other theories described earlier, there are additional limitations of the McLamore and Gray theory. Obviously, a number of triaxial tests are needed at $\beta = 0, 30$ and 90 degrees, but an important limitation of this theory is that the constant values (A and B) for prediction of the anisotropy curves must be determined in two separate parts, from 0 to 30 degrees and from 30 to 90 degrees. Another limitation of this theory is that the value of n needs to be precisely estimated.

The following strength criterion has been suggested by Ramamurthy et al. (1988) for layered or foliated rocks which shows anisotropic behaviour,

$$\frac{\sigma_1 - \sigma_3}{\sigma_3} = B_j \left(\frac{\sigma_{cj}}{\sigma_3} \right)^{\alpha_j} \qquad \textbf{(5.14)}$$

where σ_1, and σ_3 are the major and minor principal stresses, σ_{cj} is the uniaxial compressive strength at a particular orientation (β), and α_j and B_j are constants for a particular β. To evaluate the parameters α_j and B_j independently at a specific orientation, the following two equations were suggested by Ramamurthy et al.:

$$\frac{\alpha_j}{\alpha_{90}} = \left(\frac{\sigma_{cj}}{\sigma_{c90}}\right)^{1-\alpha_{90}} \qquad \textbf{(5.15)}$$

and

$$\frac{B_j}{B_{90}} = \left(\frac{\alpha_{90}}{\alpha_j}\right)^{0.5} \qquad \textbf{(5.16)}$$

where σ_{c90} is the uniaxial compressive strength at $\beta = 90°$, and α_{90} and B_{90} are values of the parameters α_j and B_j at $\beta = 90°$. These can be obtained from triaxial tests at this orientation.

The strength predictions of this criterion and the experimental data for Ashfield shale are shown in Figure 5.25. This figure shows that the criterion tends to underpredict at confining pressures of 0.1 and 10 *MPa* through the whole range of β. At a confining pressure of 1 *MPa* a better matching of the experimental data and the predicted curves is observed for orientation angles β less than 60 degrees, but the agreement is less satisfactory for higher β values.

5.6.6 Discussion of strength criteria

5.6.6.1 Strength criteria for intact rock

The applicability of the three empirical strength criteria suggested by Bieniawski (1974), Hoek and Brown, (1980), and Ramamurthy et al. (1984) was assessed for Ashfield shale samples using the triaxial test data. Although these criteria make no explicit allowance for strength anisotropy, i.e the influence of β, this was considered by changing the value of the normalising parameter σ_c for each individual value of β. Of the three criteria used, Bieniawski's criterion (Equation 5.4) appears to be the most appropriate one for Ashfield shale. The Hoek and Brown criterion is the next best. The Ramamurthy criterion slightly under

predicts the peak stress for Ashfield shale, and is limited because it can not predict satisfactorily the peak stress values when σ_3 is smaller than 5% of the uniaxial compressive strength.

5.6.6.2 Strength criteria for anisotropic material

The single plane of weakness theory has validity for Ashfield shale and fits the experimental data fairly well, except at high confining pressures where it tends to overpredict at the shoulders (β close to 0 and 90 degrees) and underpredict at β = 30 to 45 degrees. The modified variable cohesive theory proposed by McLamore and Gray fits the experimental data very well at low confining pressure, but at the higher confining pressure of 10 *MPa* an overprediction is shown in the region around β = 30 degrees. The Ramamurthy et al. (1988) criterion has shown a better matching of the test results for a confining pressure of 1 *MPa*, but tends to underpredict at confining pressures of 0.1 and 10 *MPa*.

The limitation of the single plane of weakness theory is that the cohesion intercept and friction angle of the matrix and the weakness plane must be determined by conducting a minimum of triaxial tests at β = 0, 90 and 30 degrees. Compared to the other theories described here, there are some more limitations in the modified variable cohesive strength theory as mentioned before. The value of n needs to be estimated. There seems to be no other rational procedure for determining the appropriate value of n other than curve fitting by trial and error. The main limitations of the Ramamurthy et al. theory are the requirements for a number of triaxial tests at β = 90° and the uniaxial compression test data for a range of values of β.

Of the three criteria used, the single plane of weakness theory appears to be the most appropriate one for Ashfield shale as it fits the experimental data fairly well.

5.6.7 An empirical strength criterion for Ashfield Shale

Some of the disadvantages of the existing strength criteria and their limitations when applied to Ashfield shale have been described in previous sections. For practical purposes it is desirable to have a single criterion that overcomes many of these criticisms and limitations and is capable of accurately predicting the strength of this shale. It is highly desirable that this single criterion meet the following requirements:

(a) It should be capable of accurately predicting the strength of Ashfield shale over the full range of β values, and therefore capture accurately the anisotropic nature of the strength.

(b) It should include the important influence of confining pressure on the strength.

(c) In view of the findings presented in Chapter 4, it should also allow for the significant influence of moisture content on strength.

(d) Determination of the key parameters in the criterion should be relatively straightforward and should require a minimum of testing.

In essence, if point (c) is adequately addressed then variations from one location to another within the Sydney basin should also be taken into account, since it has been demonstrated that changes in the quality of the shale are largely reflected by changes in the moisture content.

In this section an alternative, purely empirical strength criterion for Ashfield shale is presented. It will be seen that this new criterion meets all of the requirements stated above in points (a) to (d).

The new criterion is developed by combining Bieniawski's empirical strength criterion (Equation 5.4) with Equation (5.1), which is similar in form to one proposed by McLamore and Gray (1967) for variable cohesion. In Equation (5.1), A and B are constants and can be evaluated from the *UCS* tests described previously. This approach has many advantages over the criteria using c and ϕ, which are themselves stress dependent and are less straightforward to determine.

Following this approach, Equation (5.1) can be re-written in non-dimensional form as

$$\frac{\sigma_c}{\sigma_{c90}} = \acute{A} - \acute{B}\left[cos2(\beta_{min} - \beta)\right]^n \qquad \textbf{(5.17)}$$

where A', B', β and n are constants. The test data for Ashfield shale indicate that they take the following values:

$A' = 0.97$

$B' = 0.65$

for $0 \leq \beta \leq 30°$, and

$A' = 0.92$

$B' = 0.60$

for $30° \leq \beta \leq 90°$

$\beta_m =$ 30 degrees

$n = 3$

The term σ_{c90} represents the *UCS* at $\beta = 90$ degrees. The test results presented in Chapter 4 indicate that σ_{c90} can be determined from the following empirical equation

$$\sigma_{c90} = 600 p_a e^{(-0.415 m_c)} \qquad \textbf{(5.18)}$$

where m_c is the natural moisture content of the shale and p_a is atmospheric pressure (0.1 *MPa* or 14 lb/in^2). Equation (5.17) may now be used to determine a value for σ_c at any desired value of moisture content and any value of β, so the anisotropic uniaxial compressive strength is now completely defined.

It remains to substitute the value of σ_c determined in this way into the Bieniawski criterion that predicts the influence of confining pressure on the strength. For convenience this criterion (Equation 5.4) is repeated here

$$\frac{\sigma_1}{\sigma_c} = 1 + B\left(\frac{\sigma_3}{\sigma_c}\right)^{\alpha} \qquad \textbf{(5.4)}$$

where $B = 3$ and $\alpha = 0.75$ for Ashfield shale.

A comparison of the strengths predicted by this approach and the experimental test data for Ashfield shale is presented in Figure 5.26. It is important to note that this comparison covers the full range of β values and a range of confining pressures from 0 to $10MPa$. Furthermore, the experimental data shown on this figure comes from tests on core samples from both the Ryde interchange and Surry Hills sites. For the former the moisture contents were approximately between 2 to 4%, corresponding to *UCS* values at $\beta = 90$ degrees of about 25 to 11 *MPa*, and for the latter the moisture contents were around 1.2 to 2%, with corresponding *UCS* values of approximately 35 *MPa* to 25 *MPa*. The agreement between the new criterion and the test data is very satisfactory. The new criterion captures many of the effects that are important in practice. However, it should also be noted that the new criterion has been validated only for fresh and slightly weathered Ashfield shale, covering a range of natural moisture contents up to approximately 4.5%. It has not been validated beyond these limits because of the difficulty in coring the more weathered samples, particularly at smaller values of β.

5.7 EVALUATION OF THE ANISOTROPIC DEFORMATION PARAMETERS

Because of the presence of laminations, Ashfield shale is expected to show cross-

anisotropic deformation behaviour. The mechanical behaviour is expected to be isotropic parallel to the laminations (or bedding planes), but anisotropic in the direction orthogonal to the lamination. Taking the lamination planes (or the plane of isotropy) parallel to the x and y axes and the z axis perpendicular to the plane of isotropy, the general stress-strain relationships of an ideal cross-anisotropic elastic material are given by:

$$\epsilon_x = \frac{\sigma_x}{E_1} - \nu_1 \frac{\sigma_y}{E_1} - \nu_2 \frac{\sigma_z}{E_2} \tag{5.19}$$

$$\epsilon_y = \frac{\sigma_y}{E_1} - \nu_1 \frac{\sigma_x}{E_1} - \nu_2 \frac{\sigma_z}{E_2} \tag{5.20}$$

$$\epsilon_z = \frac{\sigma_z}{E_2} - \nu_2 \frac{\sigma_x}{E_1} - \nu_2 \frac{\sigma_y}{E_1} \tag{5.21}$$

$$\gamma_{xy} = \frac{\tau_{xy}}{G_1} = \frac{2(1+\nu_1)}{E_1} \tau_{xy} \tag{5.22}$$

$$\gamma_{yz} = \frac{\tau_{yz}}{G_2} \tag{5.23}$$

$$\gamma_{zx} = \frac{\tau_{zx}}{G_2} \tag{5.24}$$

In which ϵ_x, ϵ_y, ϵ_z, γ_{xy}, γ_{yz} and γ_{zx} are strain components and σ_x, σ_y, σ_z, τ_{xy}, τ_{yz} and

τ_{zx} are stress components.

The following five material constants may be used to describe the behaviour of materials of this type:

E_1= Young's modulus in the plane of isotropy, i.e. parallel to the laminations,

E_2= Young's modulus perpendicular to the plane of isotropy, i.e. perpendicular to the laminations,

ν_1= Poisson's ratio, describing the behaviour in the planes of the laminations in response to normal stress applied parallel to the laminations,

ν_2= Poisson's ratio, describing the behaviour in the direction perpendicular to the laminations in response to normal stress applied parallel to the laminations,

G_2= the independent shear modulus, describing the shearing behaviour in planes perpendicular to the laminations.

5.7.1 Determination of four of the anisotropic elastic parameters

To determine four of the five independent parameters, uniaxial and triaxial compression tests were performed on samples with β = 0 and 90 degrees as described below.

(a) By performing uniaxial and triaxial compression tests on vertical samples ($\beta = 90°$) using longitudinal and circumferential gauges, the values for E_2 and ν_2 can be obtained from application of equations (5.19), (5.20) and (5.21) after substitution of $\sigma_x = \sigma_y = 0$, i.e.

$$E_2 = \frac{\sigma_z}{\epsilon_z} \qquad \textbf{(5.25)}$$

$$\epsilon_x = \epsilon_y = -\nu_2 \frac{\sigma_z}{E_2} \tag{5.26}$$

(b) By performing similar tests on samples with $\beta = 0$ degrees, using longitudinal and circumferential gauges, the values of E_1 and ν_1 can be obtained from application of the following equations

$$E_1 = \frac{\sigma_x}{\epsilon_x} \tag{5.27}$$

$$\epsilon_z = -\nu_1 \frac{\sigma_x}{E_1} \tag{5.28}$$

An experimental study has also been made to determine the effects of the lamination direction and confining pressure on the elastic parameters of Ashfield shale. Triaxial compression tests have been performed on samples of Ashfield shale at specified orientation angles, $\beta = 0, 15, 30, 45, 60, 75$ and 90 degrees, and various confining pressures from 0 to 10 *MPa*. In this study two axial and two circumferential strain gauges were mounted on each sample of Ashfield shale, as explained previously (see also Figure 5.4).

5.7.2 Uniaxial test results

Samples of Ashfield shale from two different sites, Ryde-interchange and Surry Hills, in the Sydney metropolitan area have been tested. The results for all the specimens with different lamination directions were plotted in the form of applied axial stress versus axial and diametral strain. The modulus of elasticity and the Poisson's ratio, calculated from axial and diametral strains measured with strain gauges, were also plotted as functions of axial stress. A typical set of results for vertical ($\beta=90°$) and horizontal ($\beta=0°$) specimens of the Ashfield shale from

these two sites are shown in Figures 5.27 and 5.28, respectively.

Axial and diametral strain measurements were made on samples with orientations in the range from 0 to 90 degrees. The stress-strain curves for all samples from Surry Hills and Ryde interchange sites are shown in Figures 5.29 and 5.30, respectively. These figures show that there is a variation in the slope of the curves with the orientation of the laminations.

From a study of all the results, it is noted that the stress-strain curves are slightly nonlinear at the beginning of the loading. It may be concluded that the nonlinearity of the LVDT data at low stresses is due to seating of platens. The strain gauge data are almost linear at low stresses up to about 50% of the maximum stress. With unloading, a hysteresis loop is formed with permanent strain on removal of all load.

The four independent elastic parameters, E_1, E_2, ν_1 and ν_2 were determined by performing uniaxial compression tests in two directions (β=0, 90°) and by using equations (5.25) to (5.28). The following values for these four parameters for Ashfield shale from Surry Hills and Ryde-interchange have been obtained, respectively:

$E_1 = 21200\ MPa$

$E_2 = 6600\ MPa$

$\nu_1 = 0.1$

$\nu_2 = 0.1$

and

$E_1 = 9600\ MPa$

$E_2 = 3100\ MPa$

$\nu_1 = 0.1$

$\nu_2 = 0.1$

These are secant values measured at an axial stress of approximately 50% of the peak strength. The modulus of elasticity is a maximum for the horizontal

direction ($\beta=0$), when the load is applied parallel to the laminations, and minimum for the perpendicular direction ($\beta=90°$), when the load is applied perpendicular to the laminations.

Figures 5.31 and 5.32 show the variation of the modulus of elasticity at different lamination directions ($E_\beta = \sigma_{axial}/\epsilon_{axial}$) with axial stress for samples from the Ryde-interchange and Surry Hills sites, respectively. The values of E_β in these figures are secant values determined at the appropriate level of axial stress. These figures show that at any given value of β the modulus of elasticity becomes almost constant at around 5 *MPa* axial stress. These figures also show that E_β is minimum when $\beta = 90°$ ($E_\beta = E_2$) and E_β is maximum when $\beta = 0$ ($E_\beta = E_1$).

To compare samples of Ashfield shale from Surry Hills and Ryde-interchange, the variations of the modulus of elasticity and *UCS* in the direction perpendicular to the laminations ($\beta=90°$) were examined. The ratio of modulus of elasticity of shale from Surry Hills to Ryde is 2.13 and the ratio of *UCS* for shale from these two sites is 1.5. The difference between these two ratios seems to be because of the higher porosity of shale from Ryde than shale from Surry Hills. It was found that E also is a function of moisture content, but there is not enough data to examine this in detail.

5.7.3 Triaxial test results

Samples of Ashfield shale from two different sites, the Ryde-interchange and Surry Hills, in the Sydney metropolitan area have been tested. The test results have been plotted in the form of deviator stress (σ_1-σ_3) versus axial (ϵ_1) and diametral strain (ϵ_3). The modulus of elasticity and the Poisson's ratio, calculated from axial and diametral strains measured with strain gauges, were also plotted as a function of stress. A typical set of results for vertical ($\beta = 90°$) specimens of the Ashfield shale from the Ryde-interchange and Surry Hills sites for 2 *MPa* confining pressure are shown in Figures 5.33 and 5.34, respectively. These results are based on values measured up to a deviator stress of approximately 50% of the

peak strength.

Axial and diametral strain measurements were made on samples with orientations that range from 0 to 90 degrees. The stress strain curves for all lamination directions for samples from the Surry Hills and Ryde interchange sites are shown in Figures 5.35 and 5.36, respectively. These figures show a variation in the slope of the curves with the orientation of the laminations, and the overall pattern is the same as that shown in Figure 5.30 for specimens tested without a confining stress. From a study of all the test results, it may be concluded that the axial strain gauge data are almost linear at low stresses up to about 50% of the maximum stress, but significant departures from linearity occur for the diametral strains, particularly for the weaker material from the Ryde site.

5.7.3.1 Modulus parameters

The values for E_1 and E_2 were obtained from the axial strain gauges in the tests on samples of the Ashfield shale from Surry Hills with $\beta = 0$ and 90 degrees, respectively. These values were based on the secant values measured at a deviator stress of approximately 50% of the peak strength. The results for different confining pressures are shown in Table 5.4.

The modulus of elasticity was a maximum when the load was applied parallel to the laminations ($\beta = 0$) and a minimum when the load was applied perpendicular to the laminations ($\beta = 90°$). Table 5.4 shows that the modulus of elasticity in the direction parallel to the laminations, E_1, compared to the modulus of elasticity in the perpendicular direction, E_2, is more influenced by the confining pressure.

For correlation between the modulus of elasticity and confining pressure, Kulhawy (1975) suggested a power law expression in the form

$$E_i = K' p_a \left(\frac{\sigma_3}{p_a}\right)^{n'} \qquad \textbf{(5.29)}$$

where

E_i= initial tangent modulus

K' = modulus number

n' = modulus exponent

σ_3= confining pressure

p_a= atmospheric pressure in the same units as σ_3 and E_i to ensure that K' and n' are dimensionless numbers.

Santarelli (1987) modified this expression using of a power of $(1+\sigma_3)$. In the present study the modified form of equation (5.29) was examined.

A plot of E_1/p_a versus the σ_3/p_a is shown in Figure 5.37. This graph indicates that E_1 increases with an increase of the confining pressure. The variation shown on the figure is best described by the following equation:

$$\frac{E_1}{p_a} = 217000\left(1+\frac{\sigma_3}{p_a}\right)^{0.035} \qquad \textbf{(5.30)}$$

where E_1 and σ_3 are both measured in *MPa*. Regression analysis shows that equation (5.30) fits the data with a correlation coefficient of 0.96.

Figures 5.38 and 5.39 show the variation of modulus of elasticity (E_β) with deviator stress at a constant confining pressure (2 *MPa*) during the tests on samples from the Ryde-interchange and Surry Hills sites, respectively. These

figures show that at any given value of β the modulus of elasticity becomes almost constant at around 4 *MPa* deviator stresses. These figures also show the variations of modulus of elasticity with the angle of the laminations to the axial stress direction, i.e. E_β is minimum when $\beta = 90°$ ($E_\beta = E_2$) and E_β is maximum when $\beta = 0$ ($E_\beta = E_1$). The variation of E_β with deviator stress is similar to that in the *UCS* tests (Figure 5.32) and similar variations were observed at other confining stresses.

5.7.3.2 Poisson's ratio

Poisson's ratio was calculated from the diametral and axial strains measured by strain gauges mounted on triaxial specimens with lamination angles of $\beta = 0$ and 90 degrees. From the experimental results, it was found that Poisson's ratios were not constant and were influenced by the non-linear diametral strain responses. This problem was more pronounced for the Ryde samples. The Poisson's ratios obtained from both sites varied between 0.1 and 0.16 in both directions ($\beta = 0$ and $\beta = 90°$). There was not much change in the values of Poisson's ratio with confining pressure.

5.7.4 Evaluation of the independent shear modulus

The independent shear modulus, G_2, was determined from the uniaxial and triaxial compression tests on the specimens with laminations at various angles β. It can be shown from the theory of elasticity for a cross-anisotropic material that the modulus E_β measured on samples with laminations inclined at β to the axial direction is given by the following equation (Jaeger and Cook, 1969):

$$\frac{1}{E_\beta} = \frac{1}{E_2}\sin^4\beta + \frac{1}{E_1}\cos^4\beta + \left[\frac{1}{G_2} - \left(\frac{\nu_1}{E_1} + \frac{\nu_2}{E_2}\right)\right]\sin^2\beta\cos^2\beta \qquad (5.31)$$

It is thus possible to estimate G_2 by a curve fitting procedure using the variation of E_β with β and the values of E_1, E_2, ν_1 and ν_2 determined from the uniaxial and triaxial compression tests described previously. The values of E_β for $\sigma_3 = 0$ are shown in Table 5.5. The theoretical curves of E_β/E_2 versus β have been plotted for different values of G_2/E_2 in Figure 5.40. The experimental values of E_β/E_2 (Table 5.5) are also superimposed on these curves. It can be seen that the theoretical curves corresponding to $G_2 = 6600\ MPa$, or $G_2/E_2 = 1$, provide the best fit to the experimental data.

The secant values of the four independent deformation parameters (E_1, E_2, ν_1, ν_2) have also been obtained by triaxial compression tests at deviator stresses of approximately 50% of the peak strength. Using these values in Equation (5.31), a comparison has been made between experimental results and predicted values. This comparison is shown in Figure 5.41. The experimental results from the Ryde-interchange and Surry Hills sites for a confining pressure $\sigma_3 = 2\ MPa$ were used in this comparison. Figure 5.41 shows a graph of the modulus ratio E_β/E_2 against the angle β. The ideal anisotropic elastic model shows good general agreement with the experimental results across the full range of β values.

5.7.5 Elastic anisotropy ratio

It has been demonstrated that the Ashfield shale samples from both sites are significantly anisotropic. The ratio E_1/E_2 is defined as the elastic anisotropy ratio. The relationship between the elastic anisotropy ratio and the confining pressure is shown in Figure 5.42. As this figure shows, the elastic anisotropy ratio varies from 2.78 at σ_3=0 to 3.25 for σ_3=10 MPa i.e. the degree of anisotropy increases

with the confining pressure. This is in marked contrast to the effect of confining pressure on the strength anisotropy ratio for which an increase in the confining pressure tended to reduce the strength anisotropy ratio, i.e. the ratio between the values of the maximum and minimum strength, corresponding to the directions $\beta = 90$ and $\beta = 30$ degrees respectively, reduces from 3.1 at zero confining pressure to 1.85 at a confining pressure of 10 *MPa*.

5.8 CONCLUSION

The following general conclusions on the subject of the uniaxial and triaxial strength and deformation properties of the Ashfield shale are made. Because of the presence of laminations, Ashfield shale shows transversely isotropic behaviour. The mechanical behaviour is isotropic parallel to the bedding planes (or laminations), but anisotropic in the direction orthogonal to the laminations.

The Ashfield shale specimens showed the highest compressive strength in the direction perpendicular to laminations. The lowest value of strength occurred for $\beta = 30$ degrees. For uniaxial compression, the strength anisotropy ratio of the Ashfield shale appears to be 3.1. This is significantly greater than the anisotropy ratio of approximately 2 determined from the point load index tests. With increase of the confining pressure in the triaxial tests, there is a reduction in the strength anisotropy ratio.

An increase of the confining pressure increases the maximum strength of the Ashfield shale specimens for all values of β. The rate of increase is approximately the same for all orientations.

Failure of the laminated specimens occurs through extension fracture on the lamination planes for specimens with lamination angles in the range $\beta = 0$ to 15

degrees. For samples with laminations angles from $\beta = 30$ to 45 degrees failure occurs as a slip on the lamination planes. For $\beta = 60$ to 90 degrees, shear fracture occurs across the laminations with failure planes at 20 to 30 degrees to the axial (major principal) stress direction.

The shear strength parameters, cohesive strength and the angle of friction, were obtained from linear parts of, and the initial tangents to, the Mohr-Coulomb envelopes determined from triaxial tests on core specimens. The shear strength parameters vary with the orientation of the laminations to the axial load direction, but the variation in the friction angle is not very significant. The shear strength parameters are also functions of the confining pressure.

Some of the advantages and disadvantages of the existing strength criteria and their limitations when applied to Ashfield shale have been described. For practical purposes a single criterion that overcomes many of these criticisms and limitations has been suggested. This criterion is capable of accurately predicting the strength of Ashfield shale over the full range of β values, and therefore capture accurately the anisotropic nature of the strength. In essence, if moisture content is adequately addressed then variations from one location to another within the Sydney basin should also be taken into account, since it has been demonstrated that changes in the quality of the shale are largely reflected by changes in the moisture content.

The modulus of elasticity was a maximum when the load was applied parallel to the laminations ($\beta = 0$) and a minimum when the load was applied perpendicular to the laminations ($\beta = 90°$). The modulus of elasticity in the direction parallel to the laminations, E_1, compared to the modulus of elasticity in the perpendicular direction, E_2, is more influenced by the confining pressure.

From the study of influence of the lamination angle β, it can be concluded that the ratios of maximum to minimum Young's modulus and maximum to

minimum compressive strengths are very similar, i.e. both are approximately 3. However the angles at which they occur are different. The maximum and minimum strengths correspond to $\beta = 90$ and 30 degrees, respectively, but the maximum and minimum Young's modulus correspond to $\beta = 0$ and 90 degrees, respectively. Furthermore, an increase in the confining pressure tended to reduce the strength anisotropy ratio, defined as the ratio of maximum to minimum deviator stress at failure, but caused an increase in the deformation anisotropy ratio (defined as the ratio of maximum modulus E_1 to minimum modulus E_2).

For evaluation of the independent shear modulus, a series uniaxial and triaxial compression tests was performed on samples in which the laminations were inclined with respect to the axial load direction. Experimental results were compared with theoretical predictions (Equation 5.31). The theoretical predictions show good general agreement with the experimental values of the secant modulus of elasticity, measured at 50% of the peak strength across the full range of β values.

Table 5.1 Summary of the test programme

Type of test	No. of tests	Aim of test
Uniaxial compression test	18	To find the strength anisotropy ($0 \leq \beta \leq 90°$)
	25	To find the anisotropic deformation parameters ($0 \leq \beta \leq 90°$)
Triaxial compression test	50	To understand the variation of shear strength as a function of confining pressure and lamination direction (β) To evaluate the shear strength parameters To observe the effect of lamination direction on cohesive strength and friction angle
	77	To find the deformation parameters of the Ashfield shale and effects of rock anisotropy and confining pressure on the these parameters

Table 5.2 Values of maximum strength as a function of the lamination directions

Lamination direction β (degree)	Maximum shear strength	
	Ryde	Surry Hills
0	-	32.2
0	-	33
15	-	25
15	-	27
30	8.4	-
30	7.7	-
45	12.6	-
45	12.7	-
60	15.5	-
60	15.2	27.5
75	20.9	-
75	21	-
90	24.6	36.4
90	26.2	35.5

Table 5.3 Shear strength parameters for Ashfield shale

β	Cohesion, c (MPa)	Cohesion, c_i (MPa)	Friction angle, ϕ (degrees)	Friction angle, ϕ_i (degrees)
0	7.2	3.5	34	56
15	5.95	2.5	30	57
30	3.78	1.5	24	47
45	5.51	2.5	31	63
60	6.76	3	34	63
75	7.5	3.3	32	58
90	7.81	3.5	33	63

Table 5.4 Values of E_1 and E_2 as functions of confining pressure

Test No.	σ_3 (MPa)	E_1 (MPa) $\beta = 0°$	E_2 (MPa) $\beta = 90°$
S01, S901	0	21941	7737
S02, S902	0.1	22307	7789
S03, S903	0.5	23445	7828
S04, S904	1	23523	7924
S05, S905	2	23943	7619
S06, S906	5	24606	8232
S07, S907	10	25597	8076

Table 5.5 Values of E_β as a function of the lamination directions ($\sigma_3 = 0$)

Lamination direction β (degree)	Surry Hills		Ryde	
	E_β (GPa)	E_β/E_2	E_β (GPa)	E_β/E_2
0	21.1	3.1	-	-
0	21.2	3.1	-	-
0	21	3.1	-	-
15	19.6	2.9	-	-
15	20.6	3.1	-	-
30	16.6	2.5	7.4	2.4
30	16.7	2.5	7.6	2.5
45	-	-	5.8	1.9
45	-	-	6.2	2
60	9.4	1.4	3.9	1.3
60	9.6	1.4	4.6	1.5
75	7.1	1.1	3.7	1.2
75	6.8	1	3.1	1
90	6.6	1	3.2	1
90	7.5	1	3.1	1
90	6.3	1	3.1	1

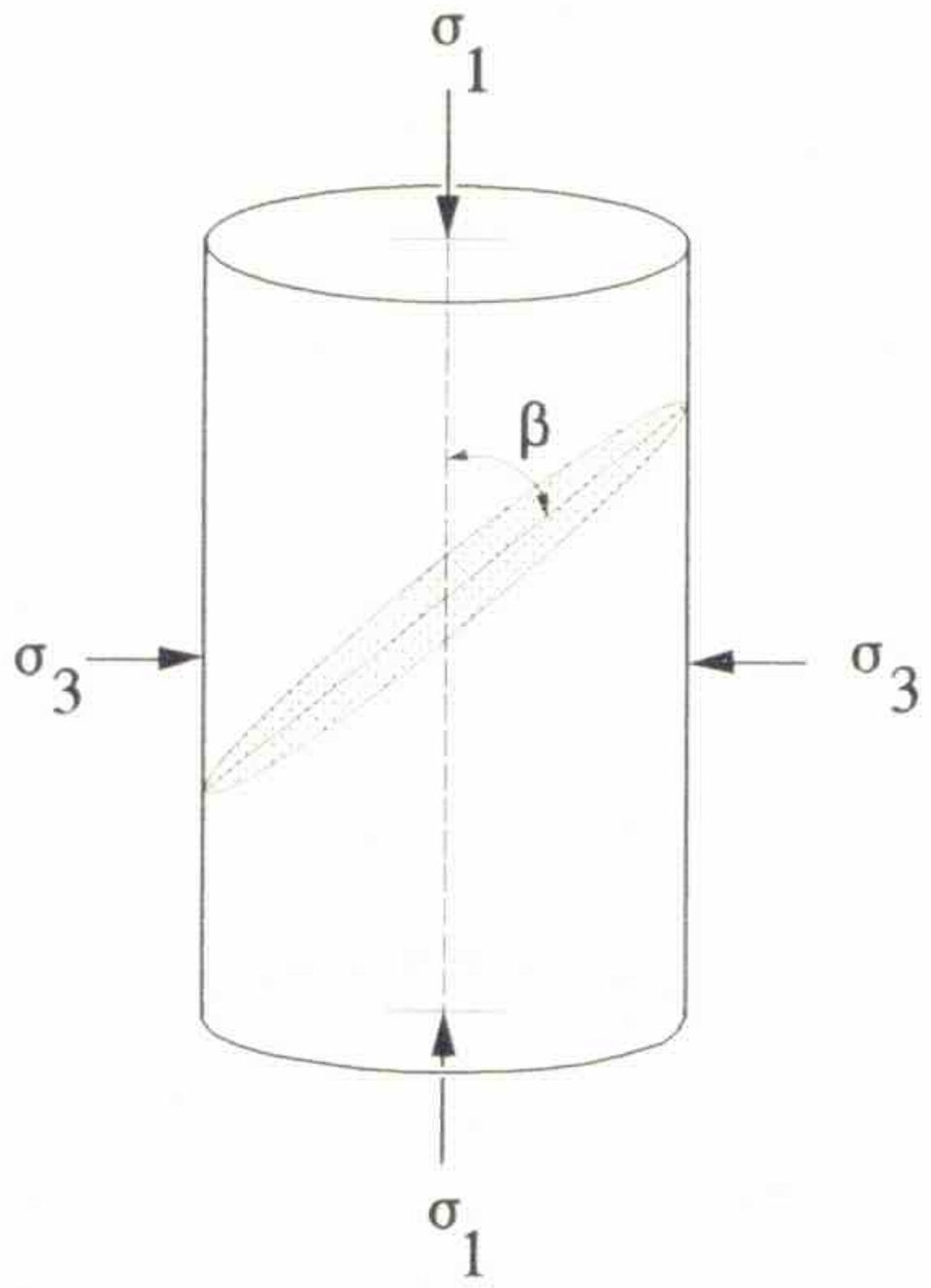

Figure 5.1 Schematic representation of anisotropic sample

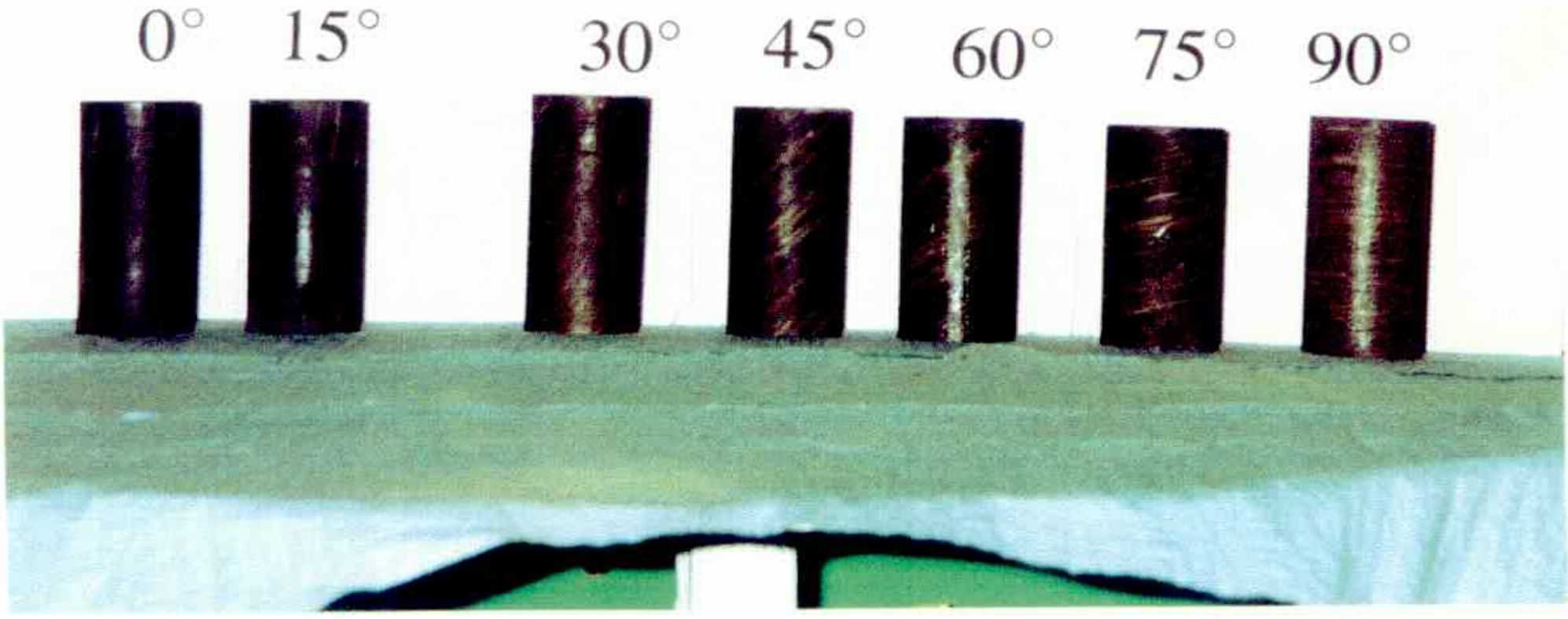

Figure 5.2 Typical anisotropic samples

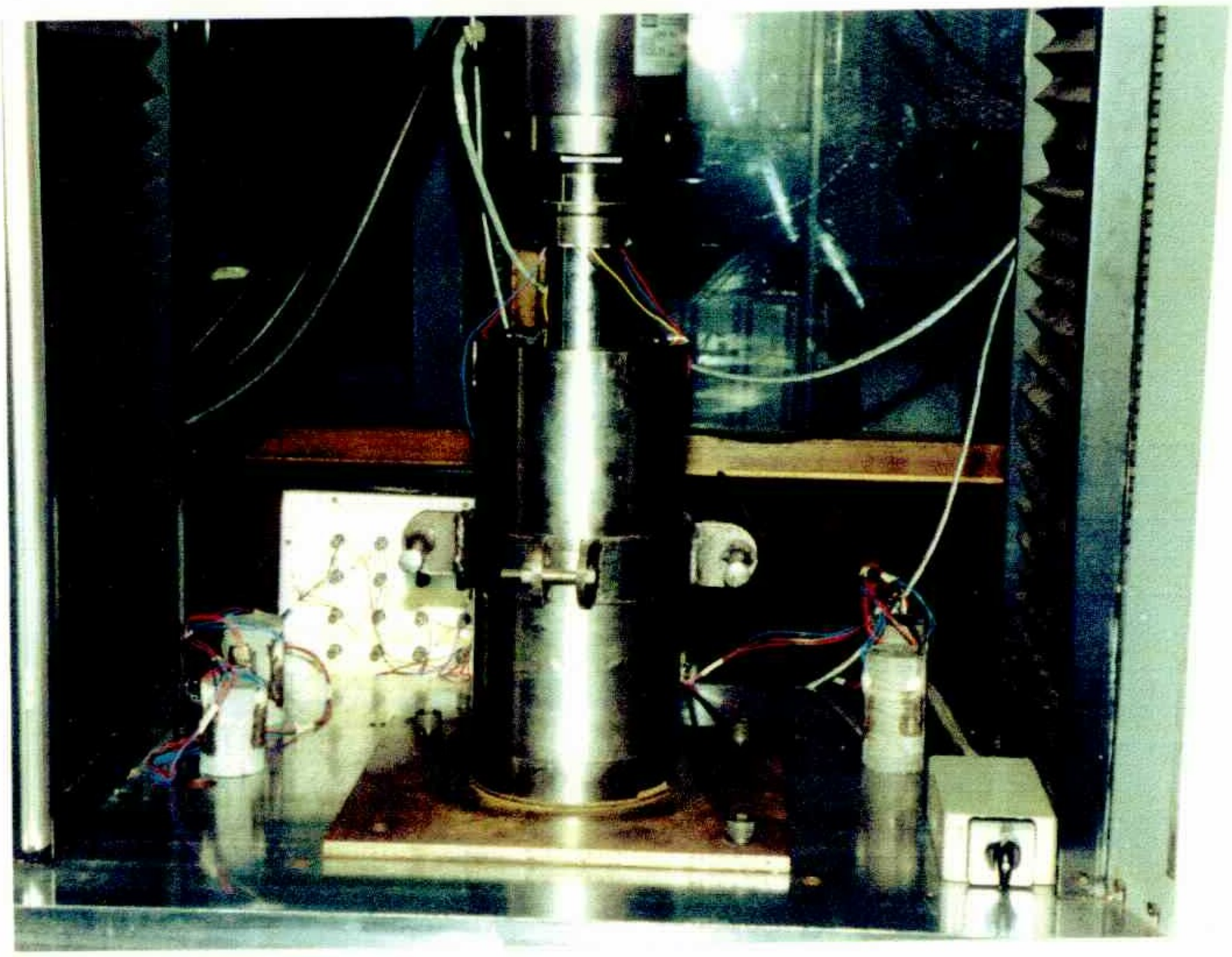

Figure 5.3 A complete set-up of the triaxial equipment

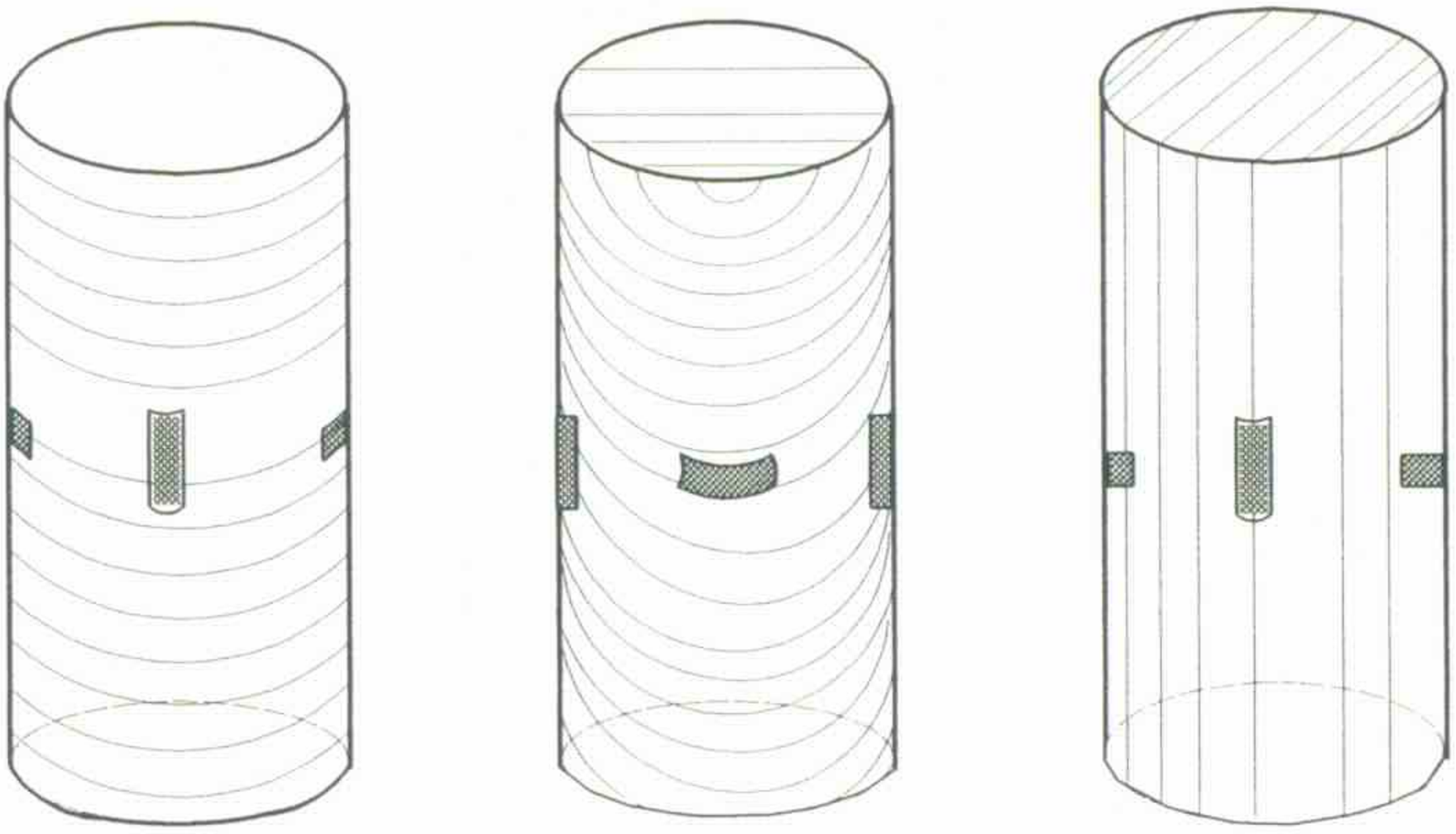

(a)

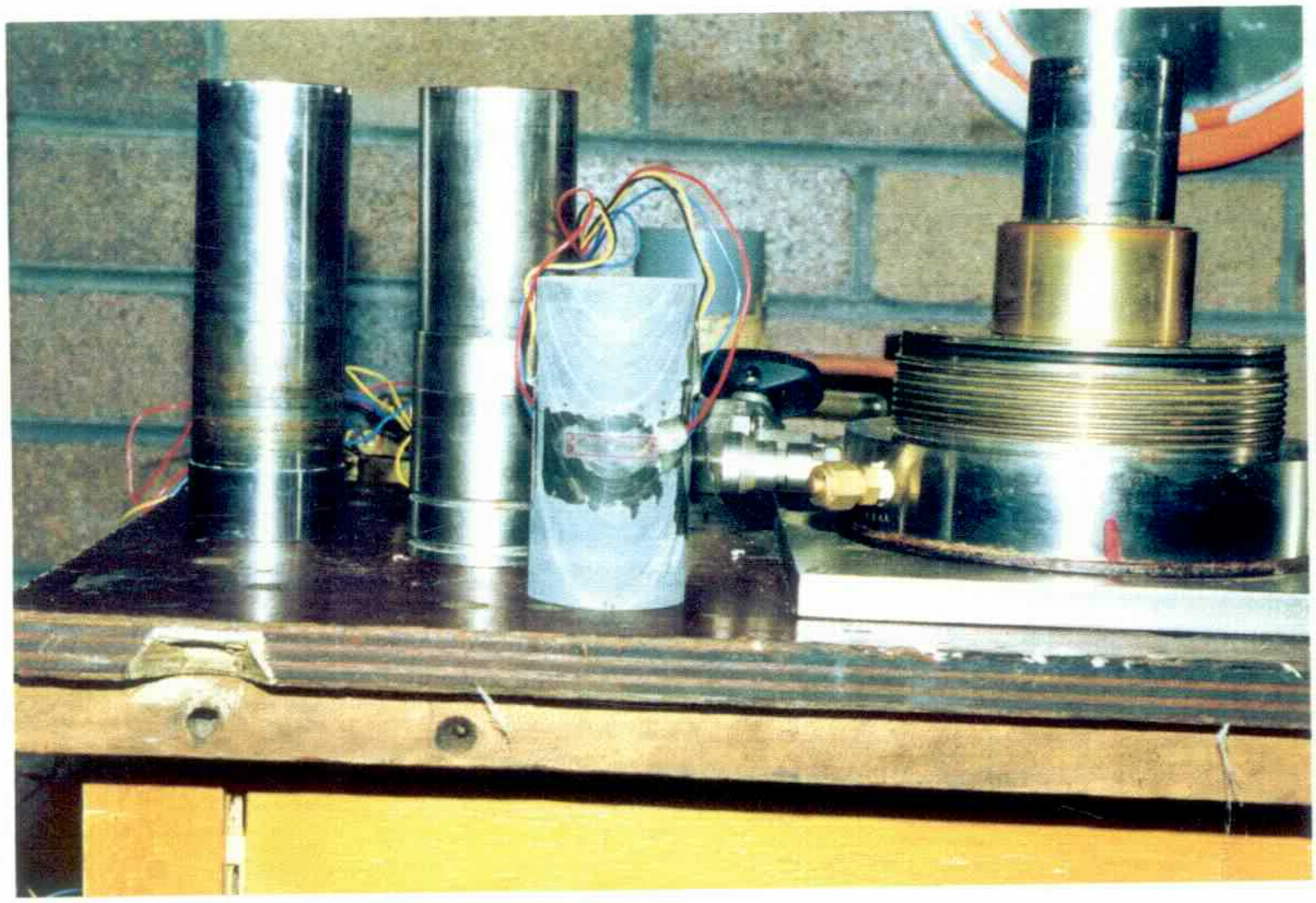

(b)

Figure 5.4 Positions of the gauges for samples with laminations

(a)

(b)

Figure 5.5 Typical view of sample (a) before test and (b) after test

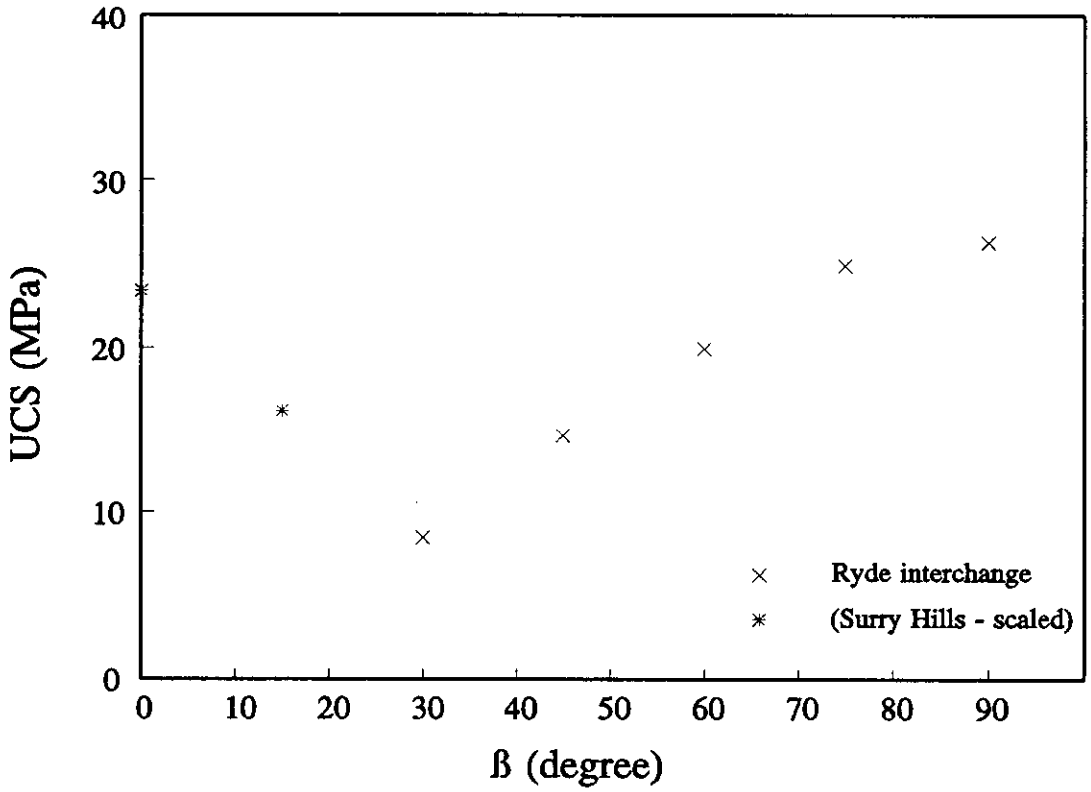

Figure 5.6 Maximum uniaxial compressive strength versus orientation angle β for Ashfield shale

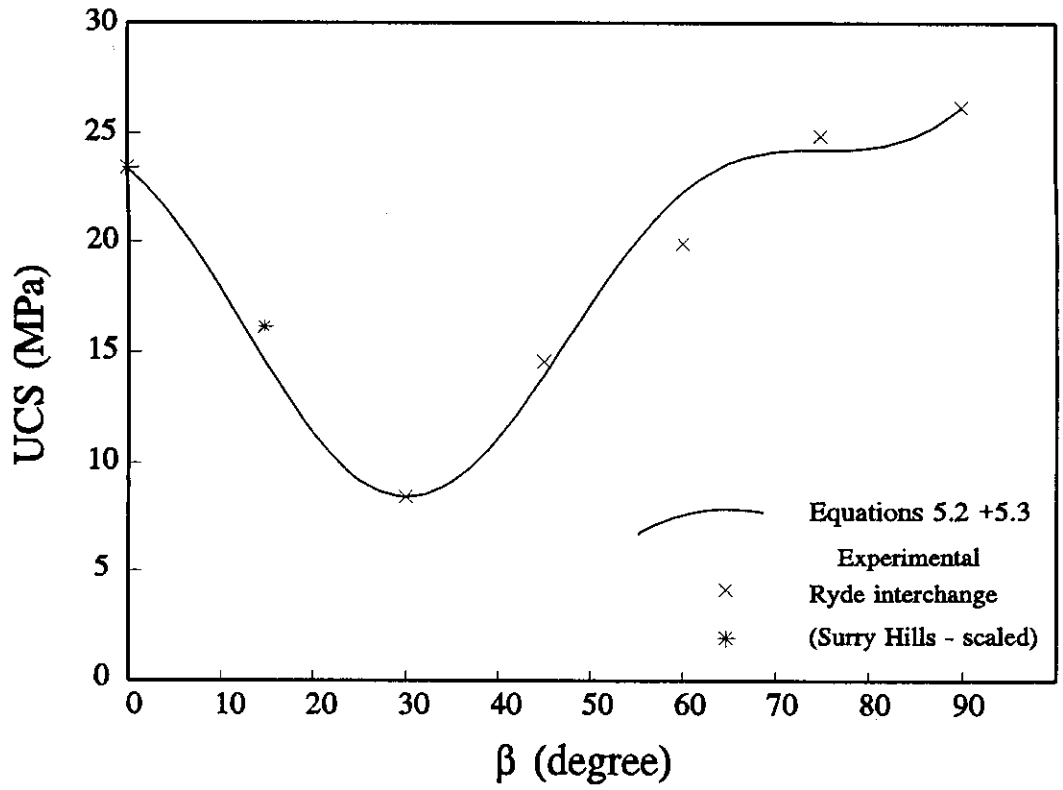

Figure 5.7 Comparison of predicted and experemimental results for Ashfield shale

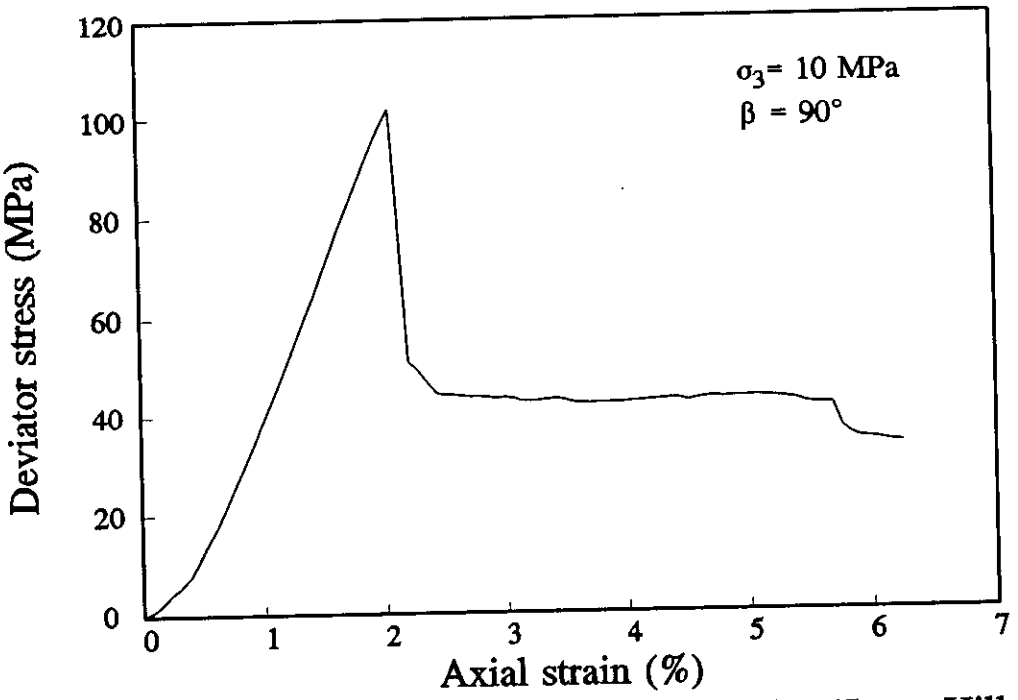

Figure 5.8 Stress-strain curve for Ashfield shale (Surry Hills)

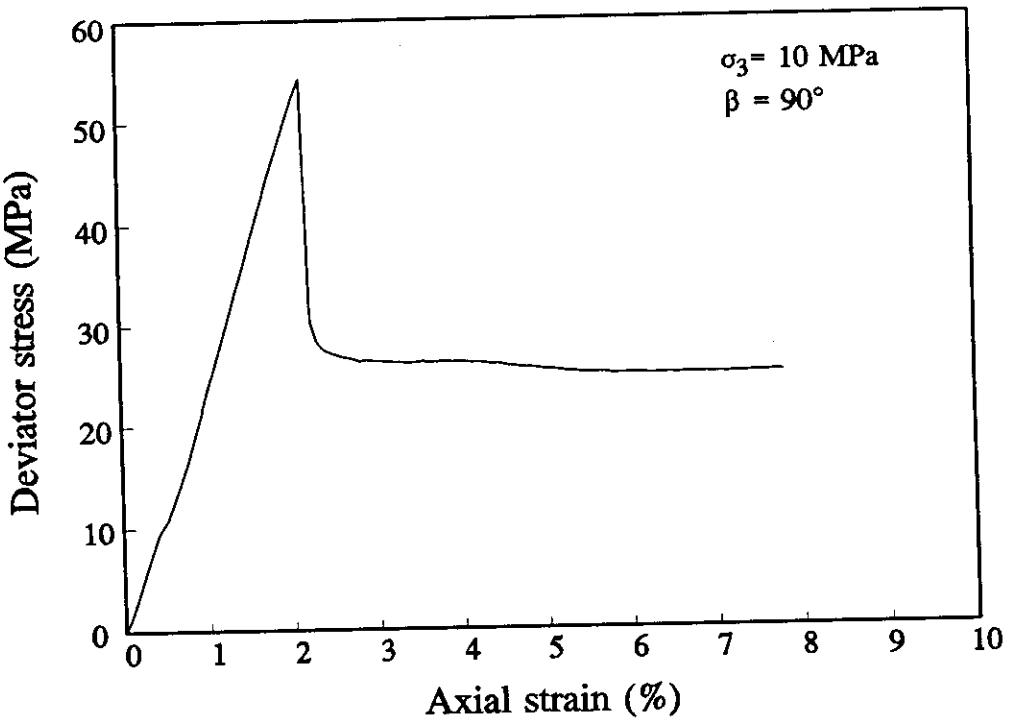

Figure 5.9. Stress-strain curve for Ashfield shale (Ryde)

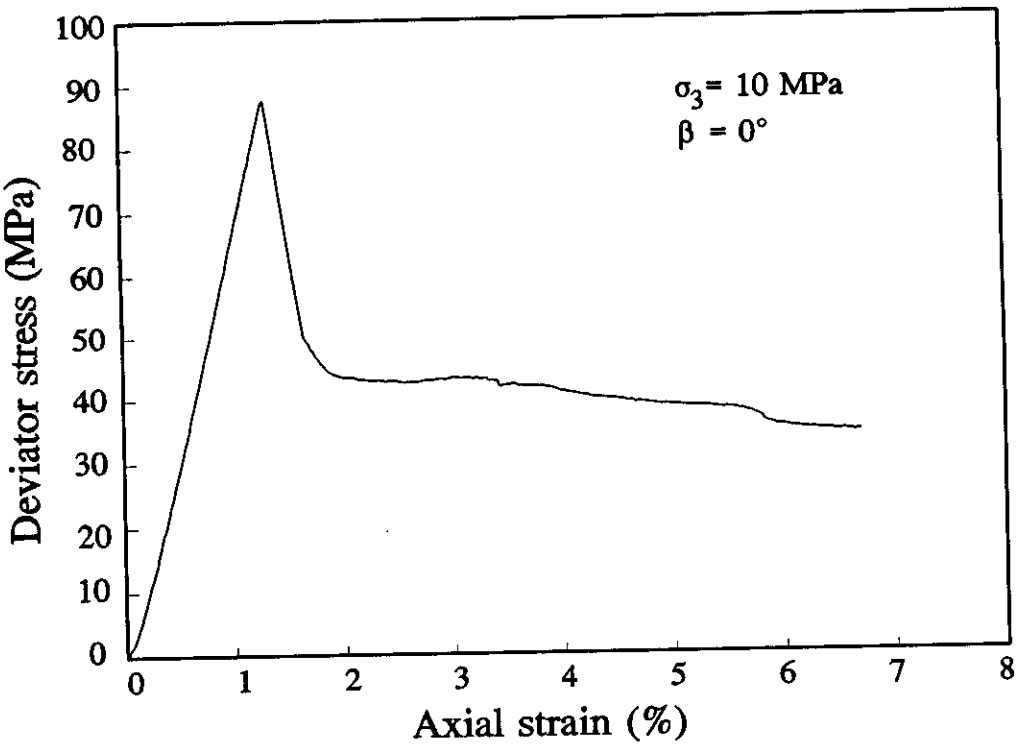

Figure 5.10 Stress-strain curve for Ashfield shale (Surry Hills)

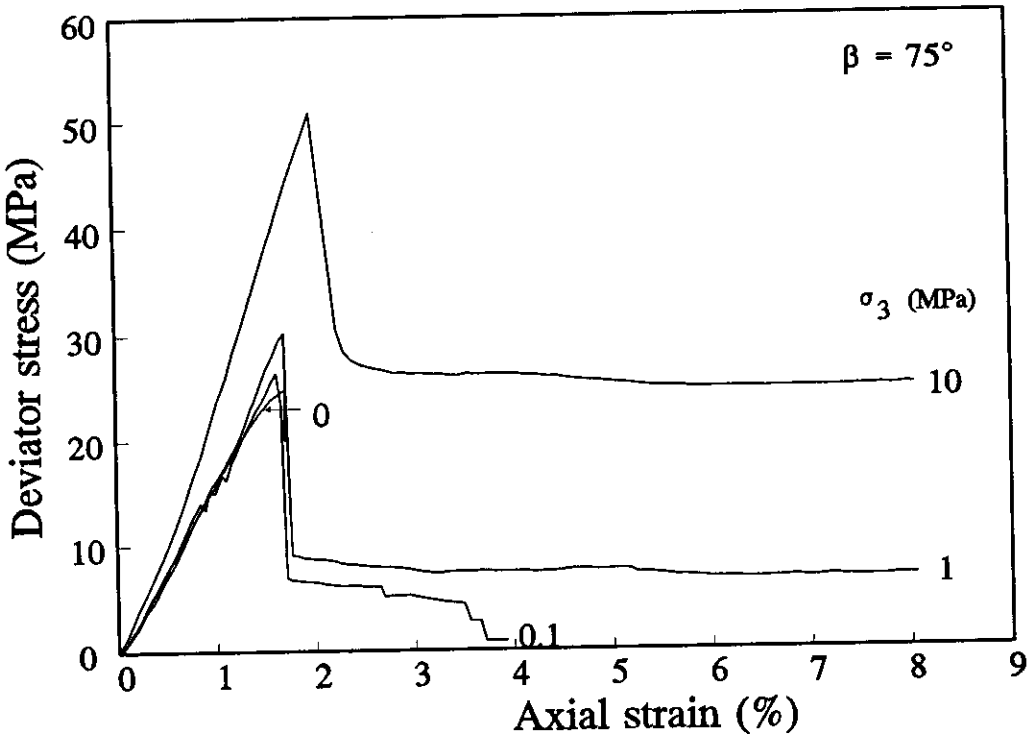

Figure 5.11 Stress-strain curves for Ashfield shale from Ryde site at various confining pressure

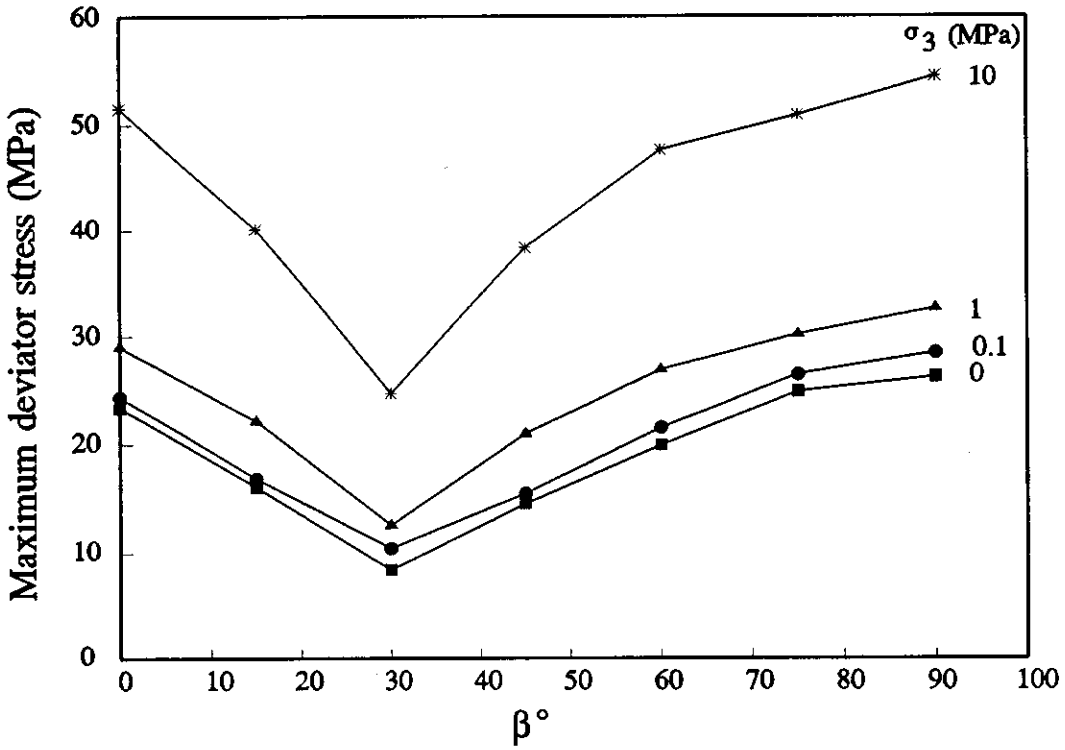

Figure 5.12 Variation of the peak deviator stress with the angle of the laminations to the principal stress direction (β) and the confining pressure (σ_3), Ryde site

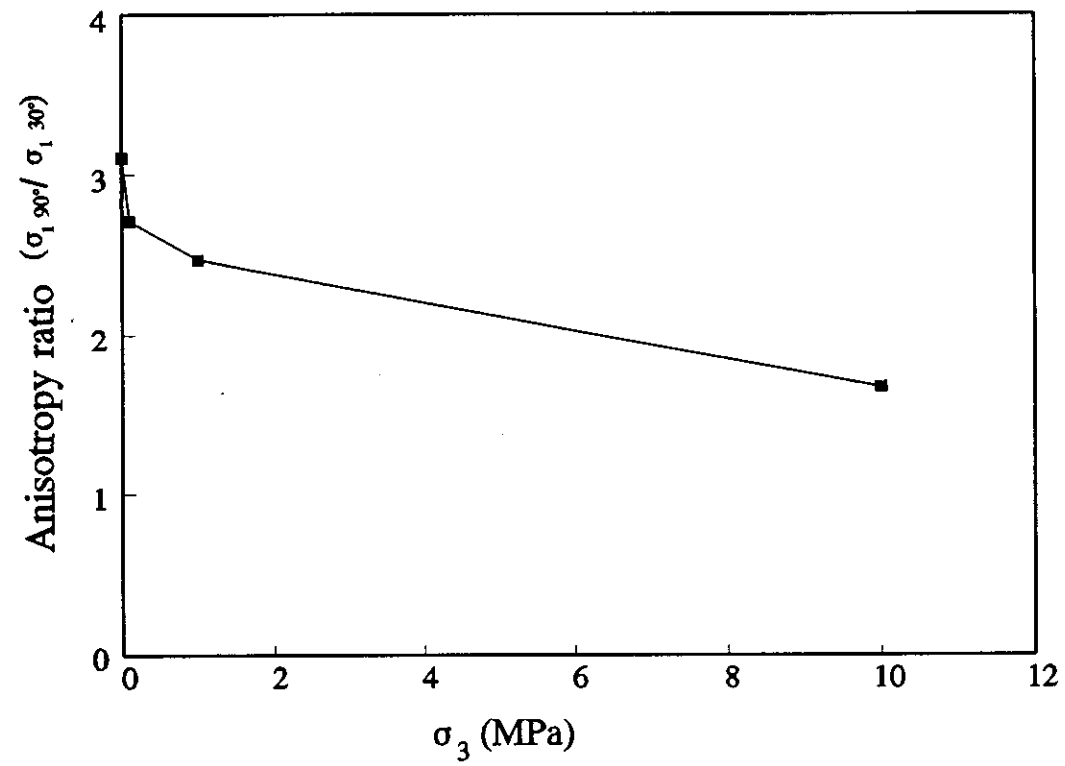

Figure 5.13 Effect of confining pressure on the strength anisotropy

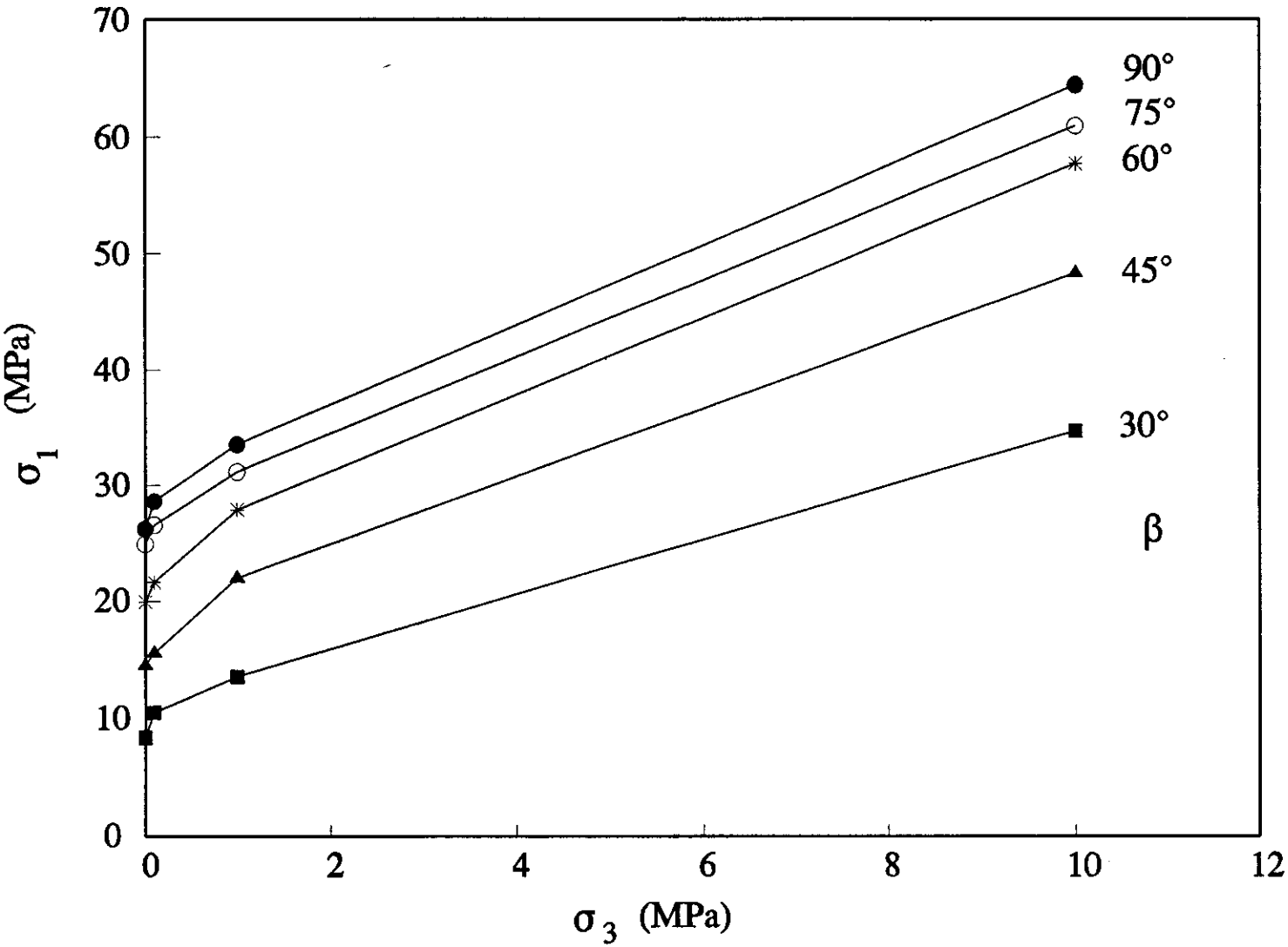

Figure 5.14 Maximum axial stress versus confining pressure for different lamination directions

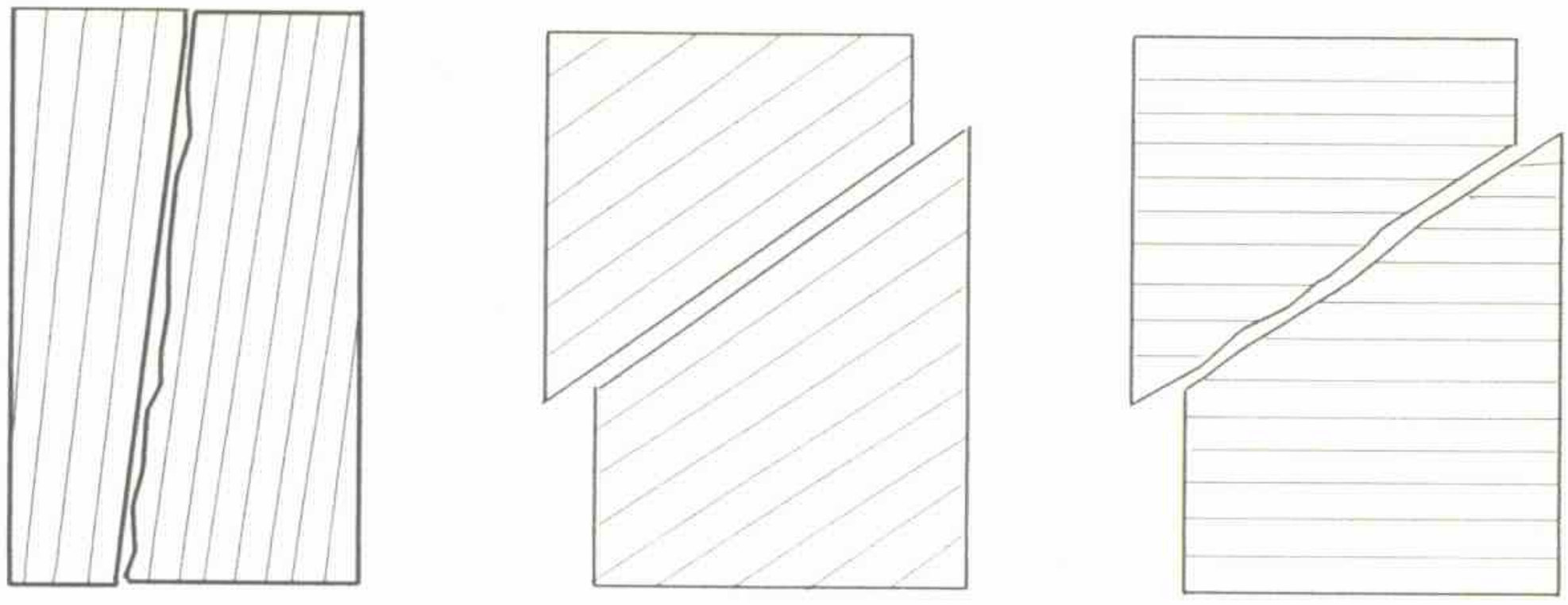

$0 \leq \beta \leq 15°$ $30° \leq \beta \leq 45°$ $60° \leq \beta \leq 90°$

Figure 5.15a Schematic representation of failure modes

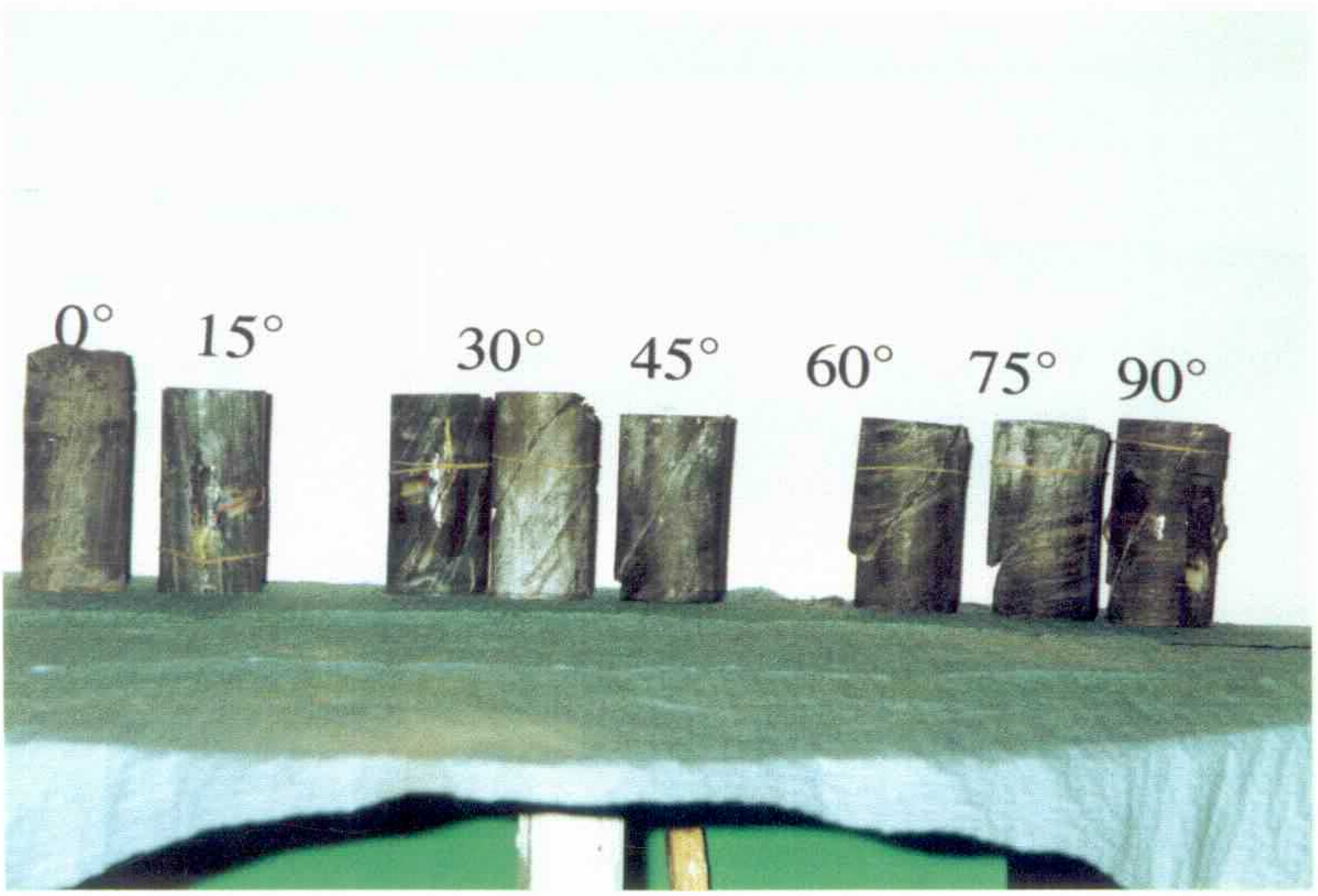

Figure 5.15b Typical representation of failure mode

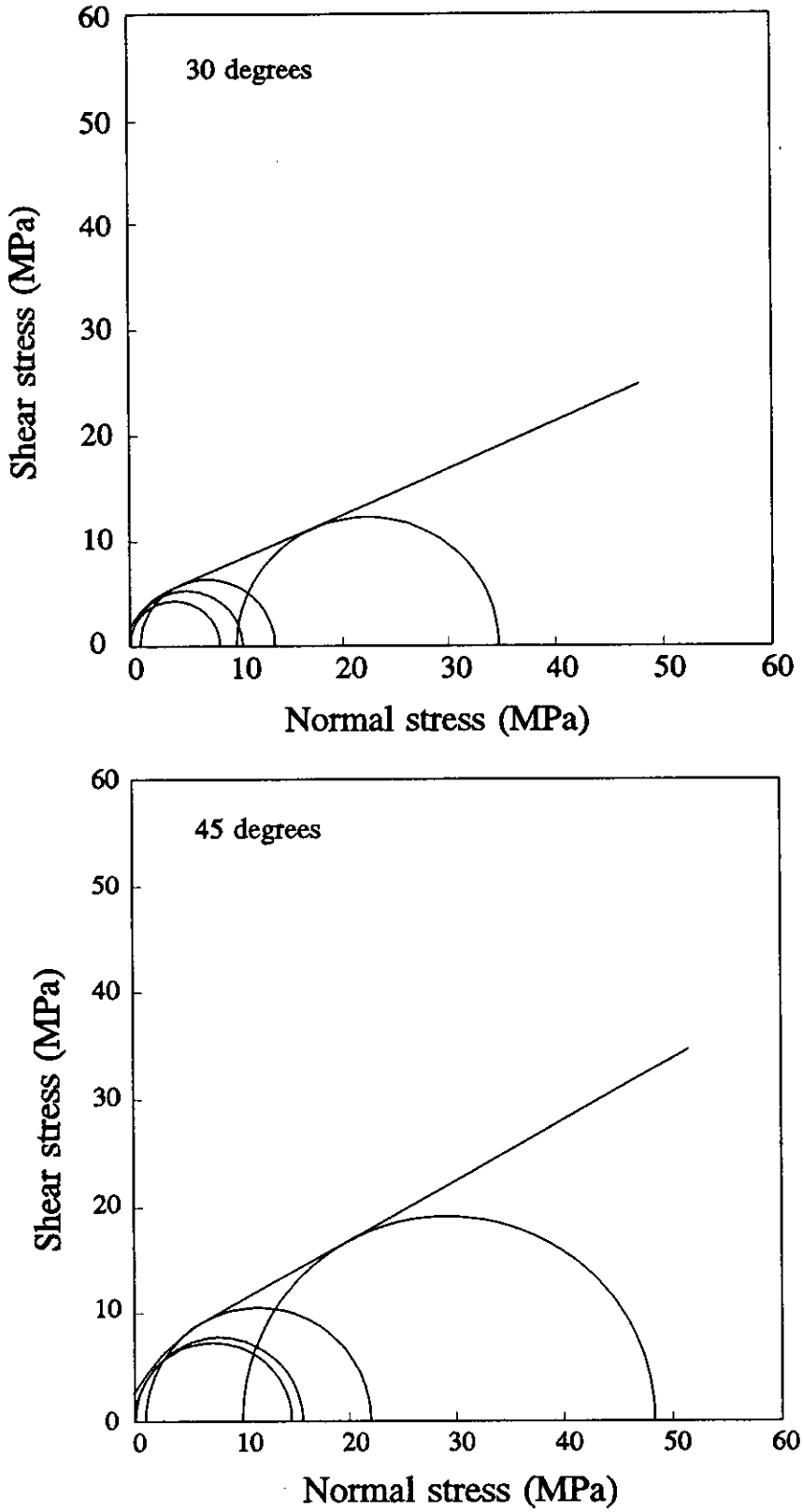

Figure 5.16 Mohr circles for Ashfield shale (Ryde)
30° and 45° lamination directions

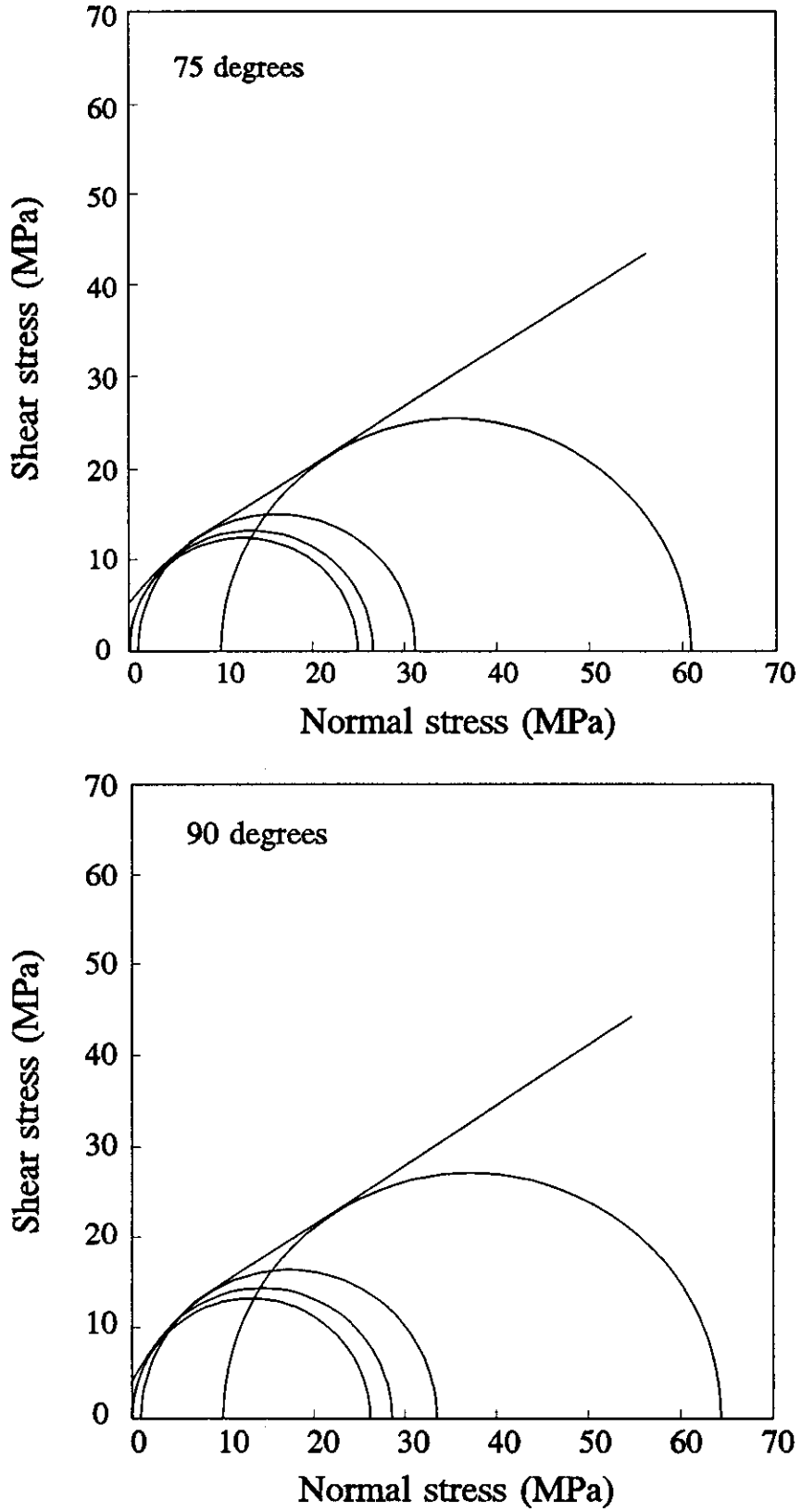

Figure 5.17 Mohr circles for Ashfield shale (Ryde) 75° and 90° lamination directions

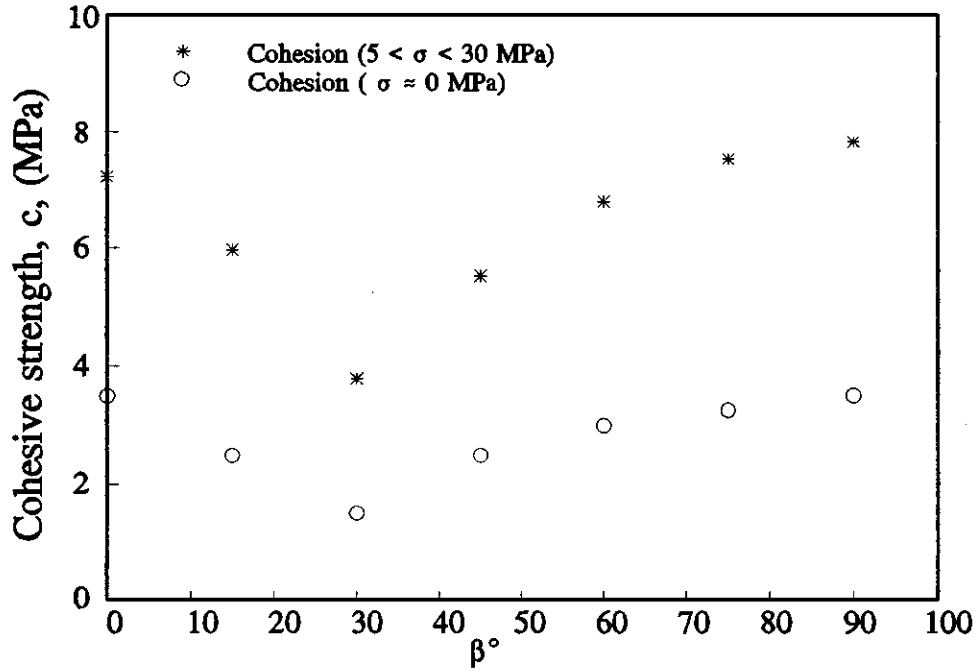

Figure 5.18 Variation of cohesive strength, c, with angle of lamination

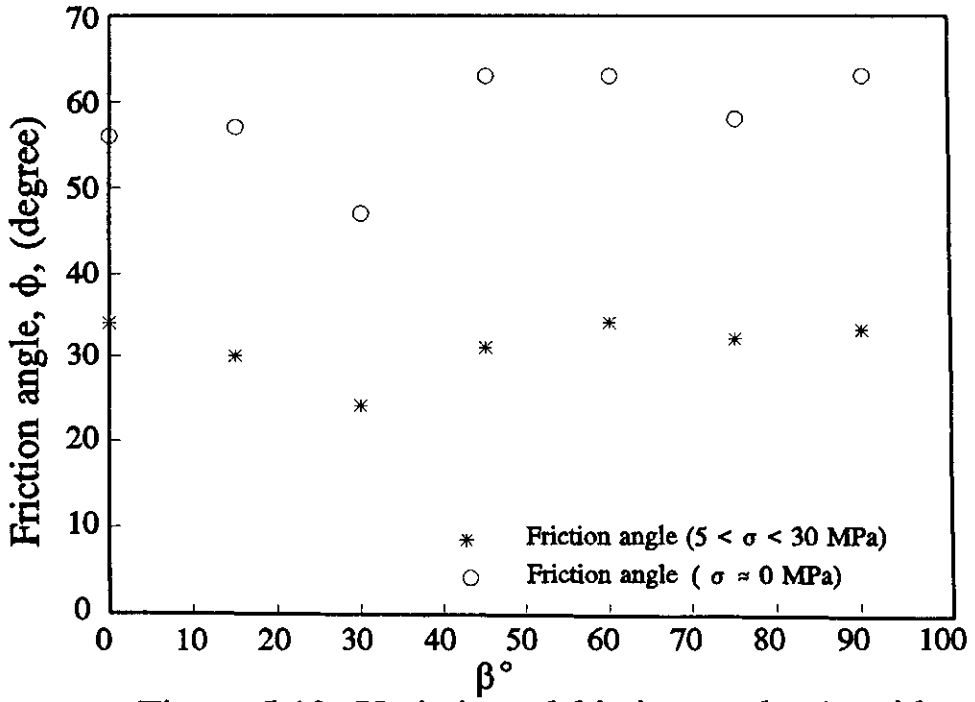

Figure 5.19 Variation of friction angle, ϕ, with angle of lamination

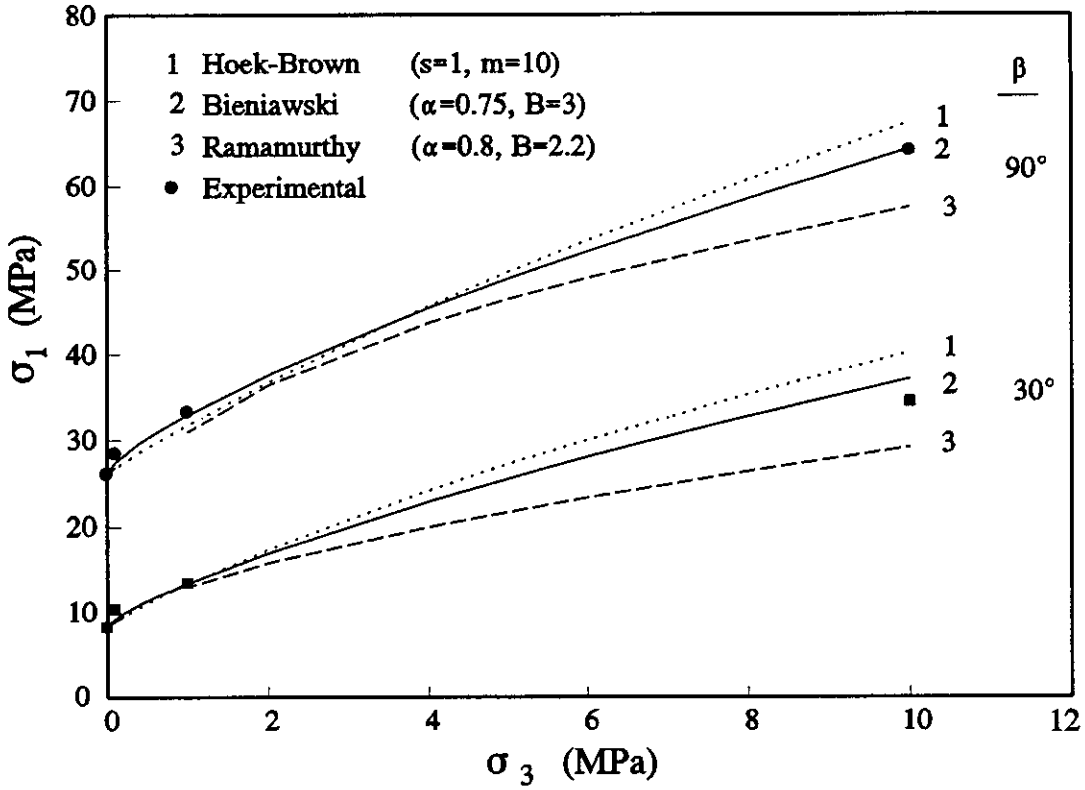

Figure 5.20 Comparison of different strength criteria

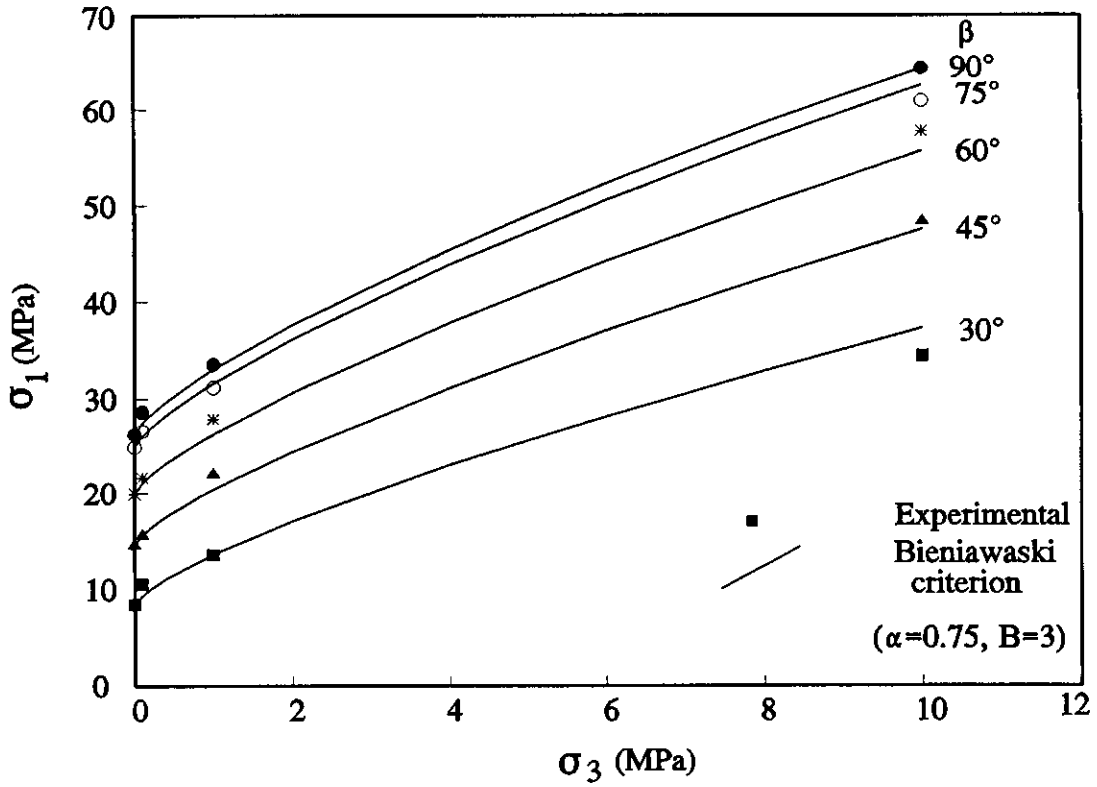

Figure 5.21 Comparison of the experimental results with the Bieniawaski criterion

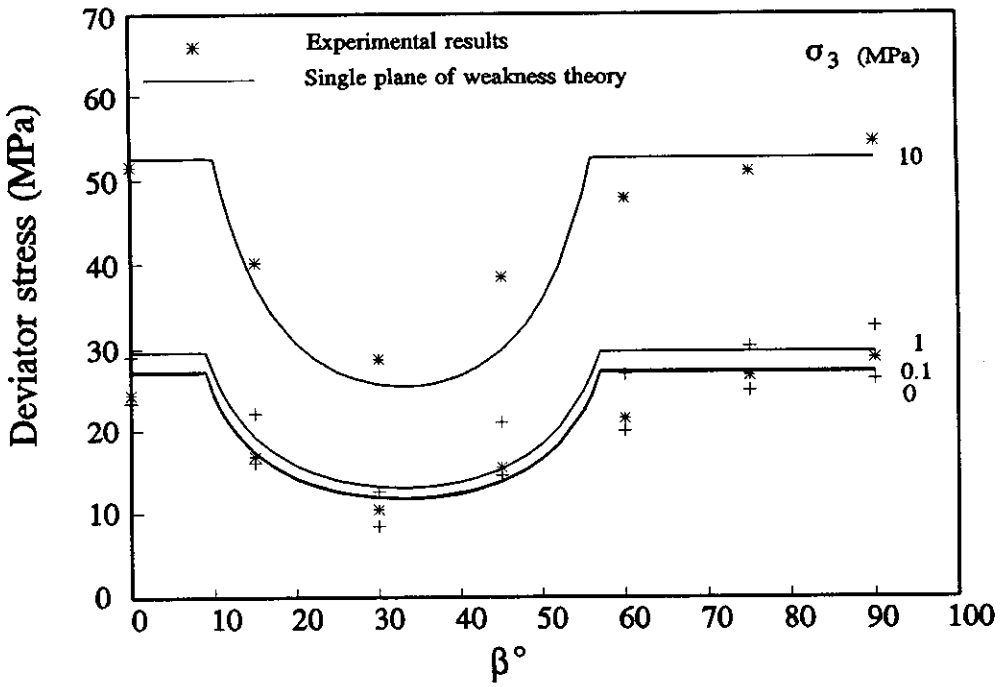

Figure 5.22 Comparison of single plane of weakness theory and experimental results

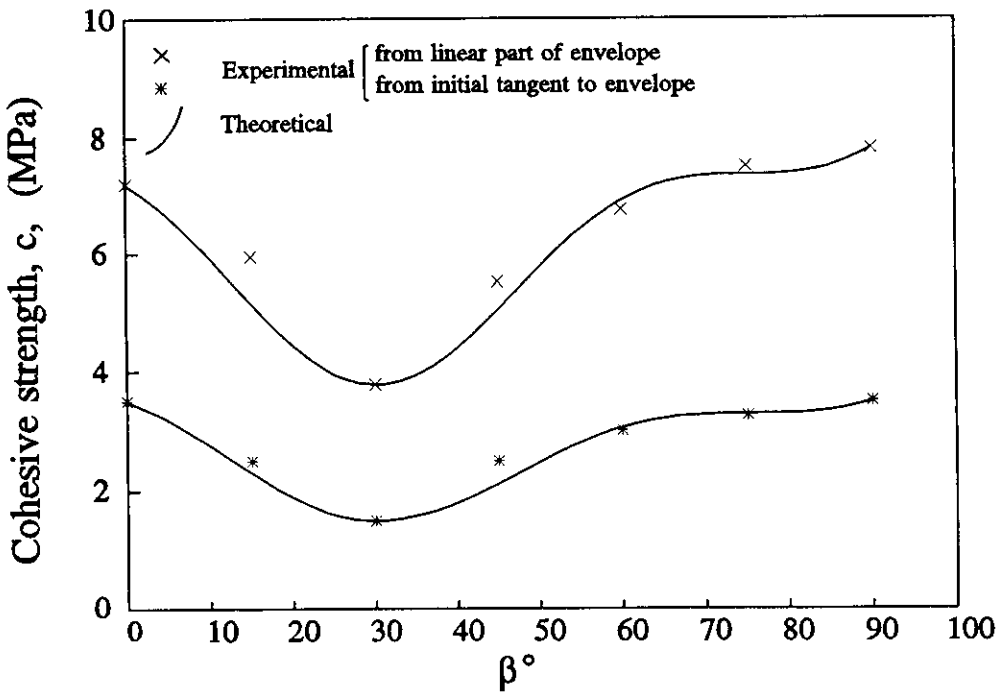

Figure 5.23 Comparison of the theoretical and experimental results

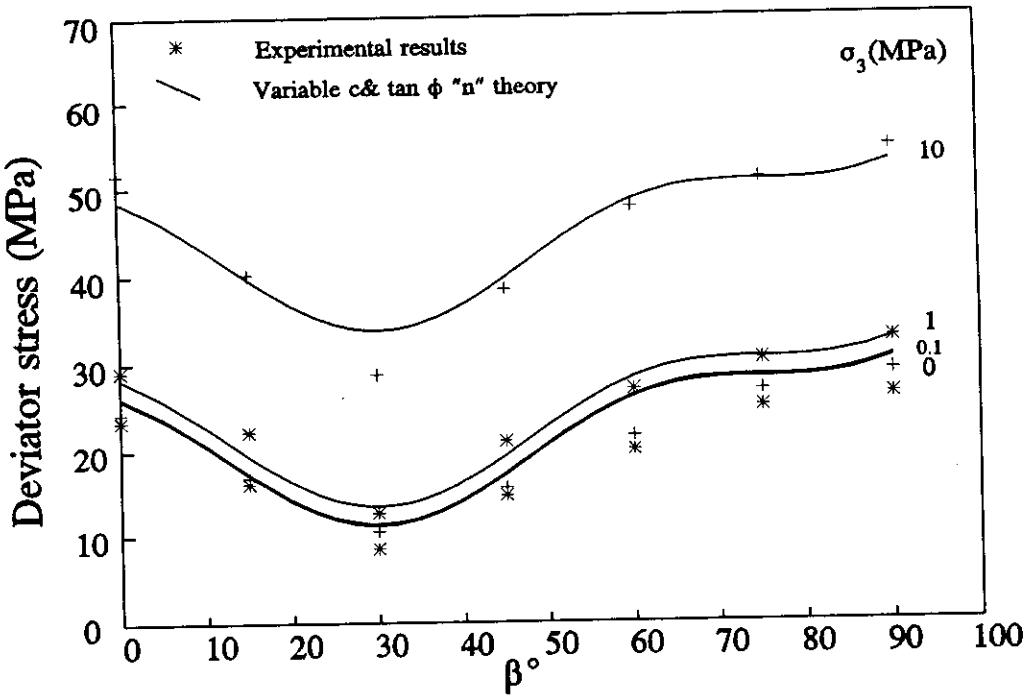

Figure 5.24 Coparison of variable c & tan ϕ "n" theory with experimental results

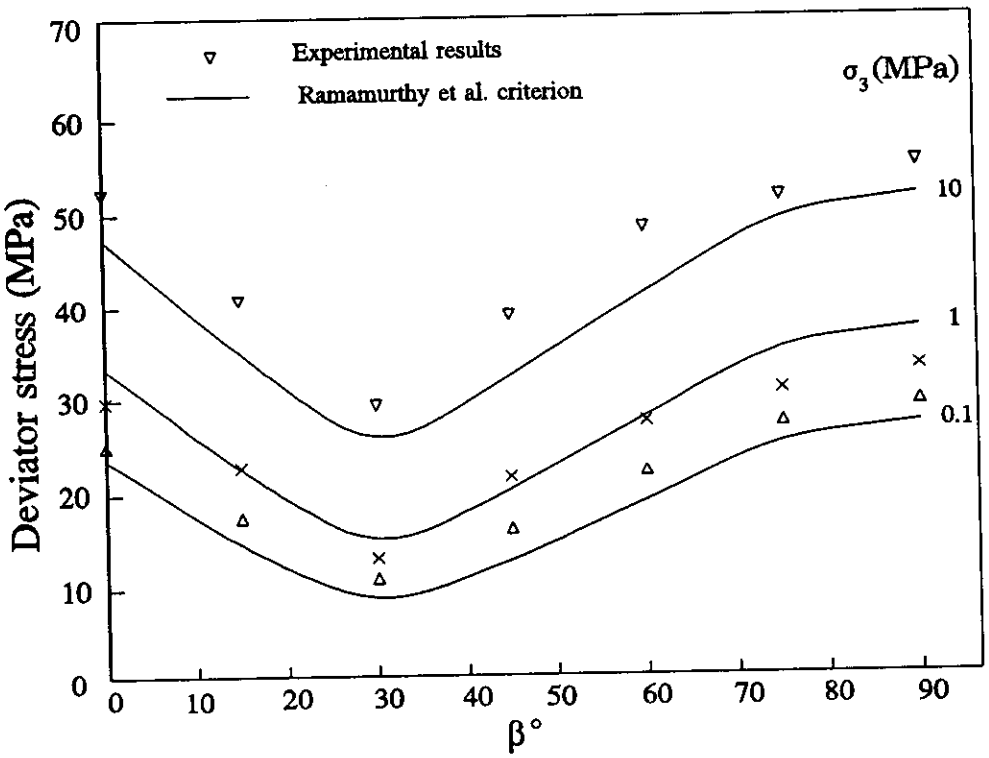

Figure 5.25 Comparison of Ramamurthy et al. criterion with experimental result

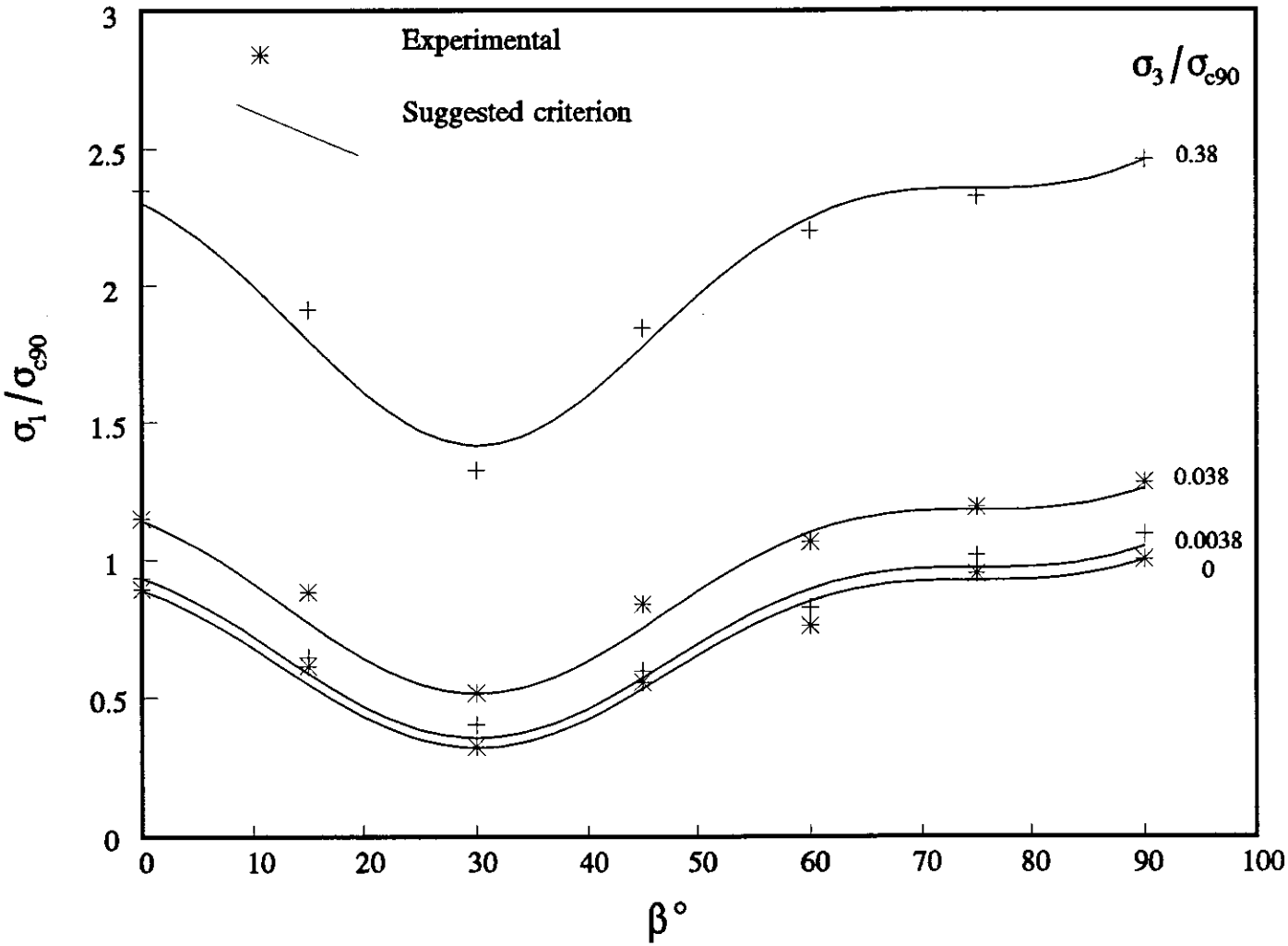

Figure 5.26 Comparison of new criterion with experimental results for Ashfield shale

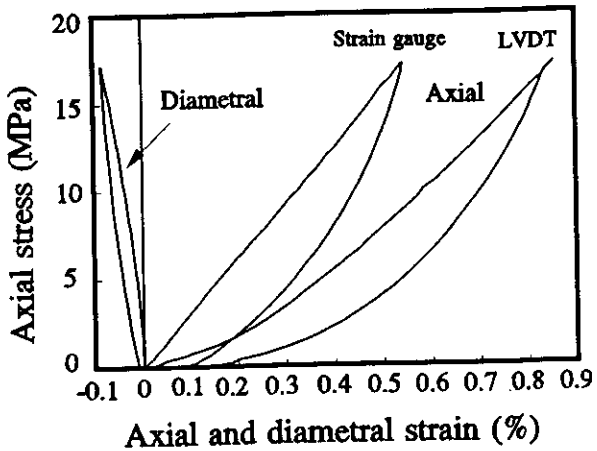

(a)

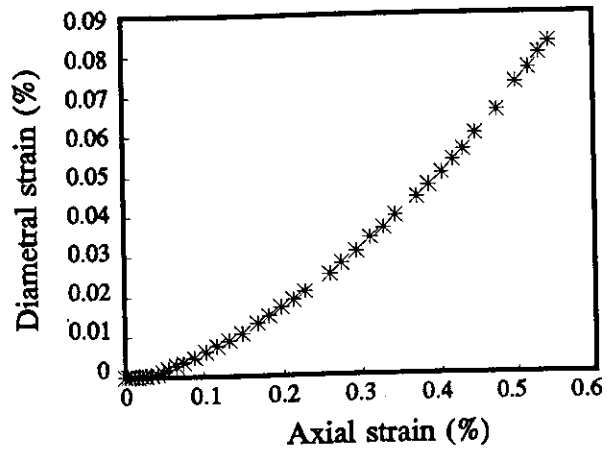

(b)

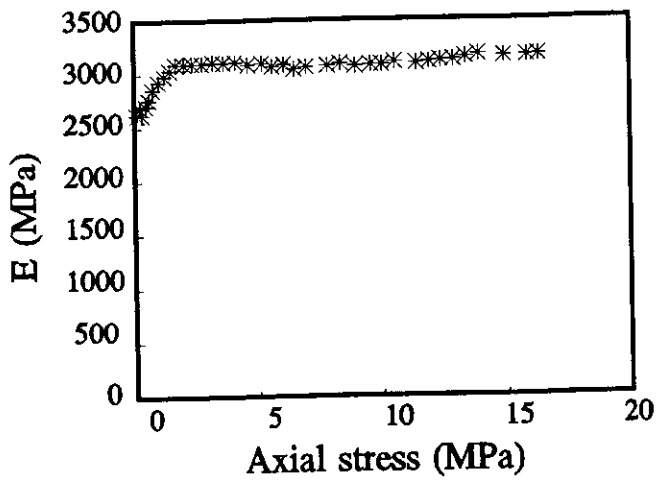

(c)

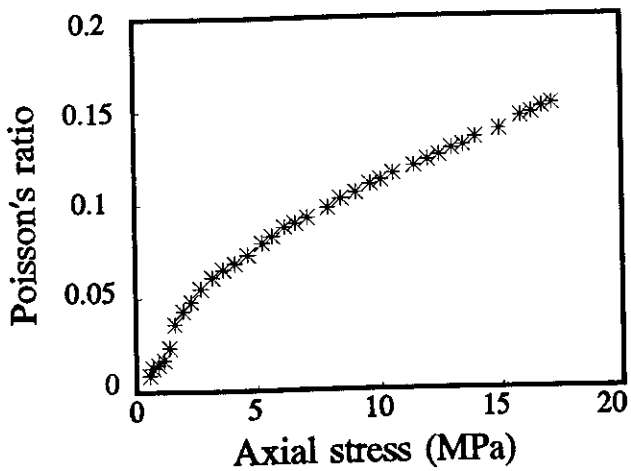

(d)

Figure 5.27 Typical test results: $\beta = 90°$ and $\sigma_3 = 0$ (Ryde)

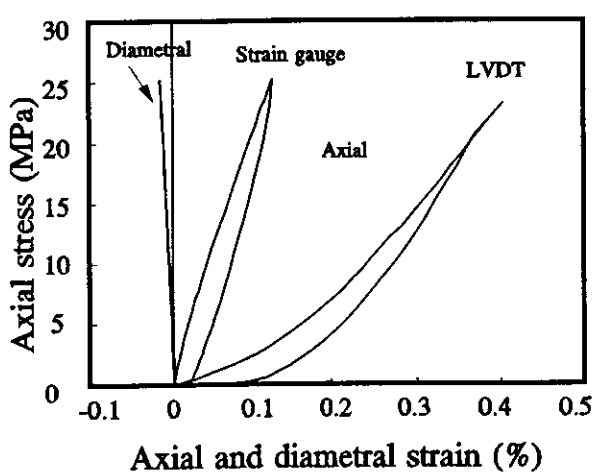

(a)

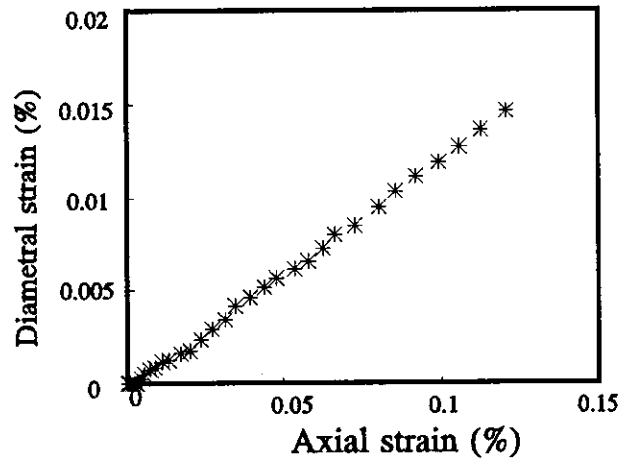

(b)

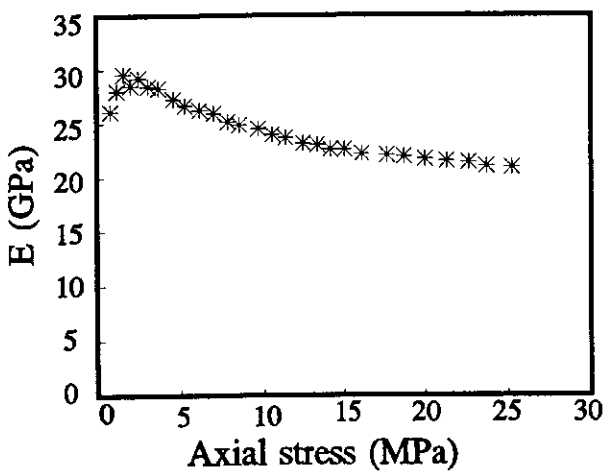

(c)

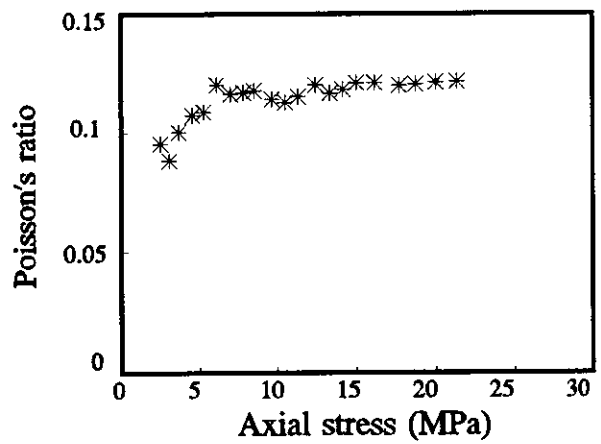

(d)

Figure 5.28 Typical test results: $\beta = 0$ and $\sigma_3 = 0$ (Surry Hills)

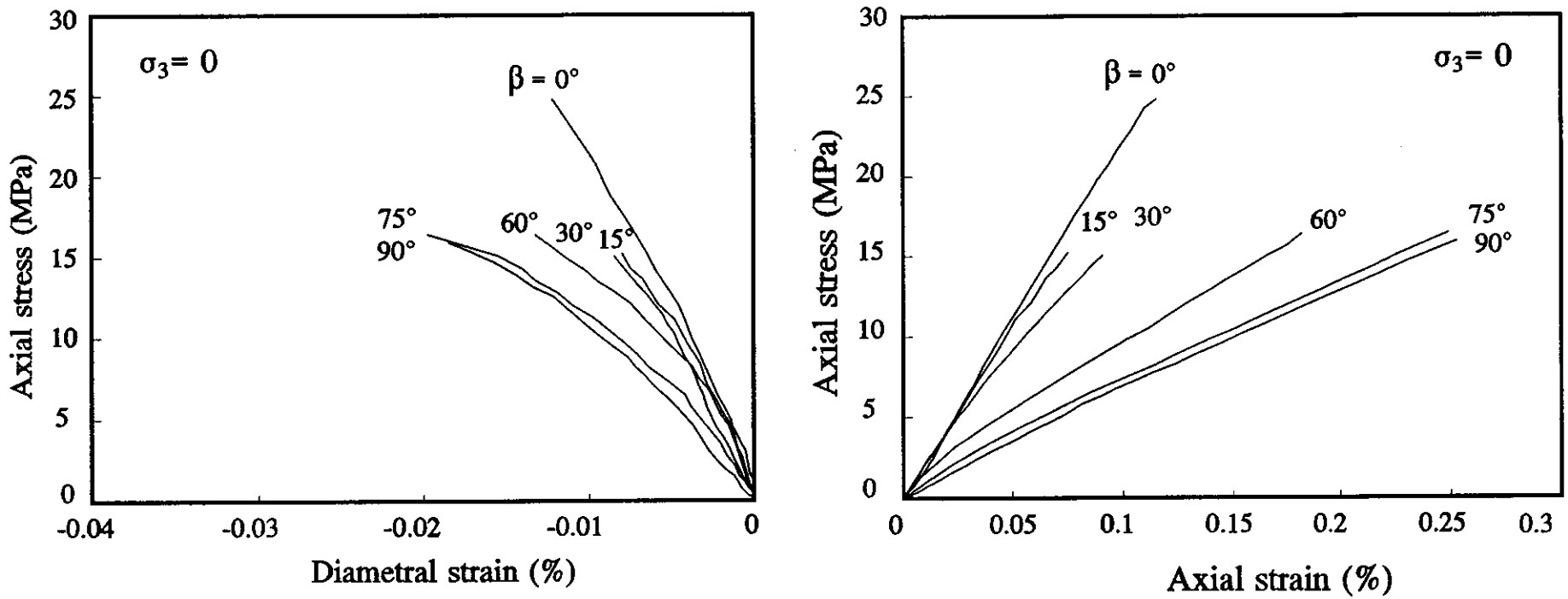

Figure 5.29 Axial stress versus axial and diametral strain for Ashfield shale from Surry Hills

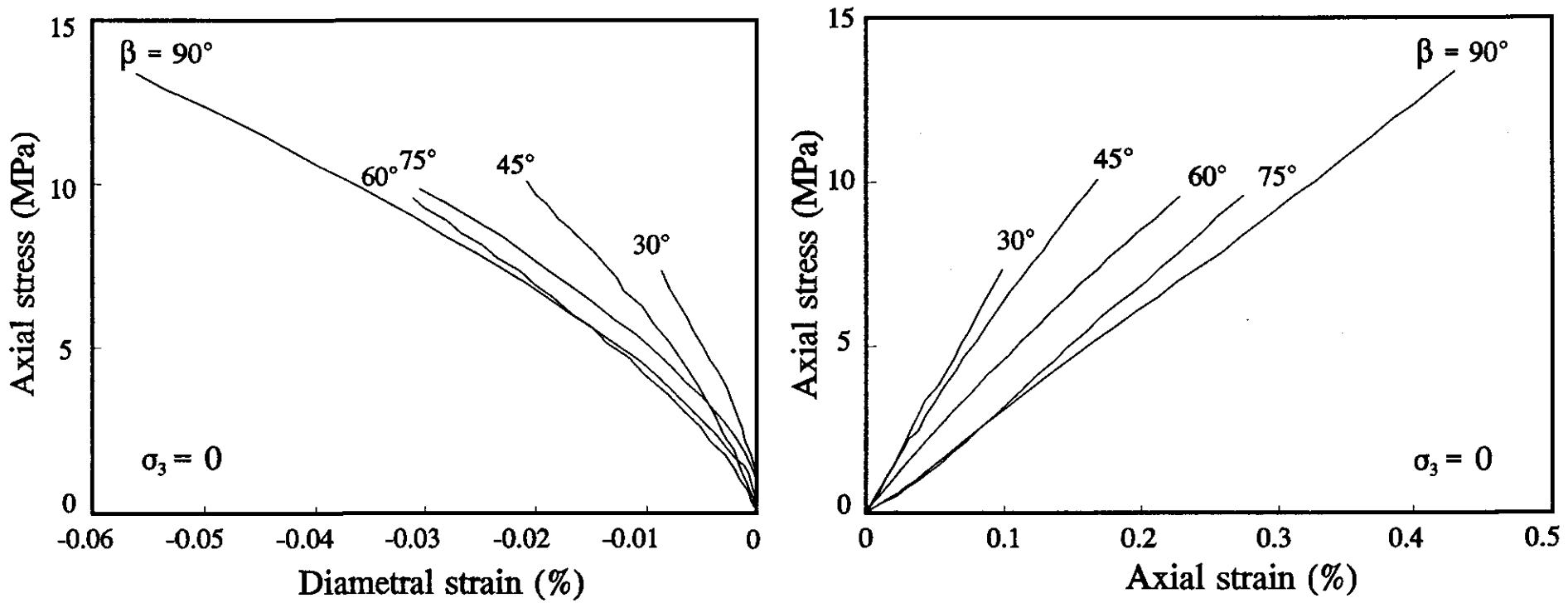

Figure 5.30 Axial stress versus axial and diametral strain for Ashfield shale from Ryde

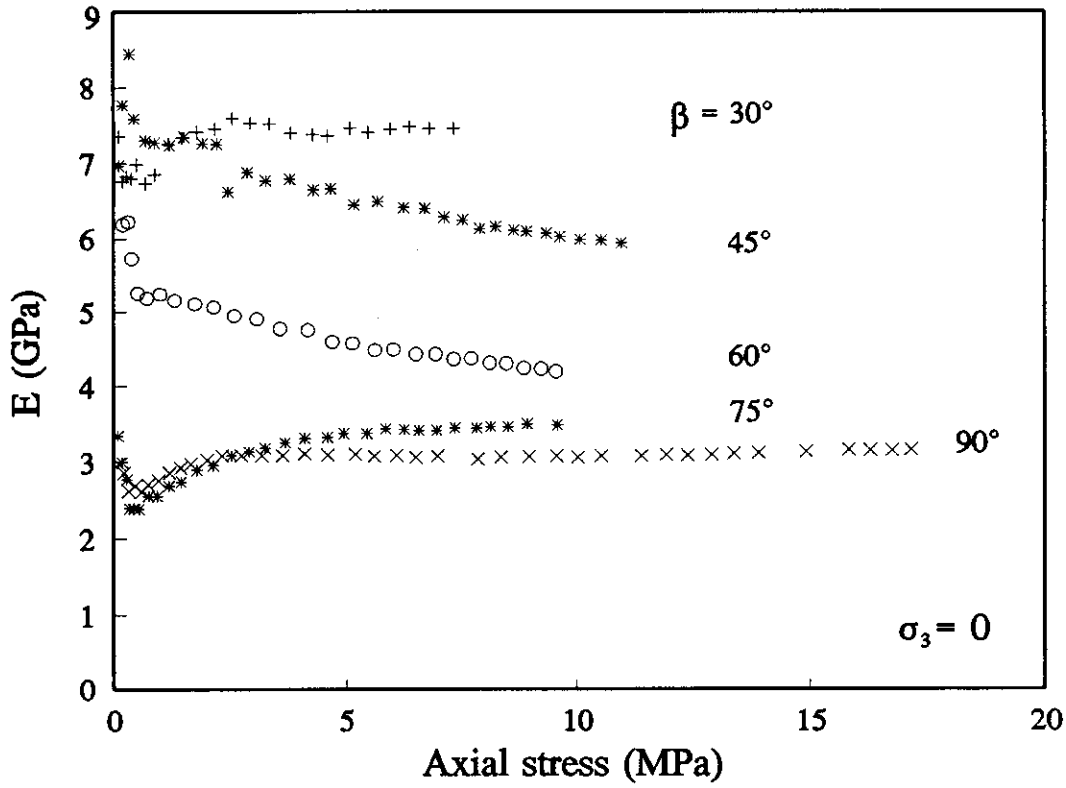

Figure 5.31 E versus stress for Ashfield shale (Ryde)

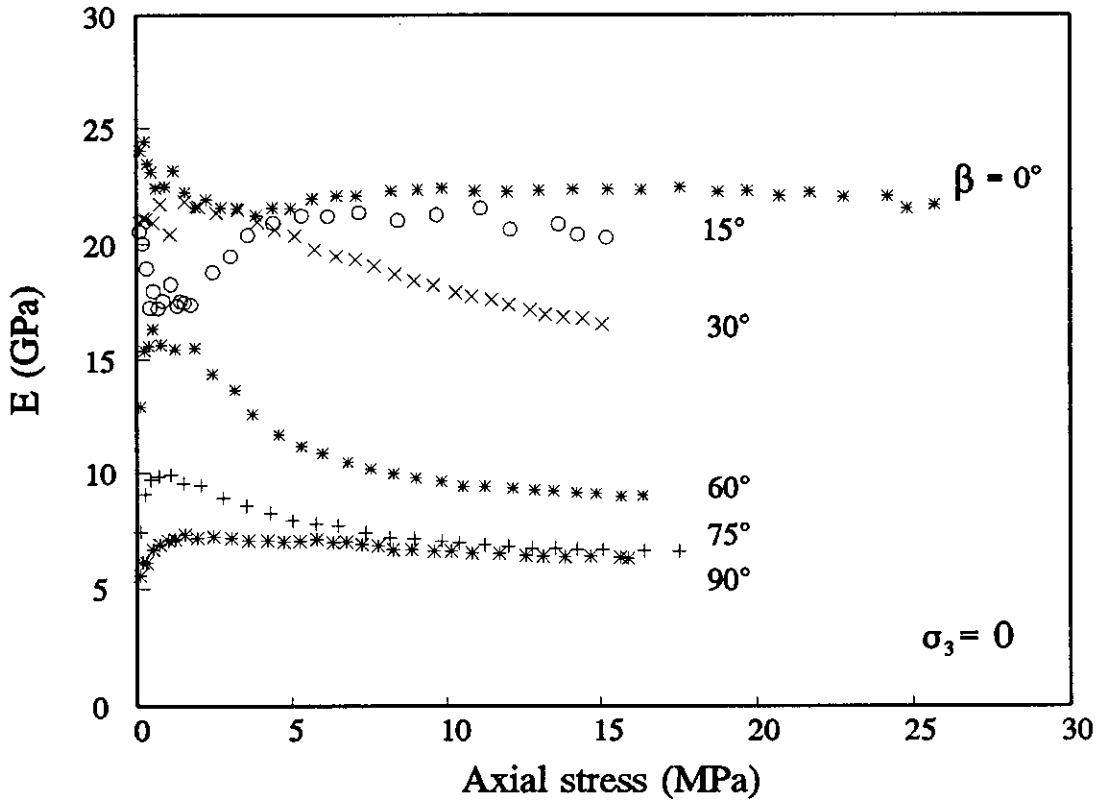

Figure 5.32 E versus axial stress for Ashfield shale (Surry Hills)

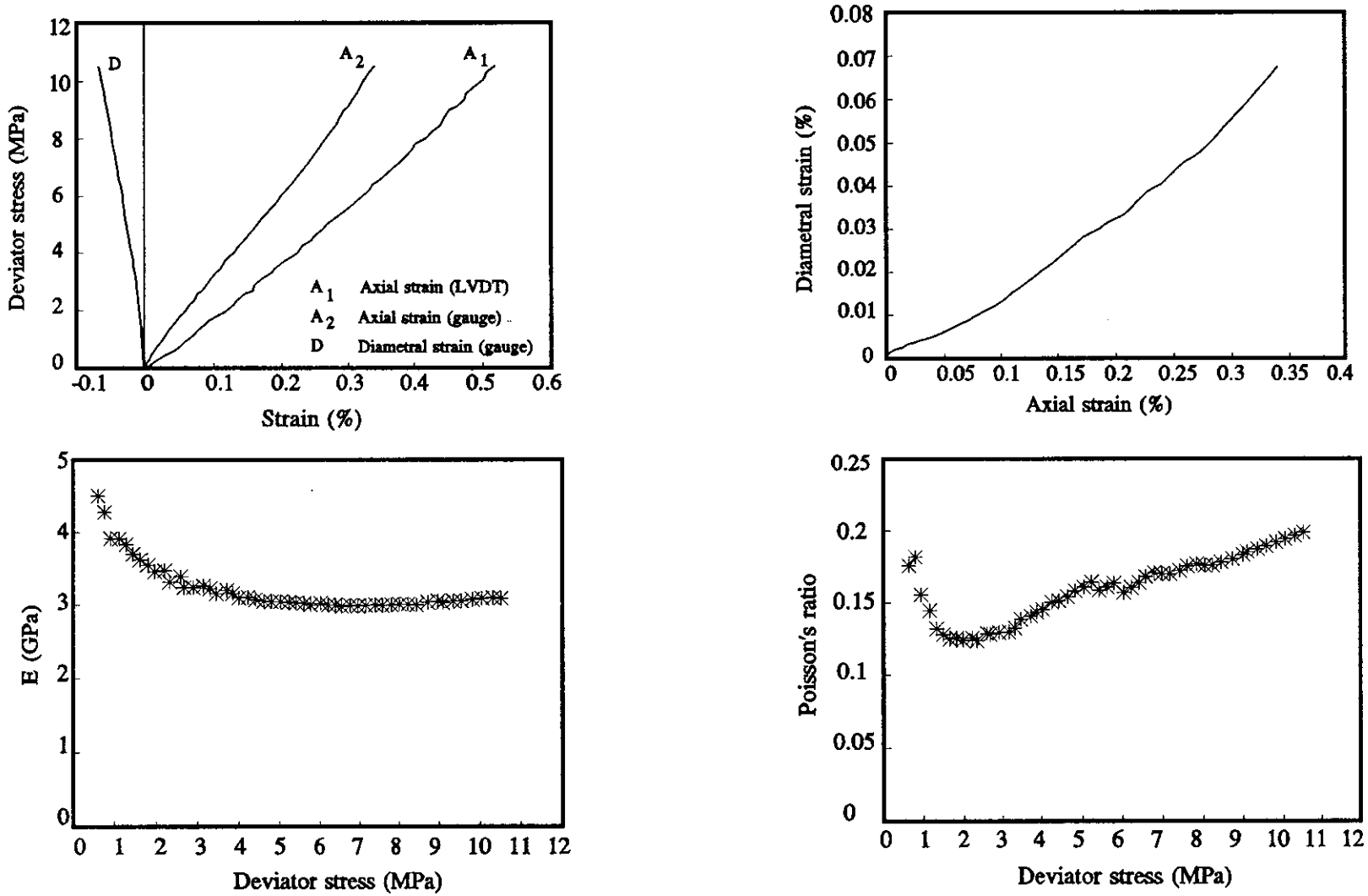

Figure 5.33 A typical set of results for Ashfield shale from Ryde (β=90°, σ_3 = 2 MPa)

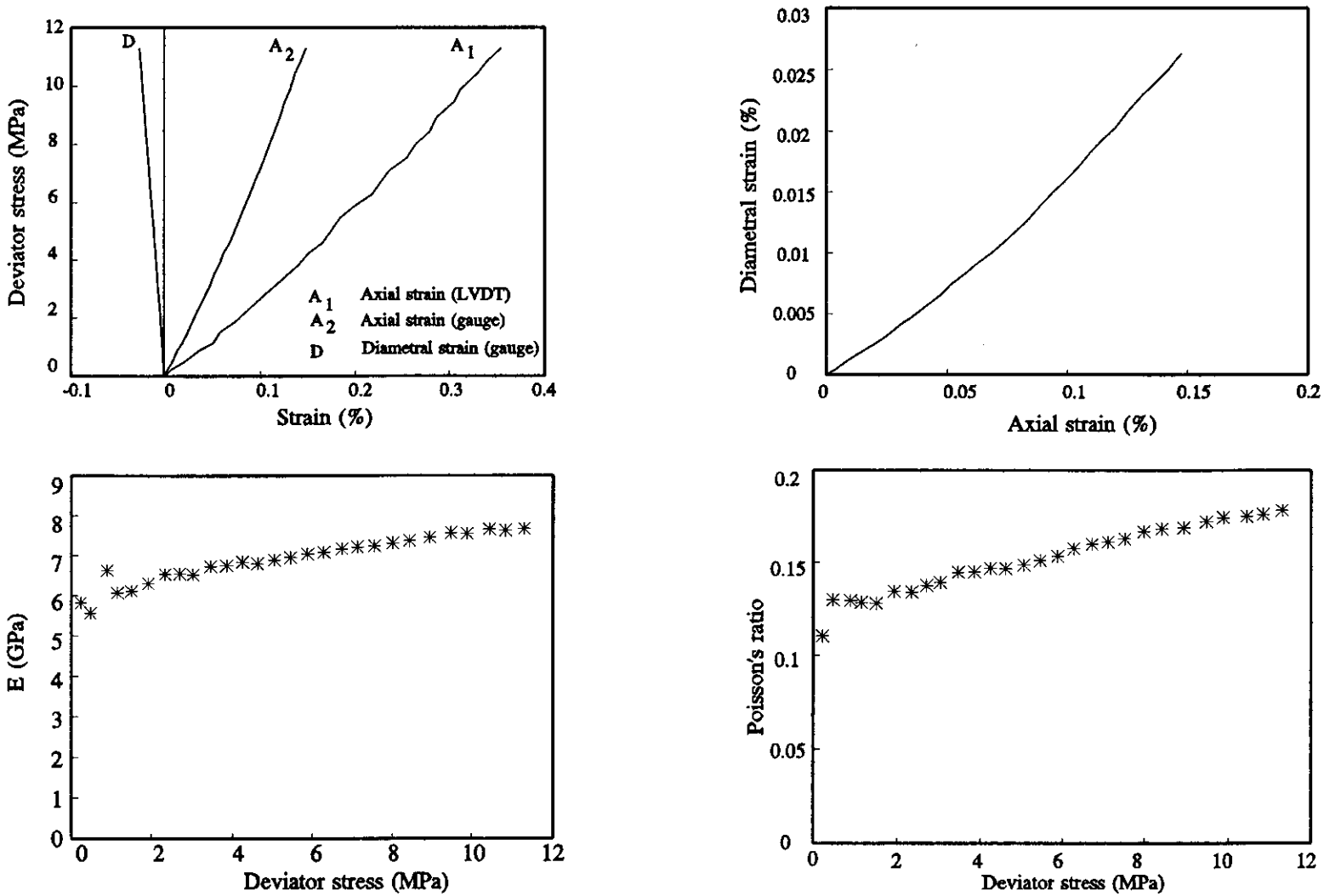

Figure 5.34 A typical set of results for Ashfield shale from Surry Hills (β=90°, σ = 2 MPa)

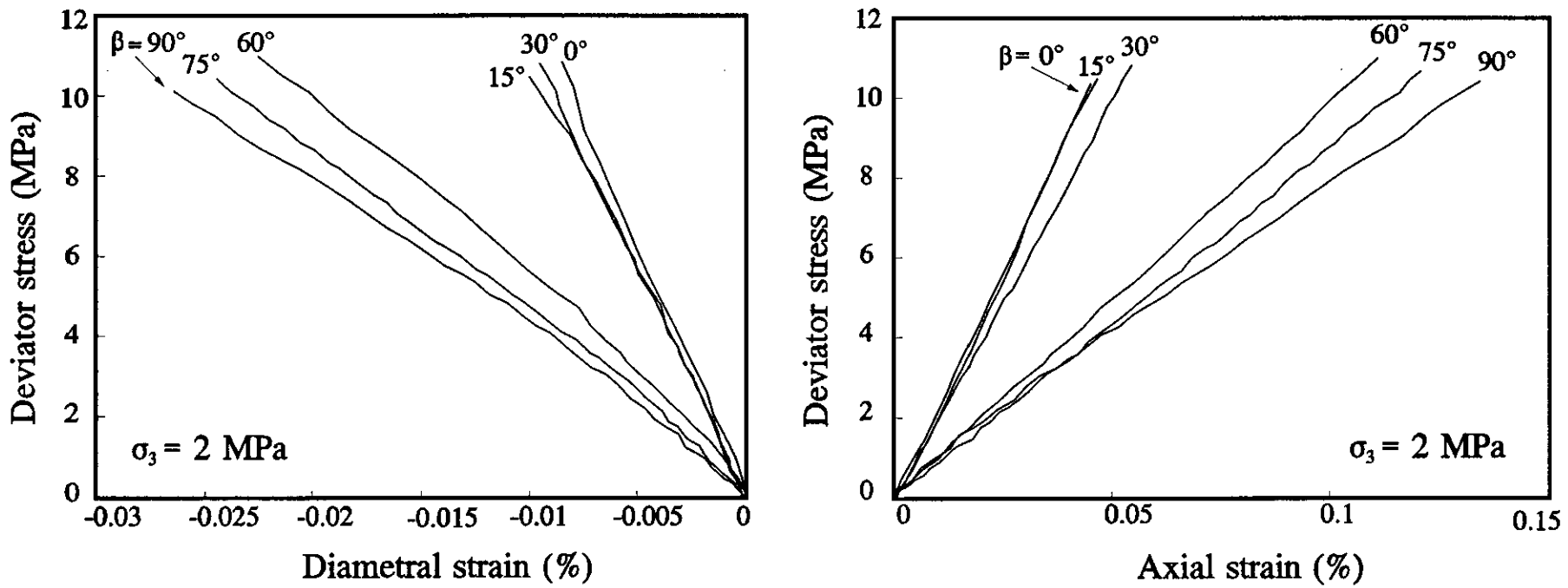

Figure 5.35 Deviator stress versus axial and diametral strain for Ashfield shale from Surry Hills

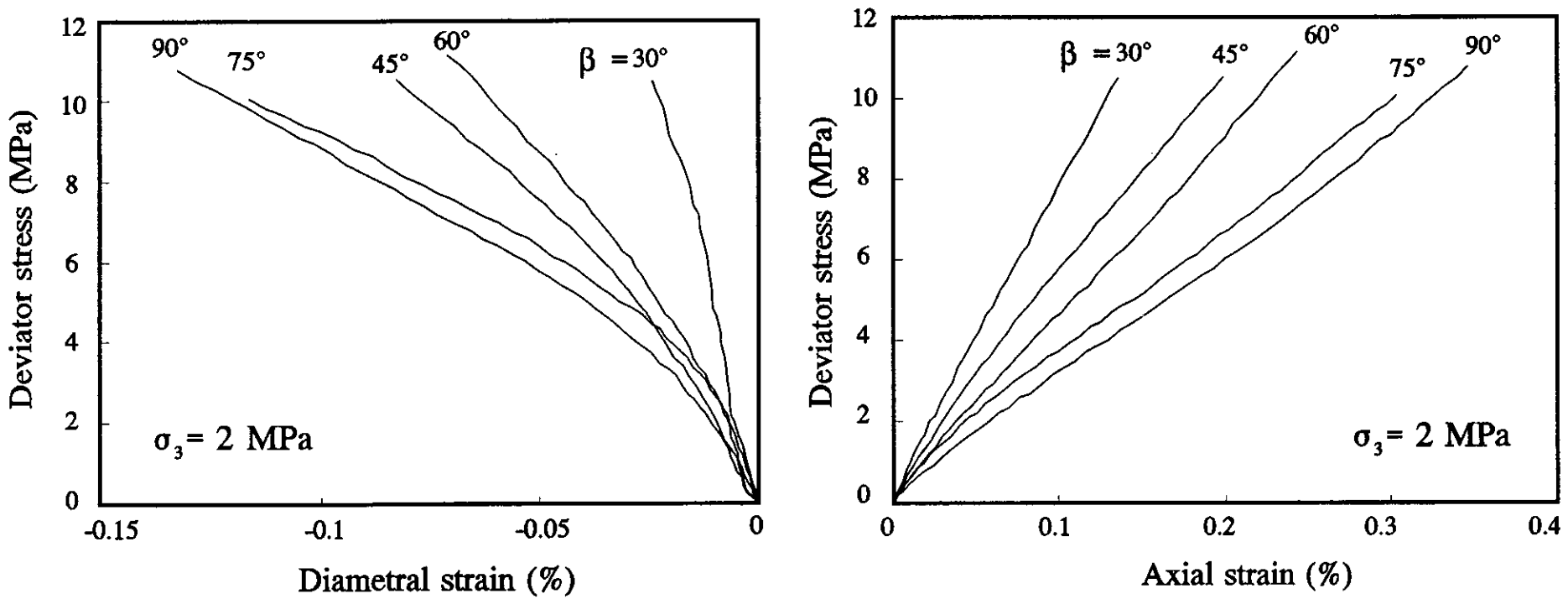

Figure 5.36 Deviator stress versus axial and diametral strain for Asfield shale from Ryde

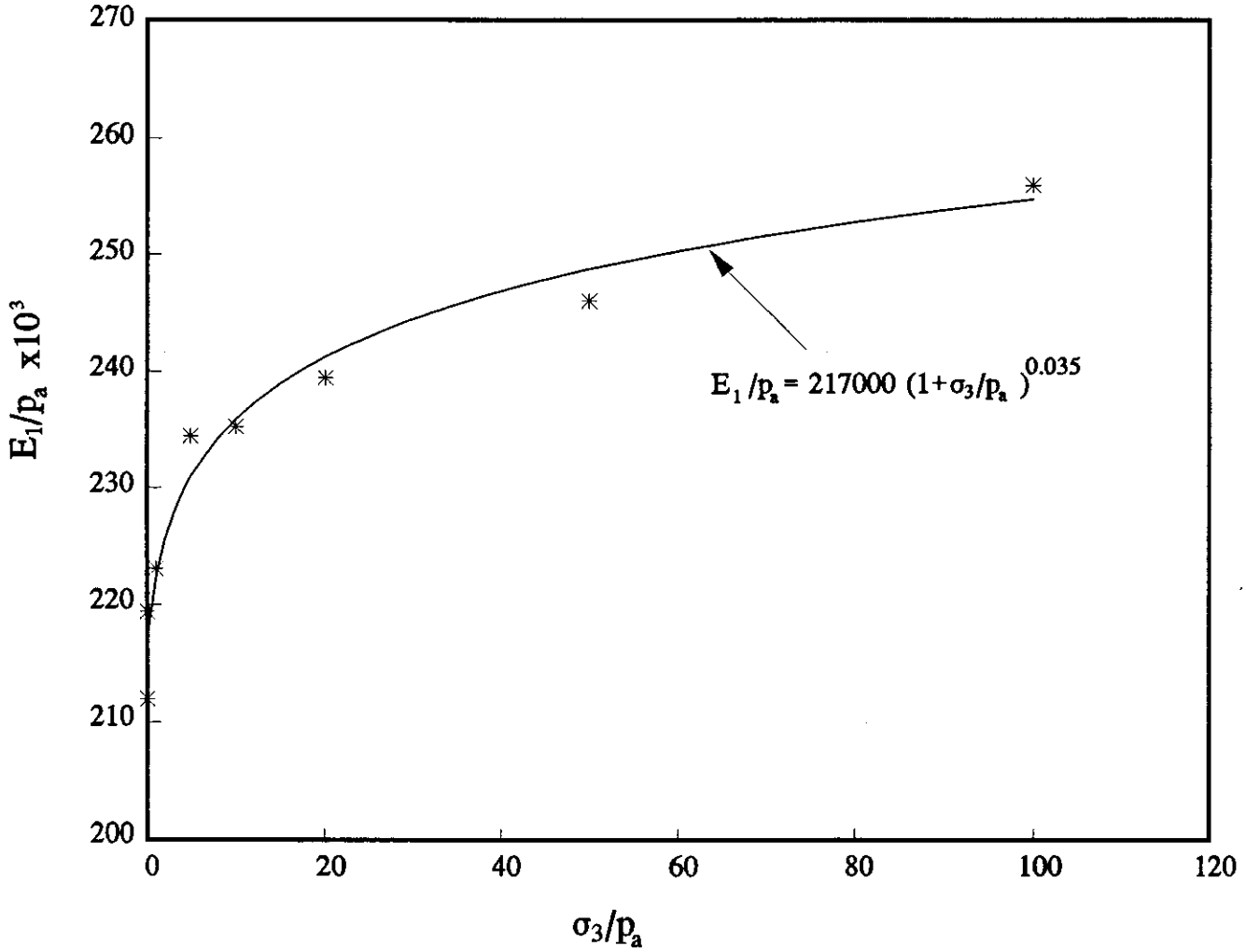

Figure 5.37 Variation of E as a function of confining pressure

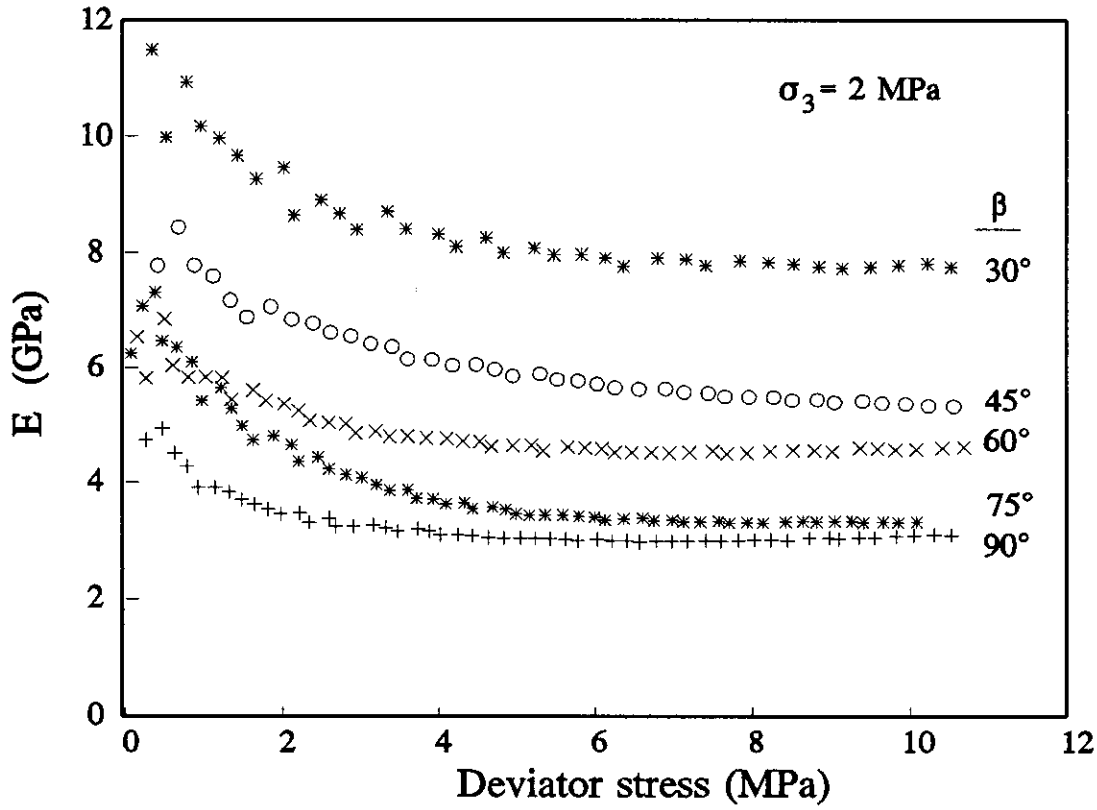

Figure 5.38 Modulus of elasticity versus deviator stress for Ashfield shale (Ryde)

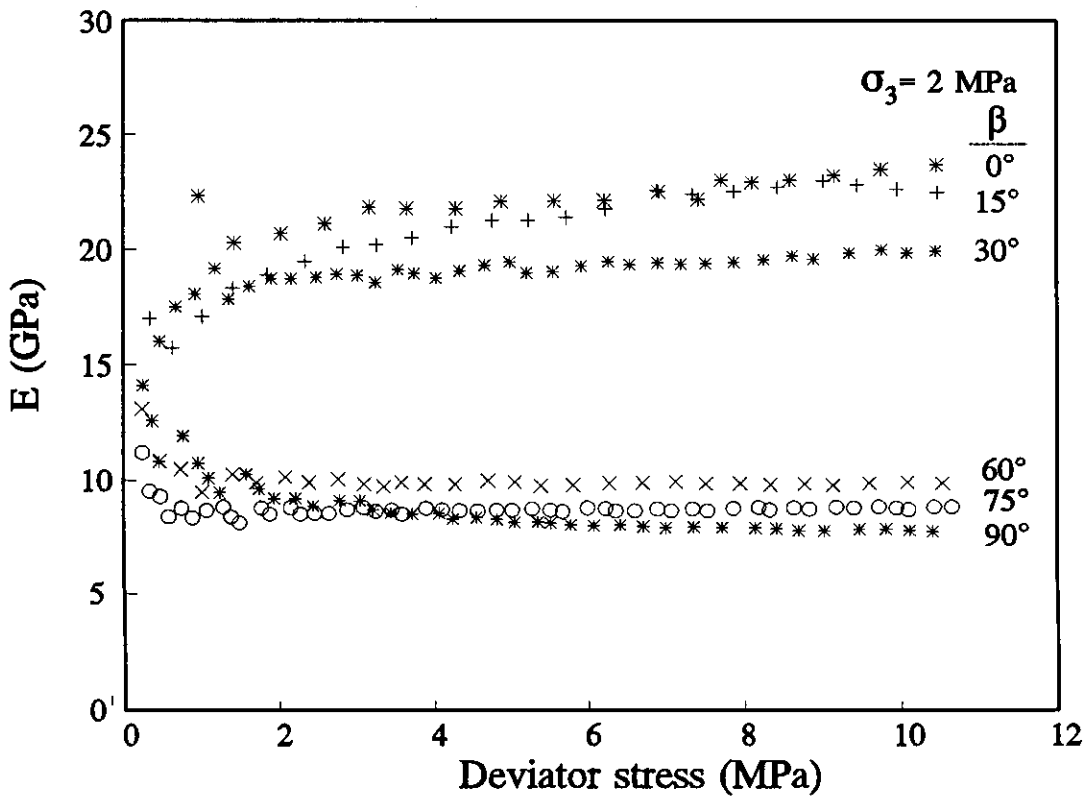

Figure 5.39 Modulus of elasticity versus deviator stress for Ashfield shale (Surry Hills)

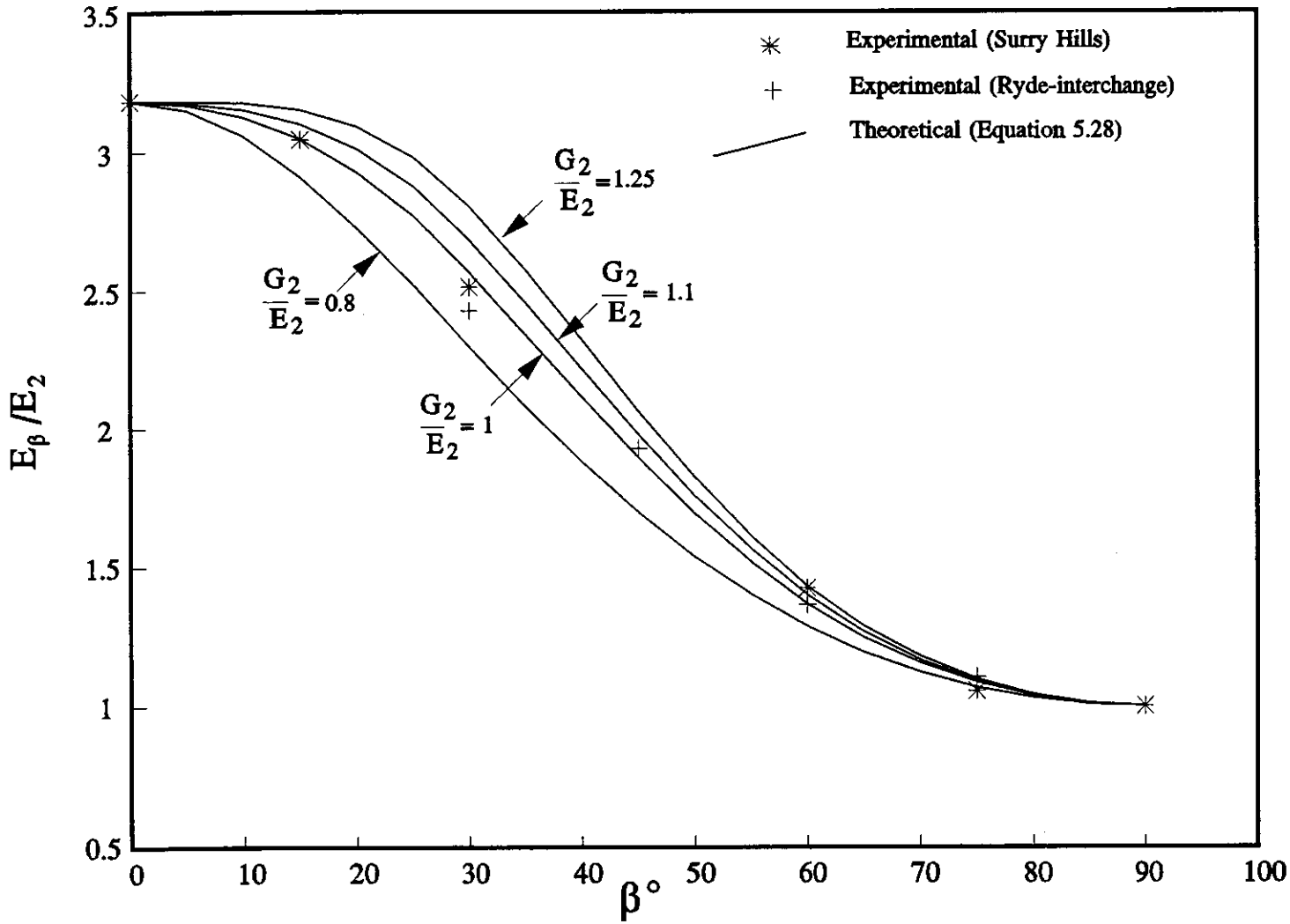

Figure 5.40 Evalution of the independent shear modulus

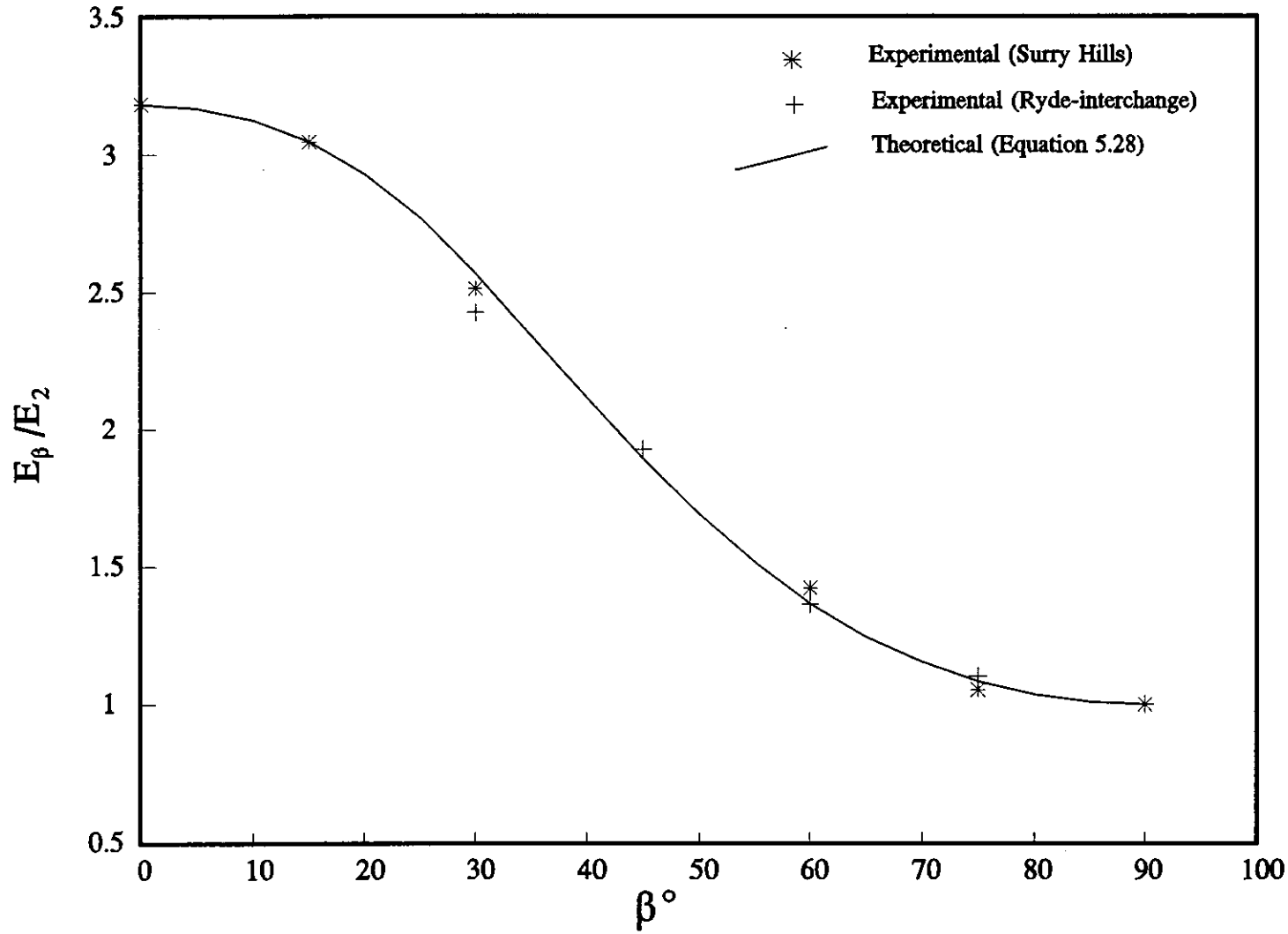

Figure 5.41 Comparison of the theoretical and experimental results for Ashfield shale

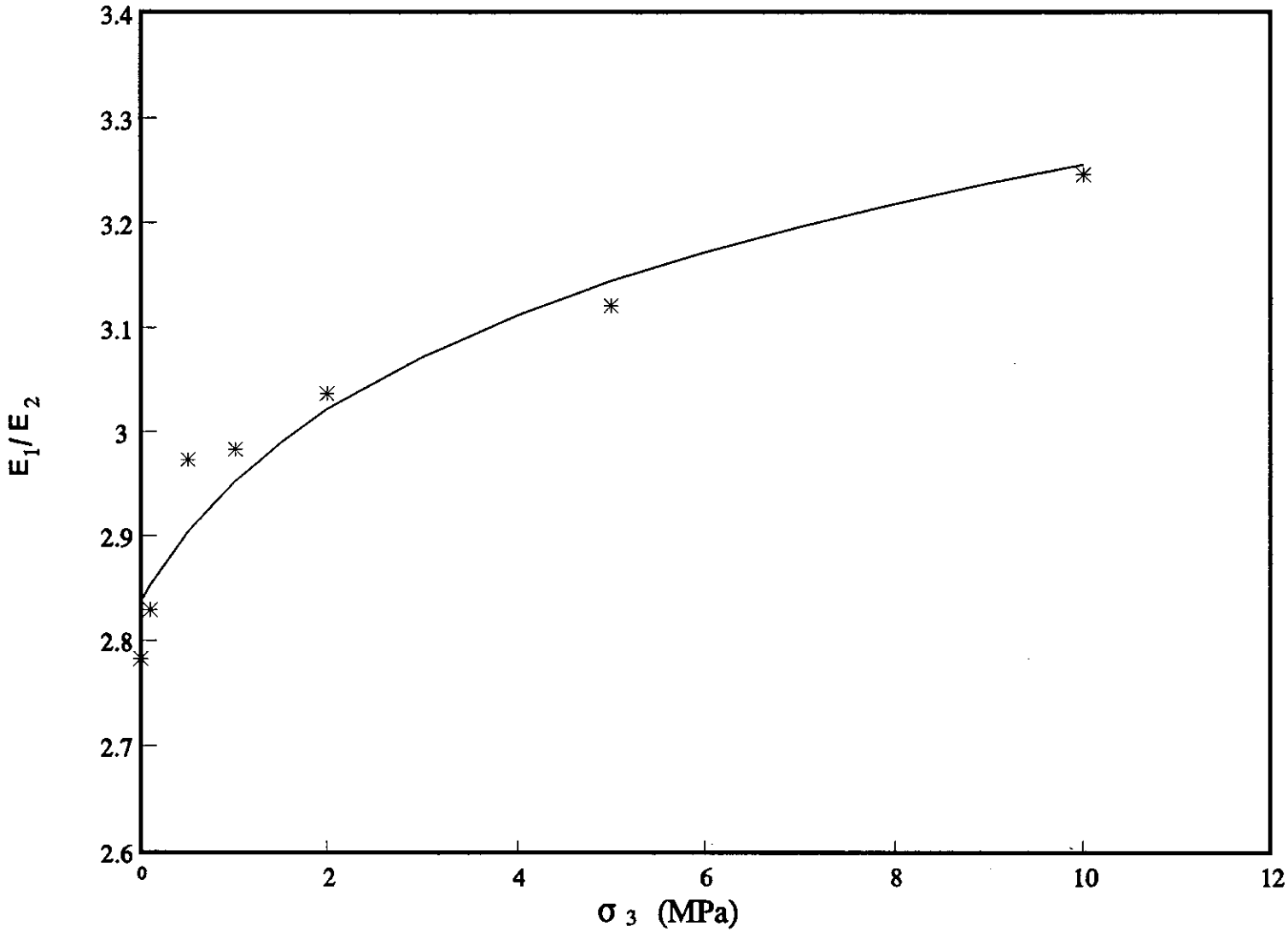

Figure 5.42 Effect of confining pressure on elastic anisotropy ratio

CHAPTER 6

DIRECT SHEAR TESTS

6.1 INTRODUCTION

In this chapter the results of a series of direct shear tests on the Ashfield shale are presented. The main objective of this chapter is to investigate the effect of normal stress and lamination direction on the shear behaviour and shear strength parameters of this shale determined in direct shear. The relation between the parameters determined from direct shear and triaxial tests is discussed. Direct shear tests have also been performed in different directions along the bedding planes to measure the variation of shear strength in one quadrant from 0 to 90 degrees. Some tests have also been carried out to investigate the effect of the rate of shearing on the behaviour of Ashfield shale. The shear stiffness has been calculated for each test and each level of normal stress. A comparison of the measured shear stiffnesses with predicted values of stiffness is presented in chapter 7.

The results presented in this study were obtained from direct shear tests performed on samples with different lamination directions using normal stresses ranging from 0.3 to 1.6 *MPa*.

6.2 TEST PROGRAMME

The laboratory test programme consisted of more than 100 monotonic direct shear tests. The tests have been conducted under constant normal stress conditions. The main aims of these tests have been:

(a) to investigate the shear behaviour of Ashfield shale specimens,

(b) to investigate the effect of lamination directions on the shear strength, shear stiffness and shear strength parameters,

(c) to investigate the effect of normal stress on the shear strength, shear stiffness, and shear strength parameters,

(d) to investigate the effect of rate of shearing on the shear behaviour,

(e) to investigate the effect of gap width between the two halves of the shear device on the shear behaviour,

(f) to investigate the variation of shear strength in one quadrant from 0 to 90 degrees along the bedding planes.

6.3 SHEAR TESTING MACHINE

The equipment used in these tests is a version of a constant normal stiffness (CNS) direct shear device designed by Ooi and Carter (1987) at the University of Sydney. The device was modified by Boey (1990) to allow tests under a condition of constant normal stress (CNL) as well as constant normal stiffness (CNS). The direct shear device is illustrated in the photograph in Figure 6.1 and a schematic layout of the major components is given in Figure 6.2. For the present series of tests the device was used with a very low normal stiffness (150 *kPa/mm*), so that the shearing was conducted at almost constant normal stress. A general purpose, servo-controlled testing machine (an INSTRON, model TT-KM), having a maximum load capacity of 250 *kN*, was used to apply the force necessary to cause direct shearing of the shale cores. Each test was controlled by a microcomputer, which also recorded the test data. The direct

shear device consists of two collars to grip the core specimens, which had diameters of either 51, 61 or 80 *mm*. The right collar (B) has a cranked rod which is connected directly to the cross-head of the servo-controlled testing machine. The cross-head applies a force normal to the axis of the cylindrical specimen necessary to cause direct shearing on a circular plane between the two collars. The movement of collar (B) causes shear deformation of the specimen, and is guided vertically by the cylindrical roller bearings (A). The lateral movement of this collar is restrained. The second collar is restrained in such a way that movement can occur only in the direction along the axis of the specimen. Movement in this direction i.e. normal displacement is due to dilation of the specimen in the immediate vicinity of the shear plane that is in the gap between the collars.

The magnitudes of the applied shear load, the normal load and the shear and normal displacements were monitored simultaneously throughout each test. The shear load was measured by a load cell mounted in the crosshead of the testing machine. This full bridge strain gauged load cell has a maximum capacity of 250 *kN*. The precision and linearity of the cell were confirmed by a calibration test prior to use. The relative shear displacement between the two collars was measured by using a strain gauge extensometer. The extensometer was calibrated using a high magnification micrometer that can read to 0.0005 *mm*. The normal load was measured using a more sensitive axial load cell (Showa DB-500k) with a maximum capacity of 5 *kN*. A linear variable differential transformer (LVDT) was used to measure the changes in normal displacement during testing. A high magnification micrometer was used to calibrate the LVDT.

Two methods were used to try to apply a constant normal stress to the specimen. Initially the reaction spring beam in Figure 6.2 was replaced with a hydraulic jack which applied a constant axial load to the specimen. A hand pump was used to provide oil pressure to the hydraulic jack. The pressure

supplied to the jack was held constant through a pressure accumulator. However, with this arrangement the normal load did not remain constant throughout the entire shear test because of friction in the jack between the plunger and seal. A significant change in normal load occurred until the friction was overcome, after which the normal stress remained constant even for significant amounts of dilation. Because of the change in normal load it was decided to use a spring of low stiffness (150 *kPa/mm*) to apply the normal load. In this case, after installing the specimen in the shear apparatus, normal stress was applied by adjustment of the spherical seat (see detail from Figure 6.2). With this arrangement the normal load remained almost constant throughout the entire shear test. The direct shear tests were carried out at a variety of normal stresses within the range from 0.3 to 1.6 *MPa*.

The voltage outputs of all the measuring transducers (load cells, extensometer and LVDT were suitably amplified and then fed into an analog-digital converter and stored on the hard disk of a microcomputer system for later processing.

6.4 SPECIMEN PREPARATION

The specimens for the direct shear test were obtained from boreholes drilled at different directions with respect to the bedding plane direction at the Ryde-interchange site and from block samples recovered from an excavation at Moorebank in the west of Sydney. The geology and mineralogy of the Ashfield shale from these sites and the preparation of core samples have been described in Chapter 3.

The specimens of Ashfield shale from Ryde-interchange site for this test were generally 61 *mm* in diameter. The length to diameter (H/D) of specimens varied between 1 and 1.5. Before testing, each specimen was

mounted inside the two collars of the direct shear device. The left collar had an oversized diameter and the right collar which was connected to the testing machine (see Figure 2) had the same diameter as the specimen. After the specimen was firmly held by the right collar, the other end of the specimen was loosely mounted in the left collar. Typically, a gap of 3 *mm* was set between the two collars. The level of the crosshead of the testing machine was carefully adjusted to position the specimen in the centre of the left collar, and to prevent any shear load being induced on the specimen due to misalignment of the collars. After this, the loose end of the specimen was cast in the oversized collar using hydrostone grout which is a mixture of hydrostone cement and water. The shale specimen was covered by a thin layer of grease and a thin plastic film to prevent the samples from absorbing moisture from the hydrostone grout. The grout was prevented from leaking out of the collar by surrounding it with absorbent paper. This method of preparing samples for testing ensured that the specimen was firmly seated in the two collars with no induced shear load. The hydrostone grout hardened after two hours and the absorbent paper was removed. The shear and normal displacement transducer and normal load cell were mounted in the correct locations. The readings of shear stress, the shear displacement, the normal stress and the normal displacement were monitored at frequent intervals during the test and stored in the memory of a computer system for later processing. The samples were generally sheared at a rate of approximately 0.2 *mm/min*.

As mentioned in Chapter 3, the shale from Moorebank site is generally stronger than shale from the Ryde-interchange site and there was no test data for $\theta = 90°$ at the Ryde site. θ is the angle of inclination between the laminations and shear load direction. This was taken into account by preparing core samples in two directions ($\theta = 0$ and $90°$) from the block of shale from Moorebank, and conducting direct shear tests in these two directions. By comparing the results of tests on samples with lamination angle of $\theta = 0°$ from these two sites, a correlation factor between the two shales was

obtained. Values of the shear strength and shear stiffness at $\theta = 90°$ for the Ryde shale were estimated by applying the appropriate correlation factors to the test data for the Moorebank shales ($\theta = 90°$). The data presented in the remainder of this chapter for all directions except 90 degrees are from Ryde samples and for $\theta = 90°$ are from Moorebank with the scale factor applied.

6.5 TESTING PROCEDURE

In order to assess the degree of anisotropy in the shearing behaviour of the shale, a series of tests has been carried out in which the angle of inclination (θ) between the direction of the shear load and the bedding planes in the specimen has been varied between -90 and +90 degrees. A second series of tests has been carried out with the shear force applied in a number of directions within the plane of the laminations, i.e. all corresponding to $\theta = 0$. A third set of tests was also conducted to study the influence of shearing rate on the peak and residual shear strength. In the latter set of tests all parameters except the shear rate were kept constant from test to test.

In the first series of tests, eight different orientations (i.e. eight values of θ) were investigated and these have been divided into two categories with respect to the shear load direction. Specimens with a value of θ in the range from 0 to 90 degrees, i.e. θ positive, were deemed to be in category *I*, while those with θ in the range from 0 to - 90 degrees, i.e. θ negative, were deemed to be in category *II*. These orientations are shown schematically in Figure 6.3. Note the convention that θ is measured positive anti-clockwise from the vertical direction. The samples in category *I* have laminations in directions which, intuitively, might be expected to be associated with lower shear strengths.

The samples tested in category *I* had laminations that were oriented at either 0, 30, 45, 60 or 90 degrees to the direction of the applied shear load. In

category *II* the laminations were oriented at 0, - 30, - 45, - 60 and -90 degrees to the direction of applied shear load.

Because of the relatively high stiffness of the Ashfield shale specimens, the system compliance must be determined. To do this a stainless steel dummy sample with the same diameter as the shale specimens was set up in the direct shear test apparatus and the relevant normal stress was applied. The system compliance was obtained from a plot of the shear displacement versus the shear stress after allowing for the known shear stiffness of steel. An approximately linear relationship between shear displacement and shear stress was obtained, once full contact between the components was completed. The initial non-linearity seems to have resulted from the seating and contact of the components involved. The shear displacements reported in this chapter have been corrected assuming the system compliance given by the linear part of the relationship between shear stress and shear displacement. The measured stiffness of each sample was corrected based on this observation.

6.6 EXPERIMENTAL RESULTS

To measure the shear strength parameters, several tests at different normal stresses (σ) have been carried out. For each test graphs of shear stress (τ) and normal displacement (v) against shear displacement (u) have been plotted. Summary plots of the peak and residual strength data have also been prepared. For brevity, only selected test results are presented in the figures of this chapter. However, all selected test data are included in the analysis of the results.

6.6.1 Typical results

The results of constant normal stress tests for different orientations of the

laminations are summarised in Table 6.1 and typical results are presented in Figures 6.4 and 6.5. Figures 6.4 and 6.5 show representative plots of the shear stress and normal displacement against the shear displacement for core specimens containing laminations oriented at 0 and -45 degrees to the shearing direction, respectively. It can be seen from the plots of shear stress against shear displacement (Figures 6.4a and 6.5a) that the shear behaviour can be divided approximately into three zones. In all cases in the pre-peak zone, an almost linear elastic response up to a pronounced peak shear strength was observed, followed by a rapid reduction in the shear strength with further relative displacement beyond the peak (second zone). A distinct rupture surface was formed close to the peak response and subsequent shearing occurred along this surface. With further displacement, a third zone was finally defined when the shear stress reached an approximately constant value (the residual strength).

The peak shear strength occurred at an early stage of shearing at relatively small shear displacements that were usually in the range from 0.1 to 0.2 *mm*. This did not change significantly with increase in normal stress. The residual response was reached generally at a shear displacement in the range from 1 to 2 *mm*. The results presented in Figures 6.4 and 6.5 were obtained from tests carried out with different normal stresses, as indicated by the labels on the curves. It is clear that increasing the normal stress generally increases the peak shear strength. The value of the shear displacement at which the residual strength was obtained varied with the orientation of the laminations and depended mainly on the magnitude of the normal stress and the nature of the failure surface. The shear displacement at which the residual strength was obtained increased with the normal stress. Similar trends to those evident in Figures 6.4 and 6.5 were observed for most of the core samples tested.

Figures 6.4b and 6.5b present the variation of normal displacement as a function of shear displacement. The figures show that shearing is accompanied

by a significant amount of dilation at the shearing surface after the peak. It is clear that increasing the normal stress generally decreases the dilation that occurs along the rupture surface. In all cases dilation was observed for the second and third zones of behaviour.

6.6.2 Peak and residual shear strength envelopes

In order to define the shear strength parameters, the peak shear stress and the shear stress at 3 *mm* displacement were plotted against normal stress for each test. Typical plots of this type are shown in Figures 6.6, 6.7 and 6.8 for cases where the laminations were inclined at -45, 45 and 0 degrees to the direction of shearing, respectively. It is evident from these figures that the peak and residual strengths appear to depend on normal stress and that the Mohr-Coulomb strength criterion provides a reasonable fit to the test data over the normal stress range from 0.3 to 1.6 *MPa*.

The peak shear strength predicted by the Mohr-Coulomb criterion is defined by the equation

$$\tau = c_p + \sigma \tan\phi_p \qquad \textbf{(6.1)}$$

and the residual shear strength is defined by

$$\tau = c_r + \sigma \tan\phi_r \qquad \textbf{(6.2)}$$

in which:

c_p = cohesion at peak shear strength,
ϕ_p = friction angle at peak shear strength,
c_r = cohesion at residual shear strength, and
ϕ_r = friction angle at residual shear strength.

The peak and residual values of c and ϕ obtained from the test results are

listed in Table 6.2, which indicates the effects of bedding plane orientation on the shear strength parameters of the Ashfield shale. The peak friction angles varied between 31 and 62 degrees and the residual friction angles varied between 15 and 37 degrees. The interpreted average strength envelopes at peak and at 3 *mm* shear displacement for the two categories of samples are presented together in Figure 6.9, which shows the variation in the peak and residual strength envelopes with the orientation of the laminations. Clearly, the samples were strongest in the case where the angle θ was 90 degrees, i.e. when the rupture plane formed entirely through intact material in a direction perpendicular to the laminations, a result which could have been anticipated. Curiously, the peak strength envelopes corresponding to θ = 0, 30, 45, and 60 degrees are quite similar to each other but are well below the peak envelope for θ = 90 degrees. The peak strength envelopes for negative values of θ (category *II* samples) are also above the envelopes for most cases of positive θ (category *I* samples). The failure patterns also depend on the direction of the laminations relative to the shearing direction. The failure surface observed for category *I* samples was smoother than for category *II* samples. Figure 6.10 shows examples of the failed specimens for category *I* and *II*.

The interpreted peak friction angles for θ = -45 and -60 degrees appear to be unusually large. However, it should be noted that these results are from best fits to only a few data points and so they may be inappropriate because of experimental error or sample variation. Nevertheless, the trend in the results for all samples is clear and is also consistent with expectations.

When evaluating the stability of rock construction, it is important to analyse the residual strength and the residual friction angle (Hoek and Bray, 1977). As indicated in Table 6.2, the residual cohesion for most cases appears to be almost zero. It is possible that the shearing was not continued far enough in cases where the residual cohesion appears to be non-zero. The residual friction angle appears to be in the range from 15 to 34 degrees.

6.7 SHEAR STIFFNESS

Before the peak shear force is mobilised, there is some prior shear displacement across the shear zone of the specimen. The slope of this rising part of the load displacement curve is defined as the shear stiffness (K_s). In all tests the response up to the peak shear strength was observed and three different shear stiffnesses were measured. These were the initial tangent shear stiffness, the secant shear stiffness at the peak and the secant shear stiffness at 50% of the peak shear strength. The average values for initial tangent shear stiffness (K_{si}), secant shear stiffness (K_{ss}) and peak shear stiffness (K_{sp}) were calculated for each test and each level of normal stress. These values include a correction for the compliance of the testing apparatus.

The shear stiffnesses found for samples of Ashfield shale tested at different normal stresses are presented in Table 6.3. A typical set of results, at a normal stress of 580 kPa, is presented graphically in Figure 6.11. As Figure 6.11 shows, the orientation of the lamination with respect to the shear force direction has a significant effect on the measured shear stiffness of the Ashfield shale. The shear stiffness appears to be smallest when θ is in the region of 60 degrees. A comparison of the results in Figure 6.11 indicates that the initial tangent shear stiffness is typically 2 to 3 times the secant shear stiffness at the peak, and that the secant shear stiffness at 50% of the peak shear strength is approximately midway between the peak and the initial value. The shale displays a limited truly elastic response, but the pre-peak response can still be reasonably described by a set of elastic parameters.

To show the effect of the normal stress on the shear stiffness of the Ashfield shale, the secant shear stiffnesses at 50% of the peak shear strength are plotted against normal stress in Figure 6.12. As this figure shows, the magnitude of the shear stiffness varies with both the lamination direction and the of normal stress. The magnitude of the shear stiffness increases

significantly with the normal stress. Table 6.3 shows that the same observations can be made for the initial tangent shear stiffness (K_{si}) and the peak shear stiffness (K_{sp}).

6.8 ANISOTROPY OF SHEAR STRENGTH AND SHEAR STIFFNESS

It is obvious that the orientation of the laminations to the shear force has a significant effect on the shear strength of the Ashfield shale. The peak shear strengths obtained in the direct shear tests have been plotted against the direction of the laminations in polar co-ordinates in Figure 6.13. This figure shows that the peak shear strength takes small values in the region of $\theta = 30$ degrees and the highest values in the region of $\theta = 90$ degrees. Figure 6.13 shows that the shear strength of the bedding planes in the Ashfield shale samples is higher in the case of negative values of θ (category *II*) than positive values of θ (category *I*), as discussed previously. The pattern of the results is similar to that obtained by Hayashi (1966), Kawamoto (1970), and also Kobayashi and Sugimoto (1981), when they conducted direct shear tests on specimens containing artificial discontinuity planes.

The secant shear stiffnesses at 50% of the peak strength have been plotted against the direction of the laminations in polar co-ordinates in Figure 6.14. This figure shows that the shear stiffness takes highest values in the region of $\theta = -30$ degrees and the smallest values in the region of $\theta = 60$ degrees. Figure 6.14 shows that the shear stiffness of the bedding planes in the Ashfield shale samples is higher in the case of negative values of θ (category *II*) than positive values of θ (category *I*), as discussed previously. Generally the shear stiffness increased with the normal stress. It is worth noting that this result would not be predicted by the theory for a cross anisotropic elastic material (described in Chapter 7). For this ideal material the elastic stiffness is symmetric about $\theta = 90°$.

From this experimental study of the influence of the lamination angle θ, it can be pointed out that the ratios of maximum to minimum shear stiffness and maximum to minimum shear strengths are very similar, i.e. both are approximately 3. However the angles at which they occur are different. The maximum and minimum shear strengths correspond to θ = 90 and 30 degrees respectively, but the maximum and minimum shear stiffness correspond to θ = -30 and 60 degrees, respectively.

6.9 EFFECT OF ORIENTATION WITHIN THE BEDDING PLANE

The shearing resistance of the Ashfield shale was also measured in one quadrant from 0 to 90 degrees along the lamination planes. Direct shear tests were conducted in the plane of the lamination at 22.5 degree intervals. Figure 6.15 shows a complete set of results of shear stress and dilation against shear displacement for angles within the bedding plane from 0 to 90 degrees. A constant normal stress of 580 *kPa* was employed in all cases. The peak and residual shear strengths along the lamination plane have been plotted against the direction of shearing in Figure 6.16. The values of residual shear strengths and the dilation appear to be constant (Figure 6.15) within the order of scatter of the peak values. The actual variation of peak shear strength is shown in Figure 6.16 where the strength is obtained for different directions along the bedding plane. Except at the 90 degrees direction, the values of peak shear strength do not change markedly with the direction of shearing in the plane of the lamination and the strength appears to be constant within the order of scatter of the peak values measured at 0 degree direction.

6.10 EFFECT OF RATE OF SHEARING

In order to investigate the effect of the rate of shearing on the behaviour of

Ashfield shale in the direct shear test, some tests were carried out under conditions of constant normal stress. In this way all parameters except the shear rate were kept constant from test to test. The range of rates of shearing for the tests was varied from 0.1 to 1 *mm/minute*. A constant normal stress of 580 *kPa* was employed in all cases.

Figure 6.17 shows the results for tests carried out with the various rates of shearing. The results in Figure 6.17a show that the peak shear strength is noticeably affected by the rate of shearing. The peak shear strength generally increased with increasing rate of shearing, whereas the residual strength remained more or less constant. The curves in Figure 6.17b indicate that the dilation under low shear rates is slightly higher than for the sample under higher rates of shearing. To show a clearer indication of this effect, the peak and residual shear strength and the stress ratio at peak (shear stress divided by normal stress) versus rate of shearing are also shown in Figure 6.18. As Figure 6.18a shows the peak shear strength increases with increasing rate of shearing. Figure 6.18b shows that the stress ratio at peak increases with increasing rate of shearing, but the stress ratio at residual strength is relatively unaffected.

6.11 EFFECT OF WIDTH OF GAP BETWEEN COLLARS

In this study, attempts were also made to investigate experimentally the effect of gap width on the direct shear behaviour of the Ashfield shale specimens under constant normal stress. The gap width used in this study was either 2, 3 or 4 *mm*. The results are plotted in Figure 6.19. As this figure shows, the peak shear strength was found to decrease slightly with increasing gap width. The shear stiffness also decreases with increasing the width of the gap between the two collars of the shear device. Since the gap width is a factor affecting the shear resistance of the specimen, it is important to maintain a consistent gap width so as to eliminate the effects of gap width variation. A gap width of

3 *mm* is therefore used consistently in the other series of tests.

6.12 DISCUSSION OF THE RESULTS

The direct shear test is capable of detecting the nature of the anisotropy of shale. The experimental results confirmed the existence of anisotropy in the shear strength parameters and shear stiffness of shale with lamination planes. The orientation of the lamination planes to the applied shear force and the magnitudes of normal stress have a great influence on the overall shear strength and shear stiffness. The lowest stiffness in direct shear was observed when the bedding planes were inclined at 60 degrees to the applied shear force. The largest shear stiffness generally occurred when the bedding was inclined at about -30 degrees to the applied force.

6.12.1 Comparison of the shear strength parameters

The Ashfield shale exhibits distinct anisotropy. The triaxial and direct shear experimental results confirmed the existence of anisotropy in the shear strength parameters as a consequence of the lamination planes. To understand further the shear strength parameters of the Ashfield shale as a function of the lamination orientation and confining pressure, Mohr-Coulomb envelopes were constructed for both triaxial and direct shear tests. The shear strength parameters for both triaxial and direct shear tests results are shown in Table 6.4.

The peak friction angles in direct shear tests on samples with $\theta = 0$ to 90 degrees varied between 31 and 47 degrees. The smallest values of friction angle were obtained for $\theta = 90°$ and the highest values in the region of $\theta = 30°$. The cohesive strength varied between 0.93 *MPa* for $\theta = 30°$ to 3.37 *MPa* for $\theta = 90°$.

In triaxial tests, all the envelopes obtained were approximately parabolic towards the origin. For the purpose of comparison, two series of shear strength parameters were calculated, i.e. the shear strength parameters from the linear parts of the envelopes, over the range of normal stress from 5 to 30 *MPa*, (c, ϕ) and the shear strength parameters from initial parts of the envelopes. The maximum cohesive strengths for both cases occur at $\beta = 90$ degrees and the minimum at $\beta = 30$ degrees. The cohesive strengths derived from the linear parts of the Mohr-Coulomb envelopes are approximately twice the cohesive strengths derived from the initial tangents to the Mohr-Coulomb envelopes. The initial tangent cohesive strength varied between 1.5 *MPa* for $\beta = 30°$ to 3.5 *MPa* for $\beta = 90°$. The friction angle from the linear part of the envelope varied only slightly between 30 and 34 degrees, except close to $\beta = 30$ degrees, where it dropped to 24 degrees. The friction angles derived from tangent to the initial part of envelope varied only between 56 to 63 degrees, except for $\beta = 30$ degrees, where it dropped to 47 degrees. A comparison of the results shows that the friction angles derived from initial tangent to the envelopes are approximately twice the friction angles derived from linear parts of the envelopes.

The maximum cohesive strengths for both cases, triaxial and direct shear tests occur at $\theta = 90$ degrees in direct shear and $\beta = 90$ degrees in triaxial compression test and the minimum at $\theta = 30$ and $\beta = 30$ degrees. There is close agreement between the cohesive strengths derived from the initial tangents to the Mohr-Coulomb envelopes in triaxial test and the cohesive strength derived from direct shear test. The friction angles derived from tangent to the initial part of envelope in triaxial test are more close to the friction angles derived from direct shear test.

In triaxial test the minimum strength occurs at an orientation of $\beta = 30$ degrees and the failure always occurred as a shear slip on the lamination planes. In direct shear test the shear strength and mode of failure of the

sample in the case of negative and positive directions (e.g. -30° and +30°, Figure 6.3) is different. The shear strength of the sample is higher in the case of negative values of θ than positive values of θ, as discussed previously.

6.13 CONCLUSIONS

To evaluate the engineering response of Ashfield shale, which is intrinsically anisotropic in nature, direct shear tests were carried out at a variety of normal stresses within the range from 0.3 to 1.6 MPa. The peak and residual shear strength parameters were determined for the Mohr-Coulomb strength criterion.

From the experimental results, it was found that the shear strength of laminated Ashfield shale depends not only on the applied normal stress but also on the lamination directions with respect to the direction of shear loading, i.e. the shale exhibited strength anisotropy. The peak shear strength was highest for category *II* samples (negative values of θ). The shear strength was also a function of the applied normal stress. The amount of dilatancy accompanying the shearing decreased with increasing normal stress.

The peak shear strengths were usually mobilised at relatively small shear displacements which range approximately from 0.10 to 0.20 mm. The shearing resistance was reduced abruptly with further shearing beyond the peak. At bigger shear displacements the residual strength was obtained.

It was also found that the peak and residual shear strengths were practically independent of the direction of shearing whenever the shear force was applied parallel to the laminations ($\theta = 0$).

The results of the testing show that there is a wide range of shearing orientations (e.g. $\theta \approx 0$ to 60 degrees) for which the strength parameters are

approximately constant and equal to about the minimum measured values. It might therefore be appropriate to use such values in geotechnical designs requiring shear strength parameters for the intact shale. However, if the shale mass in the field contains significant jointing (a feature that is often difficult to determine in practice), the strength of the rock mass may be better characterised by the residual strength values measured as part of this study. High values of cohesion and friction angle (31 to 62°) are generally observed for the peak condition. The residual shear strength parameters that are mainly obtained from direct shear tests, show very low apparent cohesion (almost zero) values with lower friction angles (15 to 34°).

From this study of the influence of the lamination angle θ, it can be pointed out that the ratios of maximum to minimum shear stiffness and maximum to minimum shear strengths are very similar, i.e. both are approximately 3. However the angles at which they occur are different. The maximum and minimum shear strengths correspond to θ = 90 and 30 degrees respectively, but the maximum and minimum shear stiffness correspond to θ = -30 and 60 degrees, respectively.

Table 6.1 Summary of results of CNL direct shear test for Ashfield shale

Sample No.	β (degree)	σ (*kPa*)	Conditions at peak			Conditions at $u = 3$ *mm*	
			τ (*kPa*)	u (*mm*)	v (*mm*)	τ (*kPa*)	v (*mm*)
ASR1	0	580	1728	0.107	0.001	249	-0.22
ASR2	0	580	1749	0.128	0.000	262	-0.26
ASR3	0	580	1760	0.107	0.003	266	-0.61
ASR4	0	580	1821	0.117	0.014	280	-0.27
ASR5	0	800	1886	0.096	0.009	321	-0.57
ASR6	0	800	2022	0.096	0.026	362	-0.86
ASR7	0	800	2068	0.107	0.013	427	-0.63
ASR8	0	1100	2230	0.096	0.025	544	-0.57
ASR9	0	1100	2263	0.096	0.000	556	-1.25
ASR10	0	1100	2289	0.096	0.019	596	-0.50
ASR11	0	1640	2347	0.093	0.004	598	-0.25
ASR12	0	1640	2547	0.099	-0.097	713	-1.70
ASR13	0	1640	2573	0.101	-0.023	782	-0.22
ASR14	30	580	1366	0.107	0.008	285	-0.60
ASR15	30	580	1396	0.118	0.043	378	-0.78
ASR16	30	580	1487	0.128	0.014	382	-0.45
ASR17	30	800	1764	0.353	0.002	398	-0.45
ASR18	30	800	1814	0.128	0.029	412	-0.92
ASR19	30	800	1895	0.128	0.014	497	-0.61
ASR20	30	800	1928	0.128	0.000	555	-0.84
ASR21	30	800	1954	0.139	0.029	556	-0.97
ASR22	30	1100	2025	0.118	0.005	571	-0.42

τ = Shear stress u = Shear displacement σ = Normal stress

v = Normal displacement

Table 6.1 (continue)

ASR24	30	1100	2125	0.118	0.028	590	-1.32
ASR25	30	1100	2181	0.460	0.021	685	-0.29
ASR26	30	1100	2186	0.128	0.009	685	-1.28
ASR27	30	1640	2451	0.106	0.016	929	-0.38
ASR28	30	1640	2602	0.110	0.026	970	-0.52
ASR29	30	1640	2857	0.120	-0.005	1136	-1.14
ASR30	-30	580	2311	0.160	-0.002	593	-0.46
ASR31	-30	580	2509	0.460	0.014	603	-0.12
ASR32	-30	800	2793	0.160	-0.119	647	-0.69
ASR33	-30	800	2883	0.139	-0.007	783	-0.05
ASR34	-30	1100	2961	0.139	-0.064	823	-0.79
ASR35	-30	1100	3006	0.118	-0.182	902	-0.37
ASR36	-30	1640	3381	0.107	-0.420	982	-0.34
ASR37	-30	1640	3772	0.118	0.019	1108	-0.66
ASR38	45	580	1775	0.182	0.000	317	-0.78
ASR39	45	800	1880	0.171	0.048	414	-1.08
ASR40	45	800	2102	0.171	0.005	480	-1.23
ASR41	45	1100	2205	0.203	0.002	491	-0.89
ASR42	45	1100	2418	0.150	0.001	618	-0.91
ASR43	45	1640	2761	0.165	0.005	753	-0.40
ASR44	-45	580	2069	0.128	0.041	124	-0.72
ASR45	-45	580	2492	0.160	-0.058	449	-0.72
ASR46	-45	800	2554	0.150	-0.088	708	-1.12
ASR47	-45	800	2693	0.502	-0.078	737	-0.56

Table 6.1 (continued)

ASR49	-45	1100	3520	0.171	-0.01	2887	-0.49
ASR50	-45	1640	3738	0.160	-0.047	1080	-1.11
ASR51	-45	1640	4721	0.203	0.009	1414	-1.01
ASR52	60	580	1612	0.214	-0.034	324	-028
ASR53	60	580	1703	0.192	0.057	435	-1.06
ASR54	60	800	1891	0.192	-0.09	465	-0.66
ASR55	60	800	2024	0.214	0.024	492	-0.38
ASR56	60	1100	2044	0.192	0.028	726	-0.60
ASR57	60	1100	2271	0.214	0.023	875	-0.05
ASR58	60	1640	2661	0.185	-0.014	1088	-1.34
ASR59	60	1640	2820	0.182	0.017	1100	-0.36
ASR60	-60	580	1837	0.214	-0.02	141	-0.96
ASR61	-60	580	1886	0.160	0.071	247	-1.13
ASR62	-60	800	2165	0.160	-0.027	375	-0.28
ASR63	-60	800	2166	0.150	-0.014	417	-1.34
ASR64	-60	1100	2654	0.160	-0.071	498	-0.96
ASR65	-60	1100	2927	0.171	-0.059	554	-0.33
ASR66	-60	1640	3250	0.171	0.022	785	-0.10
ASR67	-60	1640	3887	0.203	-0.005	907	-0.90
F51	90*	580	3075	0.256	-0.122	1108	-0.77
F52	90*	580	3024	0.246	-0.026	930	-1.73
F53	90*	800	3356	0.246	-0.07	1448.55	-0.78
F54	90*	800	3355	0.214	-0.026	1428	-1.02
F55	90*	1100	3528	0.192	0.057	1487	-0.88
F56	90*	1640	3650	0.186	0.06	1702	-1.05

* Scaled values for this direction

Table 6.2 Peak and residual shear strength parameters for Ashfield shale

Ashfield shale core samples	β *degrees*	Peak		Residual	
		ϕ_p *degrees*	c_p *MPa*	ϕ_r *degrees*	c_r *MPa*
Category I	0	34	1.42	24	0
	30	47	0.93	31	0
	45	43	1.25	22	0.116
	60	45	1.11	34	0
	90*	31	3.37	15	0.503
Category II	- 30	46	1.89	23	0.374
	- 45	62	1.16	37	0
	- 60	59	0.91	26	0

* Scaled values for this direction

Table 6.3 Shear stiffness from direct shear test

β (Degree)	Normal stress (*kPa*)	Initial tangent (*kPa/mm*)	Secant at 50% of peak (*kPa/mm*)	Secant at peak (*kPa/mm*)
0	580	45823	23389	17258
0	580	37713	19510	14449
0	580	46829	23863	46829
0	580	43872	22465	16591
0	800	58033	29037	21311
0	800	63271	31392	22988
0	800	56878	28512	20936
0	1100	71633	35071	25593
0	1100	73001	35665	29012
0	1100	74087	36133	26342
0	1640	85128	41108	28052
0	1640	87359	42041	28660
0	1640	86209	41561	28347
30	580	36152	25291	13449
30	580	33152	23265	12415
30	580	32476	22808	12180
30	800	40777	28390	15018
30	800	42909	29808	15731
30	800	43786	30390	16022
30	800	40395	28135	14890
30	1100	51127	35216	18418
30	1100	54196	37213	19398
30	1100	50830	35023	18323
30	1640	63772	49877	25464

Table 6.3 (continued)

30	1640	65922	51259	26113
30	1640	66503	48241	26298
-30	580	41690	28892	15320
-30	800	52188	35900	18760
-30	800	64530	43842	22600
-30	1100	66740	45245	23270
-30	1100	84188	56080	28344
-30	1640	113566	63500	36141
-30	1640	115495	64615	36620
45	580	28805	18873	10146
45	800	32953	21480	11490
45	800	37423	24261	12620
45	1100	38505	29200	14352
45	16400	51641	32800	17124
45	1640	53838	34219	17926
-45	580	60079	34980	17275
-45	580	57390	33540	16603
-45	800	64100	37132	18263
-45	1100	81860	46315	22422
-45	1640	97175	53900	25755
-45	1640	965659	53600	25626
60	580	21330	14753	7770
60	580	25490	17554	9190
60	800	28633	19644	10255
60	800	27369	18806	9830

Table 6.3 (continued)

60	1100	31230	21368	11110
60	1100	31120	21295	11078
60	1640	44131	29759	15256
60	1640	43220	30587	16509
-60	580	24592	16951	8880
-60	580	35050	23887	12360
-60	800	41082	27800	14309
-60	800	44330	29889	15315
-60	1100	52298	34952	17750
-60	1100	54320	36229	18357
-60	1640	61790	40877	20555
-60	1640	62373	41230	20722
90*	580	28000	16919	12602
90*	580	28769	17346	12920
90*	800	32328	19394	14412
90*	800	37880	22551	16712
90*	1100	45592	26850	19818
90*	1640	44599	31906	21274

* Scaled values for this direction

Table 6.4 Direct shear and triaxial shear strength parameters for Ashfield shale

Lamination Direction (degree)	Direct shear test results		Triaxial test results			
	Cohesion c_p (MPa)	Friction angle ϕ_p (degrees)	Cohesion c (MPa)	Cohesion c_i (MPa)	Friction angle ϕ (degrees)	Friction angle ϕ_i (degrees)
0	1.42	34	7.2	3.5	34	56
15	-	-	5.95	2.5	30	57
30	0.93	47	3.78	1.5	24	47
45	1.25	43	5.51	2.5	31	63
60	1.11	45	6.76	3	34	63
75	-	-	7.5	3.3	32	58
90	3.37	31	7.81	3.5	33	63

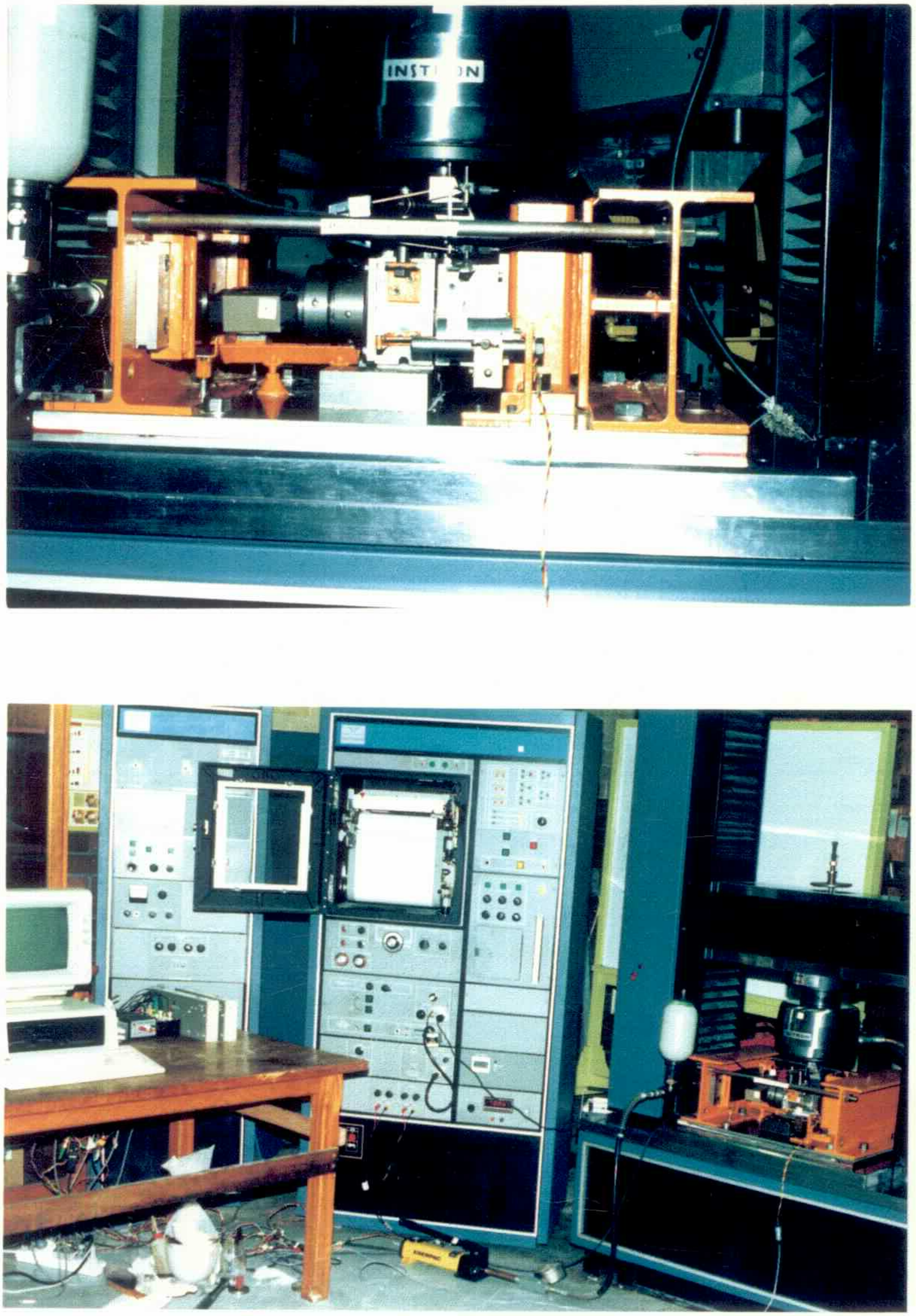

Figure 6.1 Direct shear device

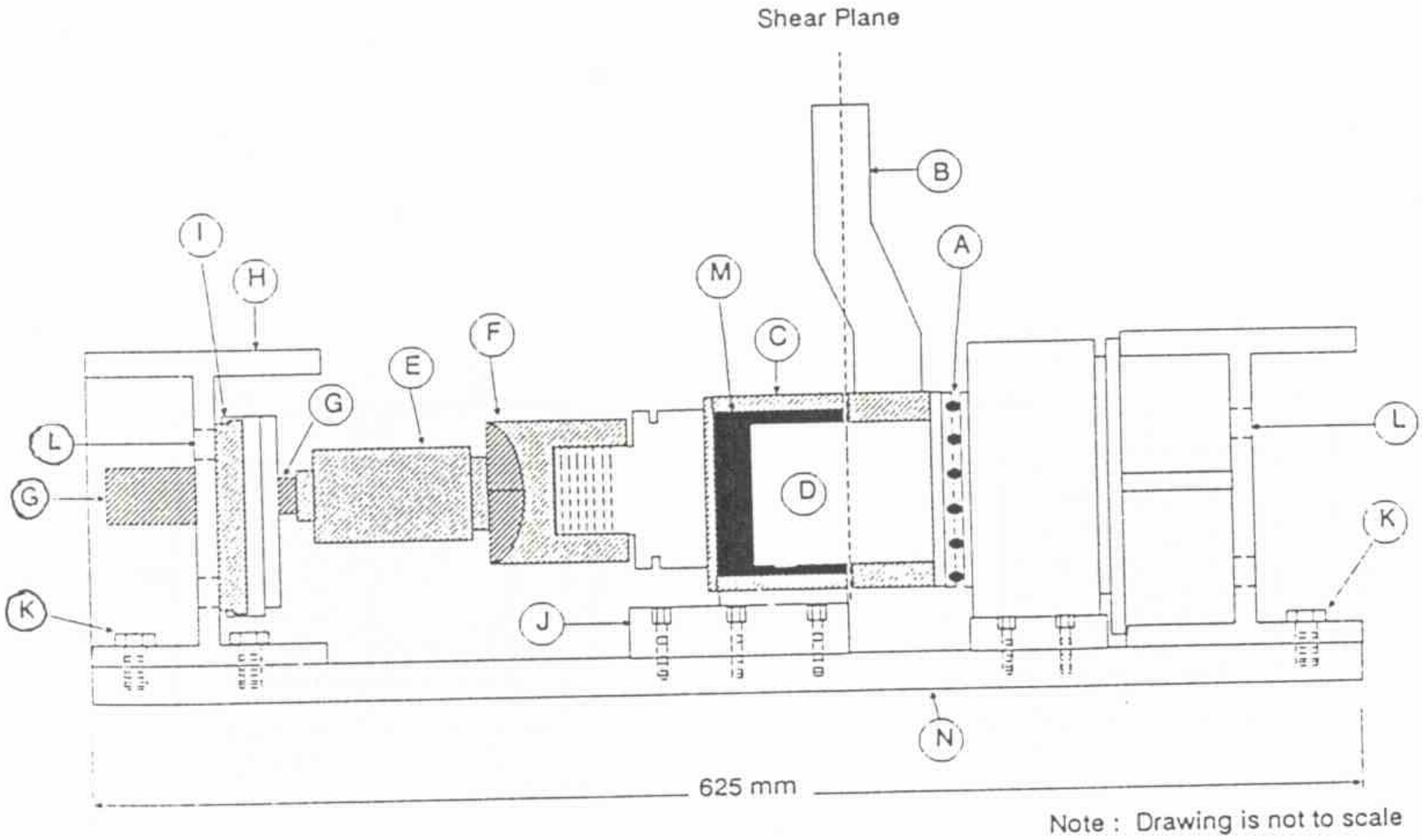

Note : Drawing is not to scale

Item	Description
A	Cylindrical roller bearings
B	Straight connecting rod of right collar : connected to testing machine for application of shear load
C	Left collar which only can slide in the slider J
D	Cylindrical specimen
E	Normal load cell
F	Spherical seat : allow application of initial normal stress
G	Hydraulic jack to apply initial normal stress (for CNL test only)
H	Reaction frame
I	Movable knife edge support (for CNS test only)
J	Slider to allow only normal displacement
K	Position of bolts for fastening to testing machine base plate
L	Long bolts to stiffen reaction frame
M	Hydrostone (plaster) grout
N	Base plate of device

Figure 6.2 Schematic Layout of the direct shear device for CNL test (after Boey, 1990)

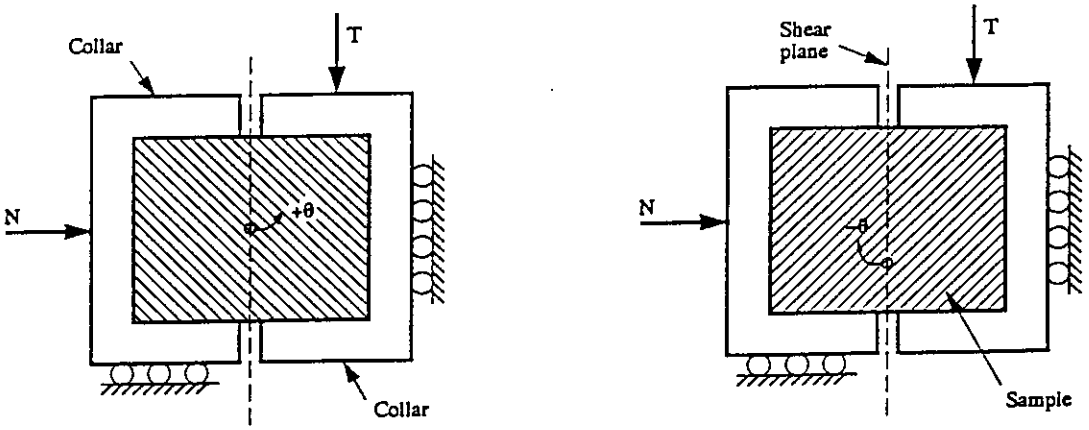

(a) Category I

(b) Category II

Figure 6.3 Orientation of laminations respect to the shear load direction

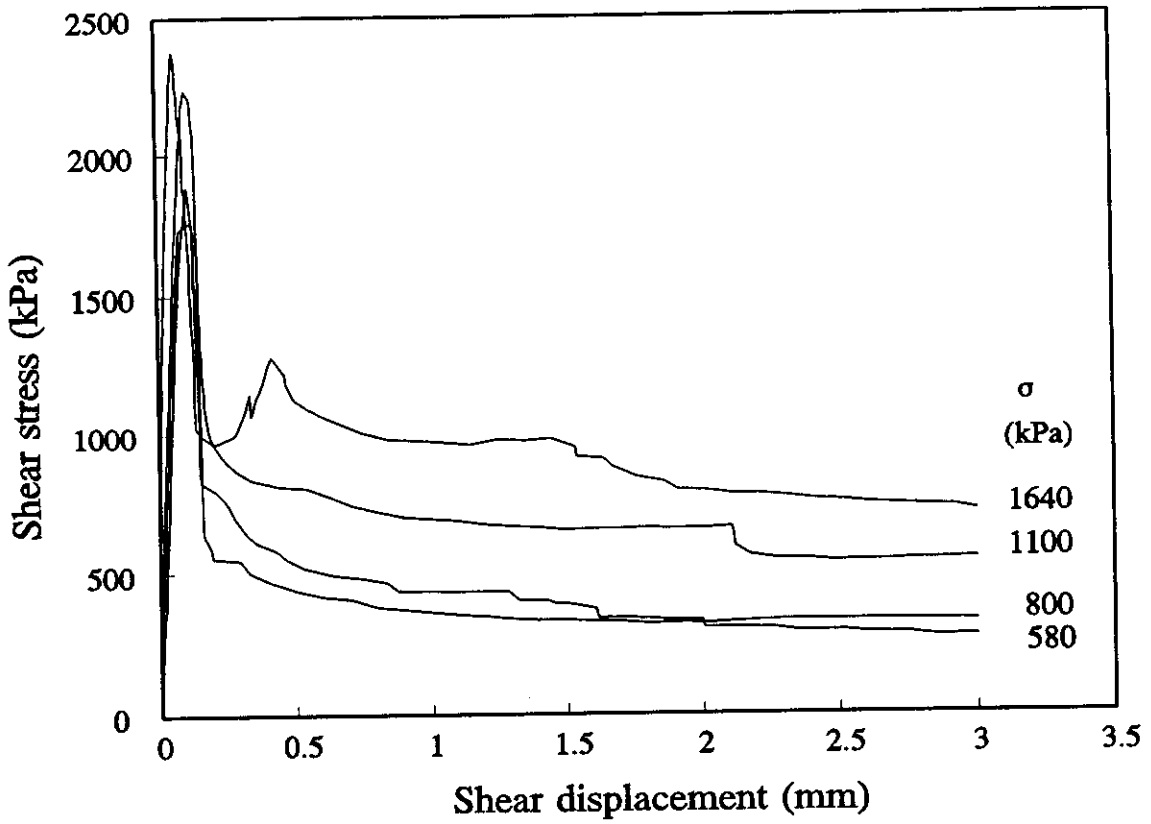

(a)

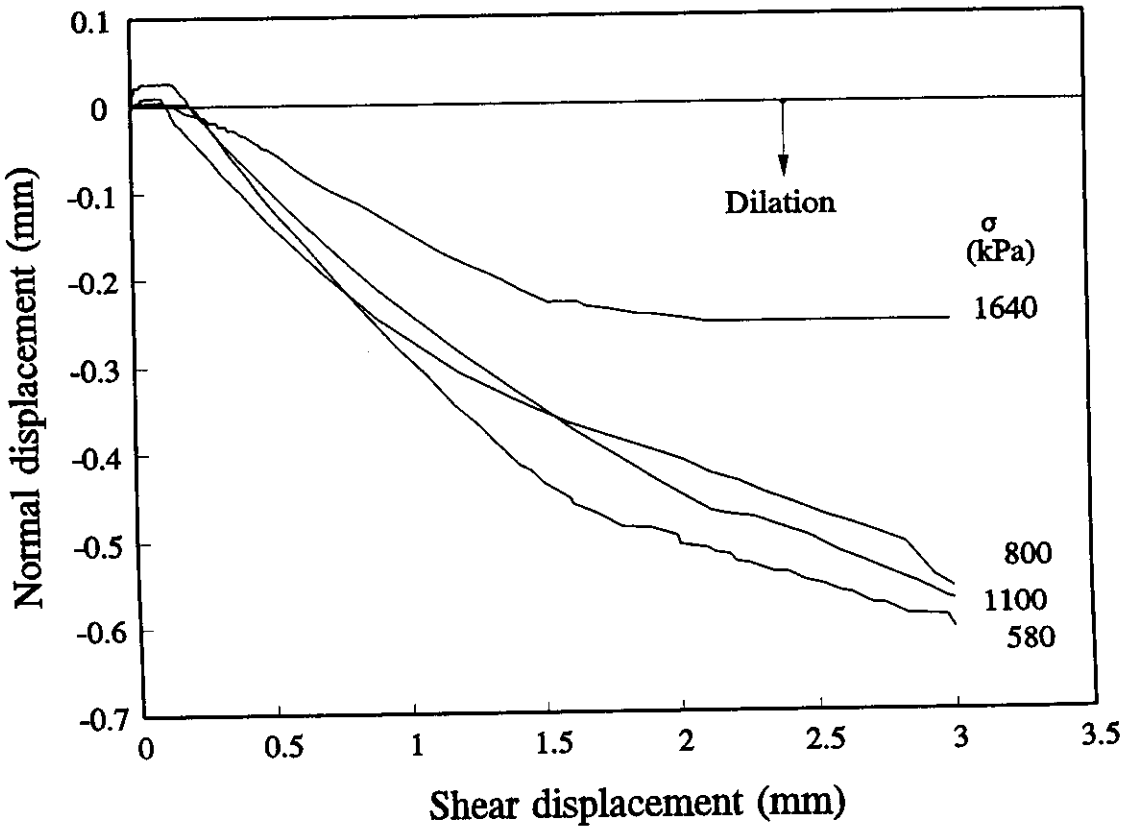

(b)

Figure 6.4 Typical test results: $\theta = 0$, (Ryde)

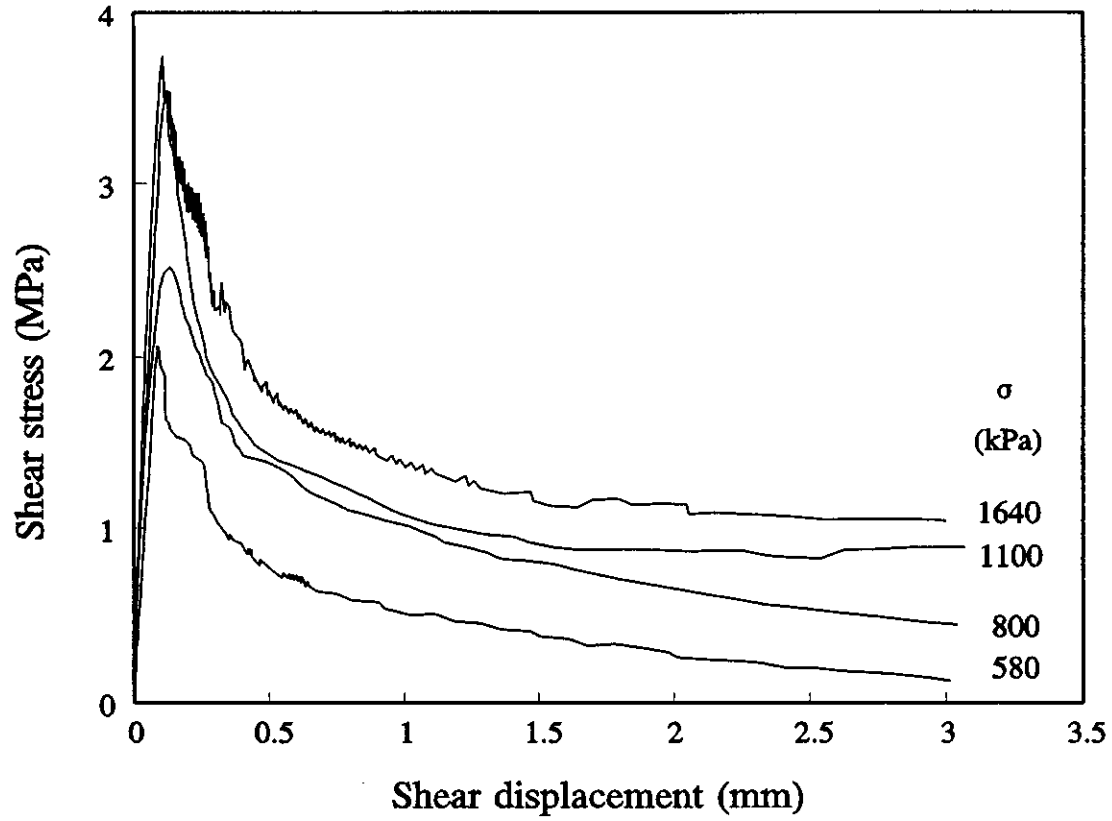

(a)

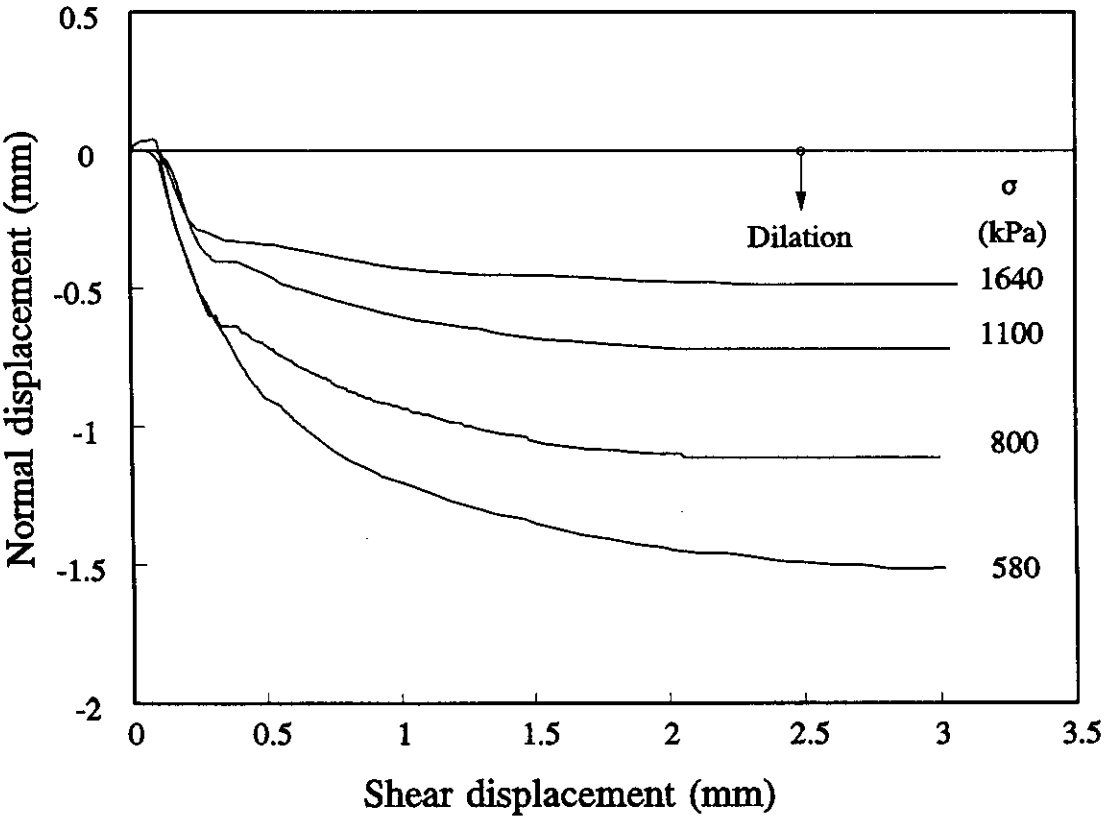

(b)

Figure 6.5 Typical test results: θ = -45°, (Ryde)

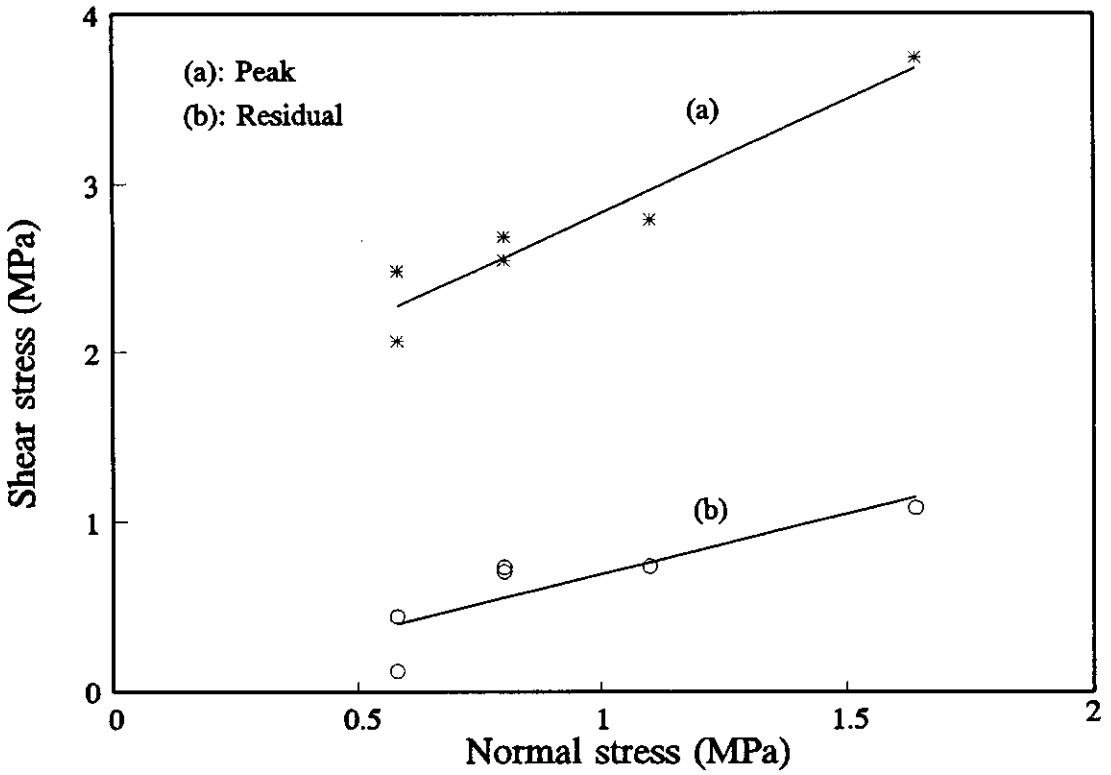

Figure 6.6 Peak and residual shear strengths for θ = -45° (Ryde)

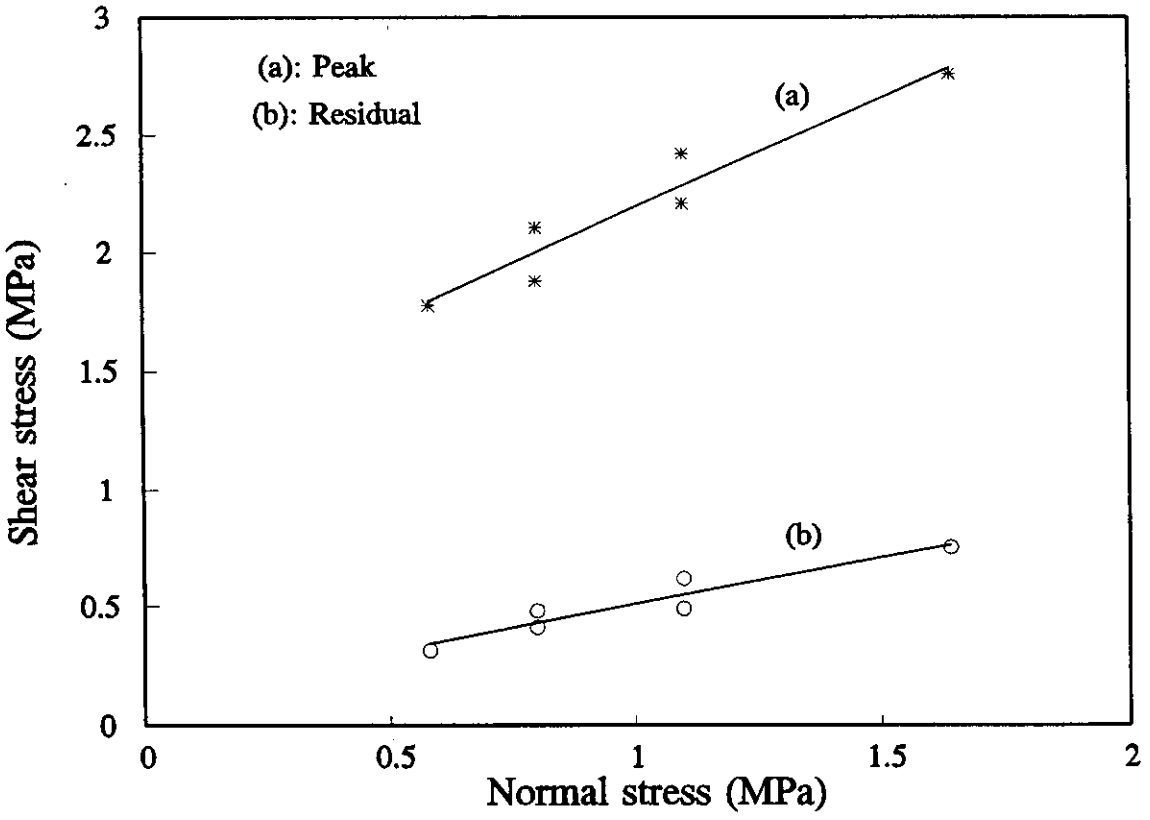

Figure 6.7 Peak and residual shear strength for θ = 45° (Ryde)

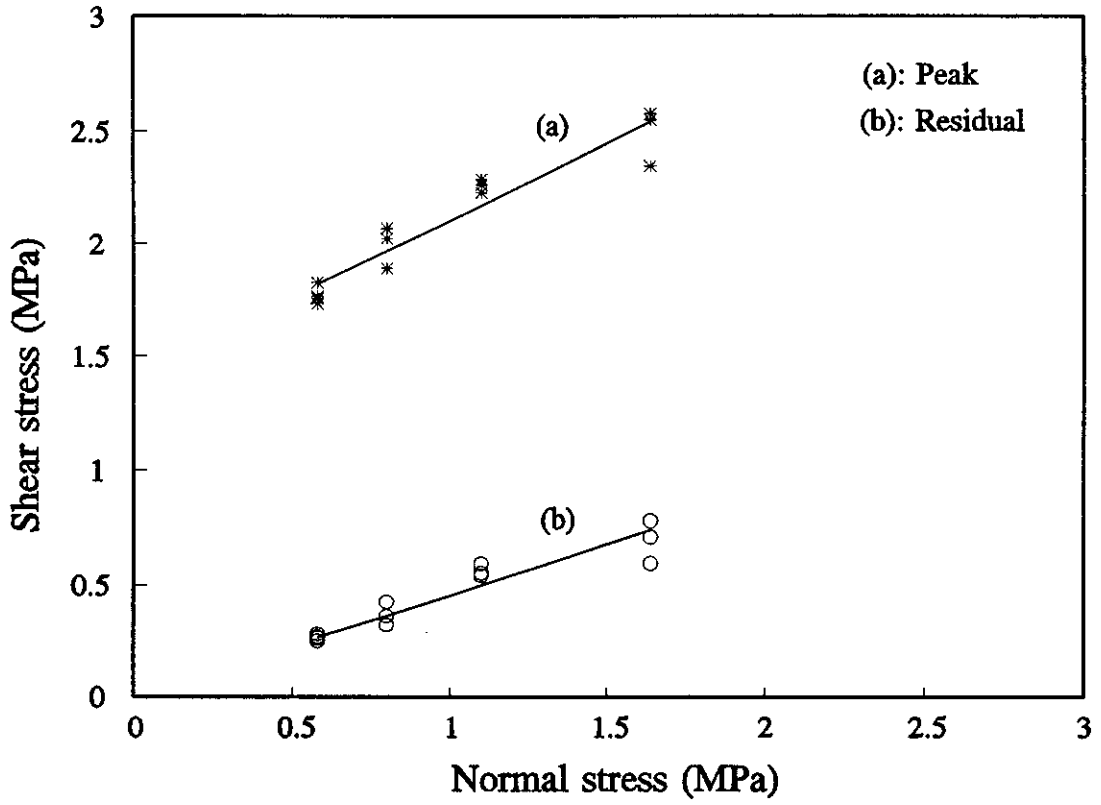

Figure 6.8 Peak and residual shear strength for θ = 0°, (Ryde)

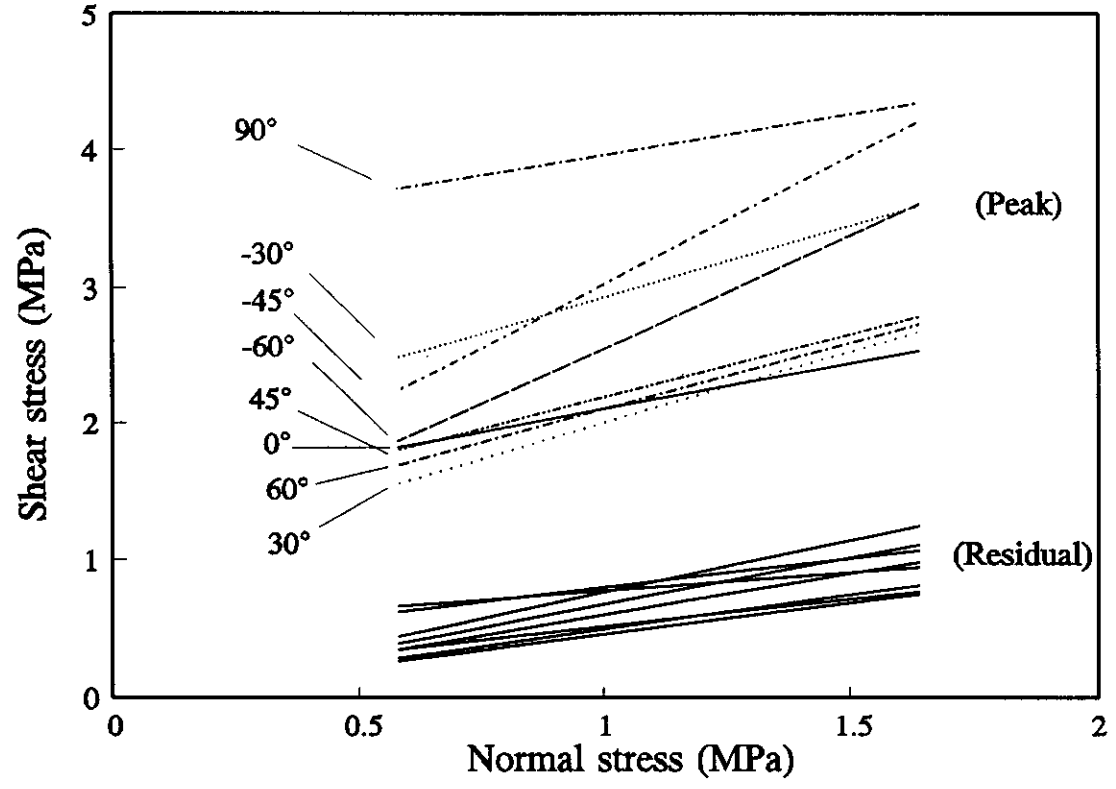

Figure 6.9 Summary of peak and residual strength envelopes (Ryde)

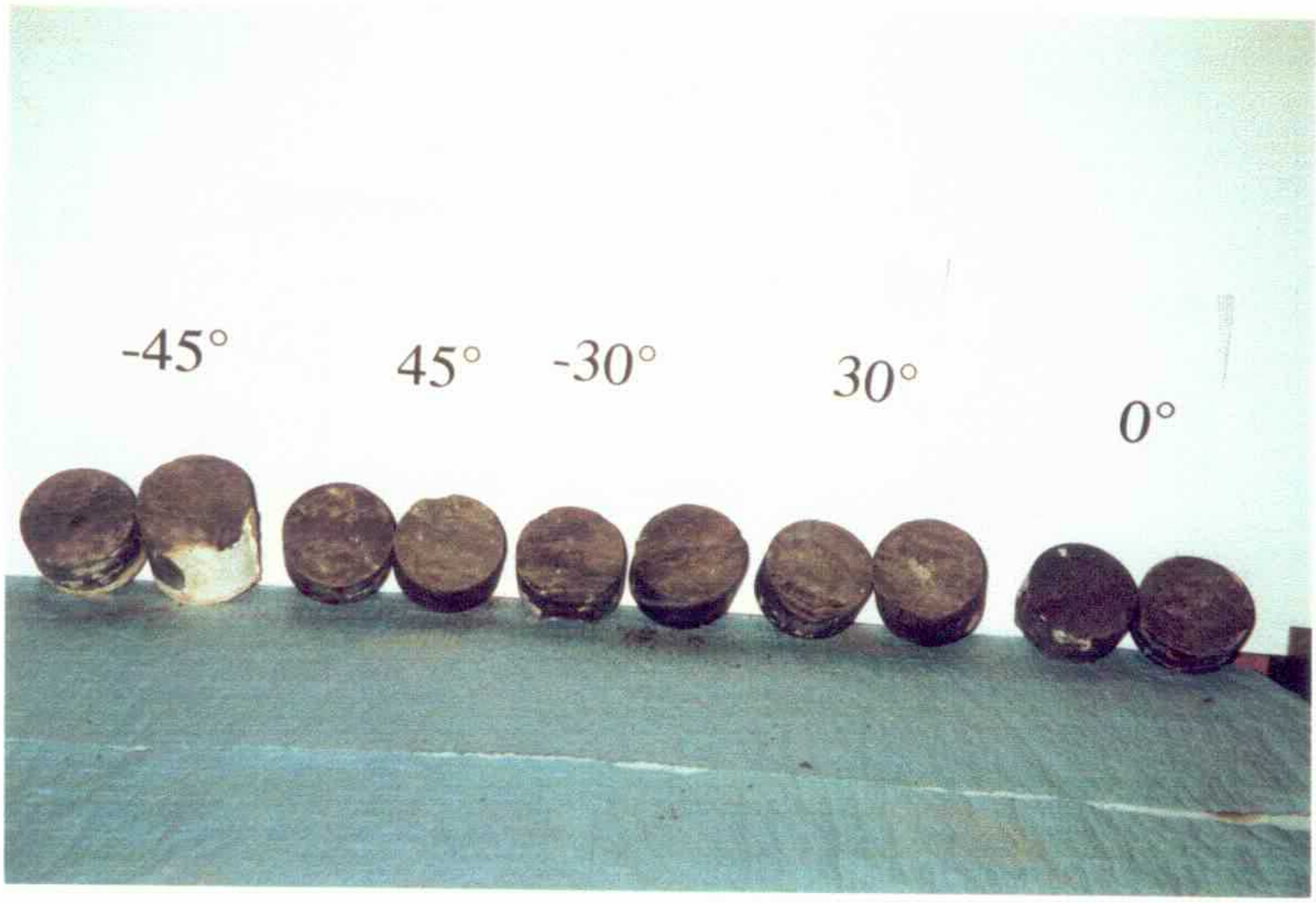

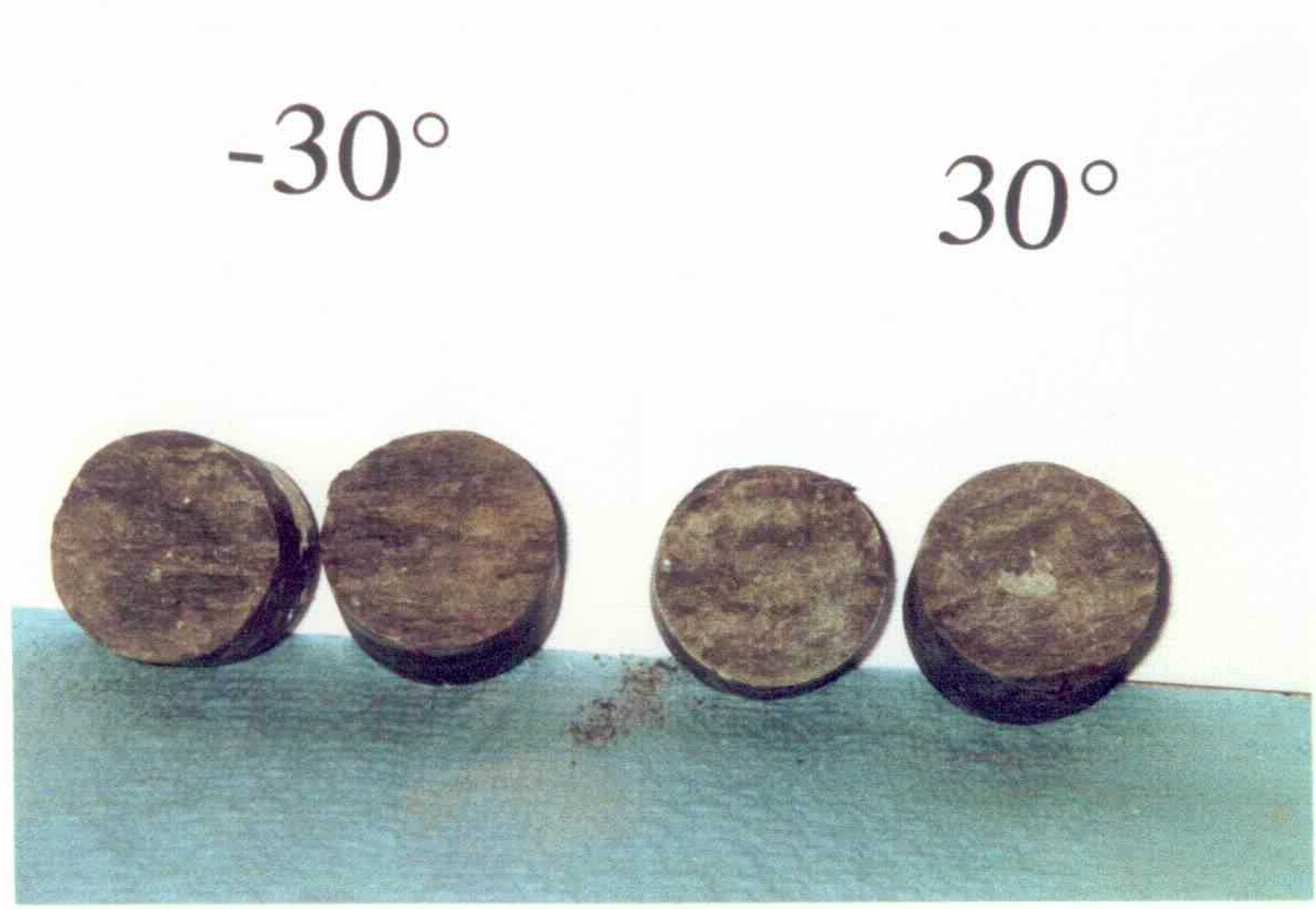

Figure 6.10 Failure surface for category I and II

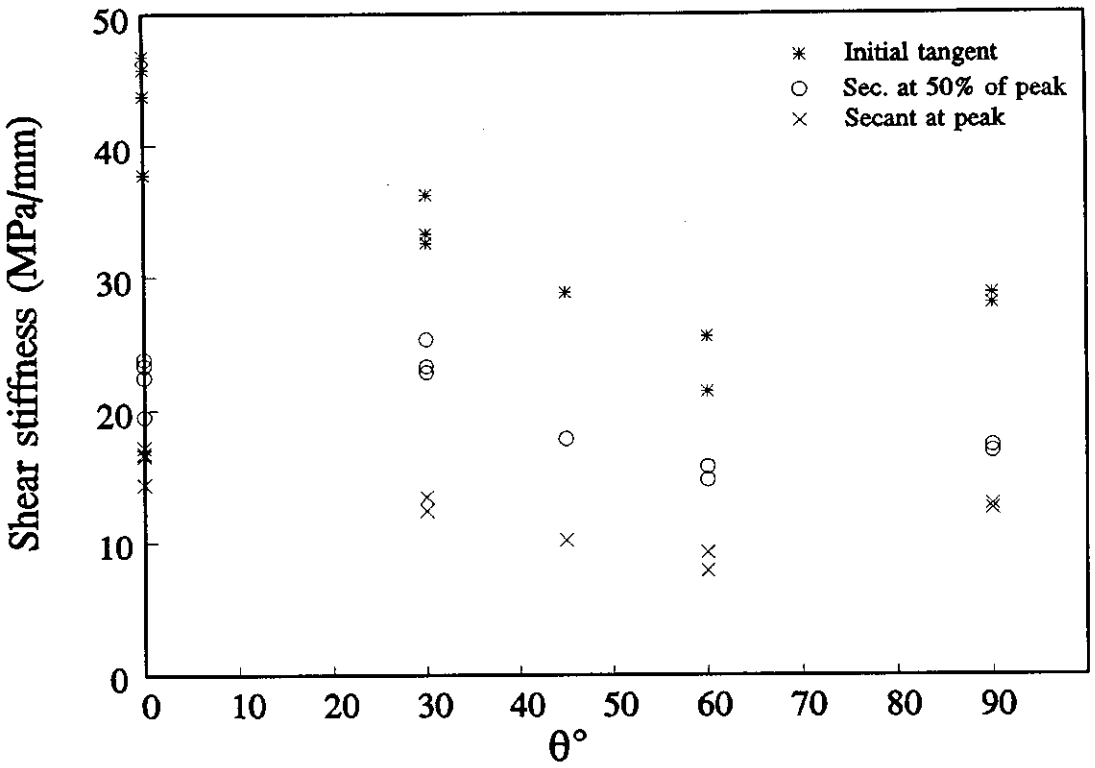

Figure 6.11 Experimental shear stiffnesses (σ_n = 580 kPa)

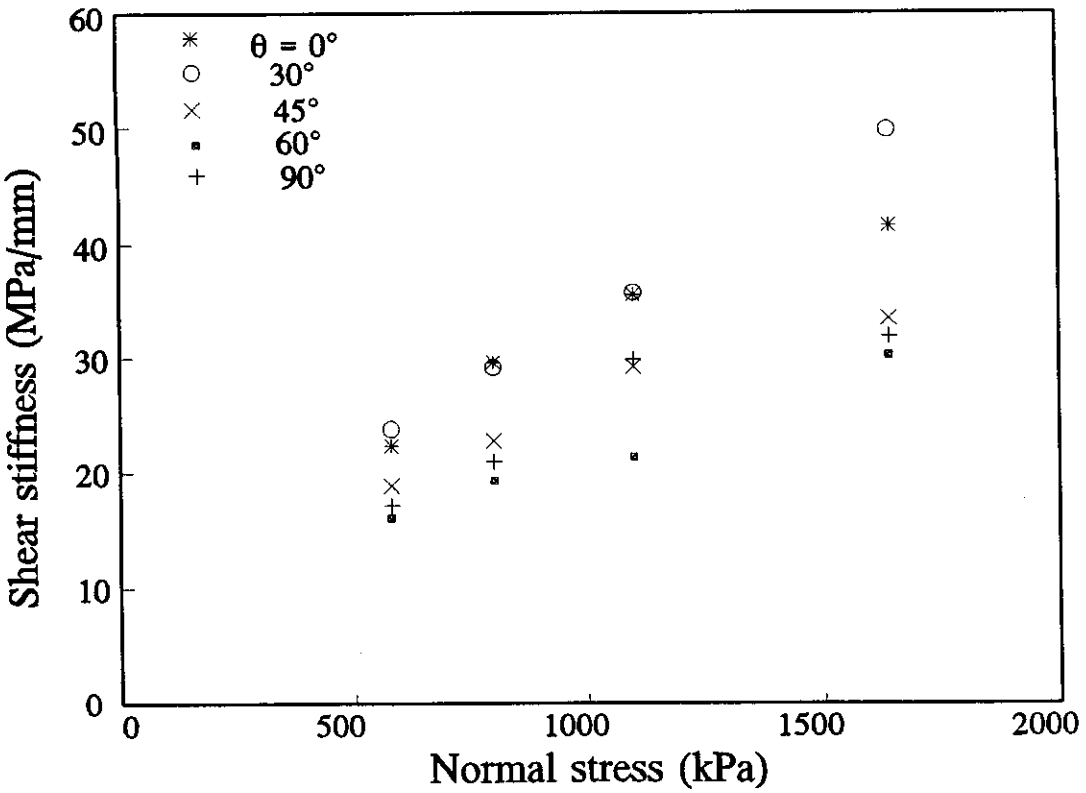

Figure 6.12 Effect of normal stress on shear stiffness
(Secant at 50% of peak)

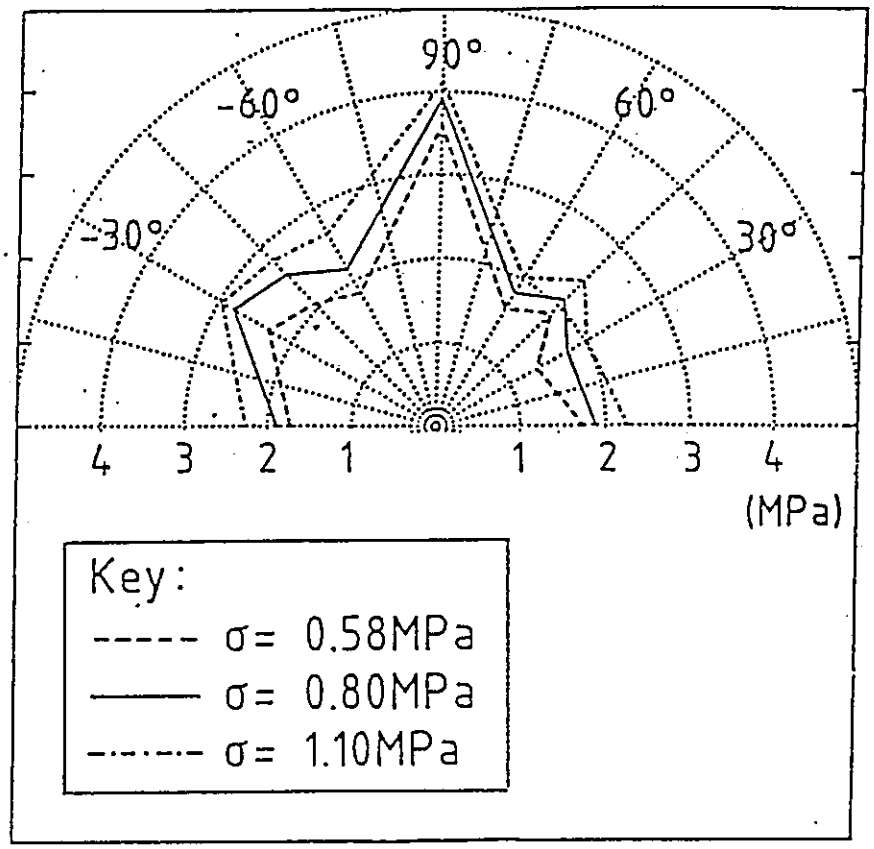

Figure 6.13 Influence of lamination orientation on peak strengths

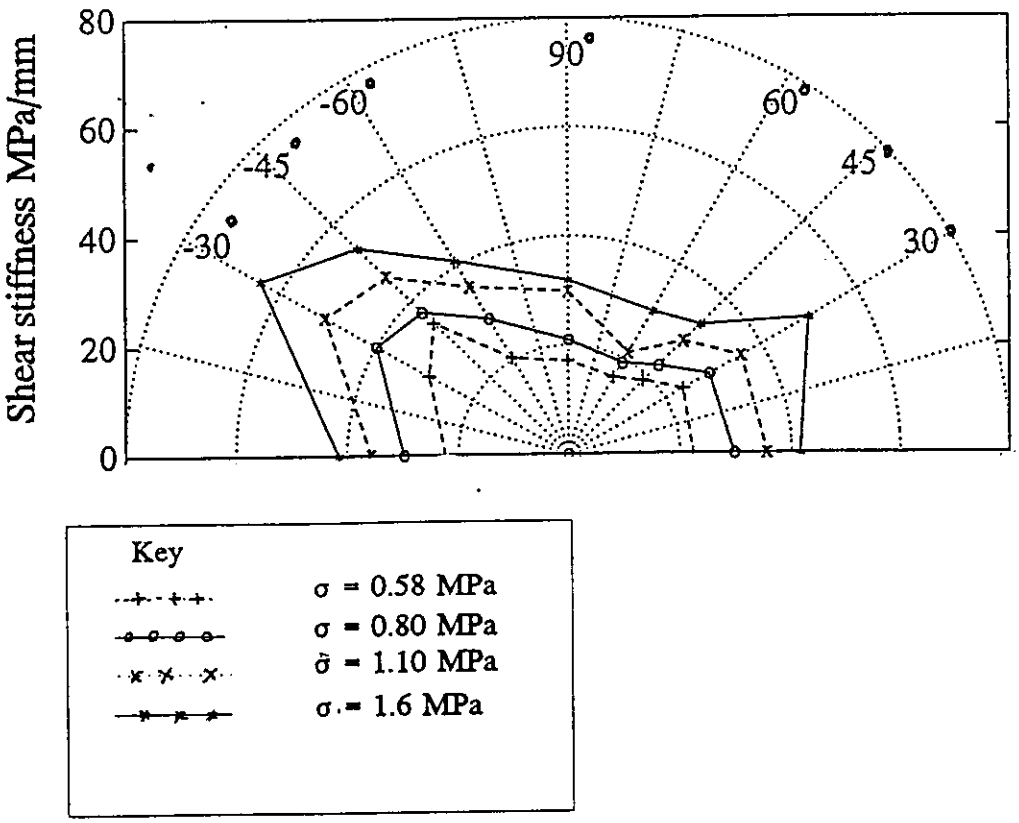

Figure 6.14 Influence of lamination orientation on shear stiffness

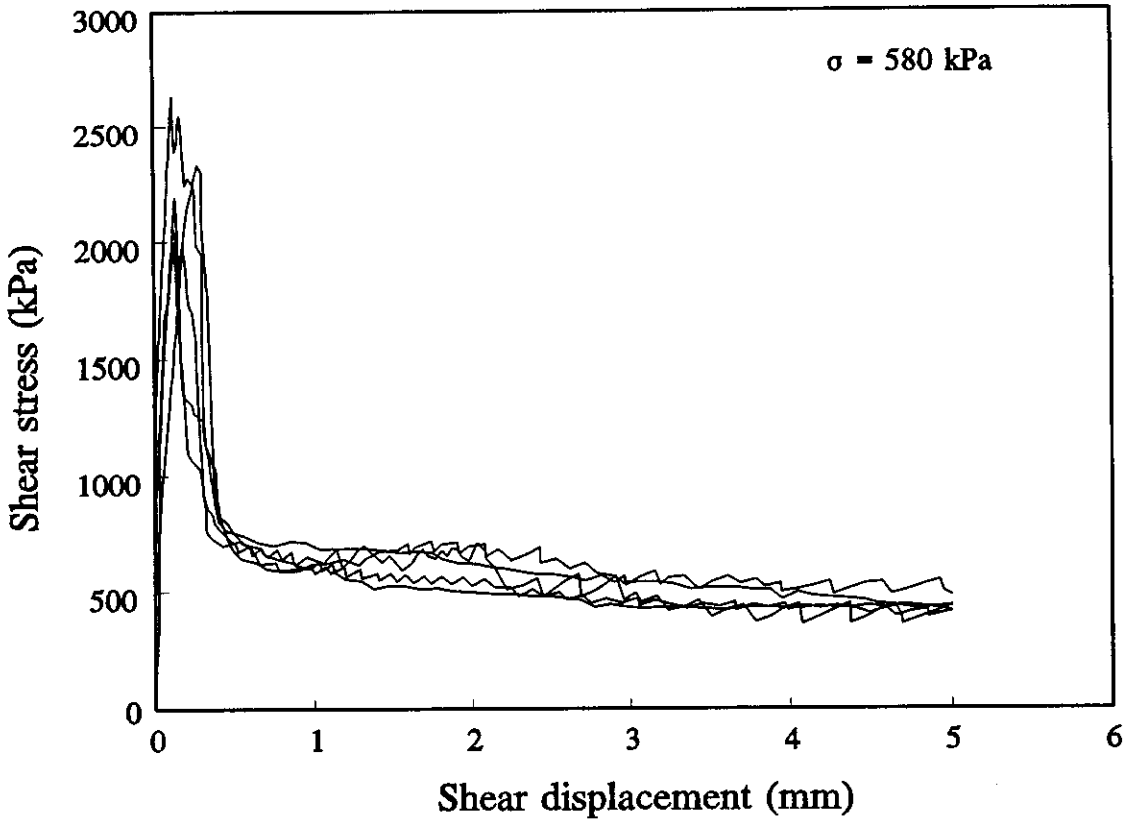

(a)

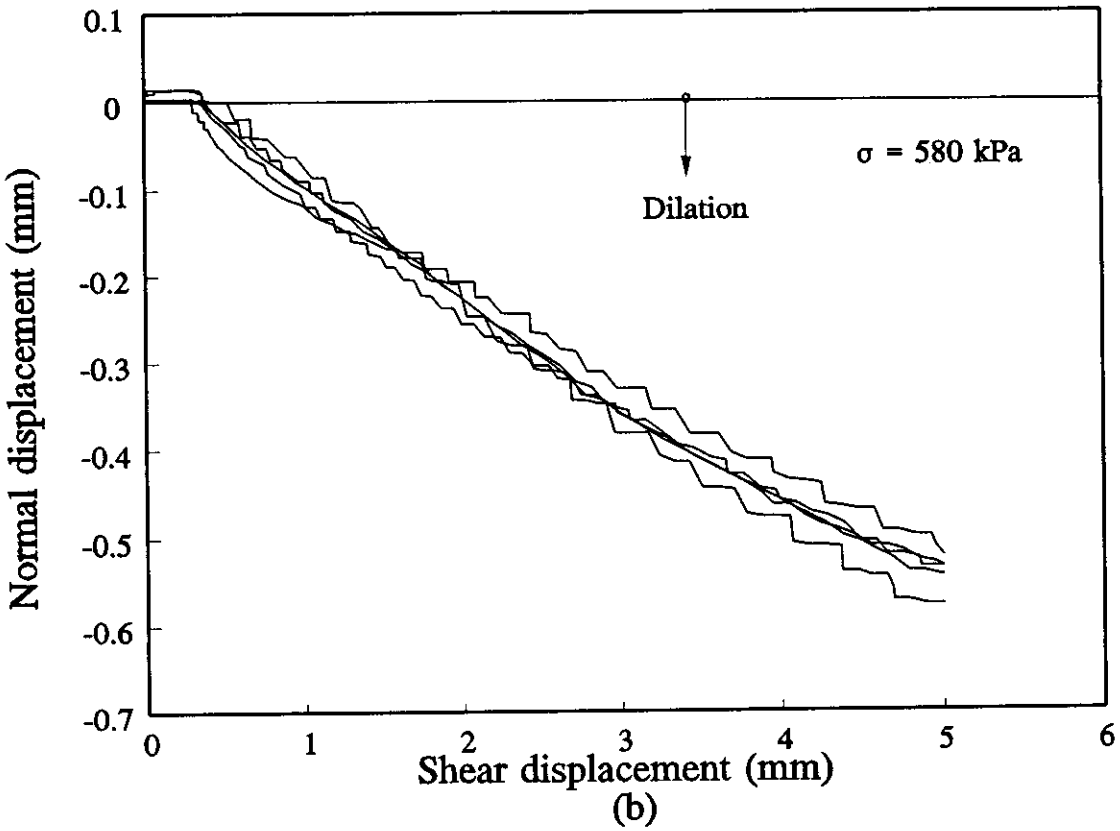

(b)

Figure 6.15 Results for shearing along the bedding planes

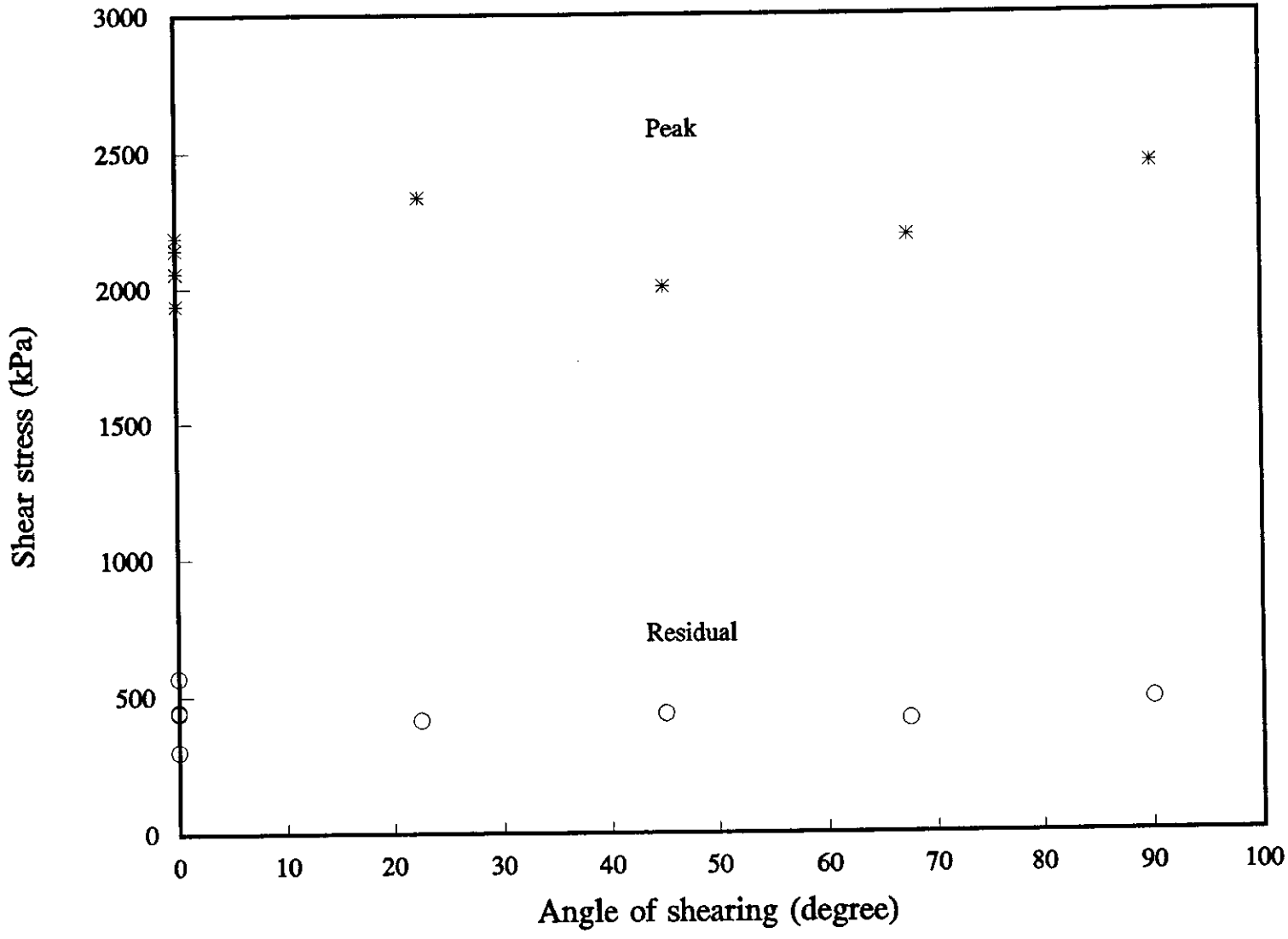

Figure 6.16 Peak and residual shear strengths along the bedding planes

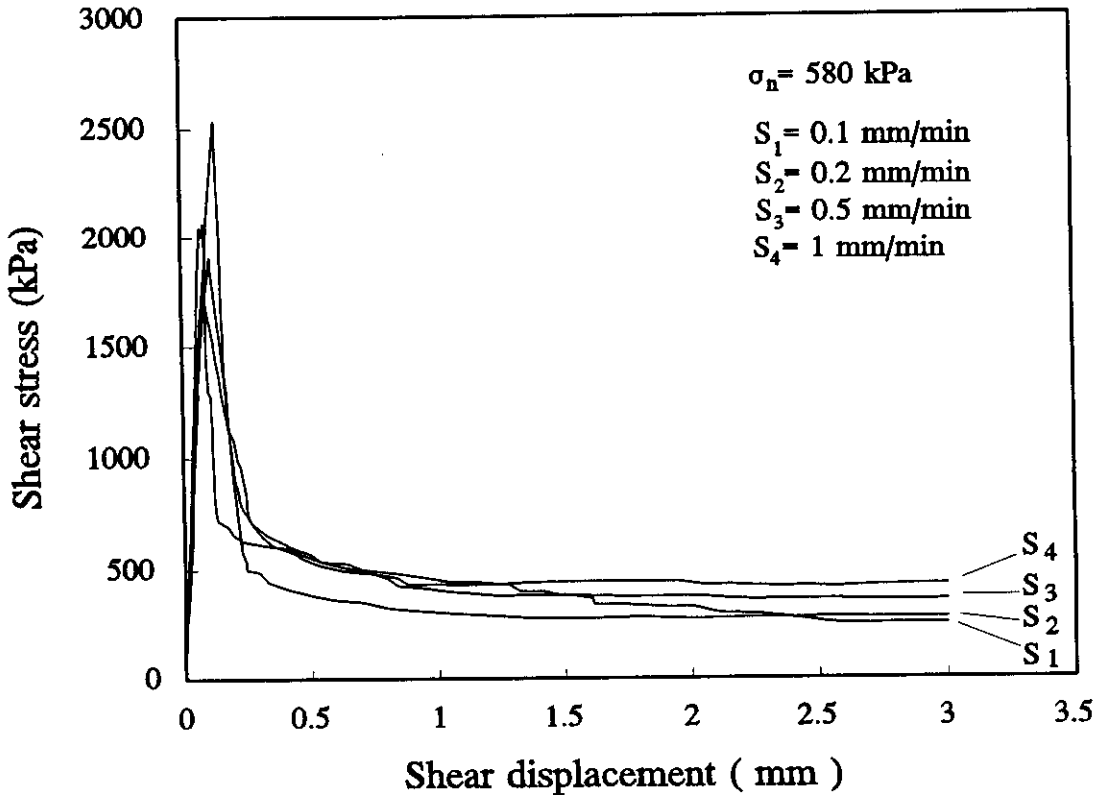

(a)

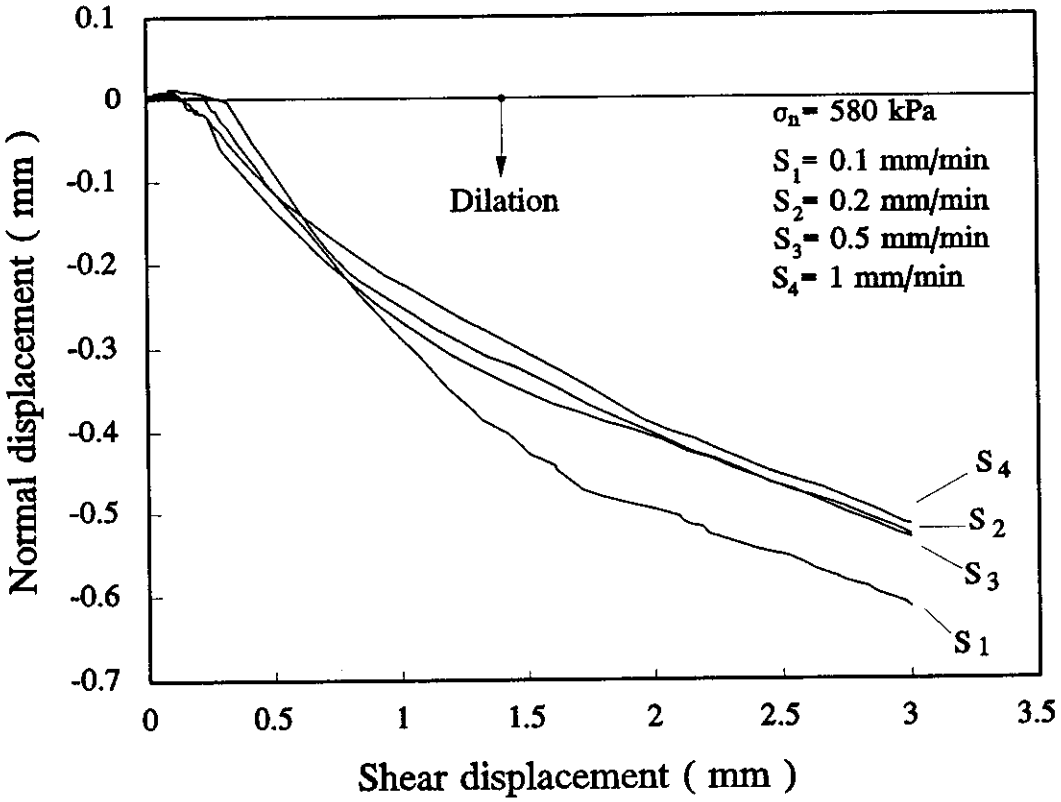

(b)

Figure 6.17 (a) Shear stress-displacement and (b) dilation-displacement curves with different strain rates

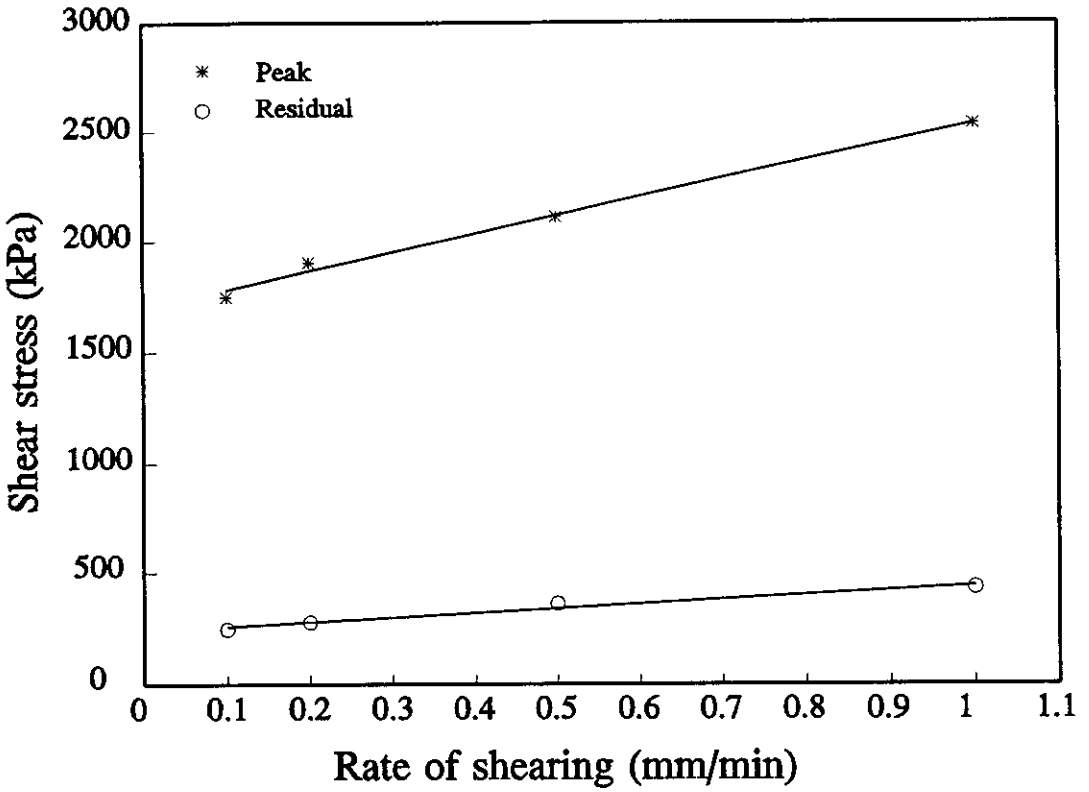

(a)

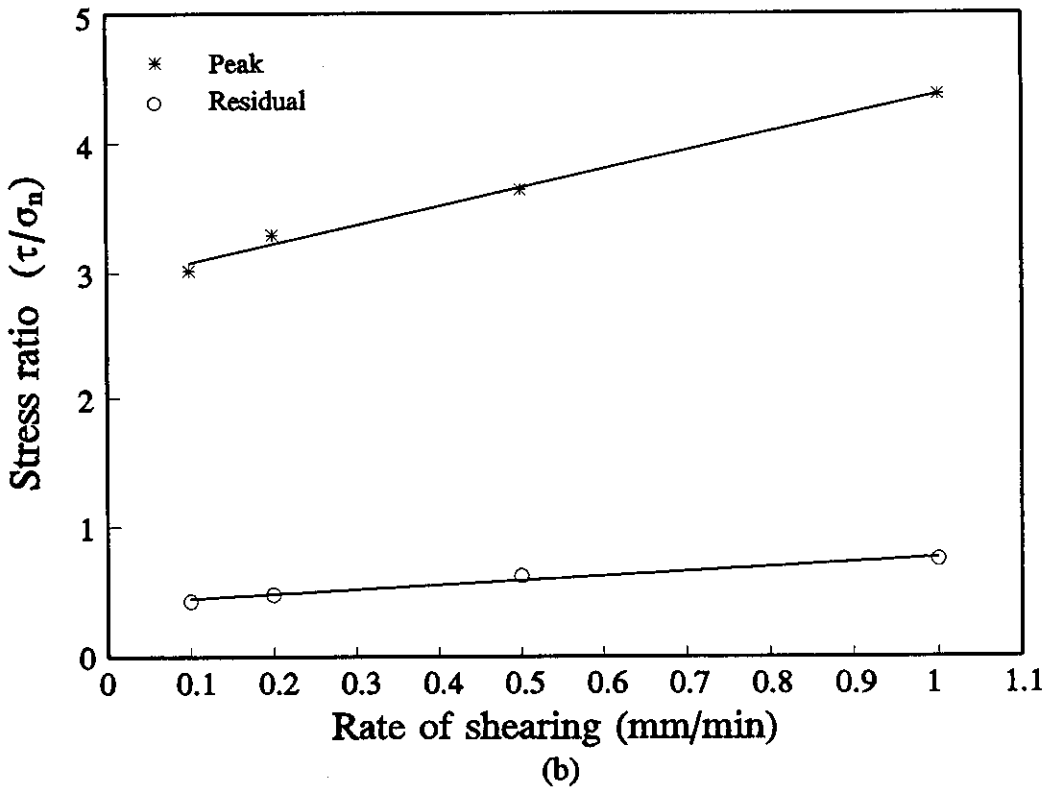

(b)

Figure 6.18 Effect of rate of shearing on (a): shear stress and (b): stress ratio (σ_n= 580 kPa)

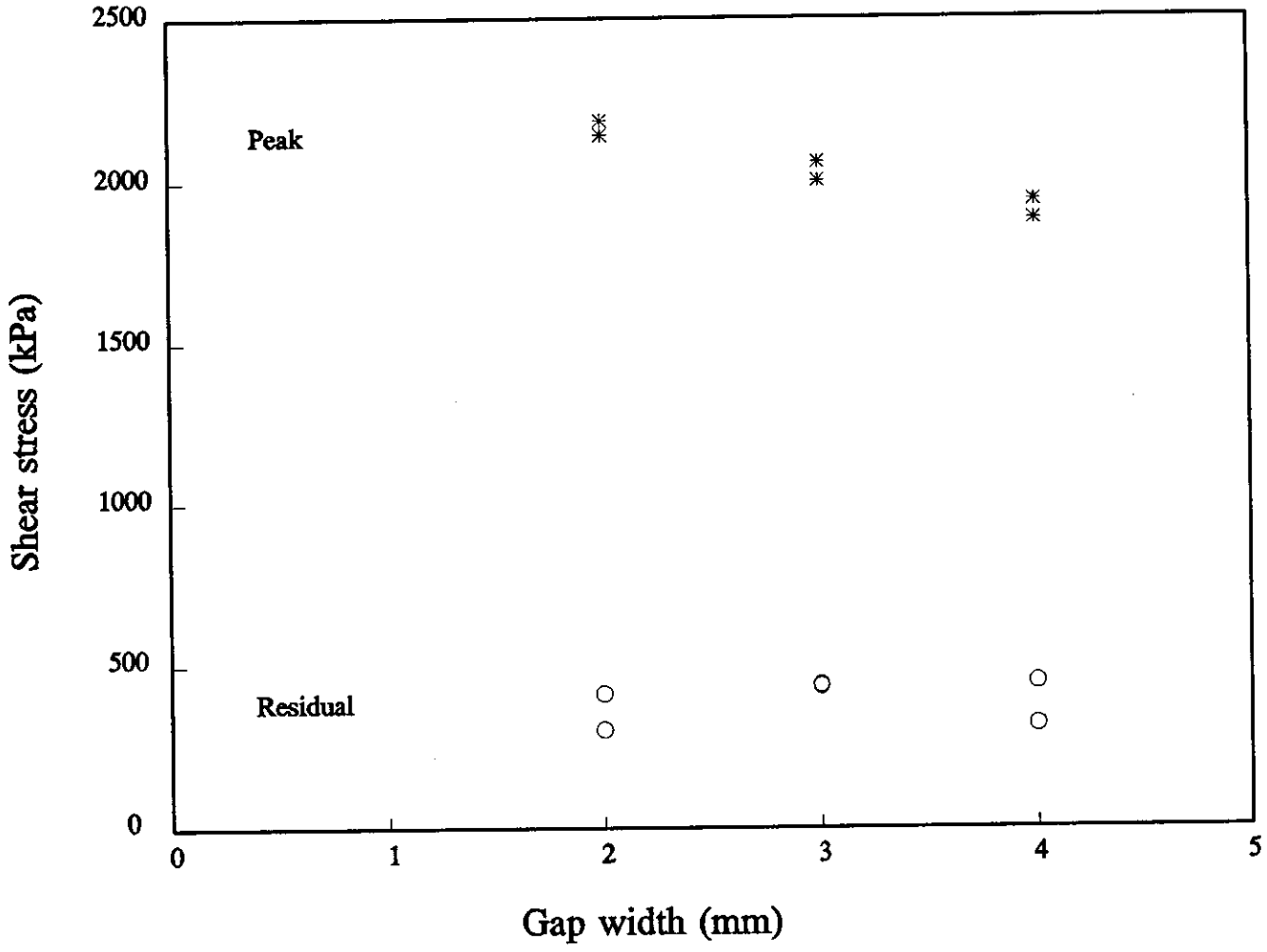

Figure 6.19 Effect of gap width on shear stress

CHAPTER 7 NUMERICAL MODELLING OF ASHFIELD SHALE IN THE DIRECT SHEAR TEST

CHAPTER 7

NUMERICAL MODELLING OF ASHFIELD SHALE IN THE DIRECT SHEAR TEST

7.1 INTRODUCTION

An extensive experimental investigation into the anisotropic behaviour of Ashfield shale has been carried out and the results have been presented in previous chapters. This chapter addresses the pre-failure behaviour of anisotropic rock during direct shear tests. The study has investigated the effect of the orientation of the bedding planes to the shearing direction, and the boundary conditions imposed in the test on the behaviour during shearing. A cross-anisotropic elastic model has been used to represent the pre-failure stress-strain behaviour of the rock. An extensive parametric study has been carried out of the behaviour of this material in direct shear.

The numerical solutions have been compared with the results of the physical experiments carried out on core samples of Ashfield shale. A detailed description of the test setup and the measured strength anisotropy has been described in chapter 6.

The deformation anisotropy deduced from the direct shear tests is also compared to that which was measured in the more conventional uniaxial and triaxial compression tests on core samples of the shale (Chapter 5).

7.2 NUMERICAL MODELLING

7.2.1 Stress-strain model

It has been demonstrated from the results of the triaxial and UCS tests that the pre-peak behaviour can be reasonably described by a cross-anisotropic elastic model. The definition of elastic constants for shale is shown in Figure 7.1. Taking the bedding planes (or the plane of isotropy) parallel to the x and y-axes and the z-axis perpendicular to the plane of isotropy as shown in Figure 7.1, the stress-strain relationships for a cross-anisotropic rock unit are given by equations (5.16) to (5.21). The transversely isotropic system is therefore completely described by five independent elastic parameters, E_1, E_2, ν_1, ν_2, and G_2 (see section 5.7 for detail).

7.2.2 Finite element model

Finite element modelling has been carried out of samples of an ideal cross-anisotropic material subjected to direct shearing. The test configuration and the relevant boundary conditions are illustrated schematically in Figure 7.2a. The test set-up modelled is similar to a conventional soil mechanics shear box test. The specimen has a height L and a width D. The top portion of the specimen is loaded horizontally through a rigid plate of height $0.5(L\text{-}T)$ and the bottom portion is restrained horizontally by a rigid plate of the same height. The specimen sits on a smooth rigid base and the interfaces between the loading and restraining plates are perfectly smooth. A vertical "gap" of width T exists between the two vertical rigid plates, so that most of the shear deformation will occur in the specimen in the region between the plates. It is assumed that a horizontal shear force is applied to the upper left-hand

loading plate at a height X above the base of the specimen. The magnitude of this shear force per unit length is denoted by F. With this configuration there may be a tendency for some bending to occur in the specimen (as well as shearing) resulting in a rotation of its top surface and the left-hand loading plate. The right-hand rigid plate is restrained against rotation. Figure 7.2b shows an exaggerated deformed shape. Additional analyses have been performed with both halves of the shear box restrained from rotation, with the bottom half rigidly restrained.

Conditions of plane strain have been assumed in the model. Parametric studies have been conducted to assess the influence on the shearing behaviour of the anisotropic material properties, and the geometry of the loading. For each parameter the angle (θ) that the plane of isotropy, i.e. the bedding planes in the shale, makes with the direction of the shearing force has been varied. Analyses similar to those described here, but for an isotropic material, have been presented previously by Noonan and Nixon (1972).

The finite element calculations were conducted using the program AFENA (Carter and Balaam, 1990). The anisotropic sample was represented using 8-noded isoparametric elements. A fine mesh, composed of 1735 nodes and 540 elements, was used. Most of the elements were located in the region of the gap where high stress gradients were expected. The analyses, based on the theory of linear elasticity, were used to predict the pre-peak stresses and displacements throughout samples of anisotropic rock subjected to direct shear. In particular, the shear stiffness of the sample was of interest, and the results of the analyses have been expressed in non-dimensional form, using the dimensionless shear stiffness

$$K = \frac{F}{E_1 D} \tag{7.1}$$

in which E_1 is the Young's modulus of the rock in the plane of isotropy, i.e. in the direction of the laminations.

7.3 PARAMETRIC STUDY

In this section the results of the numerical study for assessing the influence of the model parameters on the shearing behaviour of the anisotropic material properties are presented. The important aim of this study is the determination of the parameters which have the greatest influence on the shear stiffness of the Ashfield shale.

7.3.1 Effect of material properties

In most of the calculations presented in this chapter it has been assumed that $\nu_1 = \nu_2 = 0.1$, and that the independent shear modulus is given by $G_2 = 0.6675\ E_1$ (This can be compared to the value of $G = 0.4545\ E_1$ that would apply in an isotropic material with $\nu = 0.1$). These values have been selected because they are consistent with the values determined independently for Ashfield shale in the unconfined compression tests that were presented in chapter 5.

7.3.1.1 *Effect of modulus ratio*

Figure 7.3 shows the effect of the modulus ratio E_2/E_1 on the predicted shear stiffness for the case where the aspect ratio is $D/L = 0.67$ and the size of the gap is given by $T/L = 0.033$. Values of the modulus ratio less than or equal to 1 have been investigated. As seen in this figure, the material anisotropy and the orientation of the laminations to the shearing direction both have a large effect on the shear stiffness. As expected, materials with a smaller ratio E_2/E_1 show higher anisotropy in the overall shear stiffness of the test sample. It is obvious from Figure 7.3 that the prediction for the case where $E_2/E_1 = 1$ is not independent of the orientation θ. This is because the material is not isotropic, even though the two independent Young's moduli have the same numerical values in this case and the two independent Poisson's ratios are also equal. The reason for the anisotropy is that the independent shear modulus has been assigned a value that is not consistent with isotropy, as described previously.

7.3.1.2 *Effect of shear modulus ratio*

Further analyses have been performed to investigate the effects of variation in the ratio G_2/E_1. Figure 7.4 shows the effect of varying the ratio of the independent shear modulus G_2 to Young's modulus E_1, on the predicted shear stiffness for different angles of laminations to the shearing direction. These results are for cases where the aspect ratio is $D/L = 0.67$ and the size of the gap $T/L = 0.033$ and the modulus ratio $E_2/E_1 = 0.333$. These analyses have shown that for reasonable values of the ratio G_2/E_1, i.e. 0.86, 0.66 and 0.46, the effects on the shear stiffness are less pronounced than the effects of the modulus ratio E_2/E_1, (Figure 7.3). As figure 7.4 shows, materials with larger values of the ratio G_2/E_1 show higher anisotropy in the overall shear stiffness of the test sample. The largest shear stiffness occurred when the laminations were inclined between 15° and 35° to the applied force, and the smallest shear stiffness for $\theta = 60$ to 75 degrees.

7.3.1.3 *Effect of Poisson's ratio*

Figures 7.5 and 7.6 show the effect of varying the two independent Poisson's ratios, ν_1 and ν_2, on the shear stiffness. For these cases the aspect ratio, $D/L = 0.67$, and the size of the gap is given by $T/L = 0.033$. The modulus ratio, $E_2/E_1 = 0.333$, and $G_2/E_1 = 0.66$. In Figure 7.5 $\nu_1 = 0.1$ for all curves.

Figure 7.5 indicates that the anisotropy is more pronounced as the ratio ν_2/ν_1 is increased, as might be expected. However, it is also interesting to note from Figure 7.6 that the anisotropy is also more significant as the value of Poisson's ratio itself increases, even when the two independent ratios ν_1 and ν_2 have the same value. As in other cases, the largest stiffness occurs in the range $15° \leq \theta \leq 30°$.

7.3.2 **Influence of boundary conditions**

Figure 7.7 shows the effect of the sample width to height ratio (D/L) on the shear

stiffness, for different angles of the laminations to the shearing direction. As seen in this figure, the sample shape has only a small effect on the shear stiffness, at least for the range of aspect ratios investigated.

Figure 7.8 shows the effect of gap width on the direct shear behaviour of the anisotropic material for the case where $D/L = 0.67$ and $E_2/E_1 = 0.333$. The gap width selected for these analyses is given by either $T/L = 0.022$, 0.033 or 0.044. The shear stiffness for different angles was found to decrease with increasing gap width, but for the range of widths investigated the variation was not large.

To study the effects of the point of application of the shear load, analyses were carried out for several loading points on the upper half of the sample, i.e. several values of the ratio X/L (see Figure 7.2). Figure 7.9 shows the influence of the loading point on the shear stiffness for different angles of the laminations to the applied shear force. Generally, the further the point of application of the shear force from the "gap" at the mid height of the specimen, i.e. the higher up the specimen (Figure 7.2a) and the larger the lever arm, the more compliant is the response and the greater is the tendency for rotation of the top portion of the specimen. However, even when the load was applied almost at the mid-height significant rotation of the top half of the sample occurred. When analyses were performed in which rotation was prevented the normalised shear stiffnesses were approximately 4 times greater than for the case with $X/L = 0.51$ shown in Figure 7.9, but the same variation with θ was observed.

7.4 DIRECT SHEAR TESTS ON SHALE

To evaluate the engineering response of laminated Ashfield shale, which is intrinsically anisotropic in nature, direct shear tests were carried out on cylindrical core samples at a variety of normal stresses. The direct shear tests and the results were presented in detail in Chapter 6. The length of each core sample was 90 *mm*

and the diameter was 61 *mm* (D/L = 0.678). The width of the gap in the loading apparatus was 3 *mm* (T/L = 0.033), and the loading point was at the mid-height (X/L = 0.51). The experimental boundary conditions were such that some rotation of the two halves of the shearbox could occur, although any rotations were expected to be small.

For each test specimen a graph of shear stress against shear displacement was plotted. Figure 7.10 shows a representative plot for a core specimen containing laminations orientated at 60 degrees to the shearing direction. The data from all tests have been corrected to account for the compliance of the apparatus, which was found to be small. The shear stress versus shear deformation curve (Figure 7.10) shows some non-linearity. The portion of the curve before the peak shear strength rises steeply, and measures of the slope of this curve were used to calculate the overall shear stiffness of Ashfield shale. A detailed description of the measured strength anisotropy and analysis of the test results has been described in Chapter 6.

7.4.1 **Shear stiffness of Ashfield Shale**

In all direct shear tests the response up to the peak shear strength was observed and three different shear stiffnesses were measured. These were the initial tangent shear stiffness (K_{si}), the secant shear stiffness at the peak (K_{sp}) and the secant shear stiffness at 50% of the peak shear strength (K_{ss}). Although the average corrected shear stiffnesses were calculated for each level of normal stress, only the values found for samples tested at a normal stress of 1.6 *MPa* are listed in Table 7.1, and a typical set of results is presented graphically in Figure 7.11. Similar results corresponding to a normal stress of 580 *kPa* were presented previously in Figure 6.11. Figure 7.11 shows that the orientation of the laminations to the shear force has a significant effect on the measured shear stiffness of the Ashfield shale. The shear stiffness appears to be smallest when θ is in the region of 60 degrees. A comparison of the results in Figure 7.11 indicates that the initial tangent shear stiffness is typically 2 to 3 times the secant shear stiffness at the peak, and that the secant shear stiffness at 50% of the

peak shear strength is approximately midway between the peak and the initial value. The shale displays a limited truly elastic response, but the pre-peak response can still be reasonably described by a set of elastic parameters.

7.5 COMPARISON BETWEEN PREDICTIONS AND EXPERIMENTAL RESULTS

Independent uniaxial and triaxial compression tests have been carried out on Ashfield Shale. A description of the tests and results were presented in chapter 5. The following deformation parameters for Ashfield shale from Ryde-interchange site have been estimated from the results of these *UCS* tests:

$$E_1 = 9600\ MPa$$
$$E_2 = 3100\ MPa$$
$$\nu_1 = 0.1$$
$$\nu_2 = 0.1$$
$$G_2 = 6600\ MPa$$

These values are based on the secant values measured at an axial stress of approximately 50% of the peak strength. Value of the deformation at $\theta=0$ (E_1) for the Ryde shale were estimated by applying the appropriate correction factor to the test data for the Surry Hills shale ($\theta=0$). Using these values, predictions have been made of the stiffness of Ashfield shale in the direct shear tests, and these are compared with the experimental results in Figure 7.12. This figure shows a graph of non-dimensional shear stiffness, K, against the angle of the laminations to the shear load direction. The normalisation of the experimental results has been achieved by dividing the measured stiffness in direct shear by E_1 (= 9600 *MPa*) and multiplying it by D, the diameter of the core sample (= 0.061 *m*). The predicted direct shear stiffness shows good general agreement with the secant shear stiffness measured at 50% of the peak strength in the direct shear test. Good agreement exists across the full range of θ values. This implies that the direct shear test is capable of detecting

accurately the nature of the anisotropy of shale in the direct shear test. Furthermore, the secant values of the moduli determined from uniaxial and triaxial compression tests (Chapter 5) are consistent with the secant shear stiffnesses measured in direct shear tests. However, in view of the sensitivity of the shear stiffness to the degree of rotational restraint imposed in the numerical analyses, that is there was a factor of 4 between these analyses and analyses with no rotation permitted, the excellent agreement may be fortuitous.

7.6 INTERPRETATION OF DIRECT SHEAR TESTS

It is not possible to use the data from a single direct shear test alone to deduce the full set of elastic properties of a cross-anisotropic rock. In the direct shear test essentially only one measure of stiffness is made. If the rock were isotropic, characterised by only two independent constants, then it might be reasonable to assume a value for Poisson's ratio (say), and then to use the stiffness measured in direct shear to deduce Young's modulus of the rock. This procedure has already been suggested by Noonan and Nixon (1972). However, for a cross-anisotropic rock, there are five independent elastic constants and these cannot be determined simply from the measured shear stiffnesses. Nevertheless, by performing tests with the laminations at different orientations θ, an indication of the extent of the anisotropy can be obtained, and in principle a curve fitting procedure could be used to find reasonable sets of parameters that match the observed variation of shear stiffness with θ. The magnitudes of the estimated elastic constants could vary by an order of magnitude depending on the assumed boundary conditions, and in particular the rotational restraint, imposed by the shear box. This suggests that the shearbox test is of limited use if the pre-peak behaviour of anisotropic materials is required, but if the results can be calibrated against sets of elastic constants determined from other types of deformation test, such as the uniaxial and triaxial compression tests (Chapter 5), it may be possible to obtain useful data on anisotropic materials.

7.7 CORRELATION BETWEEN TRIAXIAL AND DIRECT SHEAR STIFFNESS

7.7.1 Deformation parameters

Two techniques, triaxial and direct shear tests have been described and compared. The experimental results on the Ashfield shale with laminations at different orientation θ, from both the direct shear and triaxial tests confirmed the existence of anisotropy in both the modulus ratio and shear stiffness. In principle a curve fitting procedure has been used to find reasonable sets of parameters that match the observed variation of shear stiffness with θ. The secant values of the moduli measured, at a deviator stress of approximately 50% of the peak strength, from triaxial compression tests (Chapter 5) are consistent with the secant shear stiffnesses measured at 50% of the peak shear strength in direct shear tests. The trend and the shape of both shear stiffnesses versus θ curves (Figures 5.39, 7.12) are the same. The lowest modulus ratio and shear stiffness was observed in both the physical and theoretical experiments when the lamination planes were inclined at between 60 to 90 degrees to the direction of applied load. The largest modulus ratio and shear stiffness generally occurred when the lamination inclined between 0 and 35 degrees to the applied force.

7.8 CONCLUSIONS

This chapter has presented the results of an investigation into the pre-failure behaviour of anisotropic materials in the direct shear test. A numerical study was conducted to investigate the effects of parameters such as the degree of anisotropy, the shape of the test specimen, and the boundary conditions of the shear test on the shear response. This chapter has also described some of the results of direct shear experiments on Ashfield shale (Chapter 6). It was found that the nature of the anisotropic response of the shale in direct shear tests was in close agreement with that observed in independently conducted, uniaxial and triaxial compression tests (Chapter 5).

For the range of parameters investigated it can be concluded from the numerical study that the shape of the direct shear specimen and the gap allowed in the loading apparatus have only small influences on the direct shear response. However, the orientation of the bedding planes to the applied shear force, the inherent anisotropy of the material, and the point of application of the shearing force each have a much greater influence on the overall shear stiffness. The lowest stiffness in direct shear was observed in both the physical and numerical experiments when the bedding planes were inclined at between 60° to 75° to the direction of the shear force. The largest shear stiffness generally occurred when the bedding was inclined between 15° and 35° to the applied force. In the experiments, the Ashfield shale was about twice as stiff when the sample was sheared parallel to the bedding compared to the case where shearing was conducted orthogonal to the bedding. Good agreement between the predicted and experimental shear stiffnesses was observed for all inclinations of the laminations.

Table 7.1 Shear stiffnesses from direct shear tests with a normal stress 1.6 *MPa*

θ (°)	Initial tangent (*MPa/mm*)	Secant at 50% of peak (*MPa/mm*)	Secant at peak (*MPa/mm*)
0	86.2	41.6	28.3
30	66.5	48.2	26.3
45	53.9	34.2	17.9
60	43.2	30.6	16.5
90	44.5	31.9	21.2
-30	113.5	63.5	36.1
-45	96.6	53.6	25.6
-60	62.4	41.2	20.7

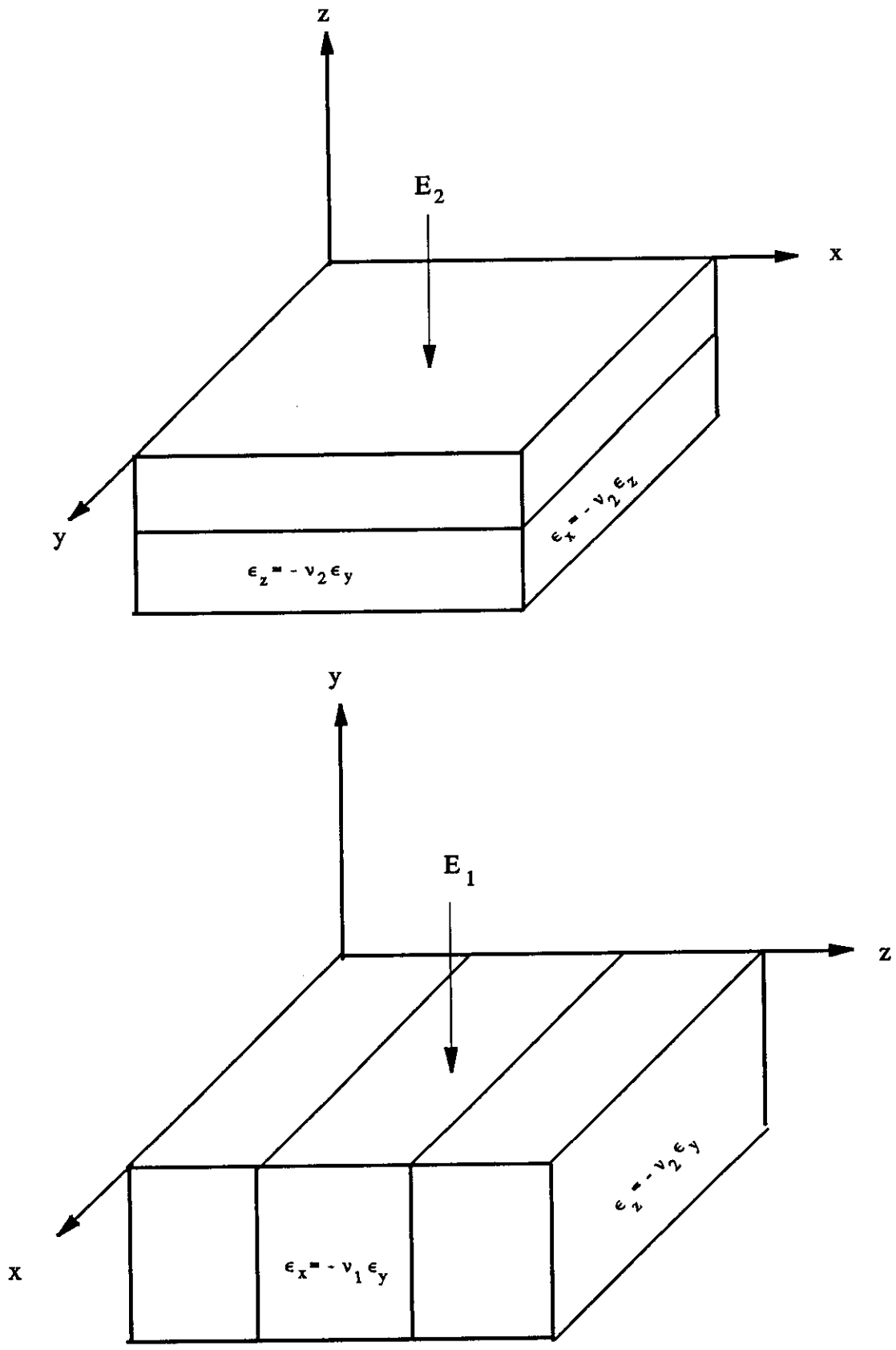

Figure 7.1 Definition of elastic constants for shale with lamination parallel to the xy plane

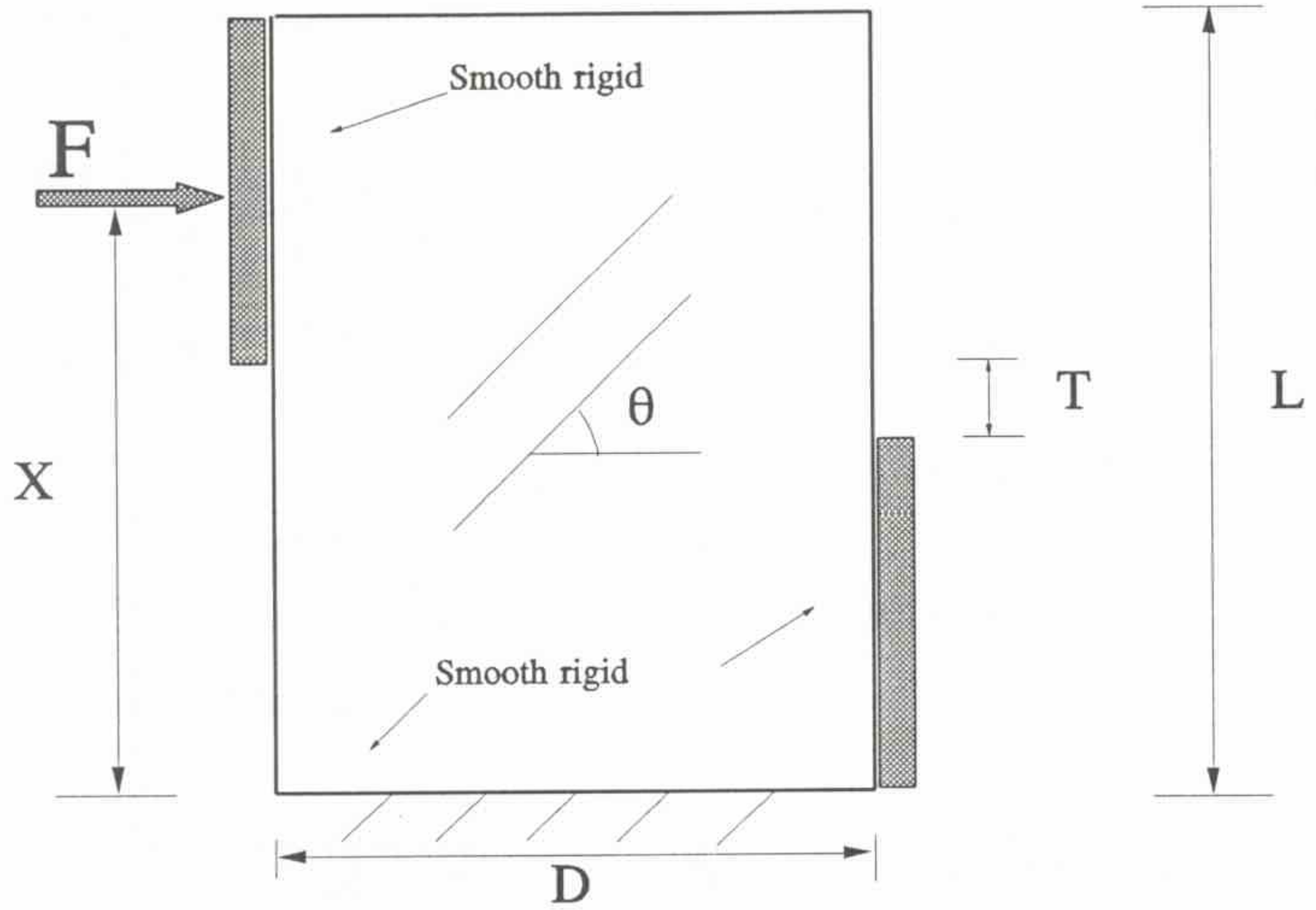

(a) Model dimensions and loading configuration

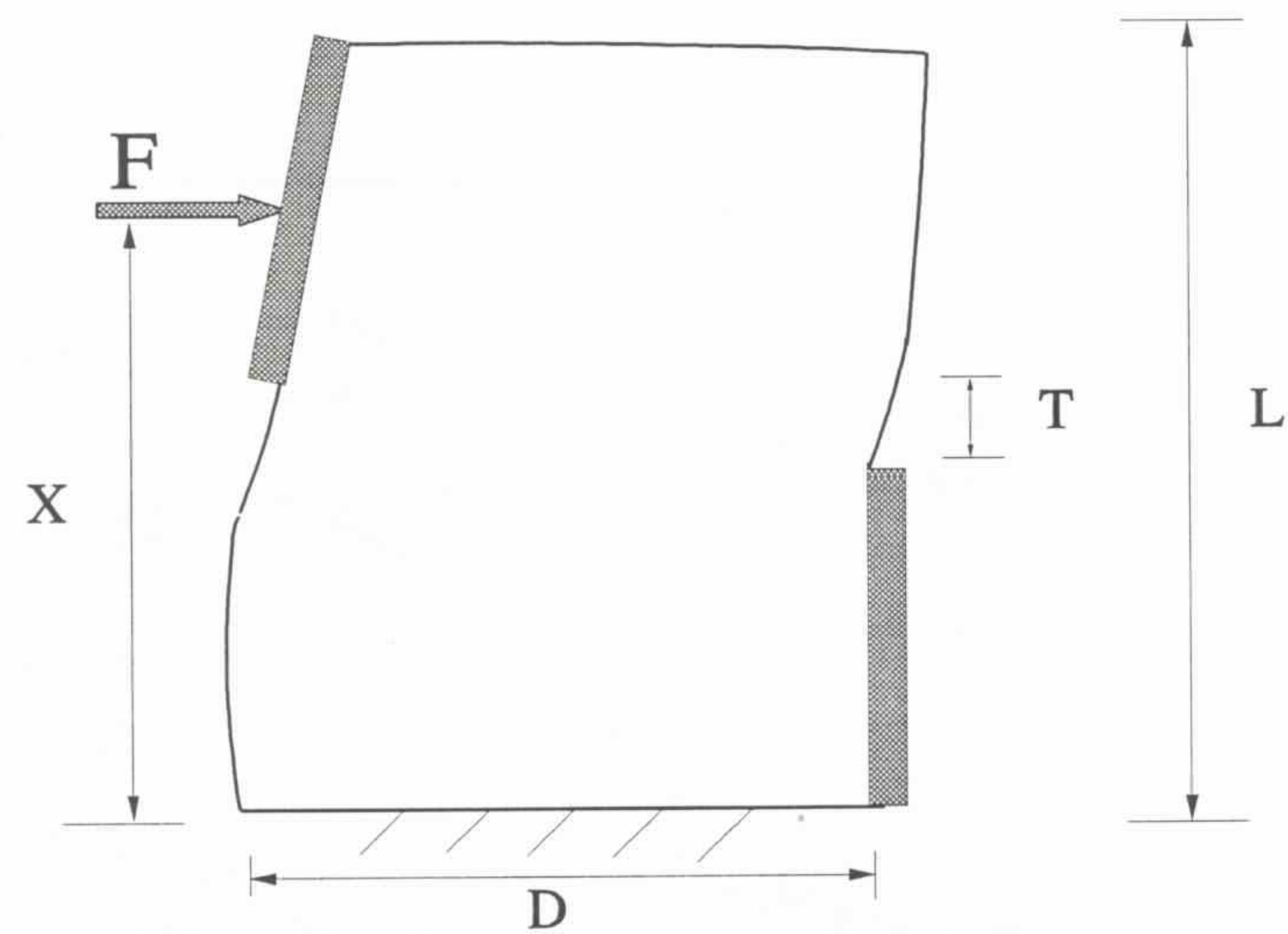

(b) Deformed sample

Figure 7.2 Problem definition

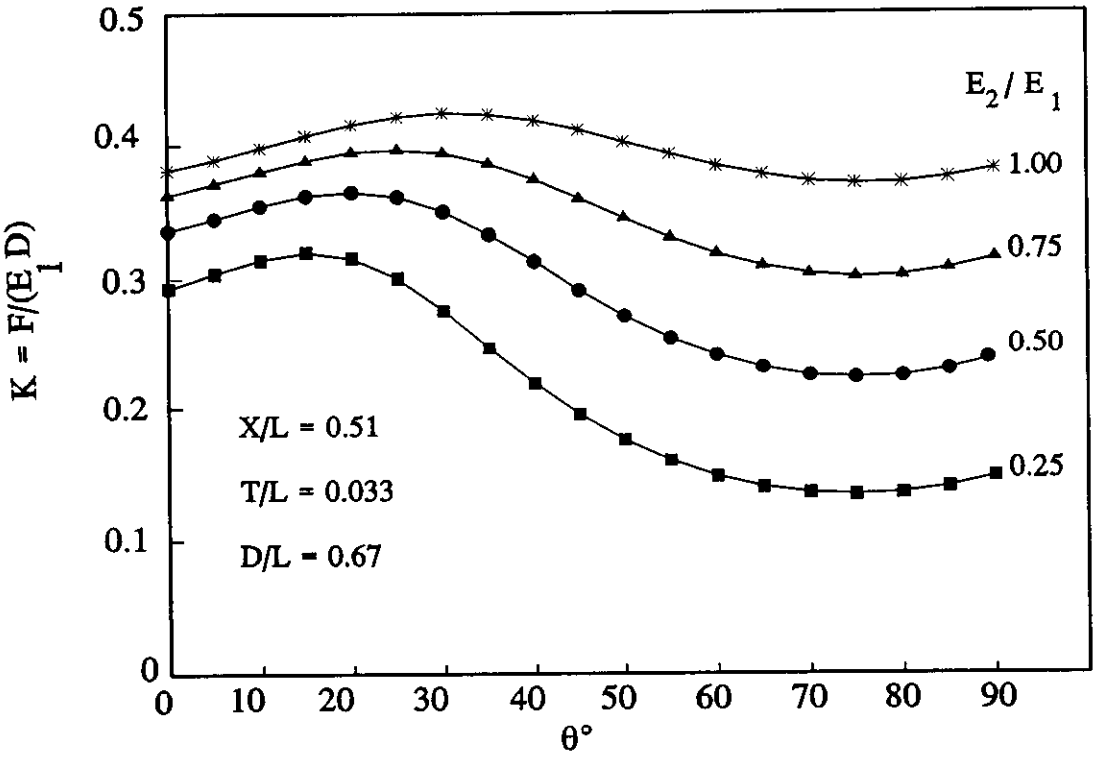

Figure 7.3 Effect of moduli on shear stiffness

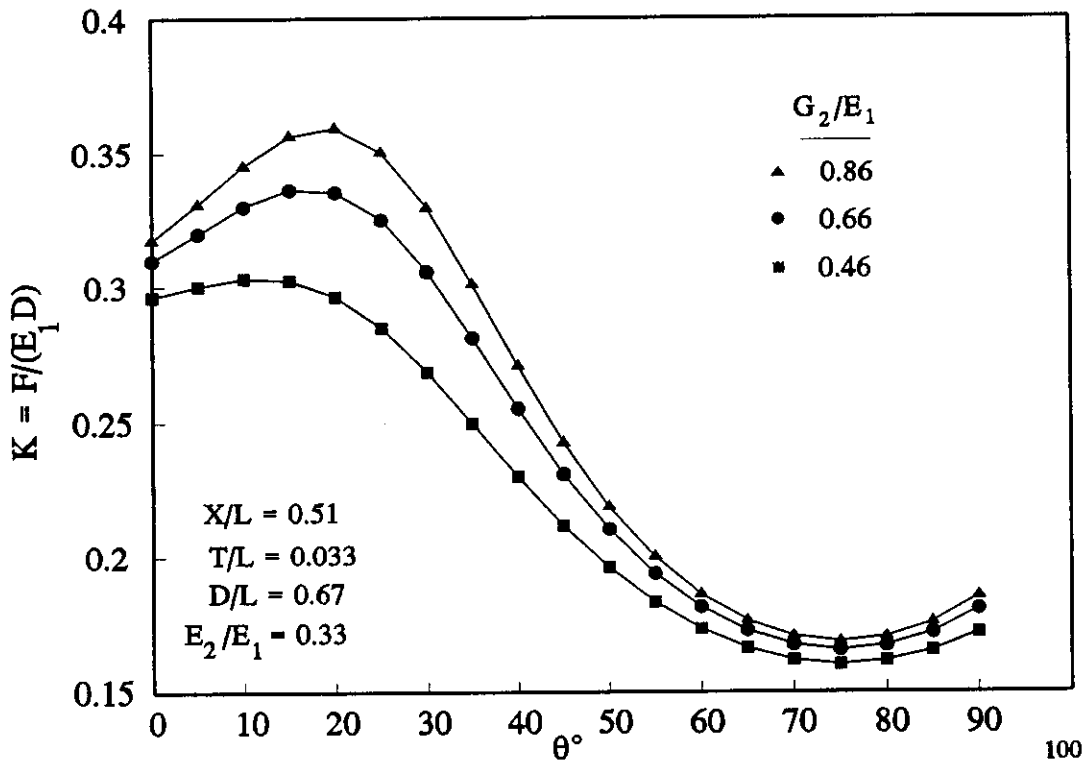

Figure 7.4 Effect of shear modulus on shear stiffness

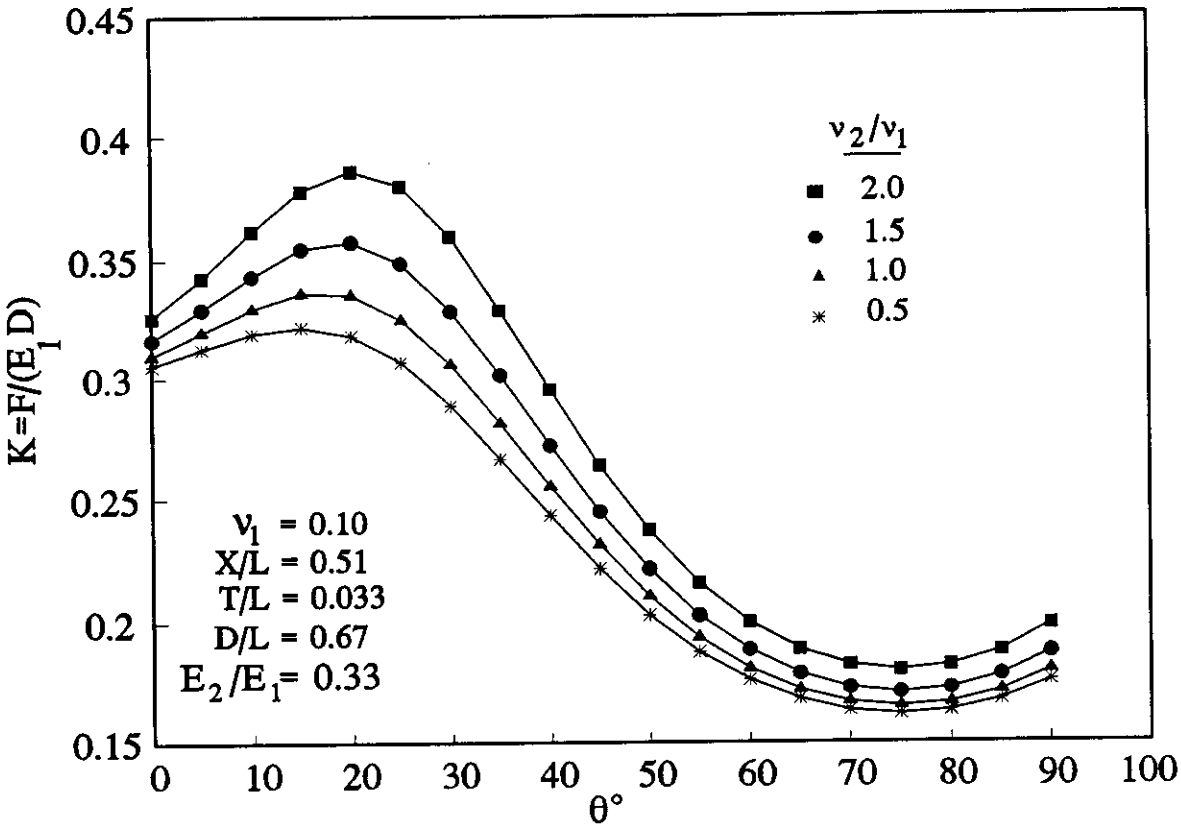

Figure 7.5 Effect of ratio of ν_2/ν_1 on shear stiffness

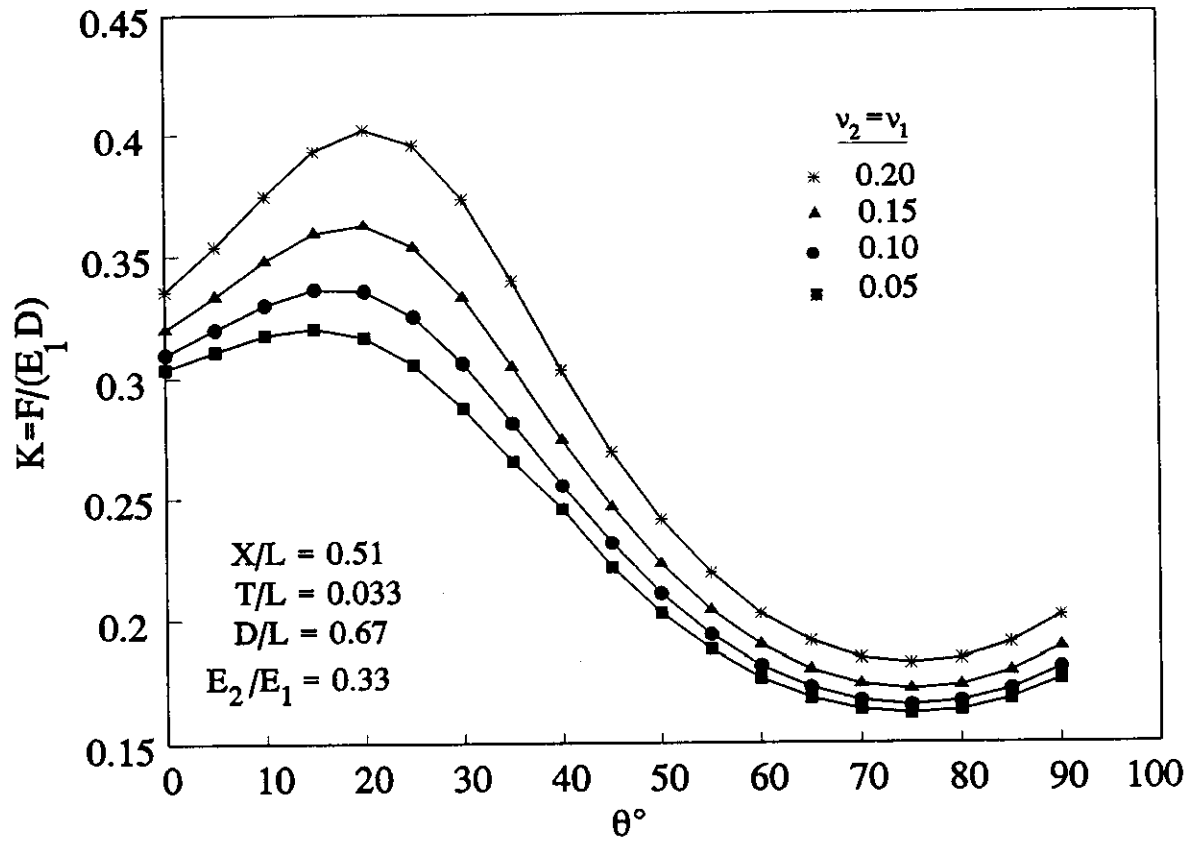

Figure 7.6 Effect of different ν on shear stiffness

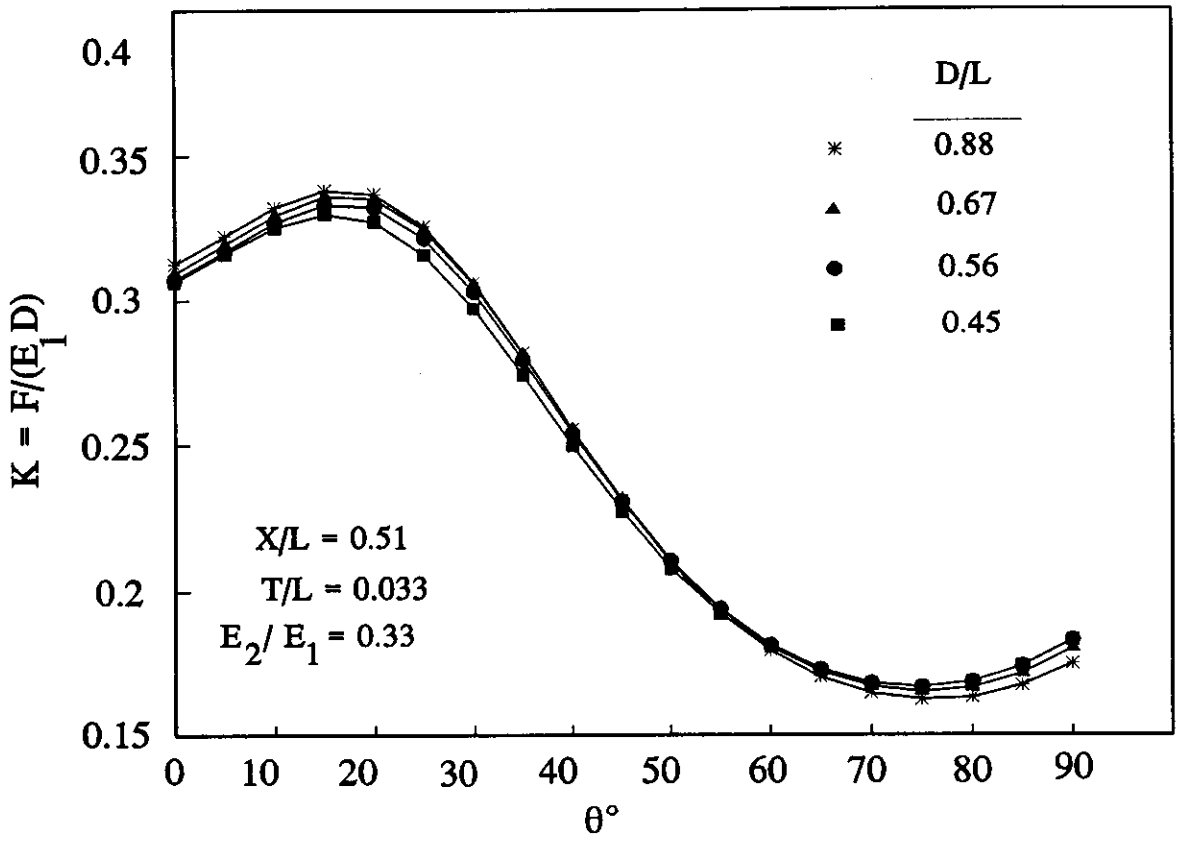

Figure 7.7 Effect of Aspect Ratio

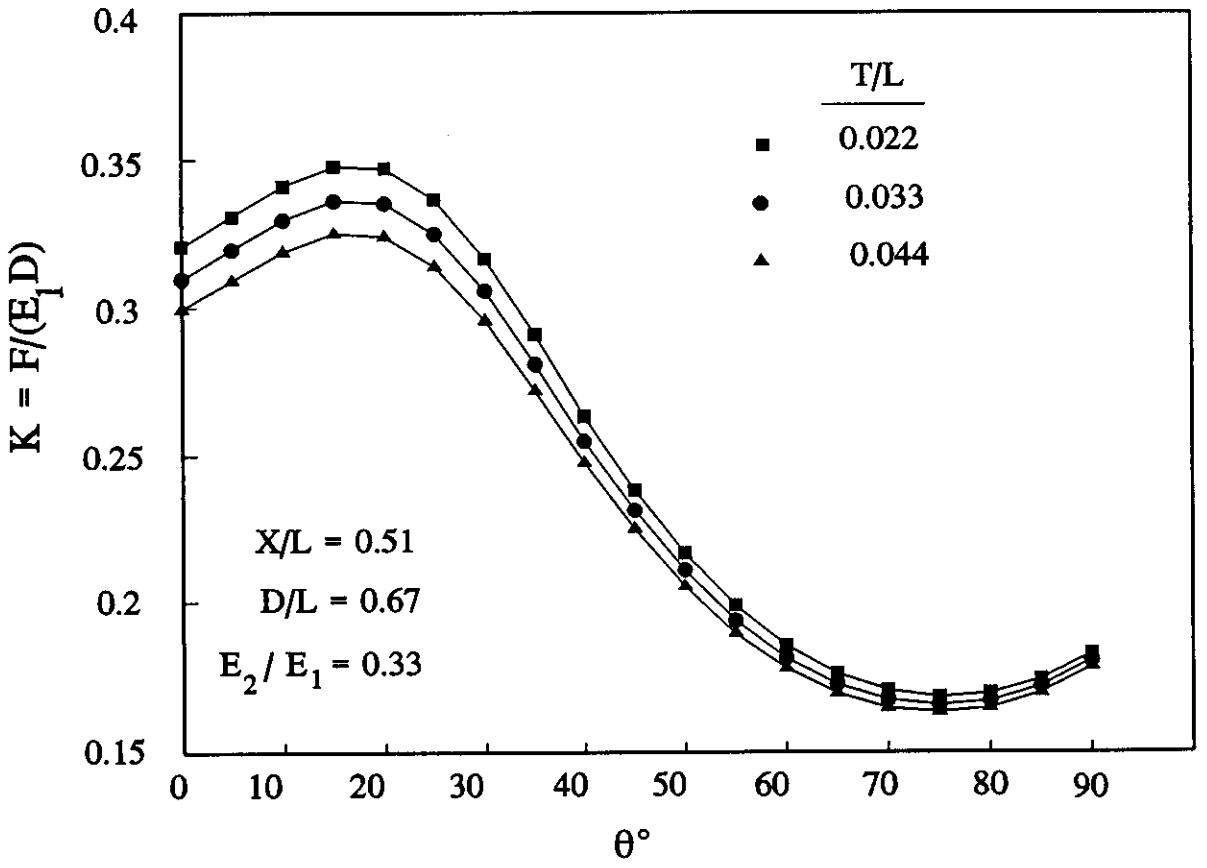

Figure 7.8 Effect of gap thickness

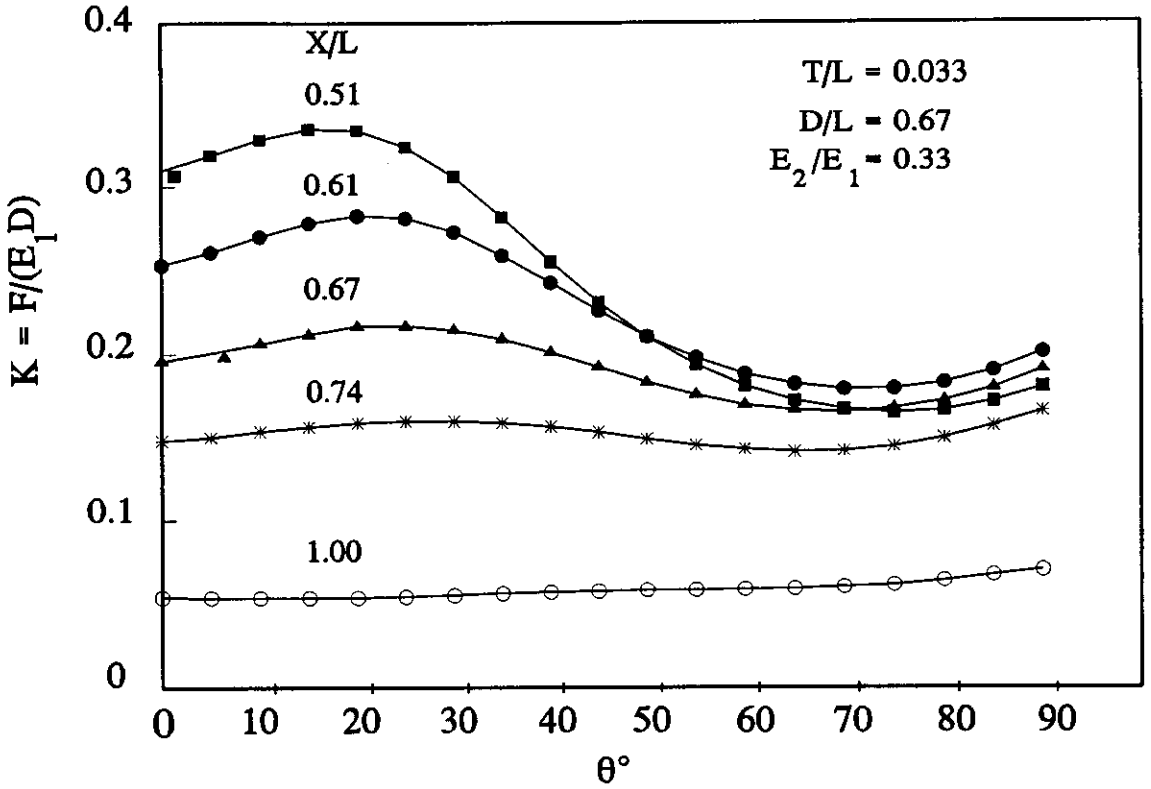

Figure 7.9 Effect of load application position

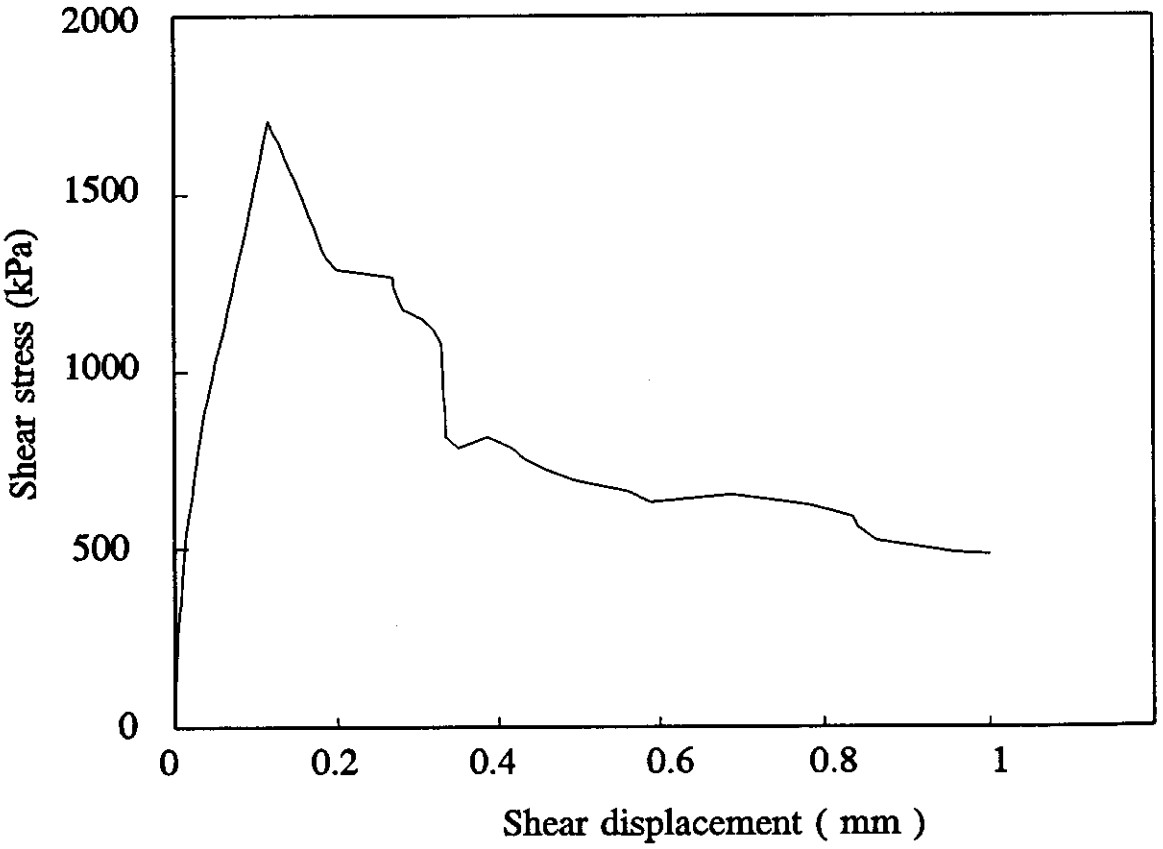

Figure 7.10 Typical shear box result

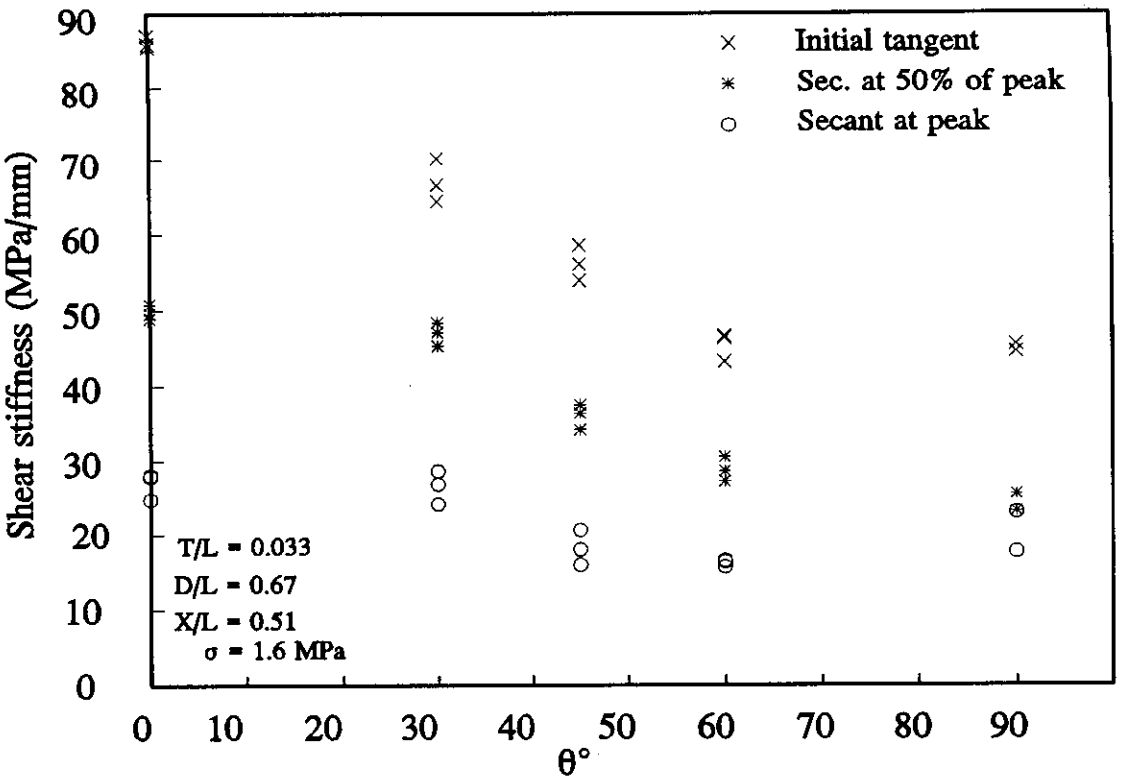

Figure 7.11 Experimental shear stiffnesses

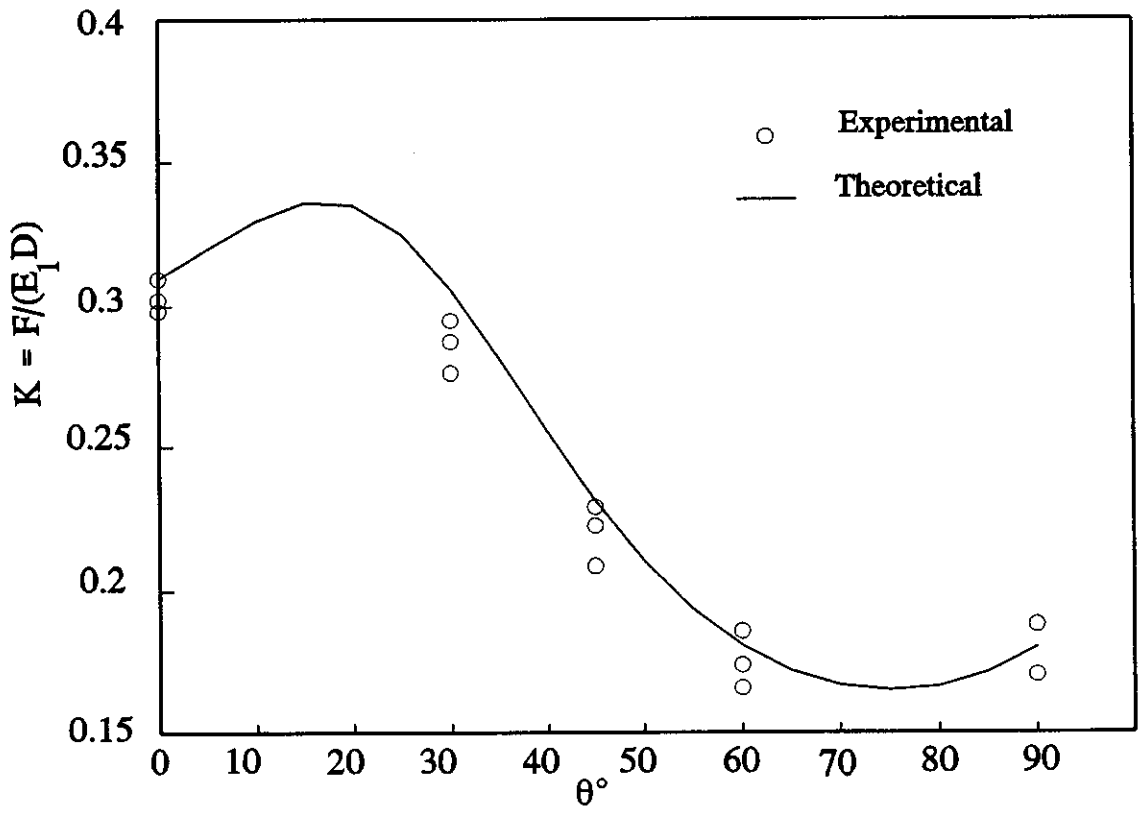

Figure 7.12 Comparison of experimental and predicted shear stiffnesses

CHAPTER 8 SUMMARY AND CONCLUSIONS

8.1 INTRODUCTION

8.2 SUMMARY

8.3 SUGGESTION FOR FURTHER STUDIES

CHAPTER 8

SUMMARY AND CONCLUSIONS

8.1 INTRODUCTION

In this chapter, the work performed in this research is summarised and conclusions are made and some suggestions for further study are described. The main purpose of this research was to study the engineering behaviour of Ashfield shale, especially the effects of lamination direction on the shear strength and deformability of this rock. A comprehensive series of tests has been carried out on Ashfield shale. Correlations between different mechanical and physical properties have been made.

8.2 SUMMARY

A review of publications concerning the mineralogy, classification and engineering behaviour of shale has been presented. The various factors influencing the strength and deformation of shales have been described and conclusions drawn which influenced the direction of the present experimental work on the Ashfield shale.

The mineralogy and petrofabric have been studied by X-ray diffraction, scanning electron microscopy and optical microscopy, and various physical properties of the Ashfield shale have been measured. The study of fabric concludes that lamination in shale is a significant feature that is useful in interpreting sedimentary processes involved in shale formation. X-ray diffraction analysis of the Ashfield shale confirmed the absence of chlorite, mixed-layer clays, and smectite in this shale, and showed that kaolinite and micaceous clay minerals (illite) were the dominant clay minerals. On average kaolinite was more abundant. Quartz was the major non-clay constituent of the Ashfield shale, and typically constituted about 50% of the non-clay mineral in this shale. Microscopic investigations were also conducted with the optical and scanning electron microscope on shale samples to identify the composition and texture of this rock. A number of large mineral grains (Phosphate) were found within the platy fine-grained matrix. Siderite was found to be finely dispersed in the Ashfield shale and no significant feldspars were detected in the samples used in this study.

The natural moisture content has been found to be a good predictor of the durability, strength, index properties and clay content of the shale. Correlations between the durability, strength and natural moisture content of the Ashfield shale have been demonstrated, with durability and strength increasing with decreasing moisture content. The effect of weathering is to increase the clay and moisture contents. However, different fresh unweathered shales had different moisture contents. The variability of the natural moisture content can be correlated with mineralogical factors. Increasing moisture content was associated with increasing clay content (particles less than 2 micron) and in turn this was associated with an increase in plasticity index and plastic and liquid limits. The clay size fraction, as determined from sedimentation analysis indicated clay fractions of about 30% whereas the mineralogical studies indicated clay fractions of about 50% in all samples. This discrepancy presumably reflects the presence of significant quantities of

large kaolin particles. This could be caused by cementation (fusing of the clay particles at high temperature and pressure). The process of weathering causes a breakdown of the cementation. Thus clay mineral content remains constant, but clay particle size fraction increases. This could also explain increasing of the liquid limit, I_p, and durability of Ashfield shale. In terms of the plasticity chart the Ashfield shale specimens used in this study fall in the low plasticity range.

Following the classification scheme established by Gamble (1971) and Franklin and Chandra (1972), based on the slaking characteristics of shales, the results indicate that the durability of Ashfield shale varies from high, for fresh intact material, to low for highly weathered material.

It was found that the porosity ranges between 5% for fresh Ashfield shale from Surry Hills and Moorebank sites to about 13% for Ashfield shale from the Ryde-interchange site. It was found that all samples of the Ashfield shale were close to being fully saturated in-situ, so the natural water content gives a direct measure of the porosity of the shale. Because the samples of the Ashfield shale were nearly fully saturated in-situ, it can be assumed that the changes in moisture content mostly reflect changes in porosity of the shale.

Plots of uniaxial compressive strength of all samples with laminations perpendicular to loading direction versus moisture content indicate that uniaxial compressive strength decreases with an increase in the moisture content, which is consistent with previous findings for other shales. It was found that the relationship between uniaxial compressive strength and moisture content was exponential. A small increase in moisture content causes a large reduction in *UCS*. The variations are described well by the following equation:

$$UCS = 600 p_a e^{-0.415 m_c} \qquad \textbf{(8.1)}$$

in which

m_c = moisture content (%), and

p_a = atmospheric pressure (0.1 *MPa* or 14 lb/in^2).

Because of the closeness of the correlation and because the natural moisture content of a shale sample is a relatively simple parameter to determine in practice, equation (8.1) provides an indirect but very convenient means of estimating *UCS* for Ashfield shale.

The point load test is widely used to determine the uniaxial compressive strength indirectly. Correlations have been made between the point load strengths and the measured values of uniaxial compressive strength in directions perpendicular to the laminations. Average correlation factors of 24.1 and 38.2 have been found between the axial and diametral point load strengths and the uniaxial compressive strength, respectively. However, owing to the scatter in the data the point load tests do not appear to be reliable for estimating *UCS* values.

The strength anisotropy, I_a, the ratio of point load strength in the strongest and weakest directions was measured for the samples tested in these two directions. The mean strength anisotropy index considered here was calculated to be 2 with a standard deviation of 0.5. However, from the correlations with *UCS* a ratio of I_a = 1.6 can be determined. The difference between the anisotropy ratios from the individual point load test results and from the correlations with *UCS* results indicates the difficulty of determining the anisotropy from point load tests. This is probably caused by natural variability in the samples which can be expected to be more significant in the smaller point load tests samples.

A series of uniaxial and triaxial compression tests and direct shear tests was performed on the Ashfield shale to study the influence of the orientation of lamination planes on the shear strength and deformation of Ashfield shale. The orientation of the plane of anisotropy was varied between 0 and 90 degrees relative to the axial load.

The maximum strength, and the shear strength parameters, c and ϕ, have been found to be functions of lamination orientation, β with respect to the axial load direction, and confining pressure, σ_3. The specimens showed the highest compressive strength in the direction perpendicular to laminations. The lowest value of strength occurred for β = 30 degrees. The strength anisotropy ratio in compression ($\sigma_{d90}/\sigma_{d30}$) has been found to be approximately 3.1. An increase of the confining pressure increases the maximum strength and decreases the ratio of anisotropy of the Ashfield shale specimens for all values of β. The rate of increase in the maximum strength is approximately the same for all orientations. The shear strength parameters, cohesion intercept and the angle of friction, were obtained from the linear and initial parts of the Mohr-Coulomb envelopes. The variation of cohesion intercept, c, with lamination orientation, β, is similar to that for the maximum strength at various confining pressures. The variation of the friction angle, ϕ, as a function of the lamination direction at a particular confining pressure is not very significant, so a constant value can be assumed, of confining pressure .

Because of its sedimentary origin, Ashfield shale shows anisotropic behaviour. The theory for a cross anisotropic elastic material has been used to analyse the deformation behaviour of this shale. Five independent elastic parameters describe this cross anisotropic system. These five independent elastic parameters have been obtained by performing uniaxial and triaxial compression tests on samples with different orientations of the laminations (β) to the principal stress direction.

Four independent elastic parameters (E_1, E_2, ν_1 and ν_2) were determined by performing uniaxial and triaxial compression tests on samples with β = 0 and 90 degrees. The independent shear modulus, G_2, was determined from a series of tests on samples with different lamination angles to the axial load direction. Experimental results were fitted to the equation (5.27). The value of shear modulus was estimated by a curve fitting procedure using the variation of E_β with

β and the values of E_1, E_2, ν_1 and ν_2 determined previously.

The modulus of elasticity was a maximum when the load was applied parallel to the laminations ($\beta = 0$) and a minimum when the load was applied perpendicular to the laminations ($\beta = 90°$). The modulus of elasticity in the direction parallel to the laminations, E_1, compared to the modulus of elasticity in the perpendicular direction, E_2, is more influenced by the confining pressure.

From the study of the influence of the lamination angle β, it can be concluded that the ratios of maximum to minimum Young's modulus and maximum to minimum compressive strengths are very similar, i.e. both are approximately 3. However the angles at which they occur are different. The maximum and minimum strengths correspond to $\beta = 90$ and 30 degrees, respectively, but the maximum and minimum Young's modulus correspond to $\beta =$ 0 and 90 degrees, respectively. Furthermore, an increase in the confining pressure tended to reduce the strength anisotropy ratio, defined as the ratio of maximum to minimum deviator stress at failure, but caused an increase in the deformation anisotropy ratio (defined as the ratio of maximum modulus E_1 to minimum modulus E_2).

Some of the advantages and disadvantages of the existing strength criteria and their limitations when applied to Ashfield shale have been described. For practical purposes a single criterion that overcomes many of these criticisms and limitations has been suggested. This criterion is capable of accurately predicting the strength of Ashfield shale over the full range of β values, and therefore capture accurately the anisotropic nature of the strength. In essence, if moisture content is adequately addressed then variations from one location to another within the Sydney basin should also be taken into account, since it has been demonstrated that changes in the quality of the shale are largely reflected by changes in the moisture content.

In triaxial and uniaxial compression tests failure of the laminated specimens occurs through extension fracture on the lamination planes for specimens with lamination angles of $\beta = 0$ to 15 degrees. For samples with laminations angles $\beta = 30$ to 45 degrees failure occurs as a slip on the lamination planes. For $\beta = 60$ to 90 degrees shear fracture occurs across the laminations with failure planes at 20 to 30 degrees to the axial stress direction.

Direct shear tests were carried out at a variety of normal stresses within the range from 0.3 to 1.6 *MPa*, and peak and residual strength parameters were determined for the Mohr-Coulomb strength criterion. The peak strengths were usually mobilised at relatively small shear displacements which range approximately from 0.10 to 0.20 *mm*. The shearing resistance was reduced abruptly with further shearing beyond the peak. At bigger shear displacements the residual strength was obtained. The orientation of the lamination planes to the applied shear force (θ) and the magnitudes of normal stress had a large influence on the overall shear strength (peak and residual), the shear stiffness and dilation, i.e. the shale exhibited strength anisotropy. Increasing normal stress generally increased the peak shear strength and shear stiffness but decreased the dilation that occurs along the rupture surface.

The results of the testing show that there is a wide range of shearing orientations (e.g. $\theta \approx 0$ to 60 degrees) for which the strength parameters are approximately constant and equal to about the minimum measured values. It would therefore be appropriate to use such values in geotechnical designs requiring shear strength parameters for the intact shale. However, if the shale mass in the field contains significant jointing, the strength of the rock mass may be better characterised by the residual strength values measured as part of this study.

The shearing resistance of the Ashfield shale was also measured along the lamination planes in various directions from dip to strike. It was found that the peak and residual shear strengths were practically independent of the direction of

shearing whenever the shear force was applied parallel to the bedding planes ($\theta = 0$).

A numerical study was conducted to investigate the effects of parameters such as the degree of anisotropy, the shape of the test specimen, and the boundary conditions of the shear test on the deformation of anisotropic rock, such as shale, in direct shear tests. The analyses, based on the theory of linear elasticity for a cross-anisotropic material, were used to predict the pre-peak stresses and displacements throughout samples of anisotropic rock subjected to direct shear. In particular, the shear stiffness of the sample was of interest. Implications for the interpretation of actual test data have been discussed, and illustrated by comparison of the theoretical predictions with experimental results for Ashfield shale.

From this study it was found that it is not possible to use the data from a single direct shear test alone to deduce the full set of elastic properties of a cross-anisotropic rock. In the direct shear test essentially only one measure of stiffness is made. For the range of parameters investigated it can be concluded from the numerical study that the shape of the direct shear specimen and the gap allowed in the loading apparatus have only small influences of the direct shear response. However, the orientation of the bedding planes to the applied shear force, the inherent anisotropy of the material, and the point of application of the shearing force each have a much greater influence on the overall shear stiffness. The lowest stiffness in direct shear was observed in both the physical and numerical experiments when the bedding planes were inclined at approximately 75 degrees to the direction of the shear force. The largest shear stiffness generally occurred when the bedding was inclined between about 15 and 35 degrees to the bedding. In the experiments, the Ashfield shale was about twice as stiff when the sample was sheared parallel to the bedding compared to the case where shearing was conducted orthogonal to the bedding.

In particular, for Ashfield shale, the results presented in Chapter 7 indicate that the secant stiffness in direct shear, measured at 50% of the peak strength, gave results that were most consistent with the secant values of the moduli determined from uniaxial and triaxial compression also at 50% of peak. The experimental results and the theoretical results in both cases (direct shear and triaxial tests) confirmed the existence of anisotropy in both the modulus ratio and shear stiffness of Ashfield shale.

The maximum cohesive strengths for both cases, triaxial and direct shear tests occur at $\theta = 90$ degrees and the minimum at $\theta = 30$ degrees. There is close agreement between the cohesive strengths derived from the initial tangents to the Mohr-Coulomb envelopes in triaxial test and the cohesive strength derived from direct shear test. The friction angles derived from tangent to the initial part of envelope in triaxial test are more close to the friction angles derived from direct shear test.

In triaxial test the minimum strength occurs at an orientation of $\beta = 30$ degrees and the failure always occurred as a shear slip on the lamination planes. In direct shear test the shear strength and mode of failure of the sample in the case of negative and positive directions (e.g. -30° and +30°, Figure 6.3) is different. The shear strength of the sample is higher in the case of negative values of θ than positive values of θ, as discussed previously.

8.3 SUGGESTION FOR FURTHER STUDIES

It would be useful for engineers and geologists, to be able to correlate the slaking durability values with relative slaking and weathering rates in the field. Long term field studies of the durability of Ashfield shale are therefore recommended. The field test results could then be correlated with the slake durability experimental results presented in this study.

Only a limited number of samples of shales was tested for their Atterberg limits. Therefore, many additional specimens from different locations should be tested to define the distribution on the classification plot. The results would be useful for the correlation of shale from different sites.

It is suggested that a database and statistical model for Sydney shales in the metropolitan area be developed, by collecting and including additional data, especially those data that allow better correlation with mechanical properties of these shales. This database would be a basis for reviewing Pell's foundation design chart for shales, for construction projects and for further investigation.

To define the behaviour of laminated shale and the mode of deformation under triaxial loading, a theoretical three dimensional model is suggested. The data obtained in this experimental study could be used as a input data for such a model.

For the design and construction of underground structures built in shaly rocks, knowledge of the time-dependent deformation is essential, so the study of the time-dependent deformation behaviour of the Ashfield and Bringelly shales is suggested.

To improve the database for shales within the metropolitan area, the study of the engineering behaviour of Bringelly shale is recommended.

REFERENCES

Alling, H.L., (1945), "Use of microlithologies as illustrated by some New York sedimentary rocks", Bull. Geol. Soc. America., Vol. 56, pp. 737-756.

Anon, (1981), "British Standard 5930: Code of practice for site investigations", London, British Standards Institution, pp. 147.

Anon, (1975), "British Standard 1377: Methods of testing soils for civil engineering purposes", London, British Standard Institution, 143 p.

Anon, (1981), "Basic geotechnical description of rock masses", International Society for Rock Mechanics Commission on the classification of rocks and rock masses, International Journal of Rock Mechanics and Mining Sciences, Vol. 18, pp. 85-110.

Anon., (1985), "Suggested method for determining point load strength (revised version)", ISRM Commission on Testing Methods, International Journal of Rock Mechanics and Mining Sciences & Geomechanic Abstract, Vol. 22, pp. 51-60.

Arora, V.K., (1987), "Strength and deformational behaviour of jointed rocks", Ph.D. Thesis, Indian Institute of Technology, Delhi.

AS 1289, (1977), "Method of testing soil for engineering purposes", Standard association of Australia, Sydney.

Athy, L.F., (1930), "Density, porosity, and compaction of sedimentary rocks", Bulletin of American Association of Petroleum Geology, Vol. 14, pp. 1-24.

Atterberg, A., (1911), "On the investigation of the physical properties of soils and on the plasticity of clays", Int. Mittfur Bodenkunde, Vol. 6, pp. 27-37.

Attewell, P.B., and Sandford, M.R., (1974), "Intrinsic shear strength of a brittle anisotropic rock - I; experimental and mechanical interpretation", International Journal of Rock Mechanics and Mining Sciences, Vol. 11,

pp. 423-430.

Attewell, P.B., and Farmer, I.W., (1976), "Principles of engineering geology", Chapman and Hall, London.

Aughenbaugh, N.B., (1974), "Effect of moisture on shale", 23rd Annual Soil Mechanics and Foundation Engineering Conference, ASCE, University of Kansas, Lawrence, Kansas, pp. 1-14.

Aughenbaugh, N.B., and Bruzewski, R.F., (1976), "Humidity effects on coal mine roof stability" Bureau of mines, Final report.

Ballivy, G., Ladanyi, B., and Gill, D.E., (1976), "Effect of water saturation history on the strength of low porosity rocks", Soil Specimen preparation for Lab. Testing, ASTM STP 599, pp. 4-20.

Barton, N.R, (1973), "Review of a new shear strength criterion for rock joints", Engineering Geology,Vol. 7, No. 4, pp. 287-332.

Bates, R.L., and Jackson, J.A., (1987), "Glossary of geology", American Geological Institute, Virginia.

Benjelloun, Z.H., Bertrand, L., and Feuga, B., (1989), "Etude du comportement mecanique de la fracture rocheuse en cisaillement", Proceedings, ISRM-SPE International Symposium, Pau, Vol. 1, pp. 433-439.

Benmokrane, B., and Ballivy, G., (1989), "Laboratory study of shear behaviour of rock joints under constant normal stiffness conditions", Proceedings, 30th U.S. Symposium on Rock Mechanics, University of Colorado, pp. 899-906.

Bergh-Christensen, J., and Selmer-Olsen, R., (1970), "On the resistance to blasting in tunnelling", Proceedings, the Second Congress of the International Society for Rock Mechanics, Belgrade, Vol. 3, Paper 5-7.

Bieniawski, Z.T., (1974), "Estimating the strength of rock materials", Journal of South Africa, Institute of Mine and Metall., Vol. 74, No.8, pp. 312-320.

Bieniawski, Z.T., (1975) "The point load test in geotechnical practice", Engng. Geol.Vol. 9, pp. 1-11.

Binger, W.V., (1948), "Analytical studies of Panama canal slides", Proceedings, second International conference on soil mechanics and foundation engineering, Rotterdam, Vol. 2, pp. 54-60.

Bjerrum, L., (1967), " Progressive failure in slopes of overconsolidated plastic clay and clay shales", Journal of the soil mechanics and foundations division, ASCE, Vol. 93, SM5, pp. 3-51.

Boey, C.F (1990), "Modelling of the behaviour of natural calcarenite", Ph.D. Thesis, Dept. Civil Engineering, University of Sydney, Australia.

Branagan, D.F., (1985), "An overview of the geology of the Sydney Region", In Engineering Geology of the Sydney Region, (ed. P.J.N Pells), pp. 3-46.

Brindley, G.W., & Brown, G. (Eds), (1980), "Crystal structures of clay minerals and their X-ray identification", Min. Soc., Great Britain 495 pp.

Broch, E., and Franklin, J.A., (1972), " The point load strength test", Int. J. Rock Mech. Min. Sci., Vol. 9, pp. 669-697.

Brown, E.T., Richards, L.R., and Barr, M.V., (1977), "Shear strength characteristics of Delabole slates", Proceedings, Conference of Rock engineering, New Castle Upon Tyne, pp. 31-51.

Brown, I., Hittinger, M. & Goodman, R, (1980), "Finite element study of the Nevis Bluff (New Zealand) rock slope failure", Rock Mechanics. 12:231-245.

Brown, E.T. (editor), (1981), "Rock characterisation, testing and monitoring", ISRM suggested methods, Pergamon Press, Oxford, 211 p.

Coates, D.F., and Parson, R.C., (1966), "Experimental criteria for classification of rock substances", International Journal of Rock Mechanics and Mining Sciences and Geomechanics Abstracts, Vol. 3, pp. 181-189.

Brown, G., ed., (1961), "The X-ray identification and crystal structures of clay mineral", Mineralogical Society (Clay minerals Group), London, 544 p.

Burgess, P.J., (1977), "The role of engineering geology in developing Sydney's environment- past, present and future", Bulletin of the Int. Assoc.

Engineering Geology, No. 15, pp. 17-20.

Burshtein, L.S., (1969), "Effect of moisture content on the strength and deformability of sandstone", In Soviet Mining Science, N4, pp. 573-576.

Carroll, D.(1970), "Clay minerals, a guide to their X-ray identification, Special paper 126, Geological Society of America, 80 p.

Carter, P.G. and Sneddon, U., (1977), "Comparison of Schmidt hammer, point load and unconfined compression test in carboniferous strata", Proc. Conf. Rock Engng University of Newcastle, the British Geotechnical Soc. London, pp. 197-210.

Carter, J.P & Balaam, N.P., (1990), "AFENA Users' Manual", Centre for Geotechnical Research, University of Sydney, Australia.

Chandra, R., (1970), "Slake-durability test for rocks", M.S. Thesis, University of London, Imperial College, Rock Mechanics Research Report, 55 p.

Chenevert, M.E., (1970),"Shale alteration by water adsorption", Journal of petroleum Technology, American Institute of Mining, Metallurgical, and Petroleum engineers, September, pp. 1141-1148.

Chenevert, M.E., (1970a), "Adsorptive pore pressures of argillaceous rocks" Proceedings, Eleventh symposium on rock mechanics, Berkeley, California, pp. 599-627.

Chenvert, M.E., and Gatlin, C., (1965), "Mechanical anisotropies of laminated sedimentary rocks", Society Petroleum Engineers Journal, pp. 67-77.

Chesnut, W.S., (1983), "Geology of the Sydney 1:100,000 sheet", New South Wales Geological Survey, Report No. 9130, pp. 182-199.

Chugh, Y.P. and Missavage, R.A., (1981), "Effects of moisture in strata control in coal mines", Engineering geology, Vol. 17, pp. 241-255.

Coats, D.F., (1964), "Classification of rocks for rock mechanics", International Journal of Rock Mechanics and Mining Sciences, Vol. 1, pp. 421-431.

Colback, P.S.B. and Wiid, B.L., (1965), "The influence of moisture content on

the compressive strength of rocks", Proc. 3rd Can. Rock Mech. Symp., Toronto, pp. 65-83.

Coulomb, C.A., (1773), "Essai sur une application des regles maximis et minimis a quelques problems de statique, relatifs a l'Architecture", Memoirs de Mathematique et de physique, Vol. 7, Paris, pp. 343-381.

Crawford, A.M., Curran, J.H. (1981), "The influence of shear velocity of the frictional resistance of rock discontinuities", International Journal of Rock Mechanics and Mining Sciences and Geomechanics Abstracts, 18, pp. 505-515.

D'Andrea, D.A., Fischer, B.L., and Fogelson, D.E., (1965), "Prediction of compressive strength from other rock properties", US Bureau of Mines, Report Investigation 6702.

Dearman, W.R, (1976), "Weathering classification in the characterisation of rock. A revision." Bulletin of the Int. Assoc. Engineering Geology, No. 13, pp. 123-127.

Deer, D.U., and Gamble, J.c., (1971), "Durability-plasticity classification of shales and indurated clay", Proceedings, 22nd Annual Highway Geological Symp., University of Oklahoma, Norman, Okla., pp. 37-52.

Deere, D.U., (1963), "Technical description of rock cores for engineering purposes", Felsmechanik und Ingenieurgeologic, Journal of the International Society of Rock Mechanics, Vol. 1, pp. 16-22.

Deere, D.U., and Miller, R.P., (1966), " Classification and index properties for intact rock", Air Force Weapons Laboratory Technical report No. AFWL-TR-65-116, Kirtland Air Force Base, New Mexico.

Deere, D.U, Merritt, A.H., and Coon, R.F., (1969), Engineering classification of in-situ rock", Air Force Weapons Laboratory Technical Report No. AFWL-TR-67-144, Kirtland AFB, New Mexico.

Deo, P., (1973), "Use of shale in embankments", Report No. 14, Joint Highway research project, Purdue university, West Lafayette, Indiana.

Deo, P., (1972), "Shales as embankment materials", Ph.D. Thesis, Purdue

university, West Lafayette, Indiana.

Dolanski, J., (1971), "X-ray identification of clay mounts from Wianamatta shale core", Rep. geol. surv. New South Wales, GS 1971/757 (unpubl.).

Donath, F.A., (1972a), "Faulting across discontinuities in anisotropic rock", Proceedings, 13th Symposium on Rock Mechanics, (ASCE), pp. 753-772.

Donath, F.A., (1972b), "Effect of cohesion and granularity on deformational behaviour of anisotropic rock", In studies in Mineralogy and Precambrian Geology (Edited by B.R Doe and D.K. Smith), Geological Society of America, Memoir 135, pp. 95-128.

Donath, F.A., and Cohen, C.I., (1960), "Anisotropy and failure in rocks (abstract)", Geological Society of American Bulletin, 71, 1851.

Donath, F.A., (1964), "Strength variation and deformational behaviour of anisotropic rocks", State of stress in the Earth's crust, W.R. Jude (editor), American Elsevier Publishing Co., New York, N.Y., pp. 281-297.

Donath, F.A., (1961), "Experimental study of shear failure in Anisotropic rocks", Bulletin of Geological Society of America, Vol. 72, pp. 985-990.

Dusseault, M.B., Loftsson, M. and Russell, D., (1986), "The mechanical behaviour of Kettle Point oil shale", Can. Geotech. J. 23, pp. 87- 93.

Farmer, I.W., (1983), "Engineering behaviour of rocks", 2nd Edition, Chapman and Hall, London.

Fayed, L.A., (1968), "Shear strength of some argillaceous rocks", International Journal of Rock Mechanics and Mining Sciences, Vol. 5, No. 1, pp. 79-85.

Fell, R., (1985), "Slope stability in the Wianamatta group", In Engineering Geology of the Sydney Region, (ed. P.J.N Pells), pp. 163-175.

Ferguson, J.A. and Hosking, J.S., (1955), "Industrial clays of the Sydney Region", New South Wales: Geology, mineralogy, and appraisal for ceramic industries. Aust. J. appl. Sci., 6, 380-405.

Fish, E.L., Turnbull, L.A, and Toenges, A.L., (1944), "A study of summer air conditioning with water sprays to prevent roof falls at the beach bottom coal mine, west Virginia", U. S. Bureau of Mines, Report of investigations 3775.

Forster, I.R., (1983), "Influence of core sample geometry on the axial point load test", International Journal of Rock Mechanics and Mining Sciences & Geomechanic Abstract, Vol. 20, pp. 291-295.

Franklin, J.A., Broch, E., & Walton G., (1971), "Logging the mechanical character of rock", Transaction of Institute of Mine and Metallurgy, 80, A1-A10.

Franklin, J.A. and Chandra, A., (1972), "The slake durability test", International Journal of Rock Mechanics and Mining Science, 9, pp. 325-341.

Franklin, J.A., (1981), "Evaluation of shales for construction projects", Research and development project 22303, Ministry of Transportation and Communications, Toronto, Ontario.

Franklin, J.A., (1981), "A shale rating system and tentative applications to shale performance", Trans. Res. 790, pp. 2-12.

Franklin, J.A., (1970), "Classification of rock according to its mechanical properties", Ph.D. Thesis, University of London, Imperial College, London.

Gamble, J.C., (1971), "Durability-plasticity classification of shales and other argillaceous rocks", Ph.D. thesis, University of Illinois at Urbana-champaign.

Ghafoori, M., Airey, D.W. and Carter, J.P. (1993), "Correlation of moisture content with the uniaxial compressive strength of Ashfield shale", Australian Geomechanics, pp. 112- 114.

Ghafoori, M., Mastropasqua, M., Carter, J.P., and Airey, D.W., (1992), "Engineering properties of Ashfield shale", Research Report No. R663, School of Civil and Mining Engineering, University of Sydney.

Gibson, M., (1965), "Application of electron microscope to the study of particle of orientation and fissility in shale", Journal of Sedimentary Petrology, No. 35, pp. 408-414.

Goldstein, J.I., Newbury, D.E., Echlin, P., Joy, D.C., Fiori, C. & Lifshin, E., (1981), "Scanning electron microscopy and X-ray Microanalysis", New York, Plenum Press.

Gonnerman, H.F., (1925), "Effect of end condition of end condition of cylinder in compression tests of concrete", Proceedings, American Society of Testing Materials, 24(2), pp. 1036-1065.

Gordon, I., (1976), "F4 Freeway, Municipality of Holroyed, reconstruction and deviation from Clyde to May's Hill, drilling investigation of proposed cutting between Williams St. and Hayes Avenue, May's Hill", DMR Internal Report No. 496 (Part II).

Gould, M.C., (1982), "Development of a high capacity dynamic direct shear apparatus and its application to testing of sandstone rock joints", M.S Thesis, University of Colorado, Boulder, CO.

Green, S.J., and Perkins, R.D., (1968), "Uniaxial compression tests at strain rates from 10-4/sec to 104/sec on three geological materials", Proceedings, 10th US Symposium on Rock Mechanics, Austin, texas.

Greminger, M., (1982), "Experimental studies of the influence of rock anisotropy on size and shape effects in point load testing", International Journal of the Rock Mechanics Sciences & Geomechanics Abstract, Vol. 19, pp. 241-246.

Grice, R.H., (1968), "The effect of temperature-humidity on the disintegration of nonexpandable shales", Bulletin of the Association of Engineering Geologists, Vol. 5, No. 2, pp. 69-77.

Grim, R.E., (1962), "Applied clay mineralogy", McGraw-Hill, Inc.

Loughnan, F.C., (1960), "The origin, mineralogy and some physical properties of the commercial clays of New South Wales", University of New South Wales, Geological Series, 2, 348 p.

Grim, R.E., (1953), "Clay mineralogy", McGraw-Hill, Inc.

Gunsallus, K.L, and Kulhawy, F.H., (1984), "Comparative evaluation of rock strength measures", International Journal of the Rock Mechanics Sciences & Geomechanics Abstract, Vol. 2, No. 5, pp. 623-640.

Hadfield, C., (1981), "Foundation investigation for proposed grade separation - SH 10 (Pacific Hwy) intersection with Mona Vale Rd. and Ryde Rd.", New South Wales Dept. Main Roads Internal Report No. 112.

Hamrol, M., (1961), "Quantitative classification of the weathering and weatherability of rocks", Int. Conference on Soil Mechanics and Foundation Engineering, Paris.

Harper, T.R., Appel, G., Pendelton, M.W., Szymanski, J.S., and Taylor, R.K., (1979), "Swelling strain development in sedimentary rock in northern New York", International Journal of Rock Mechanics, Mining sciences and Geomechanics Abstracts, Vol. 16, pp. 271-292.

Hartman, I., and Greenwald, H.P., (1941), "Effect of changes in moisture and temperature on mine roof", U.S. Bureau of Mines, Report of investigations 3588, 40pp.

Hassani, F.P., Scoble, M.J., Whittaker, B.N., (1980), "Application of the point load index test to strength determination of rock and proposals for a new size-correction chart", Proc. 21st U.S Symp. Rock Mech., Rolla, pp. 543-565.

Hawkes, I., and Mellor, M., (1970), "Uniaxial testing in rock mechanics laboratories", Engineering Geology, No. 4, pp. 177-285.

Hawkes, I., Mellor, M., and Gariepy, S., (1973), "Deformation of rocks under uniaxial tension", International Journal of rock Mechanics and Mining science, No. 10, 493-507.

Hayashi, M., (1966), "Strength and dilatancy of brittle jointed mass - The extreme value stochastics and anisotropic failure mechanism", Proceedings of the First Congress of the International Society of Rock Mechanics, Lisbon, Vol. 3, No. 1, pp. 295-302.

Hedberg, H.D., (1936), "Gravitational compaction of clays and shales", American Journal of Sciences, Ser. 5, Vol. 31, pp. 241-281.

Helby, R., (1973), "Review of late Permian and Triassic palynology of New South Wales", Geol. Soc. Aust., Spec. Publ., 4, 141-155.

Herbert, C., (1970), "The sedimentology and palaeoenvironment of the Triassic Wianamatta Group sandstones, Sydney Basin", Rec. Geol. Surv. N.S.W., 12(1), 29-44.

Herbert, C., (1976), "The depositional development of the basin", In Branagan, D.F., Herbert, C., & Langford-Smith, T., An outline of the geology and geomorphology of the Sydney Basin, Science Press, Sydney, pp. 5-38.

Herbert, C., (1979), "Sydney 1:100,000 Geological sheet, 9130, and accompanying notes. N.S.W. Geological Survey, Sydney.

Herbert, C., (1979), "The geology and resource potential of the Wianamatta group", New South Wales Geological Survey, Bulletin 25, 203 p.

Herbert, C., (1980) ,"Wianamatta group and Mittagong formation", in 'A guide to the Sydney basin', New South Wales Geological Survey, Bulletin 26, pp. 254-272.

Hobbs, D.W, (1964), "The tensile strength of rocks", International Journal of rock Mechanics and Mining science, Vol. 1, pp. 385-396.

Hoek, E., and Brown, E.T., (1980b), "Empirical strength criterion for rock masses", Journal of Geotechnical Engineering Division, ASCE, 106, pp. 1013-1035.

Hoek, E., (1964), "Fracture of anisotropic rock", Journal of South African Institute of Mining and Metallurgy, Vol. 64, No. 10, pp. 510-518.

Horino, F.G., and Ellickson, M.L., (1970), "A method of stimating the strength of rock containing planes of weakness, U.S. Bureau of Mines, Report Investigation 7449.

Hudec, P.P., (1976), "Development of durability tests for shales in embankment and swamp backfills, Ontario, Ontario Ministry of Transportation and

Communications, Research Report 216, Toronto, Ont.

Huggett, J., (1984), "An SEM study of phyllosilicates in a Westphalian coal measures sandstone using back-scattered electron imaging and wave length dispersive spectral analysis", Sediment. Geology, 40, pp. 233-247.

Hutson, R.W. and Dowding, C.H., (1987a), "Micro computer control of direct shear tests", Proceedings, 28th U.S. Symposium on rock Mechanics, Tucson, AZ, A. A. Balkema, Rotterdam, pp. 125-132.

Iliev, I.G., (1966), "An attempt to estimate the degree of weathering of intrusive rocks from their physico-mechanical properties", Proc. 1st Cong. Int. Soc. Rock Mech., Vol. 1, pp. 109-114.

Ingram, R.L., (1953), "Fissility of mudrocks", Bulletin, Geological Society of America, Vol. 64, pp. 878-889.

International Society of Rock Mechanics, (1979b), "Suggested methods for determining water content, porosity, density, absorption and related properties, and swelling, and slake-durability index properties", International Journal of Rock Mechanics and Mine Sciences & Geomech. Abstr., Vol. 15, pp. 89-97.

International Society of Rock Mechanics, Commission on Standardisation of Laboratory and Field Tests, Committee on Laboratory Tests (1978) "Suggested methods for determining swelling and slake durability index properties" , International Journal of Rock Mechanics and Mining Sciences, Vol. 16, pp. 151-156.

International Society of Rock Mechanics, Commission on Standardisation of Laboratory and Field Tests, (1972), "Suggested methods for determining the uniaxial compressive strength of rock materials and the point load strength index", Committee on laboratory tests document No.1, Final draft.

Jaeger, J.C., (1960), "Shear failure of anisotropic rocks", Geological Mag., Vol. 97, pp. 65-72.

Jaeger, J.C., Cook, N.G.W. (1969), "Fundamentals of rock mechanics", Methuen, London.

Johnston, I.W., (1985b), "Comparison of two strength criteria for intact rock", Journal of Geotechnical Engineering, ASCE, Vol. 111, pp. 1449-1454.

Johnston, I.W., (1985a), "Strength of intact geomechanical materials", Journal of Geotechnical Engineering, ASCE, Vol. 111, pp. 730-749.

Jones, O.T., (1944), " The compaction of muddy sediments", Quaternary Journal of Geological Society of London, Vol. 100, pp. 137-160.

Jumikis, A.R., (1966), "Some engineering aspects of Brunswick shale", Proceedings, 1st Congress of International Society of Rock Mechanics, Lisbon, pp. 99-102.

Kana, D.D., Chowdhury, A.H., Hsiung, S.M., Ahola, M.P., Brady, B.H.G., and Philip, J., (1991), "Experimental techniques for dynamics shear testing of natural rock joints", Proceedings, 7th International Congress on Rock Mechanics, Aachen, Deutschland, Vol. 1, A. A. Balkema, Rotterdam, pp. 519-525.

Kawamoto, T., (1970), "Macroscopic shear failure of jointed and layered brittle media", Proceedings of the Second Congress of the International Society of Rock Mechanics, Belgrade, Vol. 2, pp. 215-221.

Keller, W.D., (1946), "Evidence of texture on the origin of the Cheltenham fireclay of Missouri and associated shales", Journal of sedimentary Petrology, V. 16, pp. 63-71.

Kobayashi, R. and Sugimoto, F., (1981), "On shear behaviours of rock containing weak planes", Proceedings of the International Symposium on Weak Rock, Tokyo, pp. 15-20.

Kowalski, W.C., (1966), "The interdependence between the strength and void ratio of limestones and marls in connection with their water saturation and anisotropy", Proceedings, 1st Congress of International Society of Rock Mechanics, Lisbon, Vol. 1, pp. 143-144.

Krinsley, D., and Manley, C., (1989), "Back-scattered electron microscopy as an advanced technique in petrography", Journal of geological Education, 37, pp. 202-109.

Krinsley, D.H., Pye, K., & Kearsley, A.T., (1983), "Application of backscattered electron microscopy in shale petrology", Geological Magazine, Vol. 10, No. 2, pp. 109-208.

Krsmanovic, D. and Langof, Z. (1964), "Large scale laboratory tests of the shear strength of rocky material", Felsmechnik und Ingenieurgeologie Supp.II, pp. 20-30.

Krsmanovic, D. (1967), "Initial and residual shear strength of hard rocks", Geotechnique 17, pp. 145-160.

Krumbein, W.C, and Sloss, L.L., (1963), "Stratigraphy and Sedimentation", W.H. Freeman and Company, San Francisco.

Krynine, P.D., (1948), "The megascopic study and field classification of sedimentary rocks", Journal of the Geology, Vol. 56, pp. 130-165.0

Kulhawy, F.H., (1975), "Stress deformation properties of rock and rock discontinuities", Engineering geology, Vol. 19, Elsevier Sci. Publ. Co. Amsterdam, Netherland, pp. 327-350.

Lajtai, E.Z., (1969), "Strength of discontinuous rocks in direct shear", Geotechnique, Vol. 19, No. 2, pp. 218-233.

Lajtai, E.Z., (1969a), "Shear strength of weakness planes in rock", International Journal of rock Mechanics and Mining science, Vol. 6, pp. 499-515.

Lam, T.S.K., and Johnston, I.W., (1982), "A constant normal stiffness direct shear machine", Proceeding, 7th Southeast Asian Geotechnical Conference, Hong Kong, China, pp. 805-820.

Lama, R.D. and Gonano, L.P (1976), "Size effect considerations in the assessment of mechanical properties of rock masses", proceedings, 2nd Symposium of Rock Mechanics, Dhanbad.

Lambe, T.W., (1958), "The engineering behaviour of compacted clay" Journal of the Soil Mechanics and Foundations Division, ASCE, Vol. 84, No. SM2, pp. 1655-1 to 1655-35.

Lekhnitskii, S.G., (1981), "Theory of elasticity of an anisotropic body", Mir

Publishers, Moscow, USSR, 430 p.

Loughnan, F.C., Grim, R.E., and Vernett, J., (1962), "Weathering of some Triassic shales in the Sydney Region", Journal of Geological Society of Australia, 8(2), pp. 245-257.

Loughnan, F.C., (1960), "The origin, mineralogy and some physical properties of the commercial clays of New South Wales.", University of New South Wales, Geological Series, 2, 348 p.

Lovering, J.F., (1954a), "The stratigraphy of the Wianamatta Group, Triassic system, Sydney Basin", Rec. Aust. Mus., 23(4), pp. 169-210.

McLamore, R, and Gray, K.E, (1967), "The mechanical behaviour of anisotropic sedimentary rocks", Trans. American Soci. Mech. Engrs., Series B, Vol. 89, pp. 62-76.

McWilliams, J.R., (1966), "The role of microstructure in the physical properties of rocks", Special Tech. Publication No. 402, ASTM, pp. 175-189.

Mead, W.J., 1936, "Engineering geology of dam sites", Transactions, of Second Congress on large dams, Washington D.C., Vol. 4, pp. 171-192. Also, Civil Engineering, ASCE, 1937, Vol. 7, No. 6.

Mead, R.H., (1966), "Factors influencing the early stages of the compaction of clays and sands - Review", Journal of Sedimentary Petrology, Vol. 36, pp. 1085-1101.

Menzies, B.K., (1988), "A computer controlled hydraulic triaxial testing system", Advance triaxial testing of soil and rock, ASTM STM977, pp. 82-94.

Miller, R.P., (1965), "Engineering classification and Index properties for intact rock", Ph.D. Thesis in Civil Engineering, University of Illinois, Urbana, Illinois, 333 p.

Mogi, K., (1966a), "Some precise measurements of fracture strengths of rocks under uniform compressive stress", Rock Mechanic and engineering Geology, No. 4, pp 41-45.

Mohr, O., (1900), "Welche umstande bedingen die elastiztatsgrenze und den bruch eines materials", Z. Ver. dt. Ing., 44, pp. 1524-30; 1572-1577.

Morgenstern, N.R, and Eigenbrod, K.D. (1974), "Classification of argillaceous soils and rocks", Journal of the Geotechnical Engineering Division, ASCE, Vol. 100, No. GT10, pp. 1137-1156.

Moucharab, K.S, and Benmokrane, B., (1994), "A new combined servo-controlled loading frame/direct-shear apparatus for the study of concrete or rock joint behaviour under different boundary and loading conditions", Geotechnical testing Journal, GTJODJ, Vol. 17, No. 2, pp. 233-242.

Moye, D.G., (1955), "Engineering geology for the Snowy Mountains Scheme", Journal of the Institution of Engineers, Australia, Vol. 27, pp. 281-299.

Muller, G., (1967), "Diagenesis in argillaceous rocks", Digenesis in sediments, G. Larsem and G. Chilingar, eds., Ebevier, Amsterdam, The Netherlands, pp. 121-175.

Murayama, S., and Yagi, N., (1966), "Swelling of mudstone due to sucking in water", Proceedings, 1st Congress of the International Society of Rock Mechanics, Lisbon, Vol. 1, pp. 495-498.

Murrell, S.A.F.,(1965), "The effect of triaxial stress systems on the strength of rocks at atmospheric temperatures, Geophysics Journal, Vol. 100, No. GT7, pp. 231-281.

Natau, D., Leichnitz, W and Balthasau, K, (1979), "Construction of a computer controllrd direct shear testing machine for investigation of rock discontinuities", Proceedings, 4th International Congress on Rock Mechanic, Montreux, Switzerland, Vol. 3, pp. 241-243.

Noonan, D.K.J. & Nixon, J.F., (1972), "The determination of Young's modulus from direct shear tests", Canadian Geotechnical Journal, 9:504-507.

O'Brien, N.R., (1970), "The fabric of shale - an electron microscope study", Sedimentology, Special Issue - Lithification of clastic sediments I, Vol. 15, No. 1-2, pp. 229-246.

O'Brien, N.R., (1963), "A study of fissility in argillaceous rocks", Ph.D Thesis, University of Illinois, Urbana, Illinois.

Oakland, M.W., and and Lovell, C.W. (1982), "Classification and other standard tests for shale embankment", Joint Highway Research Project No. 82-4, Purdue University, W. Lafayette, Indiana, USA, 171 pp.

Obert, L., Windes, S.L. and Duvall, W.I., (1946), "Standardised tests for determining the physical properties of mine rocks", US Bureau of Mines, Report of Investigation No. 3891.

Odom, I.E., (1967), "Clay fabric and its relation to structural properties in Mid-continent Pennsylvanian sediments", Journal of Sedimentary petrology, Vol. 37, No.2, pp. 610-623.

Odom, I.E., (1963), "Clay mineralogy and clay mineral orientation of shales and claystones overlying coal seames in Illinois, Ph.D. Thesis, University of Illinois, Urbana, Illinois.

Olivier, H.J., (1979b), "Some aspects of the influence of mineralogy and moisture redistribution on the weathering behaviour of mudrock", Proceedings, Fourth International Congress on Rock Mechanics, Montreux, Suisse, Vol. 3, pp. 1-8.

Oliver, H.J., (1979a), "A new engineering-geological rock durability classification", Engineering geology, Vol. 14, No. 3, pp. 255-279.

Ondera, F.T. and Duangdeun, P., (1981), "Dependence of mechanical properties to the texture and water content of weak rock - A case of late Tertiary mudstone from the Mae Mo Lignite Mine, Northern Thailand", Proceedings, International Symposium on weak rock, Tokyo, Vol. 1, pp. 327-332.

Ooi, L.H. and Carter, J.P (1987a), "A constant normal stiffness direct shear device for static and cyclic loading", Geotechnical Testing Journal., ASTM, Vol. 10, No. 1, pp. 3-12.

Parker, J., (1966), "How moisture affects mine openings", Engineering and Mining Journal, November, pp. 95-97.

Pells, P.J.N., (1975), "The use of point load test in predicting the compressive strength of rock materials", Technical note. Australian Geomechanical Journal, G5, N1, pp. 54-56.

Pells, P.J.N., Douglas, D.J., Rodway, B., Thorne, C. and McMahon, B.K., (1978), "Design loadings of foundations on shale and sandstone in the Sydney region", The University of Sydney, School of Civil Engineering, Research Report No. R 315.

Perkins, R.D., Greens, S.J. and Friedman, M., (1970), "Uniaxial stress behaviour of porphyritic tonalite at strain rates up to 103/sec", International Journal of rock Mechanics and Mining science, Vol. 7, pp. 527.

Pettijohn, F.J., (1948), "A preface to the classification of the sedimentary rocks", Jour. Geol., vol. 56, pp. 112-118.

Pettijohn, F.J., (1975), "Sedimentary rocks", 3rd edition, Harper and Row, New York.

Philbrick, S.S., (1950), "Foundation problems of sedimentary rocks", Ch. 8 in Applied sedimentation, P.D. Trask, editor, pp. 147-168.

Picard, M.D., (1953), "Marlstone- a misnomer as used in Unita Basin, Utah", Bulletin of American Association of Petroleum Geology, Vol. 37, pp. 1075-1077.

Pomeroy, C.D., Hobbs, D.W., and Mahmoud, A., (1971), "The effect of weakness plane orientation on the fracture of Barnsley Hards by triaxial compression", International Journal of rock Mechanics and Mining science, Vol. 8, No. 3, pp. 227-238.

Price, N.J., (1960), "The compressive strength of coal measure rocks", Coll. Eng., Vol. 37, pp. 283-292.

Price, N.J., (1958), "A study of rock properties in conditions of triaxial stress", Proceedings, Conference Mechanical properties Non metallic Brittle materials, London, pp. 106-122.

Pye, K. and Krinsley, D., (1986), "Microfabric, mineralogy and early diagenetic

history of the Whitby mudstone Formation (Toarcian), Cleveland Basin, U.K.",Geological Magazine, 123, pp. 191-203.

Pye, K. and Krinsley, D., (1984), "Petrographic examination of sedimentary rocks in the SEM using back-scattered electron detectors", Journal of Sedimentary Petrology, 54, pp. 877-888.

Ramamurthy, T., Venkatappa Rao, G., and Rao, K.S., (1985), "A strength criterion for rocks", Proceedings, Indian Geotechnical Conference, Roorkee, Vol. 1, pp. 59-64.

Ramamurthy, T., (1986), "Stability of rock mass", Eight IGS Annual Lecture, Indian Geotechnical Journal, Vol. 16, No. 1, pp. 1-73.

Ramamurthy, T., and Arora, V.K., (1994), "Strength predictions for jointed rocks in confined and unconfined states", International Journal of Rock Mechanics and Mining sciences & Geomechanical Abstract, Vol. 31, No. 1, pp. 9-22.

Ramamurthy, T, Venkatappa Rao, G., and Sing, J., (1988), "A strength criterion for anisotropic rocks", Proceedings, 5th Australian New Zealand Conf. on Geomechanics, Sydney, pp. 253-257.

Rao, K.S., Rao, G.V. and Ramamurthy, T., (1985), "Rock mass strength from classification", Paper No. 3, Proceedings, Workshops on Engineering classification of rocks, GBIP, New Delhi, India, pp. 27-50.

Rao, K.S., (1984), "Strength and deformation behaviour of sandstones", Ph.D. thesis, Indian Institute of Technology, Delhi.

Read, J.R.L., Thornton, P.N., and Regan, W.M., (1978), "A rational approach to the point load test", Proceedings, 3rd Australian New Zealand Conference on Geomechanics, Vol. 2, Wellington, pp. 35-39.

Reichmuth, D.R., (1963), "Correlation of force-displacement data with physical properties of rock for percussive drilling systems", Rock Mechanics, (C. Fairhurst, ed.), pp. 35-39.

Reichmuth, D.R., (1968), "Point load testing of brittle materials to determine tensile strength and relative brittleness", Proceedings, 9th Symp. Rock

Mech., Colorado, pp. 134-159.

Richardson, D.N., (1984), "Relative durability of shale", Ph.D. Thesis, University of Missouri-Rolla, at Rolla, Mo..

Richardson, D.N., (1985), "Relative durability of shale: A suggested rating system", 36th Annual Highway Geol. Symp., Clarksville, Ind.

Russel, D. J., and Harman, J., (1985), "Fracture frequency in mudrocks: an example from the Queenston Formation of Southern Ontario", Canadian Geotechnical Journal, Vol. 22, No. 1, pp. 1-5.

Russel, D. J., 1982, "Controls on shale durability: the response of two Ordovician shales in the slake durability test", Canadian Geotechnical Journal, Vol. 22, No. 1, pp. 1-5.

Ruxton, B.P., and Berry, L., (1957), "Weathering of granite and associated erosional features in Hong Kong", Bull. Geol. Soc. Am., 68, pp. 1263-92.

Rzhevsky, V., and Novik, G., (1971), "The phicics of rocks", Mir publishers, Moscow, 320 p.

Salustowicz, A., (1965), "Zarys mechaniki gorotworu", Katowice, Wydawnictwo "Slask",.

Santarelli, F., (1987), "Theoretical and experimental investigation of the axisymetric wellbore", Ph.D. Thesis, Imperial College, London.

Selmer-Olsen, R., and Blindheim, O.T., (1970), "On the drillability of rocks by percussive drilling", Proceedings, The Second Congress of the International Society for Rock Mechanics, Belgrade, Vol. 3, Paper 5-8.

Sing, J., (1988), "Strength prediction of anisotropic rocks", Ph.D Thesis, Indian Institute of Technology, New Delhi.

Skempton, A.W. and Northey, R.D. (1953), The sensitivity of clays, Geotechnique, Vol. 3, No. 1.

Skinas, C.A., Bandis, S.C., and Demiris, C.A., (1990), "Experimental

investigations and modelling of rock joint behaviour under constant stiffness", Proceedings, International Symposium on rock joints, Loen, Norway, A. A Balkema, Rotterdam, pp. 301-308.

Slansky, E. (1973), "Clay mineral identification in Ashfield shale from the Maroota area", Rep. Geological Survy of New South Wales, GS 1973/396 (unpubl.).

Smith, K.C.A., (1956), "The scanning electron microscope and its field of application", PhD thesis, Cambridge University, Cambridge.

Smordinov, M.I., Motovilov, E.A, and Volkov, V.A., (1970), "Determination of correlation relationships between strength and some physical characteristics of rocks", Proceedings, 2nd Congerce of International Society of Rock Mechanics, Belgrade, Vol. 2, pp. 35-37.

Sounders, M.K., Fookes, P.G., (1970), "A review of the relationship of weathering and climate and its significance to foundation engineering", Engng. Geol., 4, pp. 289-325.

Spears, D.A. and Taylor, R.K., (1972), "The influence of weathering on the composition and engineering properties of in situ coal measures rocks", International Journal of Rock Mechanics and Mining sciences, Vol. 9, pp. 729 -756.

Spears, D.A., (1976), "The Fissility of some Carboniferous shales", Sedimentology, Vol. 23, pp. 721-725.

Standards Association of Australia Site Investigation Code, "Australian standard for site investigation", AS 1726, 1981, p. 78.

Taylor, R.K. and Spears, D.A., (1970), "The breakdown of British coal measure rocks", International Journal of Rock Mecanics and Mining Sciences, Vol. 7, No. 5, pp. 481-501.

Terzaghi, K., (1946), "Rock tunnelling with steel supports", Youngstown, Ohio, Commercial Shearing and Stamping Co.

Terzaghi, K., (1962), "Stability of steep slopes on hard unweathered rock", Geotechnique, 12, pp. 251-270.

Terzaghi, K., and Peck, R.B., (1967), "Soil mechanics in engineering practice", John Wiley and Sons, Inc., New York.

Thaulow, S., (1962), "Apparent compressive strength of concrete as affected by height of test specimen and friction between the loading surfaces", Bulletin Reunion Intern. Lab. Essais Research material Construction, 17, pp.31-33.

Trask, P.D., (1931), "Compaction of sediments", Bulletin of American Association of Petroleum Geology, Vol. 15, pp. 271-276.

Tsidzi, K.E.N., (1991), "Point load-uniaxial compressive strength correlation", Proceedings, 7th International Congress on Rock Mechanics, ed.(W. Wittke), Aachen, pp. 637-639.

Twenhofel, W.H., (1937), "Terminology of the fine-grained mechanical sediments", Report of Committee on Sedimentation 1936-1937, Nat. Res. Coun., Div. Geol. Geog., pp. 81-104.

Uff, J.F., and Nash, J.K.T.L., (1967), "Anisotropy of shale due to folding", Proceedings of the Geotechnical Conference, Oslo, pp. 301-303.

Underwood, L.B., (1967), "Classification and identification of shales", Journal of the Soil Mechanics and Foundations Division, ASCE, Vol. 93, SM6, pp. 97-116.

Van Eeckhout, E.m., (1976), "The mechanisms of strength reduction due to moisture in coal mine shales", International Journal of Rock Mechanics and Mining Sciences, Vol. 13, No. 2, pp. 61-67.

Van Eeckhout, E.M., and Perig, S.S., (1975), "The effect of humidity on the compliances of coal mine shales", International Journal of Rock Mechanics and Mining Sciences, Vol. 12, No. 11, pp. 335-340.

Venkatappa Rao, G., Priest, S.D., and Selva Kumar, S., (1985), "Effect of moisture on strength of intact rocks and the role of effective stress principle", Indian Geotechnical Journal, Vol. 15, No. 4, pp. 246-283.

Venkatappa Rao, G., Priest, S.D., and Selva Kumar, S., (1983), "Effect of moisture on strength of intact rocks and the role of effective stress

principle", Report for Project XV Indo-British Collaboration on rock mechanics, Indian Institute of Technology, Delhi.

Venter, J.B., (1980), "An investigation of slake durability test for mudrocks used for road construction", Proceedings, 7th Soil Mechanics and Foundation Engineering Conference, Regional conf. for Africa, Vol. 1, pp. 201-204.

Vernik, L., Bruno, M., Bovberg, C., (1993), "Empirical relations between compressive strength and porosity of siliciclastic rocks", International Journal of Rock Mechanics and Mining Sciences & Geomechanical Abstract, Vol. 30, No. 7, pp. 677-680.

White, S., Shaw, A., and Huggett, J., (1984), "The use of back-scattered electron imaging for the petrographic study of sandstones and shales", Journal of Sedimentary Petrology, 54, pp. 487-494.

White, W.A., (1961), "Colloid phenomena in sedimentation of argillaceous rocks", Journal of Sedimentary Petrology, Vol. 31, pp. 560-570.

Wiid, B.L., (1967), "The Influence of moisture upon the strength behaviour of rock", Ph.D. Thesis, University of Witwatersand, 184 p.

Won, G.W., (1985), "Engineering properties of Wianamatta group rocks from laboratory and in-situ tests", Engineering Geology of the Sydney Region, (Ed. P.J.N. Pells), pp. 143-161.

Youash, Y.Y., (1966), "Experimental deformation of layerd rocks", Proceedings, 1st Congress, International society for Rock Mechanics, Lisbon, pp. 787-795.